Multi-Objective Genetic based Algorithms and Experimental Beam Lifetime Studies for the Synchrotron SOLEIL Storage Ring

Xavier Nuel Gavaldà

NNT : *2016SACLS205*

THESE DE DOCTORAT
DE
L'UNIVERSITE PARIS-SACLAY
PREPAREE AU L'UNIVERSITE PARIS-SUD ET
"SYNCHROTRON SOLEIL"

ÉCOLE DOCTORALE N° 576

Particules, Hadrons, Énergie, Noyau, Instrumentation, Image, Cosmos et Simulation

Physique des Accélérateurs

Par

M. Xavier Nuel Gavaldà

Application d'Algorithmes Génétiques Multi-Objectifs et Études Expérimentales de la Durée de Vie du Faisceau de l'Anneau de Stockage du Synchrotron SOLEIL

Thèse présentée et soutenue à Synchrotron SOLEIL, Gif-sur-Yvette le 6 septembre 2016

Composition du Jury :

Dr, S. Bielawski, Laboratoire de Physique des Lasers, Atomes et Molécules de Lille, Président
Dr, M.-E. Couprie, Synchrotron SOLEIL, Directrice de thèse
Dr, L. S. Nadolski, Synchrotron SOLEIL, Co-encadrant
Dr, C. Bruni, Laboratoire de l'Accélérateur Linéaire d'Orsay, Examinatrice
Pr, J.-M. De Conto, Laboratoire de Physique Subatomique et de Cosmologie de Grenoble, Rapporteur
Pr, S. Khan, Zentrum für Synchrotronstrahlung Technische Universität Dortmund, Rapporteur

Dedicat a la meva dona
i al meu fill

ACKNOWLEDGMENTS

I would like to thank all people that have helped and supported me during this thesis.

First of all, a special thanks to L.S. Nadolski for his guidance, kindness and support during this project. He took care of me from the beginning and he showed me a lot of attitudes to be a good scientist. Thank you very much for your advice, patience and to share your knowledge with me.

I would like to thank M.-E. Couprie, to accept to be the Director of this thesis and for her guidance and advice during the writing process of the manuscript.

My warm thanks to P. Brunelle for her guidance, patience and kindness during this work.

Many thanks to the rest of my colleagues of the Accelerator Physics Group for their help and support during this project: R. Nagaoka, M.-A. Tordeux, A. Loulergue, F. Culligan, H.-C. Chao, M. Klein, J. M. Luque Raigón and S. Podgorny.

I would like to thank also A. Nadji for his cordiality, support and encouragement.

Many thanks as well to A. Díaz Ortíz to share his knowledge and to discuss with me during this project. ¡*Muchas gracias*!

Thanks to N. Béchu and C. Herbeaux for their guidance and discussions.

Thanks a lot to N. Carmignani, T. Pulampong, F. H. De Sá and O. Rudenko for his fruitful discussions during this project.

I cannot close this section without remembering my colleagues from the oPAC network. I will never forget all great times that we spent together in many activities during these 3 years. Thanks as well to C. Welsch for his cordiality and support. This experience has completely changed my live.

CONTENTS

RÉSUMÉ

Les sources de rayonnement synchrotron sont des installations scientifiques construites pour produire des faisceaux de photons de flux et de brillance élevés. Le rayonnement synchrotron est utilisé simultanément par plusieurs dizaines de laboratoires: ce sont les lignes de lumière qui utilisent les faisceaux de photons pour explorer les propriétés de la matière. Le spectre du rayonnement synchrotron s'étend typiquement de l'infrarouge aux rayons X durs, c'est-à-dire, de longueurs d'onde de quelques millimètres à quelques dixièmes de nanomètres. Il existe un grand nombre de domaines d'application qui couvre les sciences fondamentales, appliquées et industrielles: par exemple la physique, la chimie, les sciences de l'environnement, la biologie, la médecine, les applications pharmaceutiques, l'archéologie et la biotechnologie. Il existe actuellement une soixantaine de sources de lumière répartie essentiellement en Europe, en Amérique du Nord et en Asie.

Le synchrotron SOLEIL est la source de lumière de troisième génération française délivrant ses photons aux utilisateurs de façon routinière depuis 2007. En 2015, SOLEIL a accueilli 2 400 utilisateurs uniques et a délivré 4900 heures des faisceaux, 24 h/24 h avec une grande disponibilité (98,9 % du temps prévu). Un jour par semaine est dédié à la maintenance, au réglage et à l'installation de nouveaux équipements afin d'améliorer continuellement les performances des accélérateurs. SOLEIL est constitué d'un injecteur à deux étages: un accélérateur linéaire accélérant un faisceau d'électrons jusqu'à une énergie 110 MeV et un booster, anneau de 157 m de circonférence, qui permet, en un sixième de seconde, d'augmenter l'énergie des électrons jusqu'à sa valeur nominale de 2,75 GeV. Le faisceau d'électrons est alors accumulé et stocké dans un accélérateur appelé anneau de stockage pendant plusieurs jours pour produire le rayonnement synchrotron. Ce dernier est soit produit au moyen d'aimant de courbure (ou dipôle) soit au moyen de structures périodiques magnétiques appelées insertions. SOLEIL dispose actuellement d'un total de 27 lignes de lumière en opération et de deux autres en construction.

La qualité du rayonnement synchrotron dépend directement de la structure magnétique de l'anneau de stockage qui détermine la dynamique et la stabilité du faisceau d'électrons à l'intérieur de la machine. Cette structure magnétique est constituée de séries d'aimants séparées par des sections droites pour accueillir les insertions, sources les plus intenses de rayonnement synchrotron. Le faisceau d'électrons est guidé par les champs magnétiques des dipôles le long de l'anneau; des aimants particuliers, les quadripôles, focalisent le faisceau pour lui donner une taille micrométrique; d'autres aimants, les sextupôles, corrigent les aberrations chromatiques introduites par les quadripôles. Le système radiofréquence permet de restituer à chaque électron, l'énergie perdue à chaque tour par rayonnement synchrotron. Enfin, le faisceau d'électrons circule dans une enceinte à vide appelée chambre à vide, où

règne une pression extrêmement faible (quelques nanobars) afin de limiter les interactions du faisceau d'électrons avec les molécules du gaz résiduel qui génèrent des pertes d'électrons et limitent le temps pendant lequel le faisceau peut rester stocké dans l'anneau de stockage.

Pour une source de lumière, une des plus importantes figures de mérite est la brillance : elle correspond au flux de photons émis par unité de surface et d'angle solide dans 0,1 pour cent de la bande passante pour une énergie de photon donnée. La brillance est inversement proportionnelle aux tailles transverses du faisceau d'électrons et proportionnelle au courant stocké (nombre d'électrons). L'émittance est le produit de la taille du faisceau et de sa divergence. Sa valeur est typiquement de l'ordre de quelques nanomètres radians pour les sources de troisième génération comme SOLEIL (3,9 nm·rad). Aujourd'hui, il est quasiment impossible d'augmenter le courant stocké au-delà de 500 mA, car les fortes densités d'électrons induisent de très intenses effets collectifs qui viennent détruire les propriétés du faisceau et ceci, même en présence de systèmes de contre-réaction. Le seul moyen d'augmenter la brillance est donc de focaliser plus intensément le faisceau pour réduire son émittance. C'est le défi des futures sources de lumière de quatrième génération sur anneau de stockage où les émittances atteindront des valeurs de quelques dizaines à centaines de picomètres radians. La forte focalisation des quadripôles implique d'augmenter la force des sextupôles pour compenser les aberrations chromatiques introduites par les quadripôles. Or les sextupôles sont des éléments non linéaires qui affectent deux paramètres importants liés aux performances du faisceau d'électrons à l'intérieur de la machine : l'ouverture dynamique et l'acceptance en énergie qui se traduisent en termes d'efficacité d'injection et de durée de vie du faisceau respectivement.

L'ouverture dynamique est définie comme la zone de stabilité du faisceau d'électrons dans le plan transversal. Elle est calculée pour un nombre de révolutions donné de l'anneau et doit rester suffisamment grande pour permettre d'injecter le faisceau d'électrons; à SOLEIL l'amplitude d'injection est de 8 millimètres dans le plan horizontal et est fixée par le système d'injection. Le calcul précis de l'ouverture dynamique est uniquement numérique en intégrant par morceaux les équations du mouvement tout après tour. Les codes de simulation et de calculs portent le nom de codes de tracking. De même, on définit un domaine de stabilité longitudinal : il existe une déviation maximale d'énergie au-delà de laquelle le faisceau n'est plus stable dans l'anneau de stockage. Cette valeur est localement, en chaque point de l'anneau et se nomme acceptance en énergie locale; cette dernière est l'ingrédient principal intervenant dans le calcul de la durée de vie due à l'effet Touschek, un processus de diffusion élastique entre deux particules au sein d'un même paquet d'électrons. La durée de vie Touschek dépend d'autres paramètres importants de fonctionnement comme le couplage, la longueur du paquet d'électrons, le courant stocké et la tension RF. La durée de vie Touschek est la principale contribution à la durée de vie totale pour une source de rayonnement synchrotron de troisième ou quatrième génération. L'acceptance en énergie est également calculée par simulations numériques et dépend de la structure magnétique de l'anneau et des limitations physiques données par les dimensions de la chambre à vide.

Résumé

L'optimisation de l'ouverture dynamique et de l'acceptance énergie reste un des principaux défis des physiciens des accélérateurs. Depuis plusieurs décades ont été développés des outils analytiques et numériques pour minimiser des termes non linéaires, les résonances excitées par les sextupôles et les défauts magnétiques ou d'alignement afin de réduire les variations des fréquences propres du faisceau (nombres d'onde) avec l'amplitude d'oscillation transverse ou longitudinale. L'analyse en fréquence est un autre exemple d'outil numérique aidant à identifier les principales résonances limitant la dynamique transverse et longitudinale. Ce type de minimisation est complexe et peut demander des temps de calcul extrêmement long quand la structure magnétique est complexe, comme à SOLEIL par exemple, avec les 11 familles de sextupôles de l'anneau. Lorsqu'une solution est trouvée, comment peut-on assurer que l'espace des paramètres a été exploré de manière exhaustive, que tout le potentiel de la structure magnétique a été exploité ? Répondre à cette question est l'un des objectifs de ce travail.

L'objectif principal de cette thèse est d'évaluer l'apport des algorithmes génétiques (GA) comme outils complémentaires d'optimisation des structures magnétiques. Ce type d'outil a été introduit il y a environ 15 ans pour optimiser les sources de rayonnement synchrotron et a été utilisé pour d'autres machines avec des résultats très prometteurs. Le type d'algorithme utilisé dans cette thèse est appelé Algorithme Génétique Multi-Objectif (MOGA). Il a été créé à l'Advanced Photon Source par M. Borland et ses collègues afin d'optimiser la dynamique non linéaire des faisceaux et explorer de nouvelles solutions, jamais obtenues auparavant, pour la structure magnétique de l'anneau. L'outil MOGA est constitué du code tracking ELEGANT pour calculer les ouvertures dynamiques et l'acceptance en énergie, et de la librairie logicielle SDD-Toolkit pour gérer les fichiers d'entrée et de sortie de MOGA. Dans le cas particulier de SOLEIL, MOGA est relié par à la bibliothèque SLURM pour effectuer les calculs sur le cluster haute performance de SOLEIL. C'est la première fois que ce genre d'outil de force brute est utilisé à SOLEIL. Si les résultats sont satisfaisants, MOGA intégrera la boîte à outils du Groupe Physique des Accélérateurs.

Le premier chapitre de ce manuscrit introduit le lecteur aux algorithmes génétiques et à leur utilisation durant les cinquante dernières années pour optimiser des problèmes multi-objectifs avec un haut niveau de complexité en utilisant le concept darwinien de l'évolution naturelle où les individus les plus adaptés survivent et deviennent les parents de la prochaine génération. L'objectif des algorithmes génétiques est de trouver un ensemble de solutions avec le meilleur compromis entre les différents objectifs, appelé front optimal de Pareto. Ce front Pareto est unique pour chaque problème multi-objectif. Pour le définir, l'algorithme change de manière aléatoire les variables à partir d'un point de départ et classe les solutions optimisées en fonction des objectifs d'optimisation. Par la suite, il mute les variables des solutions appartenant au front de Pareto pour créer la nouvelle génération d'individus. Le processus se poursuit jusqu'à ce que le nombre maximum d'individus soit atteint ou jusqu'à ce que le front de Pareto idéal soit trouvé. Le détail de l'installation et de l'utilisation de MOGA à SOLEIL est décrit.

Le deuxième chapitre de cette thèse est consacré à la comparaison du code ELEGANT utilisé

par MOGA avec le code de référence de SOLEIL: TRACY3. Le code TRACY3 a été développé continuellement depuis 15 ans au sein du groupe Physique des Accélérateurs puis validé expérimentalement. Il est crucial de valider les résultats obtenus à partir de ELEGANT en termes de « tracking » à long terme, pour s'assurer que ce code peut être utilisé de façon fiable pour calculer les ouvertures dynamiques et les acceptances en énergie et prédire des performances qui pourront être appliquées ensuite sur le faisceau de SOLEIL. Cette étude a deux conclusions importantes: un écart entre les deux codes sur le modèle des coins du dipôle et le choix de la formule utilisée pour le calcul de la durée de vie Touschek. Le modèle du coin dipolaire de la version originale du code ELEGANT installé au SOLEIL a été mis à jour pour corriger un défaut du second ordre en énergie, qui introduisait un excès de chromaticité verticale de 1,4 unité. Cette correction est importante pour les machines de moyennes et petites circonférences. Concernant le calcul de la durée de vie Touschek, la formule de Bruck initialement introduite dans TRACY3 n'est plus assez précise pour calculer la durée de vie Touschek. Cette simplification a été remplacée par la formule complète, la formule de Piwinski. Une fois ces deux corrections réalisées, l'accord entre les deux codes est atteint pour les paramètres linéaires et non linéaires et en particulier pour les calculs d'ouverture dynamique, d'acceptance en énergie et de durée de vie Touschek.

L'étape suivante a été d'améliorer la connaissance du modèle théorique de la durée de vie totale du faisceau de l'anneau de stockage de SOLEIL en comparant les résultats prédits et simulés avec les valeurs expérimentales, en utilisant le réglage magnétique standard de l'anneau de SOLEIL. À cet effet, une liste d'expériences a été effectuée pour mesurer la durée totale du faisceau d'électrons en fonction de différents paramètres tels que le couplage (rapport entre l'émittance verticale et l'émittance horizontale), le courant stocké et les dimensions physiques des collimateurs. La durée de vie Touschek a été calculée en utilisant le code TRACY3. Les différentes contributions de la durée de vie due au vide ont été évaluées par calcul analytique et plusieurs modèles ont été testés, en particulier la valeur du numéro atomique effectif correspondant à la composition du gaz résiduel, estimée grâce à différentes analyses expérimentales du gaz résiduel. Les analyses de la composition du gaz résiduel au moyen d'un analyseur de spectre ont montré que la composition varie significativement entre les arcs et les sections droites abritant les insertions sous vide. Si le numéro atomique est proche de 2,2 dans les arcs, il est plus proche de 7 (5,5) dans les insertions sous vide où les pressions locales peuvent être jusqu'à un facteur 10 plus élevées par rapport à la pression moyenne. Ces sections droites contribuent de manière prépondérante à la durée de vie due au vide et représentent près de 10 % de l'ensemble de la circonférence de l'anneau de stockage.

Les études ont donc montré qu'il est difficile d'avoir un bon accord absolu entre les simulations et les mesures expérimentales. En revanche, de manière relative, les lois d'échelles sont respectées et l'accord entre valeurs calculées et mesurées de la durée de vie est suffisant pour poursuivre les études.

Le chapitre IV présente les résultats principaux obtenus avec MOGA pour SOLEIL. Le modèle utilisé pour l'anneau de stockage de SOLEIL inclut les limitations physiques imposées par la chambre à vide; il explore un espace des paramètres de dimension 13: deux familles de

quadripôles pour changer la partie fractionnaire des nombres d'ondes et les onze familles de sextupôles pour optimiser les chromaticités et minimiser les non-linéarités. Après un mois de calcul à l'aide de 200 processeurs, 46 000 solutions optimisées sont obtenues. À partir de la structure nominale de SOLEIL, le processus converge vers des solutions du front de Pareto qui offrent une augmentation de 70 % en termes de durée de vie Touschek et une ouverture dynamique légèrement supérieure à celle de la structure nominale. Toutes les solutions du front de Pareto ont été étudiées en détail afin de sélectionner certaines d'entre elles pour être testées expérimentalement. À cet effet, TRACY3 est utilisé pour d'une part, ajouter les composantes multipolaires des champs magnétiques dans le modèle et d'autre part, pour calculer plus précisément les ouvertures dynamiques et acceptances en énergie puisqu'elles sont approximées par ELEGANT afin de réduire le temps de calcul. L'analyse en fréquence est utilisée afin de caractériser les différentes solutions en termes de résonances. Après cette étude, trois solutions ont été sélectionnées pour être testées expérimentalement: deux appartenant au front de Pareto et une autre solution dégradée en termes de durée de vie Touschek pour vérifier la fiabilité des prédictions de MOGA.

Ces solutions ont été appliquées expérimentalement sur l'anneau de stockage de SOLEIL, depuis la salle de contrôle, dans les mêmes conditions de tension RF, couplage, nombre d'ondes et chromaticités que pour les simulations. Les expériences montrent un accord remarquable entre les durées de vie Touschek simulées et expérimentales: l'amélioration de 40-50 % de la durée de vie totale obtenue à partir des simulations est confirmée par les expériences. Il en est de même pour la réduction de durée de vie prédite pour la solution dégradée. Ce résultat est fondamental, car MOGA a permis de prédire des réglages magnétiques performants qui n'avaient jusqu'à présent pas été découverts. Les variations de forces sextupolaires sont significatives: de 10 à 15 %. La fiabilité de MOGA résulte de la qualité du modèle magnétique utilisé, de la bonne intégration des limitations physiques imposées par la chambre à vide et de la correction du code de simulation ELEGANT.

Le succès de la première application d'algorithmes génétiques pour optimiser la structure magnétique de l'anneau de stockage de SOLEIL ouvre la possibilité d'utiliser ce type d'algorithmes pour les upgrades majeurs à venir, en particulier pour le projet de diminuer l'émittance horizontale du faisceau d'un facteur 20 pour atteindre une valeur de l'ordre de 200 pm·rad. Ce type d'algorithmes est perfectible, en particulier en termes de ressources utilisées et de choix des figures de mérite. Par exemple, le taux de diffusion des cartes en fréquence est certainement une figure de mérite plus adaptée pour les optimisations du modèle. D'autres algorithmes faisant appel à la méthode « Robust Conjugate Direction Search » convergent beaucoup plus rapidement et permettraient d'être utilisés directement au sein de la salle de contrôle, en direct sur le faisceau, comme dans d'autres laboratoires : l'ESRF (Grenoble, France) ou SPEAR3 (Palo Alto, USA).

INTRODUCTION

Synchrotron light sources are research facilities designed to produce photon beams of high flux and brilliance. The radiation spectrum typically ranges from the infrared to the hard X-rays (some millimeters to some tenths of nanometers in wavelength). It is 10,000 times more intense than solar light. Synchrotron radiation is a powerful tool to study the properties of matter. Its field of application is very wide and covers fundamental and applied sciences: such as atomic and electronics physics, chemistry, geophysics, pharmaceutical industries, environmental sciences, archeology, biology, biotechnology. Today they are around 60 light sources in Europe, Middle East, North and South America, Asia, and Australia.

Synchrotron SOLEIL is one of the most recent third generation light sources and was commissioned in 2006. Photons are daily distributed to 27 beam lines with another two new beam lines in construction. An average of 2,400 single users visits SOLEIL every year. In 2015 the beam availability was 98.9 % of the time scheduled for users with a mean time between failures of 105 hours. A total of 4,900 hours was delivered to the users (24/7 operation). Ideally the beam is stored in the storage ring for six consecutive days, the last day being dedicated to maintenance and machine studies. The injector is made of a 110 MeV Linac and full energy 3 Hz Booster. The photon beam performance depends directly on that of the 2.75 GeV electron beam and more precisely of their dynamics and stability.

Storage rings for light sources are made of a series of magnets separated by drift sections dedicated to host insertion devices, main sources of photon radiation. The magnet fields of the magnets enable to guide the beam along the ring while maintaining small beam sizes. An important figure of merit is the so-called brightness that is the flux of photons emitted by unit of surface and solid angle in 0.1 % of bandwidth. Brightness is inversely proportional to the transverse emittance of the beam and linearly proportional to the beam current. The emittance is basically the product of the beam size by its divergence. Its value is typically of a few nanometers for third generation light sources (3.9 nm·rad for SOLEIL). High photon flux without beam stability and accelerator reliability is useless for users. For instance, with strong horizontal focusing and low coupling value, the vertical beam size is below 10 micrometers for instance in the in-vacuum undulators of SOLEIL. Orbit feedback systems stabilize the beam with sub-micrometer stability.

In today's accelerators, increasing the beam current beyond a few hundred milliamperes (500 mA for SOLEIL with its 354 m circumference) is very difficult since collective effects limit the beam performance. The increase in brightness and coherent flux can then only be achieved by finding ways to focus the beam even more and then reduce the horizontal emittance to tens or hundreds of picometers. This is the challenge of forthcoming fourth generation synchrotron

light sources; they are named diffraction limited light sources, since the make feasible to reach the diffraction limit in the horizontal plane. For instance, the diffraction limit is obtained at 80 picometers for energy of 1 keV. Thanks to the numerous progress obtained in technologies, diagnostics, and simulation tools over the last two decades, most of the synchrotron laboratories have established a roadmap to build such a facility or upgrade the existing one. The work of accelerator physicists is to assure that the beam dynamics is stable enough to inject the beam in the storage ring and to maintain it for several hours minimizing losses.

The transverse and longitudinal beam dynamics are related to the magnetic structure of the storage ring. Different kinds of magnets control the trajectory and the characteristics of the electron beam inside the storage ring. The strong focusing quadrupoles to increase the brilliance of the synchrotron radiation comes with a deleterious effect: large chromatic effects are generated and need to be corrected by means of sextupole magnetic fields; unfortunately they are strongly nonlinear elements that in turn impact the beam lifetime and the injection efficiency in the storage ring.

The beam lifetime is an important parameter in the synchrotron storage ring because it reflects the sensitivity of the electron beam to nonlinear dynamics. The beam lifetime is limited by two phenomena. The first one is the interaction of the electron beam with the residual gas molecules present in the vacuum chamber (gas lifetime); it depends on the vacuum pressure, the gas composition, and the size of the vacuum chamber. The second one is the scattering of the electrons inside bunches leading to a change in energy (Touschek lifetime). In both cases, the electrons become lost if their trajectory hits the walls of the vacuum chamber or if their change in energy exceeds the energy acceptance of the machine. These two important contributions can be computed analytically or by tracking along the different elements of the storage ring structure taking into account the nonlinear dynamics, the radio frequency system energy acceptance and the physical aperture of the vacuum chamber.

The injection efficiency directly depends on the on-momentum dynamic aperture, defined as the region in the transverse horizontal and vertical planes where the electrons remain stable after a large number of turns. Indeed, the injected electrons are deviated in horizontal plane for most accelerators and then have to perform hundreds of turns with large horizontal amplitude seeing off-axis magnetic field of all the magnets before being damped.

The optimization of the on- and off-momentum dynamic acceptances has become for the accelerator physicists one of the most challenging aspects of this type of accelerators. Different analytical and numerical methods and tools have been developed over the years and used until now with good results to optimize quantities like Resonance Driving Terms which are excited by sextupole and high multipolar field errors and tune shift with amplitudes and energy, native characteristic of strong nonlinear systems. Frequency Map Analysis is another example of tools that a full footprint of the transverse beam dynamics. However, for exotic lattices or new lattices with very strong focusing, these methods can be tedious and time

consuming. As a second step, a new method is required to automate the optimization of the accelerator ensuring that the full space of parameters is explored, leading to the best solutions.

A new approach, based on genetic algorithms, has been introduced and followed during the last 15 years for this purpose thanks to the development of high-performance computers. It can be used to optimize both the linear and nonlinear beam dynamics of synchrotron light sources. With this new approach, the optimization of, for instance, the on- and off-momentum dynamic acceptances can be set as a multi-objective problem; it uses the iterative optimization process of genetic algorithms to find the best solutions that are fitting the objectives. It takes into account all the complexity of the storage ring magnetic structure. A computer cluster of typically hundreds of CPUs is used to compute by tracking particles for a large number of turns through different magnets.

The work performed during this thesis focuses on two main aspects. The first one is to the study, theoretically and experimentally, the limitations of the beam lifetime and its parameterization with respect to machine and beam characteristics in the SOLEIL storage ring. The second one is to install, configure, and apply the MOGA-ELEGANT method to the optimization of the present SOLEIL lattice in order to improve the performance mainly in terms of the beam lifetime.

Chapter I is dedicated to explain in detail the kind of genetic algorithm chosen to optimize the on- and off-momentum dynamic acceptances of the SOLEIL current storage ring, called Multi-Objective Genetic Algorithm (MOGA). After a brief introduction of the transverse and longitudinal linear and nonlinear beam dynamics defining the physical concepts used along this thesis, the optimization method is explained in detail. A review of the application of genetic algorithms to optimize different parameters of particle accelerators until now is given. The second part of this chapter is dedicated to study in detail the algorithm itself and the computational architecture implemented in MOGA. Special attention is paid to validate the tracking code ELEGANT, implemented in MOGA to perform the tracking.

Chapter II compares the two tracking codes used in this thesis: ELEGANT and TRACY3. TRACY3 is the reference code of the SOLEIL Accelerator Physics Group and is suitable for long-term tracking. It is used to check the relevance of the optimized solutions obtained by MOGA adding higher order multipole field components. The comparison is made in terms of optical functions, tune shifts with amplitudes and energy, on- and off-momentum dynamic acceptances, and Touschek lifetime. Main findings are the necessity to patch ELEGANT concerning the modeling of the edge focusing of dipoles and to upgrade the simplified algorithm used by TRACY3 to compute the Touschek lifetime using the full Piwinski formula.

Chapter III is dedicated to a complementary and detailed analytical and experimental study of the beam lifetime versus important parameters of the beam and machine such as transverse coupling, physical apertures and bunch current. This study allows the improvement of our understanding of the contributions of the gas and Touschek lifetimes in the case of the SOLEIL

storage ring. The experimental Touschek lifetimes of the different experiments agree with the simulated ones. Concerning the gas lifetime, a study of the gas residual composition is performed due to the impact of the presence of NEG coated surfaces in the SOLEIL vacuum chamber. The strong impact of in-vacuum undulators or the injection section is also highlighted. They represent 10 % of the total storage ring and are characterized by molecules with much higher values of atomic number and higher values of local pressures than for the rest of the storage ring.

Finally, Chapter IV presents in detail optimized solutions obtained by MOGA for the present SOLEIL lattice. Beam-based experiments are analyzed and compared with the theoretical expectations. The increase of the beam lifetime of 40-50 % predicted by the model is confirmed by beam-based experiments.

CHAPTER I
GENERAL BACKGROUND AND COMPUTER TOOLS

CONTENTS

This chapter will introduce the main concepts and tools used in this thesis. The first section is dedicated to a brief overview of the transverse and longitudinal beam dynamics in a circular accelerator. The linear equations of the motion of a charged particle will be given together with the vocabulary and useful physics parameters and merit functions to optimize an accelerator. Scattering Effects will be introduced later on when studying in depth the beam lifetime. This type of accelerator facilities is denominated *synchrotron radiation facilities* or *light sources*.

The second part of this chapter will focus on one tool used to optimize the linear and nonlinear beam dynamics of storage rings: *genetic based algorithms*. First, the state-of-the-art of the application of genetic algorithms is reviewed. The reasons for the applications of this computational tool and the motivation of the project are also explained and more specifically the optimization of light sources like the SOLEIL storage ring. Then, the specific code used during this thesis, namely MOGA-ELEGANT, is presented in detail.

Finally, the last section shows the computational environment used at Synchrotron SOLEIL: genetics algorithms require heavy computations with hundreds of Central Processing Units (CPUs) to carry out such numerical simulations.

1. Short Introduction on Accelerator Physics

In particle accelerators, high-energy charged particles are guided based on the interaction of these particles with various electromagnetic fields. The magnetic fields are generated by magnetic elements (dipole, quadrupole, and sextupole magnets) distributed along the movement trajectory along the accelerator. Longitudinal field is mostly produced in RF-cavities to accelerate or to increase the beam energy in an injector, and to compensate for the mean energy loss in terms of synchrotron radiation over one turn. The particles oscillate transversally with respect to a special trajectory that is called the *reference trajectory* or *closed orbit*. The reference trajectory is obtained by solving the piece-wise equations of motion in a succession of regions where the magnetic field is supposed constant (*hard edge approximation*) and regions without magnetic fields called *drift spaces* or *drifts*. The arrangement of all the magnets, drift spaces, and RF-cavities constitute the electromagnetic structure named *lattice*.

Considering the Cartesian coordinate system (Wiedemann, 2007) of Figure 1, it is possible to represent the ideal movement of the charged particles in a circular accelerator around the reference orbit defined with a radius ρ. The particle coordinates are defined by a six-dimensional vector $\vec{r} = (x,\ x',\ z,\ z',\ s,\ \delta)$, where x is the horizontal coordinate, z is the vertical coordinate, the curvilinear longitudinal coordinate s is a time like coordinate, $x' = \frac{dx}{ds}$, $z' = \frac{dz}{ds}$ are the s-slopes of the horizontal and vertical positions with respect to the reference trajectory, and $\delta = \frac{p - p_0}{p_0}$ is the relative longitudinal momentum deviation normalized to the reference momentum p_0, also called *relative energy offset*.

For a circular accelerator, solving Maxwell's equations, the magnetic field B produced by the magnets can be expressed in a very compact form using *Beth's representation* in complex notation (Lee, 2004):

$$\frac{B(x,z)}{(B_0\rho)} = \frac{B_z + iB_x}{(B_0\rho)} = \sum_{n=1}^{\infty} (b_n + ia_n)\,(x+iz)^{n-1}, \qquad (1)$$

where $\mathrm{B_x}$ and $\mathrm{B_z}$ are the horizontal and vertical magnetic fields, a_n and b_n are called *skew* and *normal multipolar field coefficients* respectively, $(\mathrm{B_0\rho})$ is the *magnetic rigidity* defined by the storage ring energy $\mathrm{E_0}$ as $\mathrm{B_0\rho\ [T\cdot m]} = 3.3356\ \mathrm{E_0\ [GeV]}$ and n is the *order* of the field multipolar coefficient.

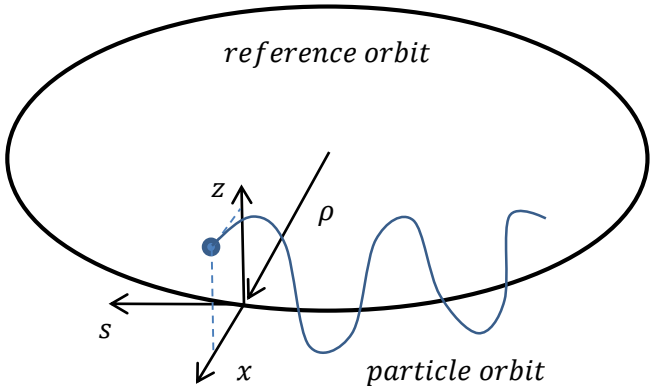

Figure 1: Cartesian coordinate system (x, z, s), of a particle moving around the accelerator reference orbit. The particle orbit is defined by the reference orbit of mean radius ρ.

By making a Taylor expansion of the magnetic field in both transverse coordinates x and z, one obtains:

$$B_{x,z}(x,z) = B_0 + \left.\frac{\partial B_{x,z}}{\partial x}\right|_{x=z=0} x + \left.\frac{\partial B_{x,z}}{\partial z}\right|_{x=z=0} z + \frac{1}{2!}\left.\frac{\partial^2 B_{x,z}}{\partial^2 x}\right|_{x=z=0} x^2 + \cdots, \qquad (2)$$

By combining Eq. 1 and Eq. 2, the multipolar field components a_n and b_n of order n-1 can be simply expressed as:

$$a_n = \frac{1}{(B_0\rho)n!}\left.\frac{\partial^n B_x}{\partial z^n}\right|_{x=z=0} \quad \text{and} \quad b_n = \frac{1}{(B_0\rho)n!}\left.\frac{\partial^n B_z}{\partial x^n}\right|_{x=z=0}. \qquad (3)$$

The effect of the electromagnetic fields over the charged particles depends on the type of magnet field represented by its multipole coefficient. There are three main types of magnets used in particle accelerators:

- The *dipole* magnets, used to bend the trajectory of the particles and then producing the circular trajectory of a storage ring. They are also intense sources of synchrotron radiation whose users can benefit from.

- The *quadrupole* magnets, used to focus the trajectory of the particles deviating from the reference trajectory. A magnetic quadrupole is called *focusing quadrupole* when it focuses the beam in the horizontal plane (and then defocuses the beam in vertical plane according to the Maxwell's equations).
- The *sextupole* magnets, whose primarily purpose is to correct chromatic aberrations (the *natural chromaticities*) resulting from the energy dependency focusing introduced by the quadrupoles (and dipole edges).
- Higher multipolar field components are often modeling magnetic errors consequences of the alignment, mechanical, assembly errors (manufacturing process). Octupole magnets are more and more employed and used together with the sextupoles to compensate for the *Resonance Driving Terms* (RDTs) introduced by the multipoles (n>2). The RDTs are related to strong resonance components excited by nonlinear magnetic fields. These resonance components must be minimized as much as possible during the lattice optimization and the machine operation to preserve a good performance (Bengtsson, 1997).

The gradient of the dipoles, quadrupoles and sextupoles are shown in Table 1.

Magnet Types	Orders n	Fields	Normalized Gradient Strengths
Dipole	0	$B_x = 0$ $B_z = B$	$b_0 = \frac{B}{(B_0\rho)} = \frac{1}{\rho}$
Quadrupole	1	$B_x = b_1 z$ $B_z = b_1 x$	$b_1 = \frac{1}{(B_0\rho)}\frac{dB_z}{dx}$
Sextupole	2	$B_x = b_2 xz$ $B_y = \frac{b_2}{2}(x^2 - z^2)$	$b_2 = \frac{1}{2(B_0\rho)}\frac{\partial^2 B_z}{\partial^2 x}$

Table 1: Definitions of magnetic field and normalized gradient strength of an ideal dipole, quadrupole and sextupole magnet. x and z are the horizontal and vertical coordinates in the Cartesian space, respectively, B_x and B_z are the magnetic field produced by the magnets in the horizontal and vertical planes respectively, $(B_0\rho)$ is the magnetic rigidity, n is the order of the multipole coefficient and b_0, b_1 and b_2 are the normalized gradient strength of dipole, quadrupole and sextupole, respectively.

1.1. TRANSVERSE MOTION: TRANSVERSE LINEAR AND NONLINEAR BEAM DYNAMICS

Following the description of the transverse motion presented by H. Wiedemann (Wiedemann, 2007), the movement of a charged particle in an accelerator under electromagnetic fields is given by the Lorentz equation:

$$\vec{F} = \frac{d\vec{p}}{dt} = e\left(\vec{E} + \vec{v} \wedge \vec{B}\right), \tag{4}$$

where $\vec{F}$ is the force applied over the charged particle, $\vec{p}$ is the particle momentum, e is the particle charge, $\vec{v}$ is the particle velocity, $\vec{E}$ is the electric field, and $\vec{B}$ is the magnetic field. In a synchrotron radiation facility, the magnetic field is used to maintain the

particles as close as possible to the reference trajectory and the longitudinal electric field is used to restore the energy lost by the particle traveling along the ring.

The equations of motion of the linear beam dynamics of a circular accelerator come from substituting the magnetic field produced by a dipole and a quadrupole expressed in Table 1 in Eq. 4. They are called the *Hill's equations* (Hill, 1884) (similar to a harmonic oscillator with a periodic s-dependent coefficient K(s)):

$$x'' + \left(b_0^2(s) - b_1(s)\right)x = 0, \tag{5}$$

$$z'' - b_1(s)\,z = 0. \tag{6}$$

Equations 5 and 6 describe a pseudo-harmonic oscillator with a constant $\mathrm{K_x(s)} = \left(\mathrm{b_0^2(s) - b_1(s)}\right)$ in the horizontal plane and $\mathrm{K_z(s) = b_1(s)}$ in the vertical one. These equations are solved applying the periodic conditions of the circular accelerators (as storage rings of synchrotrons light sources) $\mathrm{K_{x,z}(s) = K_{x,z}(s + L)}$ considering L the circumference of the ring. For instance, in the horizontal plane, the motion $\mathrm{x(s)}$ of a particle in a circular accelerator is given by:

$$x(s) = \sqrt{\varepsilon_x \beta_x(s)} \cdot cos\big(\psi_x(s) + \psi_{0,x}\big), \tag{7}$$

where:

- The constant ε_x is the *horizontal emittance*. It is a motion invariant (Liouville Theorem (Liouville, 1838)) that describes an ellipse in the phase space (x,x') following the equation expressed with the *Twiss's parameters*:

$$\varepsilon_x = \gamma_x(s)x^2 + 2\alpha_x(s)xx' + \beta_x(s)x'^2. \tag{8}$$

- The function $\beta_x(s)$ is the L-periodic *horizontal betatron amplitude function* and the two other Twiss parameters are given by:

$$\alpha_x(s) = -\frac{1}{2}\frac{d\beta_x(s)}{ds}, \tag{9}$$

$$\gamma_x(s) = \frac{1 + \alpha_x^2(s)}{\beta_x(s)}. \tag{10}$$

- The phase parameter $\psi_x(s)$ is called the *betatron phase* of the betatron motion and $\psi_{0,x}$ is the initial betatron phase. They depend on the focusing via the beta-function and are defined as:

$$\psi_x(s) = \int_0^s \frac{d\bar{s}}{\beta_x(\bar{s})}. \tag{11}$$

Another important concept resulting of Eq. 11 is the *betatron tune*, defined as the number of transverse oscillations performed by a particle during one revolution along the ring:

$$\nu_x(s) = \frac{1}{2\pi}\oint \frac{d\bar{s}}{\beta_x(\bar{s})}. \tag{12}$$

The equations of motion of a charged particle with an energy offset δ are given by Eq. 13:

$$x'' + K_x(s)x = \frac{\delta}{\rho(s)}. \tag{13}$$

The solution of this inhomogeneous differential equation is written as:

$$x(s) = \sqrt{\varepsilon_x \beta_x(s)}\, cos\big(\psi_x(s) + \psi_{0,x}\big) + \eta_x(s)\, \delta, \tag{14}$$

where the L-periodic function $\eta_x(s)$ is called the *horizontal dispersion function*. The dispersion function can also be defined as the orbit trajectory of a particle with an off-momentum energy $\delta = 1$. In vertical plane, the dispersion is very often negligible for light sources.

The dependence of the quadrupole strengths $K_{x,z}(s)$ with the off-momentum energy produces chromatic aberrations called *chromaticities* in both planes. In other words, there is a dependency between the tunes and the relative energy offset δ. The natural horizontal and vertical chromaticities are large negative numbers for strong focusing lattices and are expressed in function of the focusing introduced by the dipoles and quadrupoles of the linear lattice:

$$\xi_x^{nat} = -\frac{1}{4\pi}\oint K_x(s)\beta_x(s)ds, \tag{15}$$

$$\xi_z^{nat} = \frac{1}{4\pi}\oint K_z(s)\beta_z(s)ds. \tag{16}$$

The sextupole magnets are introduced in the magnetic lattices to correct these natural chromatic aberrations compensating Eq. 15 and Eq. 16 following the next equations:

$$\xi_x = \frac{1}{4\pi}\oint b_2(s)\beta_x(s)\eta_x(s)ds, \tag{17}$$

$$\xi_z = -\frac{1}{4\pi}\oint b_2(s)\beta_z(s)\eta_x(s)ds. \tag{18}$$

Their effect (strength b_2) is maximized when introduced at locations with a large horizontal dispersion (η_x) and large betatron functions ($\beta_{x,z}(s)$). In order to correct to zero or to slightly positive values the transverse chromaticities, a minimum of two families of sextupoles is necessary. Sextupoles located at non-zero horizontal dispersion are called *chromatic sextupoles*.

Sextupoles are intrinsically nonlinear magnets and will excite many *resonance lines* defined as linear integer combinations of the transverse tunes with the revolution frequency normalized to the unity:

$$pv_x + qv_z = rN, \tag{19}$$

where p, q and r are integers and relatively prime numbers and N is the periodicity of the lattice. The *resonance order* is defined as the positive number $|p| + |q|$.

To first order, the tune shift with amplitude can be defined as:

$$v_x(x, z, \delta) = a_{xx}x + a_{xz}z + \xi_x\delta + O(2), \tag{20}$$

where the coefficients a_{xx} and a_{xz} depend on the setting of the sextupoles (to a first approximation) and ξ_x is the total horizontal chromaticity. A similar formula is obtained in the vertical plane. To get a stable motion, the transverse tunes should be far away from any resonance condition.

The *dynamic aperture* (DA) is defined as the area of 2-dimensional surface defining the maximum transverse amplitudes where the particle motion is bounded, whence stable. The task of maximizing the DA, which is necessary for off-axis injection, is very delicate and complex. It required to minimize the so-called *Resonance Driving Terms (CDTs)*, *tune shifts with the transverse amplitude*, which are excited by all the nonlinear elements of the lattice.

Parameters	Values
Energy E (GeV)	2.739
Lorentz Factor γ	5382
Circumference C (m)	354.097
Magnetic Rigidity $(B_0\rho)$ (T·m)	9.14
Momentum Compaction Factors α/α_2	$4.2\ 10^{-4}/4.5\ 10^{-3}$
Horizontal Emittance ε_x (nm·rad)	$3.87\ 10^{-9}$
Horizontal / Vertical Betatron Tunes (ν_x/ν_z)	18.155/10.228
Synchrotron Tune (ν_s)	0.005
Horizontal / Vertical Natural Chromaticity (ξ_x^{nat}/ξ_z^{nat})	-48/-21
Horizontal / Vertical Corrected Chromaticity (ξ_x/ξ_z)	1.2/2.0
Radiation Loss per Turn (keV)	931.175
RF-Frequency (MHz)	352.2
RF-Voltage (MV)	2.665
Harmonic Number	416
Relative Energy Spread	$1.014\ 10^{-3}$
Synchronous Phase (rad)	2.815
Horizontal / Vertical Betatron Functions* (m)	11.539/7.924
Horizontal / Vertical Dispersion Functions* (m)	0.220/0
Sextupole Length (m)	0.16
Maximum sextupole Strength (T·m^{-2})	320

Table 2: Physical parameters of the SOLEIL current storage ring lattice of 2013 (obtained from Accelerator Toolbox). *All Twiss parameters are computed in the middle of the long straight section (injection location).

Table 2 shows the parameters of the SOLEIL nominal storage ring of 2013 used in this thesis. The parameters listed will be assumed for all beam-based measurements and used for the calculations if not mentioned differently.

1.2. LONGITUDINAL MOTION

The longitudinal equation of the motion is driven as a first approximation by the evolution of the energy offset and the longitudinal phase ϕ with respect to a reference particle called *synchronous particle*. All other effects such as damping or quantic excitation due to the synchrotron radiation are neglected.

A particle with an energy offset δ will have a difference of revolution frequency which can be expressed as $\frac{\Delta f}{f_{rev}} = -\eta(\delta)$, where $\eta(\delta)$ is the *phase slippage factor* and f_{rev} the revolution frequency. As a linear approximation, it can be expressed as a function the *linear momentum compaction factor* α, the relative change of the path length as function of the energy offset δ, as $\eta = \alpha - 1/\gamma^2$, with γ, the Lorentz factor. For a storage ring like SOLEIL, α is four orders of magnitude larger than the factor $1/\gamma^2$ and the slippage factor can be approximated by the momentum compaction factor (see Table 2).

In the longitudinal phase space (ϕ, δ), the equation of the motion for the longitudinal coordinate z is defined by:

$$\dot{\phi} = -\alpha\delta, \tag{21}$$

The radio frequency (RF) cavities introduce a longitudinal focusing and will ensure that particles with a given energy offset will always see the adequate RF-voltage. The RF-voltage is pulsed and given by:

$$V(t) = V_{RF}\sin(\omega_{RF}t + \phi_s), \tag{22}$$

where ϕ_s is the *synchronous phase*, V_{RF} is the peak *RF-voltage* and ω_{RF} the *RF-angular frequency* defined by $\omega_{RF} = 2\pi f_{RF} = 2\pi h f_{rev} = h\omega_{rev}$; h is the *harmonic number*, f_{rev} is the *revolution frequency* that depends on the ratio between the ring circumference and the revolution period around the ring and finally, t is the time.

The energy of a particle varies with time as:

$$\dot{\delta}(t) = \frac{\omega_{rev} h e V_{RF}}{2\pi E_0}(\sin(\phi) - \sin(\phi_s)), \tag{23}$$

where e is the charge of the particle and E_0 the energy of the synchronous particle.

By combining Eq. 21 and Eq. 23, one gets the equation of the motion for the relative phase variation with time:

$$\Delta\ddot{\phi}(t) = -\frac{\omega_{rev}^2 \alpha h e V_{RF}}{2\pi E_0}(\sin(\phi) - \sin(\phi_s)). \quad (24)$$

After linearization around the synchrotron phase ϕ_s, the longitudinal equation of the motion becomes:

$$\Delta\ddot{\phi}(t) = -\frac{\omega_{rev}^2 \alpha h e V_{RF} \cos(\phi_s)}{2\pi E_0}\Delta\phi = -\omega_s^2 \Delta\phi. \quad (25)$$

The *synchrotron tune* is defined as $\nu_s = \omega_s/\omega_{rev}$.

The RF-*energy aperture* (ε_{acc}^{RF}) can be defined as the maximum off-momentum energy that one particle can accept in longitudinal phase space, which is defined by the longitudinal RF-bucket height. In a first approximation, this can be expressed as:

$$\varepsilon_{acc}^{RF} = \pm\sqrt{\frac{2eV_{RF}\,|\sin\phi_s|}{\pi|\alpha|hE_0}\left(\sqrt{q^2-1} - \cos^{-1}\left(\frac{1}{q}\right)\right)}, \quad (26)$$

where h is the harmonic number, E_0 is the nominal energy, $q = eV_{RF}/U_0$ the *overvoltage factor*, U_0 is the *radiation loss per turn* and α is the linear momentum compaction factor. For SOLEIL, this expression is not true anymore as soon as the energy offset exceeds 2 % (Nadji, 1998). The second order of the momentum compaction factor α_2 needs to be taken into account as its value is almost 10 times larger than the first order one (Table 2).

The *electron beam lifetime* is another important figure of merit to optimize. As it will be explained in the Chapter II, its value depends on the *momentum aperture (*or *energy acceptance)* of the storage ring that is limited by the most constraining factor between the three following contributions:

1. The RF-energy acceptance.
2. The physical acceptance along the ring.
3. The transverse beam dynamics along the ring.

1.3. FIGURES OF MERIT

During this work, the two main figures of merit for a given linear lattice are the electron beam lifetime and the injection efficiency.

Large values of injection efficiency and Touschek lifetimes are necessary to ensure a good operation reducing the beam losses and increase the stability of the beam inside the machine. The strong focusing magnets used in the third generation light sources to ensure high brilliance and small horizontal emittance results in large natural chromaticities. The sextupoles are used to correct these natural chromaticities but in turns introduce nonlinearities that reduce a lot the dynamic and momentum apertures (also called on- and off-momentum acceptances respectively) and consequently the injection efficiency and the beam lifetime.

2. SINGLE BEAM DYNAMIC OPTIMIZATION BASED ON GENETIC ALGORITHMS CODES

2.1. GENERAL SCOPE

As stated earlier, the optimization of the nonlinear dynamics is a challenging problem for accelerator physicists who need to constrain the *working point* of a lattice (defined as the linear betatron tunes) in a maze of resonances from low to high orders where nonlinearities and even chaos are hidden in every corner (Wolski, 2014). The last generation of light sources is built on strong focusing lattices resulting in very large natural chromaticities needed to be compensated using large sextupolar strengths. In turn, the sextupole magnets are the main sources of nonlinearities. Today a modern light source is composed of hundreds of different elements that produce thousands of physical and technical parameters connected to each other. Taking the example of the Synchrotron SOLEIL, there are eleven families of sextupoles (122 individual magnets). On some facilities, sextupoles are even powered individually to increase the correction flexibility. The choice of the setting of their strengths will pilot the performance of an accelerator. Optimizing the dynamic aperture for injection or for lifetime for instance may lead to contrary optimal solutions. Per essence, an accelerator physicist faces a multi-objective problem composed by different objectives. The situation can be even worse since the way the linear optics is optimized (emittance, locations of sextupoles, beta-function, dispersion function, and so on) has a direct impact on the way and even the success or the failure of finding a viable nonlinear setting for a given accelerator. This aspect will not be discussed in detail from now on.

In mathematics, a classical approach to solve these kinds of multi-objective nonlinear problems has been to reduce or simplify the original problem in a scalar single-objective problem assigning a weight to each objective function. Finding the weights that optimize the scalar single-objective partially solves the optimization problem. Then, the values of the objective functions are compared to evaluate if the choice of the scalar objective function is good or not to respect to the real-life problem. In addition, the quality of this method completely depends on the way to find the weights and this choice is difficult even for experimented users.

A particular method has been highlighted in the last forty years for its robustness, efficiency, and capacity to solve multi-objective real-life problems with objectives in conflict with each other: the *Genetic Algorithms* (GAs). Genetic algorithms (Konak, 2006) are a heuristic search that mimics the process of natural selection and generates solutions to solve highly complex optimization problems using techniques inspired by natural evolution. GAs belong to the larger class of Evolutionary Algorithms (EA) (see for instance Ref. (Rudenko, 2004)) based on a big list of stochastic optimization algorithms based in the Darwinian concept of evolution. According to the Darwinian concept of evolution only the stronger and adaptable individuals survive and give their characteristics to their offspring that have, at the same time, more probabilities to survive. This concept was firstly introduced by Holland and his colleagues in the 1960s and 1970s (Holland, 1975) and has been developed until today creating a large list of algorithms with different features and characteristics.

Before to go through the method implemented into the genetic algorithms, a general definition of what the multi-objective problems are is presented below.

2.2. MULTI-OBJECTIVE PROBLEMS

The multi-objective problems are generally defined as minimizing a set of objective functions under constraints for a given range of parameters. It can be stated as (Konak, 2006):

minimize/maximize	$f_m(\vec{u})$	m = 1,…,M	(27)
subject to	$g_j(\vec{u}) \geq 0,$	j = 1,…,J	(28)
	$-\infty \leq u_L \leq u_i \leq u_U \leq \infty,$	i = 0,…,N	(29)

where $f_m(\vec{u})$ are the M-optimization objectives subject to J-constraints $g_j(\vec{u})$ depending of the N-vector $\vec{u} = (u_1, \ldots, u_N)$ containing the list of variables. This vector of variables defines the N-dimensional decision variable space that is mapped to the M-dimensional objective space as a function: $\mathbb{R}^N \rightarrow \mathbb{R}^M$.

Figure 2 shows an example of a multi-objective problem defined by two objectives $f_1(u_1, u_2)$ and $f_2(u_1, u_2)$ subject to the 2-vector variable $\vec{u} = (u_1, u_2)$. The particular solutions $f_1(\vec{u})$ and $f_2(\vec{u})$ of the objective space are defined by the set of variables $\vec{u}_1$ and $\vec{u}_2$ in the decision space. The dashed red line that defines the limit of the multi-objective problem in the objective space depends on the constraints.

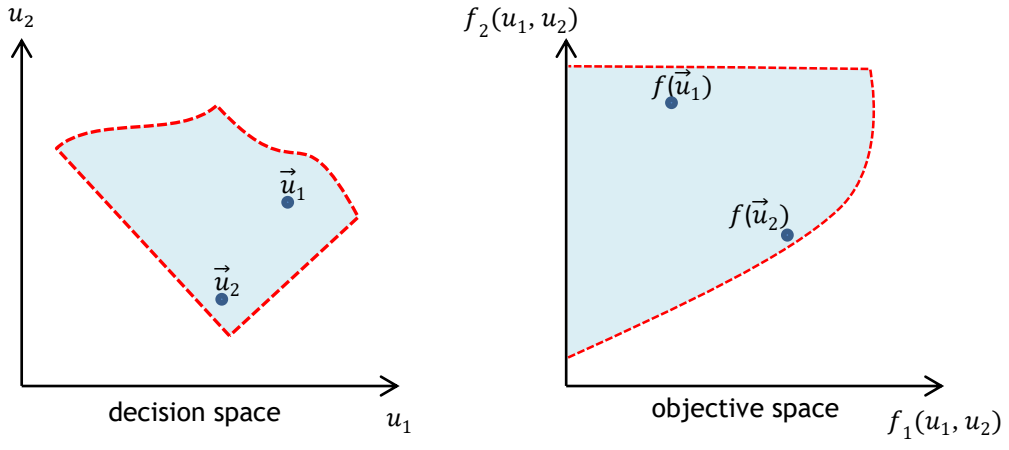

Figure 2: Relation between the decision space and the objective space limited under constraints of a multi-objective problem defined by the objectives $f_1(u_1, u_2)$ and $f_2(u_1, u_2)$ subject to the vector variable $\vec{u} = (u_1, u_2)$ defined by the variables u_1 and u_2. The particular solutions $f_1(\vec{u})$ and $f_2(\vec{u})$ of the objective space are defined by the set of variables $\vec{u_1}$ and $\vec{u_2}$ in the decision space. The constraints define the limits of the objective problem (dashed red line).

The aim of the process is to be as close as possible to the so-called *Pareto-optimal front* and to ensure its diversity (Konak, 2006). The Pareto-optimal front is the group formed by the individuals $(\vec{u})$ with the best compromise between the objectives. This Pareto-optimal set is unique for each optimization problem. The objective of the multi-objective problem is to converge to the Pareto-optimal set enlarging the "spectra of the whole problem" as much as possible. The objective problems have limits or extrema where one of the objectives is maximal (or minimal). Taking into account the more extreme of these limits ensures to enlarge the quantity of solutions present in the Pareto optimal set. Hence, the multi-objective space is divided in two regions: the region with the best solutions located in the Pareto front and the region that contains all the other solutions. The way to classify and choose individuals to reach the Pareto optimal set is different depending on the used genetic algorithm.

2.3. OVERVIEW OF GENETIC ALGORITHMS

Following the Darwinian concept of the natural evolution introduced before, genetic algorithms encode the real-life multi-objective problems linking the natural concepts to concepts that belong to the multi-objective problems. Then, in order to establish an understandable terminology, firstly some definitions of concepts and techniques commonly used in the GA environment are introduced:

- *Gene*: Independent variables involved in the optimization problem.
- *Chromosome*: Individuals formed by variables.
- *Population*: Set of individuals.
- *Crossover*: Operator in which two individuals, called *parents*, are combined to create other individuals, called *offspring*.
- *Mutation*: Operator applied on chromosomes in which a random change is introduced in the individuals to produce other individuals.
- *Fitness function*: Function assigned to the individual to measure how well the individual meets the optimization objectives.
- *Selection*: Operator to assign a fitness function based on the values of the individuals in the objective space to select viable individuals of a given population.
- *Generation*: Sequence of individuals of a given iteration.
- *Feasible*: List of individuals that belong to the optimization problem under the optimization constraints.

Figure 3 depicts the general scheme common in most of the genetic algorithms. The algorithm starts the optimization process creating a random population from an individual, generally called starting point. Thereafter, the algorithm generates an offspring population, the so-called *children's pool* applying the crossover operator combining the individuals between them. After that, the mutation operator acts on all individuals to produce new individuals. Then, the algorithm selects the individuals that have a better rating in terms of fitness functions based on their values of the objective functions. Finally, if the stopping criterion is reached, that is, if the Pareto-optimal set is found, the

process stops. If not, the process is iterative and runs until the maximum number of individuals has been produced or a good fitness level has been reached for the population.

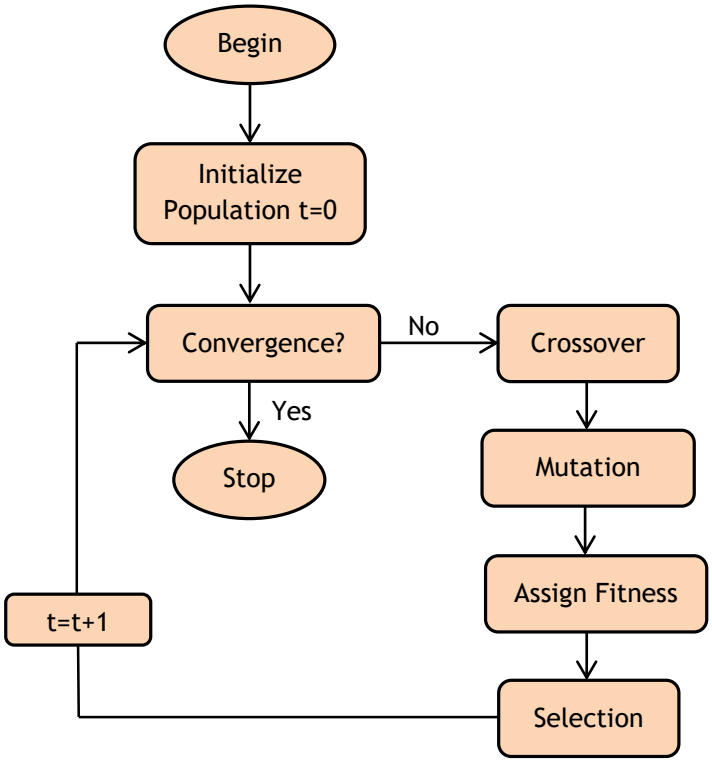

Figure 3: General diagram of genetic algorithm performance. Starting from an initial random population, if the convergence criterion is not reached, the algorithm generates an offspring population combining the individuals to each other with the operator crossover. Subsequently, the offspring population is randomly modified changing their variables, that is, applying the mutation operator. Then the algorithm selects the individuals with better objective functions to be the parents of the next generation. At the end, if the stopping criterion is reached the process stops. If not, the process runs until the maximum number of individuals has been produced or a good fitness level has been reached for the population.

The way used by the genetic algorithms to reach the Pareto-optimal set in this kind of multi-objective problem is based on two important concepts:

1. The non-domination concept, according to which the particular solution $f_m(\vec{u}_1)$ dominates the solution $f_m(\vec{u}_2)$ if:

   i. $f_m(\vec{u}_1)$ is not worse than $f_m(\vec{u}_2)$ in all objectives.
   ii. $f_m(\vec{u}_1)$ is strictly better than $f_m(\vec{u}_2)$ in at least one objective.

   In the specialized literature, the dominance of the solutions $f_m(\vec{u}_1)$ over the solution $f_m(\vec{u}_2)$ is written as $f_m(\vec{u}_1) \prec f_m(\vec{u}_2)$. For more details see the Ref. (Deb, 2001).

Then the algorithm assigns one value to rank all the solutions and classify them. Usually, this ranking process starts with 1 for the Pareto solutions and increases for the rest of solutions (called Pareto front of rank 1, 2, 3…).

2. An operator called *sharing parameter* is applied to ensure the diversity of the population and obtain solutions uniformly distributed along the Pareto front. This operator depends on the type of GA used (Konak, 2006) and tries to avoid pitfalls like being trapped in a local minimum in the objective space.

There are different methods to classify the different types of genetic algorithms created until now. The majority of the specialized literature classifies the algorithms based on the way to distinguish the Pareto-optimal set among the other solutions or depending on the method used to ensure the diversity of the population of the same Pareto-optimal set. But recently new types of genetic algorithms have appeared; they are based on the way to explore the objective space in a privileged direction: the Multi-Objective Particle Swarm Optimizers (MOPSO) (Reyes-Sierra, 2006). Following this new approach, the search space is not based on individual parameters; it is based along conjugate directions from the local minima. Conjugate direction means taking into account vectors defined in a particular topology around the minima. The search process follows the direction formed by these vectors to search for new solutions in the objective space.

2.4. History and Genesis of Genetic Algorithms in the Accelerator Community

The application of the Genetic Algorithms in particle accelerators did really take off since the early 2000 (see Ref. (Hofler, 2013) for a review). After the success of the optimization of magnets and radio frequency cavities performances at the beginning of the decade of nineties (Hajima, 1992), the optimization of linacs (Schirmer, 1996), superconducting magnets (Russenschuck, 1998), and beamline aspects (Bacci, 2007) has been become important for the accelerator community. The study of new ring-based designs have also used the genetic algorithms during the last 10 years: examples of that are the design of the International Linear Collider (Bazarov, 2005) and the pioneer work of M. Borland at the Advance Photon Sources in Argonne (Emery, 2005) for the first application on a light source. This type of optimization is based on brute force optimization and required large Central Processing Units (CPU) farms, which used to be very expensive. The huge progress in microelectronics and the reduction of the cost of a CPU or Graphical Processing Unit (GPU) farms make this technique very attractive for the storage ring community. Since then many works have been carried out in the accelerator facility across the world.

The benefit of GAs was for a long time not so appealing since brute force method seems very difficult to replace intelligence and experience of a lattice designer. Very few real improvements of machine performance have been reported until recently. The reasons are diverse. For many existing machines that were commissioned 10 to 20 years ago, often the model is not accurate enough to reproduce the daily performance. Nevertheless it is fair to report some positive results: improvement of APS operational lattice lifetime by 25 % without reduction of injection efficiency (Borland, 2010a) and improvement of Diamond lifetime as well searching new low-emittance lattice configurations (Singh, 2013).

With recent roadmap for ultra-low horizontal emittance rings, the situation has deeply changed (Borland, 2014). Almost every facility is now including GA in its nominal toolbox for optimizing a lattice for both linear and nonlinear beam dynamics. New and faster convergence algorithm begins to be evaluated also across the laboratories, more adapted to on-line optimization.

To cite a few applications:

- New ultra-low emittance rings to upgrade the actual third generation of synchrotron light sources around the world like Advanced Photon Source (Borland, 2009), European Synchrotron Radiation Facility (Carmignani, 2014a, 2014b), Advanced Light Source (Sun, 2012), SPEAR3-SLAC National Accelerator Laboratory (Tian, 2014), Brookhaven National Laboratory (Yang, 2011), Swiss Light Source (Ehrlichman, 2015, 2016) or Diamond Light Source (Bartolini, 2013; Walker, 2014). Synchrotron SOLEIL is also using the genetic algorithms to upgrade his storage ring. This thesis is the first step of the application of this computational tool at SOLEIL.
- Recently, new types of genetic algorithms have been tested for online optimization using beam-based experiments. The Robust Conjugate Direction Search (RDCS) is a genetic algorithm based in MOPSO that has been applied in SPEAR3 to reduce the vertical emittance for coupling correction and to optimize the transport line optics (Huang, 2013) and to increase the dynamic aperture by 3.5 mm (Huang, 2015). In ESRF the single bunch current was increased from 4 mA to 8 mA for the same value of beam lifetime (Carmignani, 2015). RDCS has demonstrated to be more robust and efficient than the "classical" GA due to its capacity to work with noise and bugs coming from the knobs of the control rooms of light sources and to converge to the desired parameters only in a few generations. The results are very promising.

Even if GAs seem to open new windows of optimization to benefit from the full potentiality of a given lattice, the method is complementary to existing analytical a semi-empirical methods such as minimization of Resonance Driving Terms (Bengsston, 1997), tune shift with amplitudes (Streun, 1999) or Frequency Map Analysis (FMA) (Laskar, 1990 and 1995; Nadolski, 2001 and 2003; Robin, 2000).

As explained in the introduction, the main purpose of this thesis is to explore the potentiality of the use of GAs for SOLEIL (Gavaldà, 2014); the multi-objective problem treated is the maximization of both the on- and off-momentum apertures that are strongly related to the injection efficiency and the Touschek lifetime respectively. New configurations of the current lattice of Synchrotron SOLEIL (3.9 nm·rad) should increase the on- and off-momentum apertures under a set of constraints: maintaining the same magnetic lattice configuration as the present, in terms of location of the magnets, and their maximum strengths and polarities.

It was decided from day one to start with the code MOGA-ELEGANT developed at APS (Borland, 2009), to evaluate its strengths and weakness and propose new figures of merits and new algorithms. Mostly the first part was explored during this work.

Using formalism shown in Eq. 27, Eq. 28 and Eq. 29, the multi-objective problem studied in this thesis can be written as:

$$\text{maximize} \quad [DA(\vec{u}), MA(\vec{u})], \tag{30}$$

$$\text{constrains:} \quad g_j(\vec{u}) \geq 0, \qquad j = 1,\ldots,J \tag{31}$$

$$-K_L \leq K_i \leq K_U, \qquad i = 1,\ldots,11 \tag{32}$$

$$-S_L \leq S_i \leq S_U, \qquad i = 1,\ldots,11 \tag{33}$$

where the DA and the MA are the dynamic and momentum apertures, that is, the optimization objectives as it is said before, $g_j(\vec{u})$ is the list of constraints that restrict the objectives, namely the strengths K_i and S_i of the quadrupoles and sextupoles of the storage ring restricted to certain lower (L) and upper (U) limits.

3. COMPUTATION ARCHITECTURE AND ENVIRONMENT AT SOLEIL

The code MOGA-ELEGANT uses a computer grid or a computer cluster; each CPU can work and perform independently different tasks to reach one goal. This architecture is typical in high performance computing systems as the SOLEIL cluster used in this thesis.

This section is dedicated to describe globally the architecture of MOGA-ELEGANT (software) and the computational structure (hardware) of the SOLEIL cluster used to run the algorithm.

3.1. COMPUTATIONAL ARCHITECTURE OF MOGA-ELEGANT

The software used to optimize the linear and nonlinear beam dynamics of SOLEIL is composed of the following elements:

1. The algorithm called MOGA-ELEGANT and a group of scripts written in the language Tcl-Tk to perform the optimization process required.
2. The tracking code ELEGANT to compute with tracking the dynamic and momentum apertures of the storage ring.
3. The SDDS-Toolkit to manage and process the input and output files.
4. The computational resource manager SLURM to control and manage the computation process in the SOLEIL cluster.

A detailed explanation of each component is given below.

3.1.1. THE MOGA-ELEGANT CODE

The type of GAs used in Synchrotron SOLEIL is called Multi-Objective Genetic Algorithm (MOGA) (Borland, 2009). It was created at APS ten years ago and it has been used in many light sources to optimize important parameters of the synchrotron light source as is seen in the last section.

MOGA-ELEGANT is based on the *Non-dominated Sorting Genetic Algorithm II* (NSGA-II) (Deb, 2002). NSGA-II classifies the individuals of a population using an *elitist type* of the non-dominated concept and keeping the diversity of each Pareto-optimal front using a sharing process called *crowding-distance* before to apply the classic operators of reproduction, crossover, and mutation in order to create a new generation of individuals.

Elitism means preserving and keeping always the best solutions found in the process of the next generation. The initial random character of the process does not ensure to keep the best solutions to the next generation of solutions. In NSGA-II, the population of individuals is classified in a list of fronts using the non-dominated concept assigning a number per front. The best solutions are usually enumerated by 1 and the rest of solutions are ranked each other with higher numbers. Then, the non-dominated individuals are identified from the dominated ones. This ranking process is shown in Figure 4, where a list of individuals of the objective space defined by the objective functions f_1 and f_2 is classified in different fronts called rank 1 (blue color), rank 2 (orange color) and rank 3 (green color). In a minimum multi-objective problem, the solutions that belong to the front with rank 1 dominate all the other solutions of rank 2 and rank 3.

Once the ranked fronts are formed and the Pareto front is identified, the algorithm maintains the diversity among the population members using the *crowding-distance* operator. Given an r-vector of solutions $\vec{s} = (s_1, \dots, s_r)$ of a certain ranked front, the crowding-distance of a given k-objective function $f_k(s_i)$ of the solution s_i between the extreme solutions s_1 and s_r is defined as (Deb, 2002):

$$cd_k(s_i) = \frac{f_k(s_{i-1}) - f_k(s_{i+1})}{f_k^{max} - f_k^{min}} \tag{34}$$

where $f_k(s_{i-1})$ is the value of the k-objective function of the solution s_{i-1}, $f_k(s_{i+1})$ is the value of the k-objective function of the solution s_{i+1}, $f_k^{max} = f_k(s_1)$ is the value of the k-objective function of the solution s_1 where the objective is maximum and $f_k^{min} = f_k(s_r)$ is the value of the k-objective function of the solution s_r where the objective is minimum (Figure 4). In other words, the crowding-distance is the perimeter of the cuboid formed between one solution and the nearest neighbors inside each solution front. Hence, the algorithm privileges the most isolated solutions, that is, penalizes the solutions concentrated in high-density population size.

Following the nomenclature followed by the specialized literature and using the crowed-comparison operator, NSGA-II classifies the solutions as follows (Deb, 2002):

$$f_m(\vec{u}_1) \prec f_m(\vec{u}_2) \quad \text{if} \quad \text{Rank}(f_m(\vec{u}_1)) < \text{Rank}(f_m(\vec{u}_2)) \tag{35}$$
$$\text{or} \quad \text{Rank}(f_m(\vec{u}_1)) = \text{Rank}(f_m(\vec{u}_2)) \tag{36}$$
$$\text{and} \quad \text{cd}(f_m(\vec{u}_1)) > \text{cd}(f_m(\vec{u}_2)) \tag{37}$$

Given two solutions, NSGA-II privileges the solution with less rank value. If this rank value is equal, that is the two solutions belong to the same front, the algorithm prefers the most isolated solution.

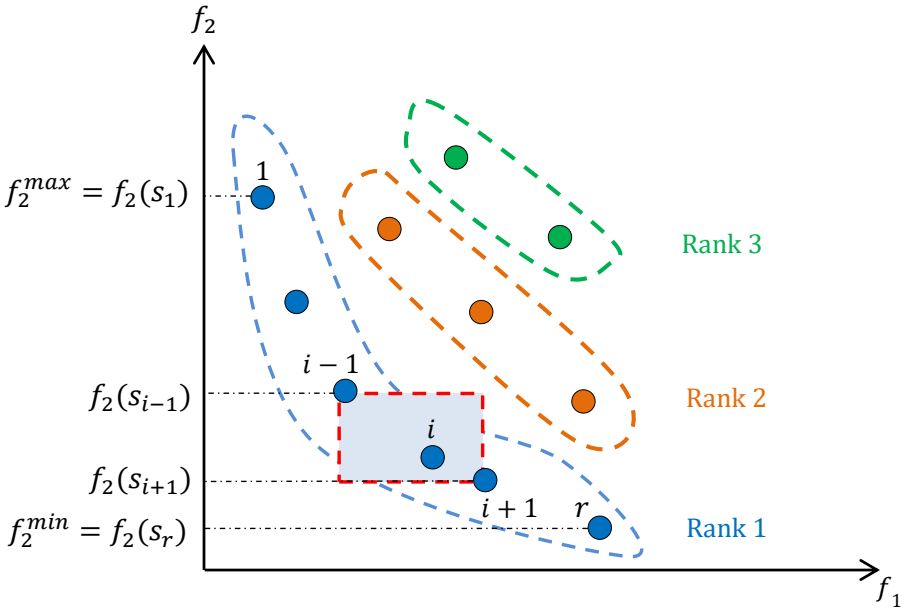

Figure 4: Scheme of the non-dominated ranking and the crowding-distance operator that characterizes the algorithm NSGA-II implemented in MOGA-ELEGANT. The solutions of the objective space defined by the objectives f_1 and f_2 are classified in fronts called rank 1 (blue dot), rank 2 (orange dot) and rank 3 (green dot). The Pareto-optimal set corresponds to the front with rank 1. In addition, NSGA-II takes into account the perimeter of the cuboid formed between each solution i and the nearest neighbors i+1 and i-1 inside each solution front. This perimeter (dashed red cuboid) is called crowding-distance and depends on the value of the k-objective function of the solution s_{i-1} ($f_1(s_{i-1})$) the value of the k-objective function of the solution s_{i+1} ($f_k(s_{i+1})$), the value of the k-objective function of the solution s_1 ($f_k^{max} = f_k(s_1)$), where the objective is maximum and the value of the k-objective function of the solution s_r where the objective is minimum ($f_k^{min} = f_k(s_r)$), defined in Eq. 34.

NSGA-II is an improved version of one of the first Multi-Objective Evolutionary Algorithms (MOEAs) called Non-Dominated Sorting Genetic Algorithm (NSGA) in the sense of the computational complexity and efficiency of the process (Deb, 2002). First of all, the computational effort is reduced by NSGA-II from the order $O(MN^3)$ of NSGA to the order $O(MN^2)$, where M is the number of optimization objectives and N is the population size. This means that with NSGA-II, it is possible to use larger population sizes to speed up the computation process. Secondly, the elitism introduced by NSGA-II also improves the speed of the process and ensures the presence of the best solutions in the breeding process of the next generation. Finally, NSGA-II defines a general rule to maintain the diversity of the population without depending on the sharing function previously defined for the user in NSGA.

There are other versions of NSGA-II improved during the last 5 years bearing in mind to reduce the computation effort to introduce a new ranking scheme that replaces the traditional ranking process shown at Eq. 35, Eq. 36 and Eq. 37 (D'Souza, 2010).

As an advantage, NSGA-II is robust, efficient and very well tested. It does not depend of human manipulations: all the process is automatized. However, it requires heavy

computations and it is very time consuming. It is necessary to run the code in a computation cluster.

3.1.2. ELEGANT AND SDDS-TOOLKIT

MOGA is based on ELEGANT as a simulation code and the SDDS-Toolkit as a protocol to control (pre and post-processing of data) and to manage the input and output files. "ELEctron Generation And Tracking" (ELEGANT) (Borland, 2000) is a multi-purpose accelerator simulation code created in APS in the decade of 1990s and used to model single- and multi-pass machines. Its capabilities are numerous, like lattice design, calculation of physical parameters (Twiss parameters, radiation integrals, matrices, orbit/trajectory, tunes and chromaticity correction, etc.) and including a 6D-tracking among others using symplectic formalism. The symplectic formalism is a powerful tool implemented in the majority of accelerator tracking codes that takes into account the area conservation to integrate the equation of particle motion over thousand and millions of turns. The dynamics of the particle is based on matrix formalism representing each magnet with an individual Hamiltonian; the Hamiltonian of the full ring is obtained concatenating the Hamiltonian of each individual element. ELEGANT is always in evolution incorporating new features like the on- and off-momentum acceptances and the Frequency Map Analysis (Laskar, 1990 and 1995; Nadolski, 2001 and 2003; Robin, 2000).

The Self Describing Data Set (SDDS) is at the same time a protocol for data storage, a toolkit of programs that transform files, and a set of function libraries (>90) working with these files. In particular, all pre- and post-processing, but also sorting, plotting, are performed by the SDDS-Toolkit (see Ref. (Borland, 2010b) for more details). The toolkit was inspired by UNIX, its power of pipes, command lines acting as filters on files. It assures quality control of the data by structuring the data in a container made of three parts: a dedicated header, a parameter page, and a structured page.

The ELEGANT version 25.1.0 and the SDDS-Toolkit were installed at SOLEIL cluster in March 2013. A considerable effort was done to install the packages and customize the different scripts that form the code MOGA-ELEGANT to the SOLEIL cluster: it was necessary to install new libraries to compile the scripts packages. This installation process depends on the operating system used and the version of software already installed in the cluster. As it explained later in more detail, the operating system in the SOLEIL cluster is GNU/Linux and the software implemented to submit and control the computation process is SLURM. Another version of ELEGANT, version 26.0.2 was installed later in November 2014 with new capabilities as it explained more precisely in Chapter II.

3.1.3. THE ALGORITHM: LIST OF SCRIPTS AND FILES

MOGA-ELEGANT is written using Tcl-Tk computer language and is structured in two parts: 1) the genetic algorithm NSGA-II implemented in the script `geneticOptimizer` and 2) the list of scripts that connects the code with the cluster, performs the tracking calculations and defines the optimization objectives with penalty functions. This list consists on the following filenames:

- The input.sdds file, where the variables of the starting point are defined.
- The `geneticOptimizer.local` script, responsible to send jobs to the cluster.
- The script `runJob1`, responsible to compute the tunes of the optimized solutions with `matchtemplate.ele` script, the on- and off-momentum acceptances using ELEGANT via the script `evalTemplate.ele` and post-process the optimized solutions via the script `processJob1`.

Table 3 shows the functions, the output files and the objectives of all the scripts implemented in the `geneticOptimizer` script. The main output files created in each part of the process to avoid errors and processing issues are also mentioned. All optimized solutions are identified with a run Identification (ID) number.

Figure 5 shows the scheme of the MOGA-ELEGANT architecture: the `geneticOptimizer` script launches the new solutions to be computed with the settings of the initial lattice defined in input.sdds. The file `geneticOptimizer.local` is facility dependent and defines the cluster language: this is SLURM for SOLEIL. ELEGANT computes the on- and off-momentum acceptances defined in `matchtemplate.ele` and `evalTemplate.ele` inside `runJob1`. After post-process the solutions with the script `processJob1`, the algorithm determines the Pareto-optimal set. The input and output files are treated by the SDDS-Toolkit. The process starts again with the information of the last solutions. At the end, a list of solutions is obtained by trade-off.

Scripts	Functions	Outputs	Output Functions	Observations
geneticOptimizer.local	Submit jobs to the cluster using SLURM management	runID.csh	Write the bash script to run with ELEGANT runJob1 into the cluster	
runJob1	Run ELEGANT to track the DA and MA and post-process solutions	runID.done	Confirm the process ending	
		runID.main-log	Write all the information of ELEGANT computations	
matchTemplate.ele	Linear matching to the target tunes	runID-linear.param	Write the parameters of lattice elements	Implemented inside runJob1
		runID-linear.fin	Write the final beam and transport parameters	
		runID-linear.twi	Write the Twiss parameters	
		runID-linear.done	Confirm the process ending	
		runID.log	Write all information of linear ELEGANT computation	
evalTemplate.ele	Fit the desired chromaticities and compute the DA and MA	runID.param	Write the parameters of lattice elements	Implemented inside runJob1
		runID.mag	Write the magnet structure	
		runID.w1	Write the phase space computation results	
		runID.aper	Write the DA calculation results	
		runID.mmap	Write the MA calculation results	
		runID.done0	Confirm the process ending	
processJob1	Post-process the solutions	runID.finc	Write the final beam and transport parameters	Implemented inside runJob1
		runID.naff	Write FFT computation results	
		runID.proc	Merge all information of runID computed before	
computeLifetime	Compute the Touschek lifetime using the Piwinski formula	runID.mmapxt	Write MA along the ring	Implemented inside processJob1
		runID.ltime	Write Touschek lifetime using the ELEGANT's subroutine touschekLifetime	
7geneticOptimizer	Define the first generation and create the next generation using selection, crossover and mutation with the algorithm NSGA-II	runID.inp	Write the runID and new variables of new generation to submit to the cluster	
		runID.all	Write information of all solutions	
		runID.sort	Write the ranking process of solutions done by NSGA-II	
		runID.best	Write information of Pareto's solutions	
		runID.children	Write information of breeding process	

Table 3: List of scripts, their functionalities, output files and objectives of the scripts implemented in MOGA-ELEGANT code.

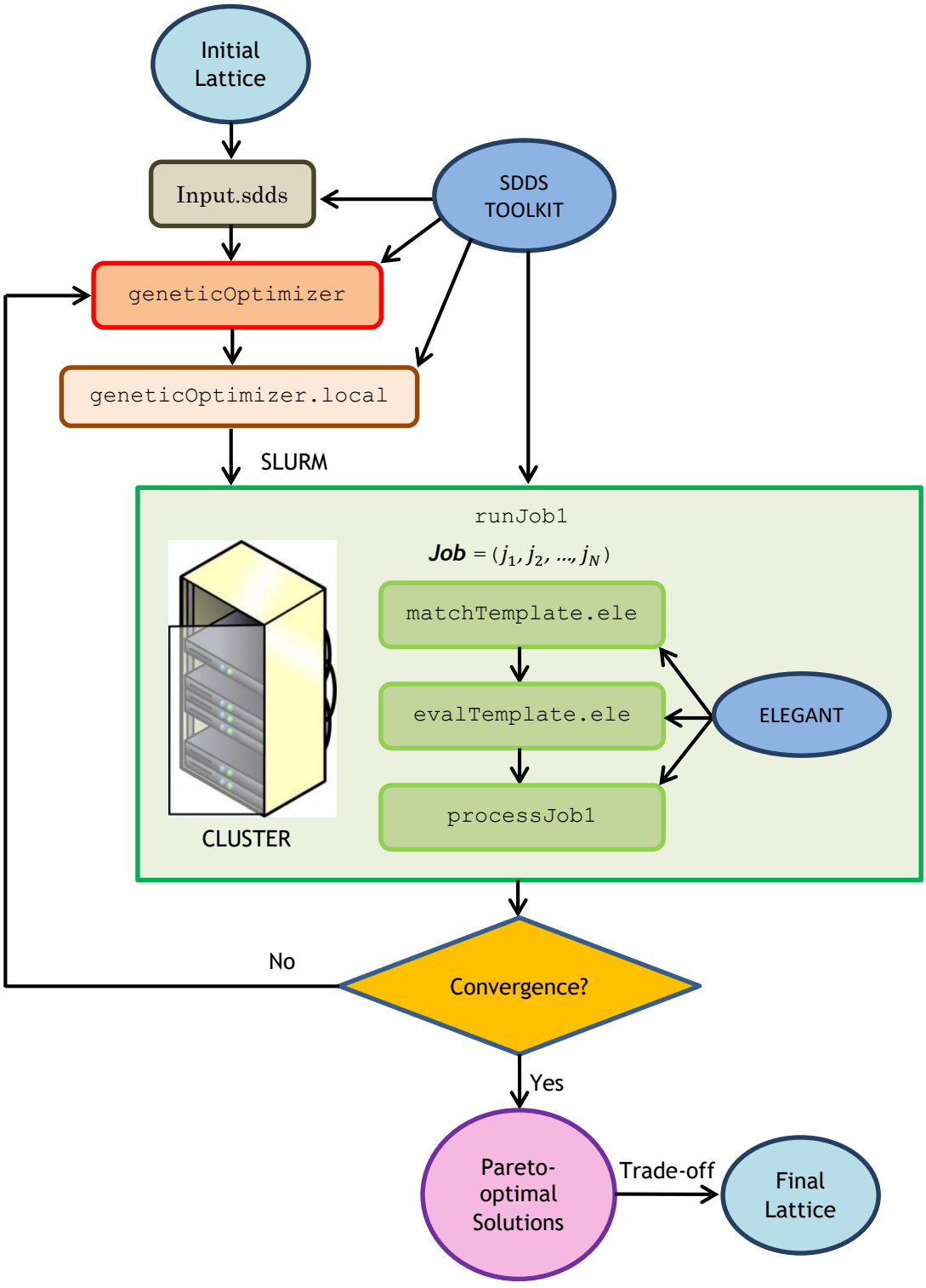

Figure 5: Scheme of the MOGA-ELEGANT architecture: the `geneticOptimizer` script launches to the cluster the new solutions with the new variables settings of the initial lattice defined in the input.sdds file via `geneticOptimizer.local`. ELEGANT computes the on- and off-momentum acceptances defined in `matchtemplate.ele` and `evalTemplate.ele`. After post-process the solutions with the script `processJob1`, the algorithm determines the Pareto-optimal set with new solutions. The process starts again with the information of the last solutions. At the end, a list of solutions is obtained.

3.1.3.1. Input File

The first file is the input.sdds file (Table 4). It defines the initial optimization variables, that is for this work, the sextupole strengths and the horizontal and vertical tunes of the optimization starting point. The input file is formed by the next list of columns:

- *parameterName*: the name of the parameters to optimize.
- *initialValue*: the initial values of each parameter.
- *errorLevel:* RMS of the Gaussian random errors to add to the parameters values as mutations. The *errorLevel* value is particularly important because it decides the size of searching the new solutions in the variable space.
- *lowerLimit:* the smallest allowable values of the parameters.
- *upperLimit:* the largest allowable values of the parameters.

Initial Values	Parameter Names	errorLevels	Lower Limits	Upper Limits
18.8125	S1	0.250	0.0	73.0
-40.8750	S2	0.250	-73.0	0.0
-21.1250	S3	0.250	-73.0	0.0
43.5625	S4	0.250	0.0	73.0
-44.6250	S5	0.250	-73.0	0.0
41.6875	S6	0.250	0.0	73.0
-62.0000	S7	0.250	-73.0	0.0
48.6250	S8	0.250	0.0	73.0
-52.7133	S9	0.250	-73.0	0.0
31.6465	S10	0.250	0.0	73.0
15.1250	S11	0.250	0.0	73.0
18.1566	nuxTarget	0.025	18.1	18.4
10.2285	nuyTarget	0.025	10.1	10.4

Table 4: Example of input.sdds file used in this thesis. The first column shows the settings of the sextupole families for the SOLEIL nominal lattice, the second column shows the variables taking into account during the optimization (11 families of sextupoles and the horizontal and vertical tunes), the third column shows the noise introduced into the algorithm to explore the variable space. The fourth and fifth columns show the limits of the optimization variables.

The variables optimized are the settings of the quadrupole and sextupole families. The limits of the SOLEIL sextupole families range are between 0 m^{-3} and ± 73 m^{-3} depending on the magnet polarity and using the convention of magnet strength K_n in ELEGANT (Borland, 2012):

$$K_{n-1} = \frac{1}{n}\frac{G_n}{(B\rho)L_n} \tag{38}$$

where the index n=1 corresponds to the dipole, n=2 to the quadrupole, n=3 to the sextupole and so on, G_n is magnet field, $(B_0\rho)$ is the rigidity and L_n is the length of the magnet. The maximum strength available for the sextupole magnets in SOLEIL is 320 $T{\cdot}m^{-2}$. For the simulations, the horizontal and vertical tunes range in [18.1, 18.4] in the

horizontal plane and [10.1, 10.4] for the vertical plane to avoid crossing the integer and half-integer resonance lines that completely destroy the performance of the storage ring lattice.

This input.sdds file contains as parameters the number of jobs, the number of parents and the number of children taking into account in the optimization process. The total number of nodes used is the product between parents and children. The total number of generations is the ratio between the total number of jobs and the number of nodes used during the optimization. These parameters are selected by the user and depend on the simulation and the available resources.

The input file is a SDDS file and can be edited with the functions of the SDDS-Toolkit, for example with *sddsmakedataset* (Borland, 2010b).

3.1.3.2. Interface with Computer Cluster and SLURM

`geneticOptimizer.local` is the script used by MOGA-ELEGANT to send the jobs to the cluster and run the ELEGANT scripts of `runJob1`. This script was customized because it depends on the management software implemented in the cluster used. In SOLEIL, the control of the cluster is performed by SLURM version 14.11.8, an open-source resource manager designed to control the performance of a cluster with hundreds or thousands of CPUs. It was created and firstly developed at Lawrence Livermore National Laboratory (LLNL) in 2002 (Jette, 2002) and now it is implemented in the majority of the clusters built to the present day.

Basically, SLURM launches and manages parallel computation jobs in a queue and control access to the cluster CPUs depending on the pending work to optimize the computation effort. The CPUs are usually organized in different partitions depending on characteristics like memory and computation performance. In SOLEIL, the CPUs dedicated to computation performance are also organized in partitions (see for instance the Appendix). One of them with a total of 200 CPUs has been reserved to run MOGA-ELEGANT due to then single task feature of the code: each solution is run in the same CPU during all the process. Then, the initial population size determines the number of CPUs necessary to run the code. Figure 6 shows the schematic function of SLURM: SLURM submits the N-jobs j_1 , …, j_N of a computation process to the cluster assigning them to a list of M-CPUs in function of its availability.

There are a large number of useful commands implemented in SLURM. But one of them is particularly used and precious to connect MOGA-ELEGANT to the SOLEIL cluster, the so-called `sbatch`. This command is used to submit a bash script for the GNU/Linux operating system to the cluster and consists in different options like the partition used, the memory required per CPU or the time limit on the job allocation as highlights. For example, to run MOGA-ELEGANT at SOLEIL is enough taking into account 2 Gb of real memory and the maximum time as possible due to the large quantity of time necessary to obtain results, typically some weeks.

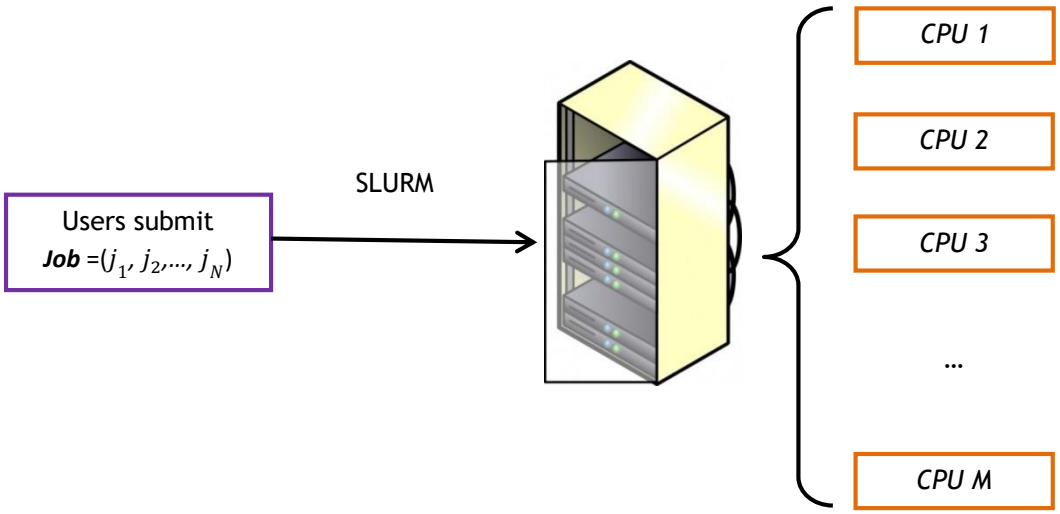

Figure 6: Scheme of the SLURM function. SLURM submits the N-jobs $j_1, \ldots, j_N$ of a computation process to the cluster assigning them to a list of M-CPUs in function of its availability.

3.1.3.3. ELEGANT Computation

The central script `runJob1` evaluates the linear and nonlinear beam dynamics of a given lattice. It performs the linear matching using `matchTemplate.ele` and calculates by symplectic tracking the on- and off-momentum apertures using the script `evalTemplate.ele`. It defines the number of turns of the tracking process and the desired chromaticities (see Table 5 and Table 6).

Secondly, it calculates with the script `processJob1` the Touschek lifetime using the Piwinski formula (Piwinski, 1998) by calling the ELEGANT's command `touschekLifetime`. The Piwinski formula computes the Touschek lifetime taking into account a Coulomb scattering process where the transverse momentum of a bunch particle is transformed to the longitudinal momentum and operational parameters as bunch current, bunch length, coupling and RF-voltage, among others.

Finally, it defines the Penalty functions taken by `geneticOptimizer` script to rank the solutions of each generation and determine the next generation to evaluate.

The variable $TMPDIR defines the temporal directory to store the results. It is necessary to customize the path definition of the variable $TMPDIR into the login shell script of GNU/Linux operating system ~/*.bash_profile* to keep the optimization output.

The script `runJob1` calls ELEGANT to calculate the tunes, the dynamic and the momentum aperture using the scripts given below.

3.1.3.3.1. Linear Matching

The script `matchTemplate.ele` fits the horizontal and vertical tunes of each solution to the previous setting of tunes defined in the input.sdds file. A "soft operator" enables to define a certain tolerance (t=0.01); then the horizontal and vertical tunes ($\nu_{x,z}$) are adjusted to the desired ones ($\nu_{x,z}^{target}$) using the following condition:

$$\left|\nu_{x,z} - \nu_{x,z}^{target}\right| \leq t, \tag{39}$$

that is, returning a non-zero value if and only if the difference between both $\nu_{x,z}$ and $\nu_{x,z}^{target}$ is more than t.

The user also has the possibility to define other optimization constraints as for example, limitations in the maximum betatron functions in the straight sections. The case taken into account in this thesis is simple: taking the settings of the quadrupole families Q7 and Q9 as optimization variables to fit the horizontal and vertical tunes to the desired ones.

The output files are (Table 3):

- runID-linear.param, a SDDS file to write the parameters of the new lattice solution.
- runID-linear.twi, a SDDS file with the Twiss parameters of the new lattice solution.
- runID-linear.done, a SDDS file that acts as a semaphore to inform the end of the process.
- runID.log, an output file to check the linear matching process.

3.1.3.3.2. Nonlinear Computation

The output files of `matchTemplate.ele` are then forwarded to the script `evalTemplate.ele` to correct the linear chromaticities defined in `runJob1` and calculates the dynamic and momentum apertures by tracking. This is the computation sequence followed by the script:

- Chromaticity correction is made using two sextupole families. The new lattice resulting of this correction is saved in the file runID.new. In this thesis, the chromaticity values are corrected with the sextupole families S9 and S10 to the nominal values used during the daily operation with users: 1.2 in the horizontal plane and 2.0 in the vertical one.

- A phase space portrait is computed using a misalignment of the beam called MALIGN (Borland, 2012). This data will be used by `processJob1` script to calculate the tune shift with energy to avoid major resonance line crossing and it is stored in the file runID.w1. The number of turns used is 128 and the computation is done from an off-momentum energy range from -10 % to 10 % and with an optimized step size of 0.4 %, that is, a total of 50 points.

- Calculation of the dynamic aperture (DA) is approximate with the "n-lines" mode tracking particles since this is a time-consuming task (Borland, 2010a). The particles are launched at intervals from (0,0) to (x_{max} sinθ, z_{max} cosθ), where θ goes from $^{\pi}/_{2}$ to $-^{\pi}/_{2}$, along a series of lines beginning at the origin chosen by the user (Figure 7). The boundary of the dynamic aperture is determined by the locations of the horizontal and vertical x and z amplitudes of the first particle loss. Clipping is applied to the boundary of the dynamic aperture to avoid any artificial enlargements induced by resonance islands (Borland, 2009) and to avoid considering vertical size of the dynamic aperture beyond the requirements (e.g. aperture limitation). This will then reject any large artificial dynamic aperture that could fake the optimization process.

  In this case, the calculation results of the dynamic aperture are stored into the file $\mathrm{runID.aper}$. Typically, the computation of the SOLEIL dynamic aperture with 1,000 turns takes 20 minutes.

  The parameters used in this thesis to compute the dynamic aperture are shown in Table 5: 21 lines for the n-line mode, 1,000 turns, (x_{min}, x_{max}) = (-0.035, 0.035) m and (z_{min}, z_{max}) = (0.000, 0.010) m as the maximum and minimum values in the horizontal and vertical planes for tracking. The number of interval subdivisions taken into account to explore both planes is 31.

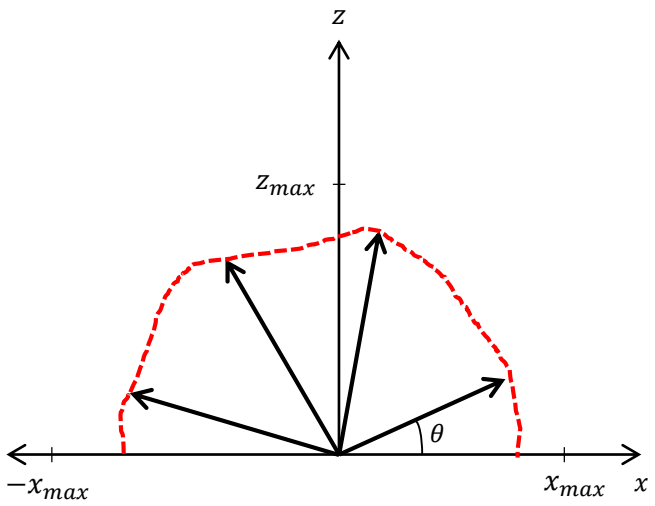

Figure 7: "n-lines" mode used by ELEGANT to compute the boundary of the dynamic aperture in the real space x-z. A certain number of lines chosen by the user are launched at intervals from (0, 0) to (x_{max} sinθ, z_{max} cosθ), where θ goes from $^{\pi}/_{2}$ to $-^{\pi}/_{2}$.

Parameters	Values
Number of Turns	1,000
Number of Lines	21
$(-x_{max}, x_{max})$ (m)	(-0.035, 0.035)
$(-z_{min}, z_{max})$ (m)	(0.000, 0.010)
Interval Splitting Number	1
Number of Subdivisions	31

Table 5: Main parameters used to compute the boundary of the SOLEIL dynamic aperture using the program `find_aperture` defined in ELEGANT.

- The local momentum acceptance (LMA) is the parameter to be used later for computing the Touschek lifetime: the boundary of the LMA is defined by the positive and negative energy offsets for particles along the ring. When a loss is detected, the script takes a certain number of step backs $\Delta\delta_b$ chosen by the user and proceeds with a smaller step size $d\delta$ to refine the determination of the boundary (Figure 8). All this information is saved in the file $\mathrm{runID.mmap}$.

  For SOLEIL (Table 6), the tracking number to determine the LMA was optimized to 1,000 turns, $(x_0, z_0) = (10^{-6}, 10^{-4})$ m as initial conditions, $\Delta\delta$ = 1 % as the step size and $\Delta\delta_b$ = 1 step back with $\mathrm{d}\delta$ = 10 steps to divide the last interval of energy. In addition, the tracking is computed in one quarter of the SOLEIL circumference and it is done in the exit of sextupole magnets to save computation time. The reasons for choosing these tracking parameters are explained in Chapter II. Nevertheless, this is the most time-consuming part of the tracking process: as average, the tracking of the SOLEIL LMA takes two hours and thirty minutes per lattice.

  The LMA computation includes radiation damping, synchrotron oscillation (6D tracking) and the dimensions of the vacuum chamber. It is studied deeply in Chapter II.

Parameters	Values
Number of Turns	1,000
(x_0, z_0) (m)	$(10^{-6}, 10^{-4})$
$\Delta\delta$ (%)	1
$\Delta\delta_b$(%)	1
$\mathrm{d}\delta$	10

Table 6: Main parameters used to compute the SOLEIL local momentum aperture using the program `momentum_aperture` implemented in ELEGANT.

- Finally, if the process is correct, a semaphore file $\mathrm{runID.done0}$ is generated.

In `runJob1` there are two important files to check the ELEGANT processes: $\mathrm{runID.log}$ after the computation of `matchTemplate.ele` and $\mathrm{runID\text{-}main.log}$ after the computation of `evalTemplate.ele`. Both files enable the 'online' checking of the performance of the ELEGANT's scripts.

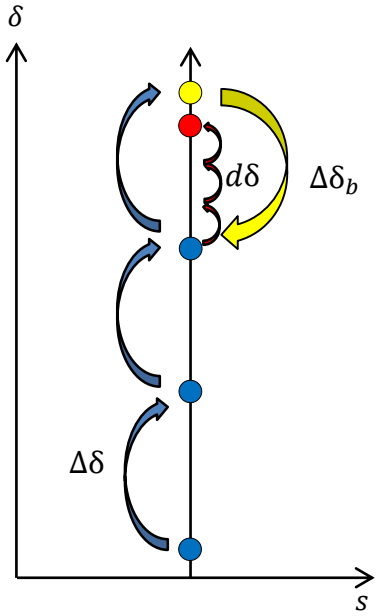

Figure 8: Searching process of the local momentum acceptance performed by ELEGANT. When a loss is detected with a step size $\Delta\delta$ (yellow point), the script steps backs by $\Delta\delta_b$ and proceeds with a smaller step size $d\delta$ to refine the determination of the boundary (red point).

3.1.3.3.3. Post-Processing

The script `processJob1` is run by `runJob1` to post-process the data previously produced by ELEGANT, that is, to compute the optimization objectives (DA area and Touschek lifetime) and to define the penalty functions. Both parameters are essential.

The Touschek Lifetime is calculated by the script `computeLifetime`. This script replicates the local momentum acceptance of one quarter of the machine along the ring stored in runID.mmap and puts all the information in runID.mmapxt.

The Touschek lifetime is calculated using the Piwinki formula of the ELEGANT command `touschekLifetime` taking into account the coupling, the bunch current, the number of bunches defined by the user, the horizontal emittance, and the energy spread previously computed for each solution in runID.twi files. For the computation and comparison the following parameters were selected (Table 7): a coupling value of 1 %, a bunch length of 6 mm, and 400 mA of beam current in 400 bunches, that is, 1 mA per bunch. The Touschek lifetime is stored as a parameter in the runID.ltime SDDS file.

Thereafter, `processJob1` calculates the area of the DA by integration (called Area1) taking into account the clipping method explained before and the penalty functions for chromaticities, DA, and LMA:

- *ChromPenalty* is computed comparing the horizontal and vertical chromaticities $\xi_{x,z}$ with the target chromaticities $\xi_{x,z}^{target}$ previously defined by the user using a tolerance factor t=0.1 (soft-operator). The penalty functions $P(\xi_{x,z})$ are given by the following equations:

$$P(\xi_{x,z}) = \frac{(\xi_{x,z} - \xi_{x,y}^{target} - t)^2}{t^2} \quad \xi_{x,z} > \xi_{x,z}^{target}, \tag{40}$$

$$P(\xi_{x,z}) = \frac{(\xi_{x,z}^{target} - \xi_{x,z} - t)^2}{t^2} \quad \xi_{x,z} < \xi_{x,z}^{target}. \tag{41}$$

$P(\xi_{x,z})$ is a positive number and will be smaller for closest chromaticity values to the target ones.

- *DAPenalty* and *LMAPenalty* are simply computed changing the sign of the area of DA (Area1) and the Touschek lifetime calculated previously because the algorithm minimizes the penalty functions.

Finally, all the information is merged inside the file $\mathrm{runID.proc}$. This file has all the computed information of each individual.

Parameters	Values
Coupling Value (%)	1
Bunch Current (mA)	1
Bunch Length (mm)	6

Table 7: Parameters used by MOGA-ELEGANT to compute the Touschek lifetime during the optimization of the SOLEIL storage ring lattice.

3.1.4. THE OPTIMIZATION PROGRAM

`geneticOptimizer` defines the algorithm itself, that is, the way chosen by the algorithm to mutate the variables, to select the best parents from each generation to breed children and to mutate these children to start the next generation of individuals. At it is already said, it is based on the algorithm NSGA-II (Deb, 2002).

Firstly, `geneticOptimizer` randomly creates the first generation changing the initial quadrupole and sextupole settings using the following expression:

$$S_i^{(1)} = S_i^{(0)} + f_{BMG}(3) \cdot errorLevel \cdot errorFactor, \tag{42}$$

where $S_i^{(0)}$ and $S_i^{(1)}$ are initial and final settings of the optimization variables (the horizontal and vertical tunes and the settings of the sextupoles families of SOLEIL). $f_{BMG}(3)$ is a non-biased centered and normalized Gaussian function N(0, σ=1) generated by the Box-Muller generator (Box, 1958) with a cut-off at 3σ following the expression:

$$\left|\cos(2\pi\, d_1) \cdot \sqrt{(-2\log(d_2))}\right| \leq 3, \tag{43}$$

where the values d_1 and d_2 are random numbers uniformly distributed in the interval [0, 1].

errorLevel is a parameter initially chosen by the user in the input file that defines the area searched into the objective space and *errorFactor* is a parameter introduced when using of the command `geneticOptimizer` to change the convergence of the optimization process.

At the end of this process, the file runID.inp is created. It contains the new values of the optimization variables: the horizontal and vertical tunes and the settings of the sextupoles families.

To select the parents, the algorithm uses the non-dominate sorting process and the penalty functions. Basically, the algorithm choses the best non-dominated solutions from all the possible solutions expressed in the file runID.all taking into account the penalty functions already calculated in `processJob1`. These non-dominated solutions are ranked in the file runID.sort. After that, another file called runID.best is created with all the non-dominated solutions with a rank number equal to 1. These non-dominated solutions define the points of the Pareto-optimal front.

Thereafter the algorithm defines the population of children as following: firstly, the algorithm mutates the value of the optimization variables using Eq. 44:

$$S_i^{(1)} = rnd \cdot Spread\left(S_i^{(0)}\right) + min\left(S_i^{(0)}\right) + f_{BMG}(3) \cdot errorLevel \cdot errorFactor, \qquad (44)$$

where $S_i^{(1)}$ are the new variable settings, rnd is as function generating a number between the interval [0, 1] distributed in a normalized Gaussian distribution, $\mathrm{Spread}\left(S_i^{(0)}\right)$ is the standard deviation of the variables i, $\min\left(S_i^{(0)}\right)$ takes the minimum value of the variables i, $f_{BMG}(3)$ is the Box Muller generator with a cut-off at 3σ defined in Eq. 43 (Figure 9).

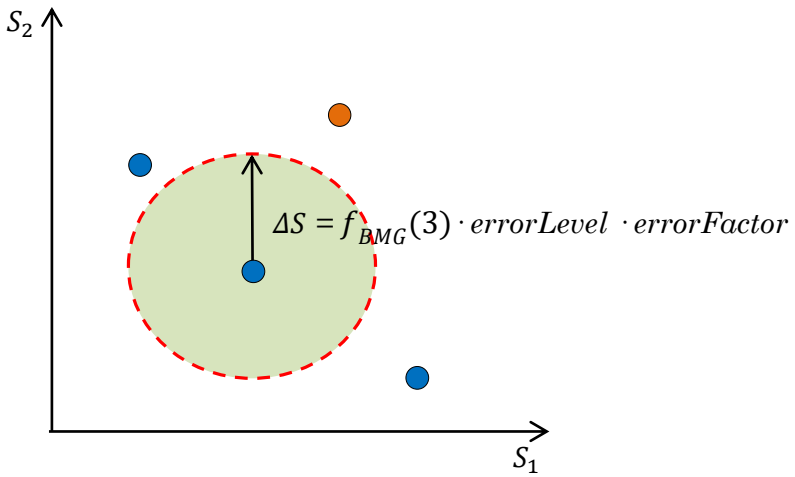

Figure 9: The randomized perturbations are close to the starting point and it depends on $f_{BMG}(3)$ a non-biased centered and normalized Gaussian function N(0, σ=1) generated by the Box-Muller generator with a cut-off at 3σ, the errorLevel and the errorFactor.

Secondly, the algorithm creates a *children pool* replicating the Pareto-optimal front the same number as the product between the numbers of variables and the number of children previously defined in the input.sdds files. For each group of Pareto-optimal front, two parents are randomly chosen. Then, the algorithm blends that attributes of the parents to breed a new generation.

For example, considering the optimization problem in 13 variables, 5 parents and 8 children, each variable will have a children pool consisting in 13·8=104 individuals from which only two will be privileged for the next generation.

Once the new variables are known, the script sends the next generation of individuals to the cluster taken into account the number of jobs still running and the maximum population available for the computation process. In other words, the algorithm sends to the cluster a job once another job is complete and a CPU is available. This process is iterative and starts again for each generation.

As convergence criteria, the process continues until the results stops improving or the maximum number of generations is reached.

3.2. COMPUTATIONAL ENVIRONMENT AT SOLEIL

MOGA-ELEGANT is time consuming and needs a large computer cluster to calculate by tracking the on- and off-momentum acceptances due to the tracking computation. A computer cluster is composed of a large number of computers connected between them in a local area network to perform heavy computations. The number of CPUs used is high (typically hundreds and thousands) because MOGA-ELEGANT needs one CPU per job, that is, it is a single task process: the tracking of the on- and off-momentum acceptances are calculated on a dedicated CPU for each lattice (job) evaluation.

For the purpose of this thesis, a partition of 200 CPUs has been reserved in the SOLEIL cluster for MOGA's calculations.

For interested readers, the details and specifications of the cluster installed in SOLEIL are explained in Appendix.

4. CONCLUSIONS

The main concepts of the transverse and longitudinal motion of a particle in particle accelerators used along this thesis have been introduced at the first part of the chapter. The second part has been dedicated to define what the genetic algorithms are and to summarize the benefits of its applications in the scientific and engineering community specially solving multi-objective problems where the objective to optimize are in conflict to each other. Thereafter, the performance of the genetic algorithm has been explained in

detail linking the different concepts and operators with the Darwinian natural evolution theory where the genetic algorithms come from.

Once the motivation of this thesis has been clarified, the application of the genetic algorithms in the accelerators community has been reported emphasizing the case of the synchrotron light sources. A large number of applications and examples have been referenced and listed reporting the important role played for the genetic algorithms in synchrotron light sources until now, as for example, the upgrading of the current third generation storage rings to the new diffraction-limited ones.

The last part of the chapter has been dedicated to deeply study the computational structure of the Multi-Objective Genetic Algorithm (MOGA), the particular case of genetic algorithms used in this thesis. The main characteristics and scripts have been listed adding their characteristics and functionalities. Special attention has been done describing ELEGANT, the tracking code used by MOGA for long tracking computations, SLURM, the open-source resource manager implemented in the SOLEIL cluster to control and manage the computational performance of MOGA, and the way used by MOGA to explore the optimization dimensions.

APPENDIX: THE SOLEIL CLUSTER

The SOLEIL cluster is a computational environment composed by hundreds of CPUs dedicated to high-level scientific computations. It is used every year to dozens of experimental researchers that come to the Synchrotron SOLEIL beamlines and for the SOLEIL staff to study and test a great variety of simulation studies.

Figure 1 shows a diagram of the SOLEIL cluster architecture (Gatineau, 2015). The cluster of synchrotron SOLEIL is divided in two machines called ISEI-KONA and IDAI that can use a total of 1,296 processors of different characteristics of memory and performance dedicated for computational purposes. The machine IDAI consists of one interactive node with 8 processors Intel Xeon Westmere EX hexa-core running at 2 GHz and a total of 80 cores with 4 TB of memory RAM.

On the other hand, the machine ISEI-KONA consists of one interactive node with 16 processors Intel Xeon Dunnington hexa-core running at 2.66 GHz and 512 GB of memory RAM and the next computational nodes:

- 112 computation nodes bi-socket Intel Nehalem X5560 quad-core running at 2.5 GHz and 36 GB of RAM. The total memory RAM available is 4 TB.
- 16 computation nodes bi-socket Intel Ivy Bridge E5-2670v2 10-core running at 2.5 GHz and 128 GB of RAM. The total RAM available is 6.4 TB. In SOLEIL, this group of nodes is identified as Ivy partition.
- 2 computation nodes bi-socket Intel Ivy Bridge E5-2670v2 10-core running at 2.6 GHz and 64 GB of RAM. Each card is composed of an accelerator card GPU NVIDIA K20M.
- 2 computation nodes bi-socket Intel Ivy Bridge E5-2670v2 10-core running at 2.6 GHz and 64 GB of RAM. Each card is composed of an accelerator card INTEL XEON PHI 31S1P.

The data storage system consists of the LUSTRE and FLASH high performance file systems with a capacity of 58 TB and 30 TB, respectively.

Figure 2 shows a frontal panel of the SOLEIL cluster. The machine ISEI-KONA (orange square) and IDAI (red square) are identified as well as the IVY partition (green square), the storage system LUSTRE (cyan square) and the systems OSCAR (magenta square) and DOSS (sweet green square) used for administration purposes. The computation section is highlighted in yellow color.

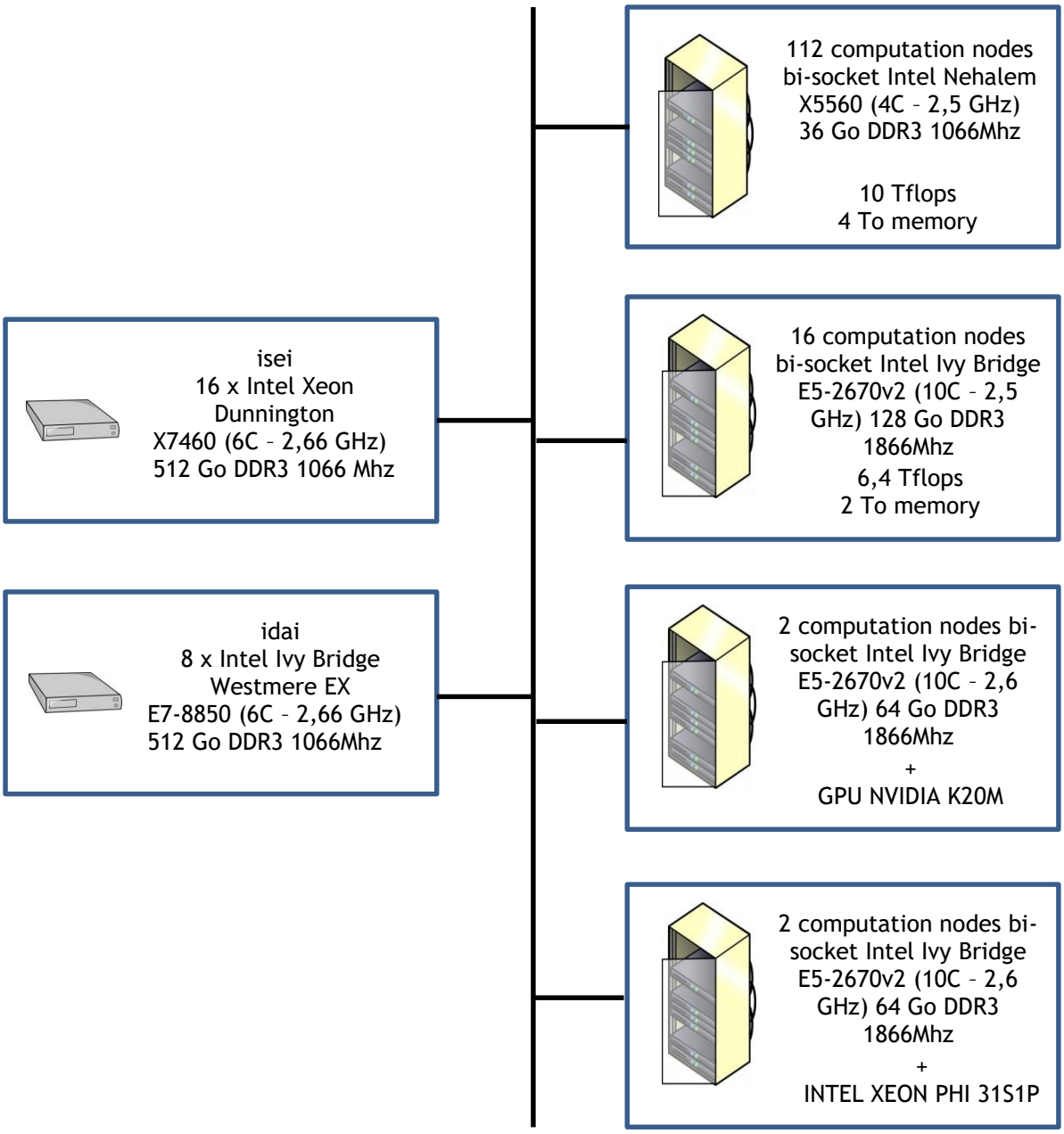

Figure 1: Computational architecture of the SOLEIL cluster. The cluster of synchrotron SOLEIL is divided in two machines called ISEI-KONA and IDAI that can use a total of 1296 processors of different characteristics of memory and performance dedicated for computational purposes: 112 nodes Intel Nehalem for computation purposes with 4 TB of memory, 16 nodes Ivy with 2 TB of memory, 2 nodes Ivy with an accelerator card NVIDIA and 2 nodes with and accelerator card XEON (Gatineau, 2015).

Figure 2: Frontal panel of the SOLEIL cluster. The machines ISEI-KONA and IDAI are identified as well as the IVY partition, the storage system LUSTRE and the systems OSCAR, and DOSS used for administration purposes.

BIBLIOGRAPHY

(Bacci, 2007) A. Bacci, V. Petrillo, A. R. Rossi and L. Serafini. Optimization of the Beamline Characteristics by Means of a Genetic Algorithm. Proceedings of the 2007 Particle Accelerator Conference, pp. 3295-3297, Albuquerque, USA, 2007.

(Bartolini, 2013) R. Bartolini, N. Hammond, J. Kay, T. Pulampong, and R. P. Walker. Ultra-Low Emittance Upgrade Options for the Diamond Light Source. Proceedings of the 2013 International Particle Accelerator Conference, pp. 25-26, Pasadena, USA, 2013.

(Bazarov, 2005) I. V. Bazarov and I. Padamsee. Multivariate Optimization of ILC Parameters. Proceedings of the 2005 Particle Accelerator Conference, pp. 1736-1738, Knoxville, USA, 2005.

(Bengtsson, 1997) J. Bengtsoon. The Sextupole Scheme for the Swiss Light Source (SLS): An Analytic Approach. Internal report of Swiss Light Source, 1997.

(Borland, 2000) M. Borland. Elegant: A Flexible SDDS-compliant Code for Accelerator Simulation. LS-287, Advanced Photon Source, 2000.

(Borland, 2009) M. Borland, V. Sajaev, L. Emery, and A. Xiao. Direct Methods of Optimization of Storage Ring Dynamic and Momentum Apertures. Proceedings of the 2009 Particle Accelerator Conference, pp. 3850-3852, Vancouver, Canada, 2009.

(Borland, 2010a) M. Borland, V. Sajaev, L. Emery, and A. Xiao. Multi-Objective Direct Optimization of Dynamic Acceptance and Lifetime for Potential Upgrades of the Advanced Photon Source. Advanced Photon Source LS-319, 2010.

(Borland, 2010b) M. Borland, L. Emery, H. Shang, and S. Soliday. User's Guide for SDDS Toolkit Version 2.8. Advanced Photon Source, 2010.

(Borland, 2012) M. Borland. User's Manual for Elegant. Program Version 25.1.0. Advanced Photon Source, 2012.

(Borland, 2014) M. Borland, G. Decker, L. Emery, V. Sajaev, Y. Sun and A. Xiao. Lattice Design Challenges for Fourth-Generation Storage-Ring Light Sources. Journal of Synchrotron Radiation, ISSN 1600-5775, 2014.

(Box, 1958) G. E. P. Box and M. E. Muller. A Note on the Generation of Random Normal Deviates, The Annals of Mathematical Statistics. Vol. 29, No. 2 pp. 610–611, 1958.

(Carmignani, 2014a) N. Carmignani. Dynamic Aperture Optimization of the ESRF Lattices: New and Old. Talk in the 2014 Low Emittance Ring Workshop, Grenoble, France, 2014.

(Carmignani, 2014b) N. Carmignani. Touschek Lifetime Studies and Optimization of the ESRF: Present and Upgraded Lattice. PhD Thesis, Pisa University, Italy, 2014.

(Carmignani, 2015) N. Carmignani, L. Farvacque, S. M. Liuzzo, B. Nash, T. Perron, P. Raimondi, R. Versteegen, and S. White. Linear and Nonlinear Optimizations of the ESRF Upgrade Lattice. Proceedings of the 2015 International Particle Accelerator Conference, pp. 1422-1424, Richmond, USA, 2015.

(Deb, 2001) K. Deb. Multi-Objective Optimization Using Evolutionary Algorithms. New York. John Wiley and Sons, pp. 28-30, 2001.

(Deb, 2002) K. Deb, S. Agrawal, A. Pratap, and T. Meyarivan. A Fast Elitist Non-Dominated Sorting Genetic Algorithm for Multi-Objective Optimization: NSGA-II. Internal report Kanpur Genetic Algorithm Laboratory (KanGAL), Kanpur, India, 2002.

(D'Souza, 2010) R. G. L. D'Souza, K. Chandra Sekaran, and A. Kandasamy. Improved NSGA-II Based on a Novel Ranking Scheme. Journal of Computing, vol. 2, ISSUE 2, pp. 91-95, 2010.

(Ehrlichman, 2015) M. Ehrlichman, M. Aiba, and A. Streun. Optimizing SLS2 Nonlinearities Using a Multi-Objective Genetic Algorithm. Proceedings of the 2015 International Particle Accelerator Conference, pp. 486-488, Richmond, USA, 2015.

(Ehrlichman, 2016) M. P. Ehrlichman. Genetic Algorithm for Chromaticity Correction In Diffraction Limited Storage Rings. Phys. Rev. ST Accel. Beams 19, 044001, 2016.

(Emery, 2005) L. Emery. Global Optimization of Damping Ring Designs Using a Multi-Objective Evolutionary Algorithm. Proceedings of the 2005 Particle Accelerator Conference, pp. 2962-2964, Knoxville, USA, 2005.

(Gavaldà, 2014) X. N. Gavaldà, L. S. Nadolski, and A. Díaz-Ortiz. Multi-Objective Optimization of the Nonlinear Beam Dynamics of Synchrotron SOLEIL. Proceedings of the 2014 International Particle Accelerator Conference, pp. 388-400, Dresden, Germany, 2014.

(Gatineau, 2014) L. Gatineau and L. Prévoust. Introduction au Gestionnaire de Ressources SLURM. Technical report NEC HPC Europe, 2014.

(Hajima, 1992) R. Hajima, N. Takeda, H. Ohashi, and M. Akiyama. Nucl. Instrum. Methods Phys. Res., Sect. A (318), pp. 822 (1992).

(Hill, 1884) G. W. Hill. On the Part of the Motion of Lunar Perigee which is a Function of the Mean Motions of the Sun and Moon. Acta Math. 8 (1): 1-36.

(Hofler, 2013) A. Hofler, B. Terzi, M. Kramer, A. Zvezdin, V. Morozov, Y. Roblin, F. Lin, and C. Jarvis. Innovate Applications of Genetic Algorithms to Problems in Accelerator Physics. Phys. Rev. ST Accel. Beams 16, 010101, 2013.

(Holland, 1975) J. Holland. Adaptation in Natural and Artificial Systems. University of Michigan Press, 1975.

(Huang, 2013) X. Huang, J. Corbett, J. Safranek, and J. Wu. Online Optimization Algorithms for Accelerators and Experimental Results. Proceedings of the 2013 International Particle Accelerator Conference, pp. 2012-2013. Shanghai, China, 2013.

(Huang, 2015) X. Huang and J. Safranek. Online Optimization of Storage Ring Nonlinear Beam Dynamics. Phys. Rev. ST Accel. and Beams 18, 084001, 2015.

(Jette, 2002) M. Jette, C. Dunlap, J. Garlick, and M. Grondona. SLURM: Simple Linux Utility for Resource Management. Lawrence Livermore National Laboratory, 2002.

(Konak, 2006) A. Konak, D. W. Coit, and A. E. Smith. Multi-Objective Optimization Using Genetic Algorithms: A Tutorial. Reliability Engineering and System Safety, vol. 91, ISSUE 9, pp. 992-1007 (2006), ISSN 0951-8320, 10.1016/j.rss.2005.11.018.

(Laskar, 1990) J. Laskar. The Chaotic Motion of the Solar System. A Numerical Estimation of the Size of the Chaotic Zones. Icarus, Vol. 88, pp. 266-291, 1990.

(Laskar, 1995) J. Laskar. Introduction to Frequency Map Analysis. Proceedings of 3DHAM95 NATO Advanced Institute, C. Simo Ed., pp. 134-150, S'Agaro, June 1995.

(Lee, 2004) S. Y. Lee. Accelerator Physics. Word Scientific Publishing Co. Pte. Ltd, pp. 40, 2nd Ed. (2004).

(Liouville, 1838) J. Liouville. Sur la Théorie de la Variation des Constantes Arbitraires. J. Math. Pures Appl. 3, pp. 342-3469, 1838.

(Nadji, 1998) A. Nadji, J. L. Laclare, M. J. Level, A. Mosnier, and P. Nghiem. The Effect of Nonlinear Synchrotron Motion on the SOLEIL Energy Acceptance. Proceedings of the 1999 International Particle Accelerator Conference, New York, USA, 1999.

(Nadolski, 2001) L. S. Nadolski. Application de l'Analyse en Fréquence à l'Étude de la Dynamique des Sources de Lumière. PhD Thesis, Paris XI University, France, July 2001, 2001PA112120.

(Nadolski, 2003) L. S. Nadolski and J. Laskar. Review of Single Particle Dynamics for Third Generation Light Sources through Frequency Map Analysis. Phys. Rev. ST Accel. and Beams 6 (11), 114801, 2003.

(Piwinski, 1998) A. Piwinski. The Touschek Effect in Strong Focusing Storage Rings. Technical Report 98-179, DESY, November 1998.

(Reyes-Sierra, 2006) M. Reyes-Sierra and C. Coello-Coello. Multi-Objective Particle Swarm Optimizers: A Survey of the State-of-the-Art. International Journal of Computational Intelligence Research, 2(3), pp. 287-308, 2006.

(Robin, 2000) D. S. Robin, C. Steier, J. Laskar, and L. S. Nadolski. Global Dynamics of the Advanced Light Source Revealed through Experimental Frequency Map Analysis. Physical Review Letters, 85(3): 558-561, 2000.

(Rudenko, 2004) O. Rudenko. Application des Algorithmes Évolutionnaires aux Problèmes d'Optimisation Multi-Objectif avec Constraintes. PhD Thesis, École Polytechnique, France, 2004.

(Russenschuck, 1998) S. Russenschuck and S. Ramberger. Genetic Algorithms for the Optimal Design of Superconducting Accelerator Magnets. Proceedings of the 2006 European Particle Accelerator Conference, pp. 2014-2016, Stockholm, Sweden, 2006.

(Schirmer, 1996) D. Schirmer, M. V. Hartrott, S. Khan, D. Krämer, and E. Wheireter. Beam Transport Lines at BESSY-II. Proceedings of the 1996 Particle Accelerator Conference, pp. 1879-1881, Dallas, USA, 1996.

(Singh, 2013) B. Singh, M. Apollonio, R. Bartolini, E. C. Longhi and T. Pulampong. Investigation and Test of the Possibility of Reducing the Emittance of Diamond Storage Ring. Proceedings of the 2013 International Particle Accelerator Conference, pp. 234-236, Shanghai, China, 2013.

(Streun, 1999) A. Streun. Practical Guidelines for Lattice Design. Technical report SLS-TME-TA-1999-0014, Paul Scherrer Institute, Switzerland, 1999.

(Sun, 2012) C. Sun, D. S. Robin, H. Nishimura, C. Steier, and W. Wan. Small Emittance and Low-Beta Lattice Designs and Optimizations. Phys. Rev. ST Accel. and Beams 15, 0540001, 2012.

(Tian, 2014) K. Tian, J. Safranek, and Y. Yan. Machine Based Optimization Using Genetic Algorithms in a Storage Ring. Phys. Rev. ST Accel. and Beams 17, 020703, 2014.

(Walker, 2014) R. P. Walker, M. Apollonio, C. P. Bailey, M. P. Cox, R. T. Fielder, N. P. Hammond, M. T. Heron, J. Kay, I. P. S. Martin, S. P. Mhaskar, G. Rehm, E. C. M. Rial, B. Singh, V. Smaluck, A. Thomson, R. Bartolini, and T. Pulampong. The Double-Double Bend Achromat (DDBA) Lattice Modification for the Diamond Storage Ring. Proceedings of the 2014 International Particle Accelerator Conference, pp. 331-333, Dresden, Germany, 2014.

(Wiedemann, 2007) H. Wiedemann. Particle Accelerator Physics. Springer-Verlag Berlin and Heidelberg GmgH & Co. K, 3rd Ed., 2007.

(Wolski, 2014) A. Wolski. Beam Dynamics in High Particle Accelerators. Imperial College Press, 1st Ed., pp. 360-373, 2014.

(Yang, 2011) L. Yang, Y. Li, W. Guo, and S. Krinsky. Multi-Objective Optimization of Dynamic Aperture. Phys. Rev. ST Accel. and Beams, 14(5), 054001, 2011.

CHAPTER II
BENCHMARKING BETWEEN TRACY3 AND ELEGANT CODES FOR THE SOLEIL LATTICE

CONTENTS

The tracking code ELEGANT (Borland, 2000) is used for the genetic-based optimization with MOGA in this thesis. The first step is then to benchmark the code against the TRACY3 code (Nishimura, 1988), the reference code extensively used for Synchrotron SOLEIL. This fundamental study is mandatory before using the MOGA code because ELEGANT is the main tool to do tracking for finding new settings of quadrupoles and sextupoles. Indeed, each simulation code follows different formalism (reference frame, matrix code, Hamiltonian code, integration scheme, high/low energy approximations) that can be more or less adapted to a given accelerator depending on its circumference, energy, and complexity of its elements. This type of comparison was already performed at SOLEIL when TRACY3 was identified as the reference code in 2002. Similar studies were carried out to ensure that the code was compliant with codes MADX-PTC and BETA (Einfeld, 2009; Nadolski, 2009a). Moreover, the results given by TRACY3 have been compared with SOLEIL beam-based measurements, leading to a very good agreement (Brunelle, 2010; Nadolski, 2009b; Tordeux, 2009).

The first part of this chapter is dedicated to a brief introduction of both tracking codes. ELEGANT and TRACY3 are concisely presented emphasizing the definitions of the dipole edge focusing model, the tracking process of the on- and off-momentum apertures, and the energy acceptance computation.

The second part is dedicated to compare the linear optics and the tune shifts with amplitudes and energy between both codes, using a simplified lattice of SOLEIL called SOLEIL2009 that exhibits a 4-fold symmetry.

The third part focuses on the choice of parameters in ELEGANT in order to compute the on-momentum dynamic aperture, the off-momentum aperture, and the Touschek lifetime since the philosophy of both tracking codes are rather different. The lattice used in this study corresponds to the one deployed at SOLEIL since 2013. It incorporates in straight section SDL13 a double vertical low—beta optics for hosting two in-vacuum insertion devices breaking down the 4-fold symmetry of the lattice. Moreover, the dimensions of the vacuum chamber are included in the model at the end.

1. Brief Introduction to Tracking Codes

The “tracking codes” used for Accelerator Physics simulations are designed to study the stability of particles over many turns and in the presence of nonlinear effects. For synchrotron light sources, an electron beam is mostly used. The accelerator is modeled piece-wise. Each magnetic element or drift space is described by its magnetic field (including multipolar field components) and misalignment errors can be added to be as close as possible to the real machine. The number of turns is chosen to take into the damping time due to synchrotron radiation.

Commonly, an element of an accelerator is described by a linear or nonlinear mapping M propagating 6-dimensional coordinates from the entrance $s=s_1$ and $\overrightarrow{w_1}=(x_1, x'_1, z_1, z'_1, \tau_1, \delta_1)$ to the exit s_2 and $\overrightarrow{w_2}=(x_2, x'_2, z_2, z'_2, \tau_2, \delta_2)$ (Figure 1), where x (z) is the horizontal (vertical) coordinate, x' (z') is its derivative in the horizontal and vertical plane with respect to the curvilinear abscissa s, τ the longitudinal coordinate with

respect to the synchronous particle, and δ is the relative energy offset with respect to the nominal energy. The full machine is modeled by concatenation of the maps of all the elements of the magnetic structure.

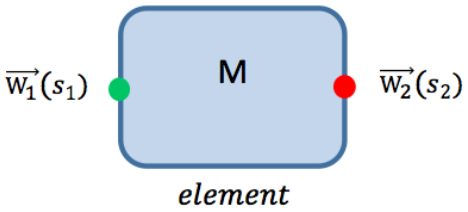

Figure 1: Principe for modeling of elements of a magnetic structure in tracking codes. The map M propagates the initial coordinate $\overrightarrow{w_1}$ at s_1 to the coordinates $\overrightarrow{w_2}$ at s_2.

There are several ways to represent the elements along the machine depending on the required level of precision: from the simplest one using matrix formalism and approximating the nonlinear magnets as thin lenses to methods using traditional numerical computations as Taylor series truncated up to a certain order, canonical integrator (i.e. conjugated variables like (x, p_x) satisfying a null Poisson bracket $[x, p_x] = 0$) or symplectic integrator (i.e. preserving the 2-form $x \wedge p_x$) using a Hamiltonian formalism. The integrators used can be implicit or explicit (for interested readers see Ref. (Forest, 1998, 2006; Herr, 2013; Wolski, 2014).

A brief description of the two tracking codes used in this thesis is given below focusing especially on the dipole edge focusing, the computation of the on- and off-momentum dynamic apertures and on the definitions of the Touschek lifetime. The good modelization of the dipole edge focusing becomes crucial to avoid the discrepancies observed in the vertical chromaticity values (see section 2). Moreover, the benchmarking of on- and off-momentum dynamic apertures between ELEGANT and TRACY3 is necessary since TRACY3 was benchmarked with the beam-based measurement performed at SOLEIL.

1.1. ELEGANT

ELEGANT (Borland, 2000) is a reference tracking code developed at the Advanced Photon Source (APS). It can perform 6D-tracking computation for linear and circular accelerators using matrix formalism up to the third order and numerical and canonical integration, or any combination of them. As any tracking code, ELEGANT describes the accelerator using a sequence of elements as magnets, radio-frequency cavity, vacuum chamber aperture among others in different levels of precision depending on the accuracy chosen by the user. As it has been explained in Chapter I, computation and optimization of Twiss parameters, closed orbit and on- and off-momentum dynamic apertures are also implemented in several ways. Physical phenomena like synchrotron radiation and damping, effect of the errors like multipolar field components and misalignments are included. The capabilities of such codes have been increased over the years for linear and nonlinear beam dynamic studies as well as collective effects and impedance studies (Borland, 2013).

For interested readers, see the Ref. (Borland, 2000) for a quick description of all functions implemented in the code and the extended user's manual of the last version (Borland, 2016) for detailed descriptions.

ELEGANT is written in C programming language (Kernighan, 1988) and is executed in a sequence of commands in UNIX shell. The input and output files are managed for a list of pre- and post-processing programs called SDDS Toolkit (Borland, 2010) used for plotting, preparing and analyzing data. These programs are written in Tcl-Tk programing language (Ousterhout, 1994; Wheeler, 2011) that allows a high level of flexibility and adaptive capacity by the user.

1.1.1. DIPOLE EDGE FOCUSING MODEL

The dipole edge focusing in ELEGANT version 25.1.0 is modeled using the first order Brown formula (Brown, 1982) in non-canonical variables as follows:

$$x' = x'_0 + \frac{1}{\rho(1+\delta)}\tan(\theta/2)z_0 \quad (1)$$

$$z' = z'_0 - \frac{1}{\rho(1+\delta)}\tan(\theta/2 - \psi)z_0 \quad (2)$$

In these equations x (z) is the horizontal (vertical) coordinate, x' (z') its derivative with respect to the curvilinear abscissa s, x_0 (z_0) is the horizontal (vertical) coordinate at the entrance of the edge field region, θ is the dipole angle, ρ is the dipole curvature radius and ψ is a parameter related to the length of the dipole fringe field (the peak magnetic field has a continuous s-dependence at entry and exit of the dipole leading to extra focusing in the vertical plane) defined as:

$$\psi = \frac{1}{\rho} Kg \frac{1+\sin\theta^2}{cos\,\theta}, \quad (3)$$

where g is the full-magnet gap and

$$K = \int_{-\infty}^{\infty} \frac{B_z(s)(B_0 - B_z(s))}{gB_0^2} ds, \quad (4)$$

where B_0 is the dipole peak field at the center of the magnet and $B_z(s)$ is the variation of the vertical magnetic field versus *s* in the fringe field region (Figure 2). The K parameter is defined by the magnetic measurements to be equal to 0.724 for SOLEIL dipoles (Brunelle, 2016).

1.1.2. ON-MOMENTUM DYNAMIC APERTURE

In ELEGANT, the dynamic aperture (DA) is computed by selecting "n-lines" as described in Chapter I, Figure 7. Technically the precision of the calculation depends on the amplitude mesh size along a line called *step size* and on *n_split* and *split_fraction* that are related to refining the computation by making steps back when the last survival particle is identified during the first stage of the DA computation.

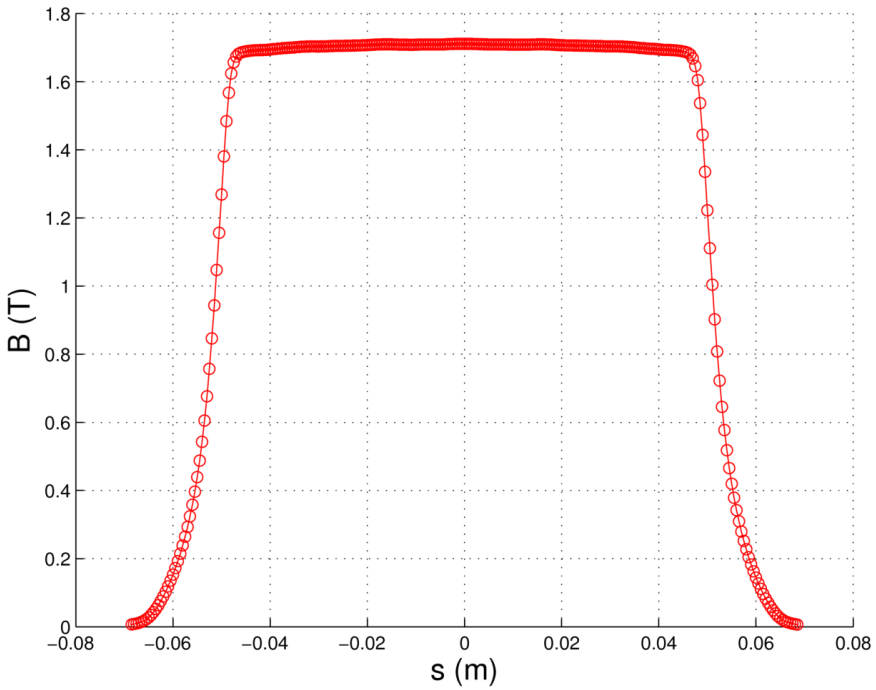

Figure 2: Measurement of the dipole magnetic field B versus s. Example of dipole n°2 of the cell n°13 of SOLEIL storage ring for a current of 540 A. Courtesy of F. Briquez.

1.1.3. MOMENTUM APERTURE

The momentum aperture at a given position s corresponds to the maximum particle energy deviation that remains stable after a Touschek event has occurred at this location. The most accurate way to make this computation is to track a particle over M subsequent turns for different energy offsets and look for the minimum energy amplitude leading to a particle loss. This particle loss can occur because of instability in the transverse plane where the particle transverse amplitude exceeds the size of the vacuum pipe, or in the longitudinal plane because the energy deviation exceeds the energy acceptance fixed by the RF-system or the transverse dynamics. As the energy deviation can be either positive or negative, this procedure can be applied to find the positive s-dependent local momentum acceptance and the negative one. Asymmetry of the momentum aperture arises from nonlinearities in the transverse plane (sextupole effect) and in the longitudinal plane (second order momentum compaction factor) (Belgroune 2003, 2005).

The computation of the momentum aperture in ELEGANT, is inspired by the work done for TRACY3 in SOLEIL, is characterized by a second refining process that divides the last energy offset step where the particle is still stable, in a certain number of steps chosen by the user (Figure 8 in Chapter I). This refining process increases the precision of the momentum aperture computation along the ring.

1.1.4. TOUSCHEK LIFETIME FORMULA USED BY THE ELEGANT CODE

The Touschek lifetime results from the particle losses during Coulomb elastic intra-beam scattering events. Two electrons within a same bunch exchange energy. If the energy deviation exceeds the momentum acceptance at the location of the scattering, one or both electrons get lost.

The Touschek lifetime (τ_{Tous}) is calculated in ELEGANT using the Piwinski formula (Piwinski, 1998) implemented in the routine `touschekLifetime` (Borland, 2012) given by:

$$\frac{1}{\tau_{Tous}} = \langle \frac{R}{N} \rangle, \tag{5}$$

where N is the number of particles in a bunch, R is the total number of scattering events per unit time and $\langle \ \ \rangle$ the average operator along the storage ring. R is given by (Xiao, 2007):

$$R = \frac{r_0^2 c \beta_x(s) \beta_z(s) \sigma_h(s) N^2}{8\sqrt{\pi}\beta^2\gamma^2\sigma_{x\beta}^2(s)\sigma_{z\beta}^2(s)\sigma_l\sigma_E} F(\tau_m, B_1, B_2), \tag{6}$$

where r_0 is the classical electron radius, c is the speed of light, β_{x} and β_{z} are the horizontal and vertical betatron functions, $\beta = {}^{\mathrm{V}}/_{\mathrm{C}}$ and γ are the Lorentz factors, σ_{E} is the beam energy spread, $\sigma_{\mathrm{x}}(\mathrm{s})$ and $\sigma_{\mathrm{z}}(\mathrm{s})$ are the total beam sizes in horizontal and vertical planes defined as

$$\sigma_x(s) = \sqrt{\varepsilon_x \beta_x(s) + \sigma_E^2 \eta_x^2(s)}\,, \tag{7}$$

$$\sigma_z(s) = \sqrt{\varepsilon_z \beta_z(s) + \sigma_E^2 \eta_z^2(s)}\,. \tag{8}$$

where $\eta_{\mathrm{x}}(\mathrm{s})$ and $\eta_{\mathrm{z}}(\mathrm{s})$ are the horizontal and vertical dispersion functions.

σ_{l} is the bunch length at zero current and depends on the momentum compaction factor α, the harmonic number h, the RF-frequency f_{RF}, the synchronous phase ϕ_{s}, the relative energy spread σ_{E} and the RF-voltage V_{RF} as follows:

$$\sigma_l = \sqrt{\frac{2\pi\alpha h c^2}{(2\pi \cdot f_{RF})^2 \cdot cos\phi_s} \frac{E}{eV_{RF}}}\sigma_E. \tag{9}$$

$\sigma_{\mathrm{x}\beta}(\mathrm{s})$ and $\sigma_{\mathrm{z}\beta}(\mathrm{s})$ are the betatron beam sizes excluding momentum spread

$$\sigma_{x\beta}(s) = \sqrt{\varepsilon_x \beta_x(s)}\,, \tag{10}$$

$$\sigma_{z\beta}(s) = \sqrt{\varepsilon_z \beta_z(s)}\,, \tag{11}$$

and

$$\tau_m = \beta^2(\varepsilon_{acc}(\mathrm{s}))^2, \tag{12}$$

where $\varepsilon_{acc}(s)$ is the s-dependent local energy acceptance.

$\sigma_h(s)$ is given by:

$$\sigma_h(s) = \frac{\sigma_{x\beta}(s)\sigma_{z\beta}(s)\sigma_E}{\sqrt{\tilde{\sigma}_x^2(s)\sigma_{z\beta}^2(s) + \tilde{\sigma}_z^2(s)\sigma_{x\beta}^2(s) - \sigma_{x\beta}^2(s)\sigma_{z\beta}^2(s)}}, \tag{13}$$

where

$$\tilde{\sigma}_x^2(s) = \sigma_{x\beta}^2(s) + \sigma_E^2(\eta_x^2(s) + \tilde{\eta}_x^2(s)), \tag{14}$$

$$\tilde{\sigma}_z^2(s) = \sigma_{z\beta}^2(s) + \sigma_E^2(\eta_z^2(s) + \tilde{\eta}_z^2(s)), \tag{15}$$

$$\tilde{\eta}_x(s) = \alpha_x(s)\eta_x(s) + \beta_x(s)\eta_x'(s), \tag{16}$$

$$\tilde{\eta}_z(s) = \alpha_z(s)\eta_z(s) + \beta_z(s)\eta_z'(s), \tag{17}$$

with $\eta_x'(s)$ and $\eta_z'(s)$ are the slope of the dispersion functions and $\alpha_x(s)$ and $\alpha_{zx}(s)$ the Twiss parameters. The function $F(\tau_m, B_1, B_2)$ is defined by:

$$F = \int_{\tau_m}^{\infty} e^{-B_1\tau} I_0(B_2\tau) \frac{\sqrt{\tau}d\tau}{\sqrt{1+\tau}} \left(\left(2 + \frac{1}{\tau}\right)^2 \left(\frac{\tau/\tau_m}{1+\tau} - 1\right) + 1 - \frac{\sqrt{1+\tau}}{\sqrt{\tau/\tau_m}} - \frac{4\tau+1}{2\tau^2} ln\left(\frac{\tau/\tau_m}{1+\tau}\right) \right), \tag{18}$$

where I_0 is the modified Bessel function. Finally, the functions B_1 and B_2 are given by:

$$B_1 = \frac{1}{2\beta^2\gamma^2}\left[\frac{\beta_x^2(s)}{\sigma_{x\beta}^2(s)} - \frac{\beta_x^2(s)\sigma_h^2(s)\tilde{\eta}_x^2(s)}{\sigma_{x\beta}^4(s)} + \frac{\beta_z^2(s)}{\sigma_{z\beta}^2(s)} - \frac{\beta_z^2(s)\sigma_h^2(s)\tilde{\eta}_z^2(s)}{\sigma_{z\beta}^4(s)}\right], \tag{19}$$

$$B_2^2 = B_1^2 - \frac{\beta_x^2(s)\beta_z^2(s)\sigma_h^2(s)}{\beta^4\gamma^4\sigma_{x\beta}^4(s)\sigma_{z\beta}^4(s)\sigma_E^2}(\sigma_x^2(s)\sigma_z^2(s) - \sigma_E^2\eta_x^2(s)\eta_z^2(s)). \tag{20}$$

The total Touschek lifetime is obtained by averaging the positive and negative contributions of Eq. 5 along the ring.

1.2. TRACY3

TRACY is written in Turbo-Pascal programing language (Obrien, 1989) and was created at the Advanced Light Source (Nishimura, 1988) in the 90s for accelerator lattice design work, closed orbit calculations and particle tracking taken into account errors as multipolar field components and misalignments. The code has evolved over the years and has been translated in C and in C++ (Bengsston, 1997; Boege, 1999; Nadolski, 2002b; Zhang, 2013). The version of TRACY3 code used in this thesis is an improved version of TRACY code adapted for SOLEIL requirements. During the last fifteen years a great effort has been made at SOLEIL to improve the capabilities of TRACY for long-term tracking and for post-

processing as for example the implementation of Frequency Map Analysis. The parallelization of the code in the SOLEIL cluster has also been an important improvement to reduce the computation time, especially for long-term tracking of dynamic and momentum apertures (Zhang, 2013).

1.2.1. DIPOLE EDGE FOCUSING

In TRACY3 the edge focusing is expressed in terms of canonical variables $(\mathrm{x}, \mathrm{p_x}, \mathrm{z}, \mathrm{p_z})$ as follows (Forest, 1994 and 1998):

$$p_x = (1+\delta)x' = p_{x0} + \frac{1}{\rho}\tan(\theta/2)x_0, \tag{21}$$

$$p_z = (1+\delta)z' = p_{z0} - \frac{1}{\rho(1+\delta)}\tan(\theta/2 - \psi)z_0, \tag{22}$$

where $\mathrm{p_{x0}}$ $(\mathrm{p_{z0}})$ are the horizontal (vertical) canonical momenta at the entrance of the dipole edge region, $\mathrm{p_x}$ $(\mathrm{p_z})$ is the horizontal (vertical) canonical momentum at the exit, and $\mathrm{x_0}$ $(\mathrm{z_0})$ is the horizontal (vertical) coordinate at the entrance of the edge field region. This formulation includes additional energy dependence in the vertical plane, as a term $(1+\delta)$ (Forest, 1994). This term is only an approximation that needs to be introduced in small machines and was discussed already by Bengtsson for the ALS 196-meter circumference storage ring (Bengtsson, 1994). A complete and precise treatment of the chromatic term of a dipole is done in the code MADX-PTC when a rectangular dipole is integrated using the non-truncated Hamiltonian (Nadolski, 2009b). Hence, the transformation from one set of coordinates to the other one is not strictly equivalent to the model in ELEGANT in terms of momenta especially at large transverse amplitudes or energy offset.

1.2.2. DYNAMIC APERTURE

In TRACY3, the dynamic aperture is computed by pure tracking over 1,000 turns, number optimized using the convergence properties of the Frequency Map Analysis (Nadolski, 2001). The computation is performed by sampling the transverse plane and by tracking the particle around the closed orbit in four dimensions and assuming zero transverse momenta. To save time, the sampling rate of the horizontal and vertical amplitude follows a root square law, since the beam dynamics is more linear for small amplitudes than for large ones (Nadolski, 2001). This process is slower but more exhaustive than the DA computation approximation performed by ELEGANT. Nevertheless, the parallelization of the SOLEIL local version of TRACY3 in the SOLEIL cluster allows a significant increase of computation speed.

1.2.3. MOMENTUM APERTURE

The local momentum acceptance is computed in TRACY3 searching the minimum relative energy offset where the particle becomes lost using an energy step size to share the total energy offset range defined by lower and upper limits. Once the maximum stable energy offset is determined at a given location, the code starts the same process for the next element of the machine lattice.

1.2.4. TOUSCHEK LIFETIME CALCULATION FROM TRACY3 CODE

The Touschek lifetime is calculated in Matlab using the output results of TRACY3 in terms of optical functions and momentum acceptance. The total Touschek lifetime (τ_{Tous}) is defined by the combination of the half beam lifetime for the positive ($\tau^{\mathrm{p}}_{\mathrm{T}_{1/2}}$) and negative ($\tau^{\mathrm{n}}_{\mathrm{T}_{1/2}}$) momentum acceptances expressed as (Belgroune, 2003 and 2005; Zhang, 2013):

$$\frac{1}{\tau_{Tous}} = \frac{1}{2}\left(\frac{1}{\tau^{p}_{T_{1/2}}} + \frac{1}{\tau^{n}_{T_{1/2}}}\right). \tag{23}$$

To calculate the half Touschek beam lifetime, a simplified expression of the Piwinski formula is used, called Bruck formula (Bruck, 1966):

$$\frac{1}{\tau^{p,n}_{T_{1/2}}} = \left(\frac{r_0^2 cq}{8\pi e\gamma^3\sigma_l}\right)\frac{1}{C}\int_0^C \frac{\Sigma\left[\left(\frac{\varepsilon^{p,n}_{acc}(s)}{\gamma\sigma'_x(s)}\right)^2\right]}{\sigma_x(s)\sigma_z(s)\sigma'_x(s)\left(\varepsilon^{p,n}_{acc}(s)\right)^2} ds, \tag{24}$$

where q = Ne is the bunch charge, e is the electron charge, N the number of electrons per bunch, $\sigma_{\mathrm{x}}(\mathrm{s})$, $\sigma_{\mathrm{x}}'(\mathrm{s})$, $\sigma_{\mathrm{z}}(\mathrm{s})$ are the total beam sizes and divergence in horizontal and vertical planes, $\varepsilon^{\mathrm{p,n}}_{\mathrm{acc}}(\mathrm{s})$ is the positive (p) or negative (n) local s-dependent momentum acceptance along the ring and σ_{l} is the bunch length at zero current. $\Sigma(\mathrm{x})$ is a special function defined by

$$\Sigma(x) = \int_0^1 \left(\frac{1}{u} - \frac{1}{2} ln\frac{1}{u} - 1\right) e^{-x/u} du. \tag{25}$$

Then, the calculation of the beam lifetime is obtained by averaging the positive and negative contributions as in ELEGANT.

The Bruck approximation is valid for flat beams and non-relativistic transverse momenta.

2. BENCHMARKING BETWEEN CODES USING A SIMPLIFIED LATTICE

2.1. SOLEIL2009 LATTICE: MAIN PARAMETERS

The SOLEIL2009 storage ring lattice is based on a double bend lattice with non-zero dispersion everywhere and exhibits a 4-fold symmetry. With an electron energy of 2.75 GeV, its strong focusing lattice enables the reach of a natural emittance of 3.6 nm·rad. It provides three different kinds of straight sections to host insertion devices: 4 long straight sections (LSS) of 12 m, 12 medium straight section (MSS) of 7 m, and 8 small straight sections (SSS) of 3.6 m. The injection section is located in one LSS and two MSS host the four RF-cavities. Ten families of quadrupoles and 10 families of sextupoles compose the lattice. The sextupoles were optimized in order to reduce the phase dependent driving terms excited by the sextupoles at first order and to control the linear chromaticities and the tune shifts with amplitude (second order phase independent driving terms). The main parameters of the lattice SOLEIL2009 are summarized in Table 1.

2.2. OPTICAL FUNCTIONS

For this first part of the benchmarking, the lattice names are SOLEIL2009.lat for TRACY3 code and SOLEIL2009.lte for ELEGANT code.

The comparison of the horizontal and vertical betatron functions and horizontal dispersion functions, computed by ELEGANT version 25.1.0 and TRACY3 over one super-period of the SOLEIL storage ring lattice of 2009, are given in Figure 3a, Figure 3b, and Figure 4, respectively. The agreement is very good in all cases.

Parameters	Values
Energy E (GeV)	2.739
Lorentz Factor γ	5360.2
Natural Emittance ε_x (nm·rad)	3.60
Magnetic Rigidity $(B_0\rho)$ (T·m)	9.14
Circumference C (m)	354.097
Symmetry/Super Period	4/4
Horizontal / Vertical Betatron Tunes (ν_x/ν_z)	18.200/10.300
Horizontal / Vertical Natural Chromaticities $(\xi_x^{nat}/\xi_z^{nat})$	-53/-23
Horizontal / Vertical Corrected Chromaticities (ξ_x/ξ_z)	0/0
Momentum Compaction Factor (1/2 order) (α/α_2)	$4.155\ 10^{-4}/4.6\ 10^{-3}$
Energy Spread σ_E	$1.034\ 10^{-3}$
Dipole Number/Angle (°)/Field (T)	32/11.25/1.71
Quadrupole Number/Family Number/Max. Field (T/m)	160/10/23
Sextupole Number/Family Number/Max. Field (T/m^2)	120/10/320
Damping Partition Number H/V/L	0.995/1.000/2.005
Energy Loss per Turn U_0 (keV)	928.9
RF-Frequency f_{RF} (MHz)	352.2
Harmonic Number h	416
Number of Straight Sections (LSS/MSS/SSS)	4/12/8
Horizontal Betatron Function β_x (LSS/MSS/SSS) (m)	10.87/4.18/18.19
Vertical Betatron Function β_z (LSS/MSS/SSS) (m)	8.00/1.73/1.94
Horizontal Dispersion Function η_x (LSS/MSS/SSS) (m)	0.22/0.15/0.24

Table 1: Physical parameters of the SOLEIL2009 storage ring lattice (obtained from TRACY3 code).

(a)

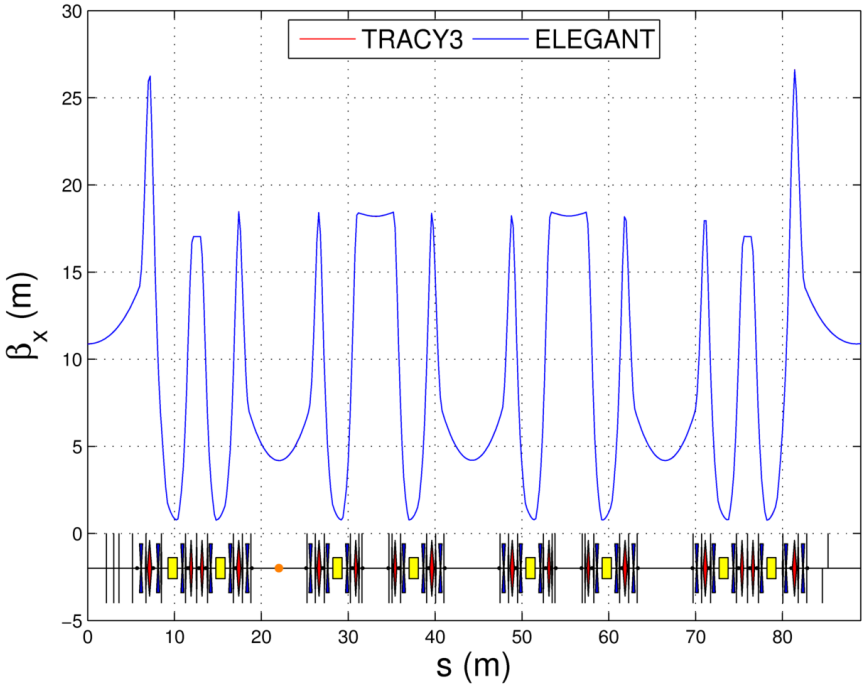

(b)

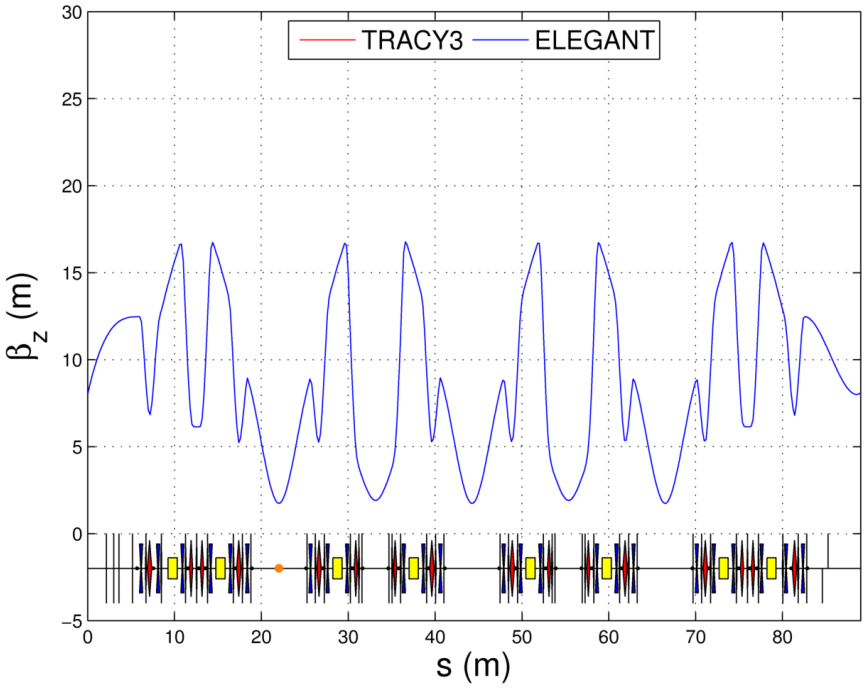

Figure 3: Comparison of the horizontal (a) and vertical (b) betatron functions (β_x, β_z) computed by TRACY3 (red line) and the ELEGANT version 25.1.0 (blue line) over one quarter of the SOLEIL2009 storage ring lattice.

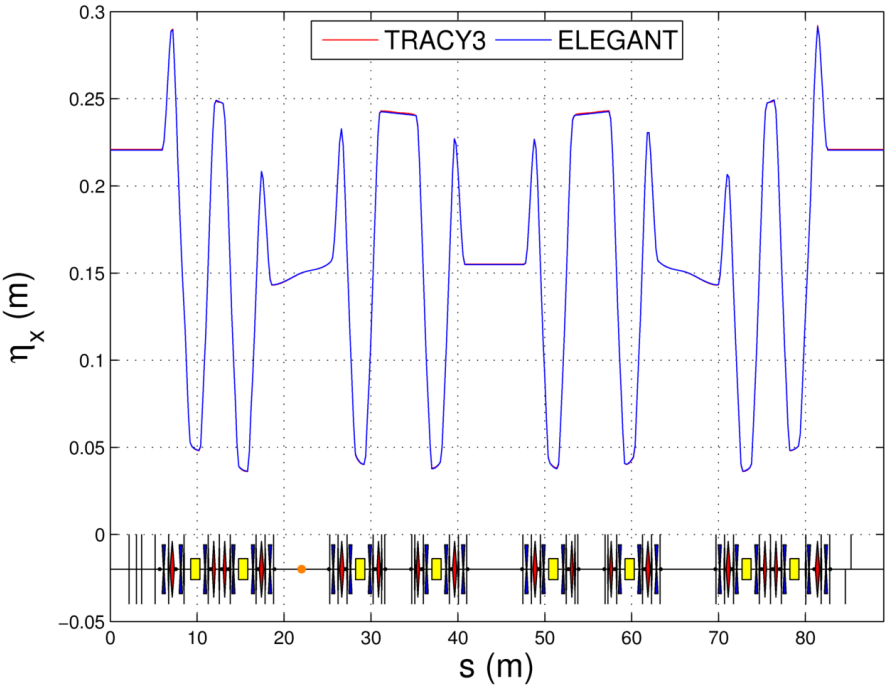

Figure 4: Comparison of the horizontal dispersion function (η_x) computed by TRACY3 (red line) and the ELEGANT version 25.1.0 (blue line) over one quarter of the SOLEIL2009 storage ring lattice.

2.3. Tunes and Chromaticities

Table 2 shows the horizontal and vertical tunes (ν_x, ν_z), the horizontal emittance (ε_x) and the horizontal and vertical chromaticities (ξ_x, ξ_z) computed by the ELEGANT version 25.1.0 and TRACY3 codes. The parameters agree with the precision of the codes as expected except for the chromaticity in the vertical plane: there is a discrepancy of 1.4 units.

Parameters	ELEGANT 25.1.0	TRACY3
(ν_x, ν_z)	(18.200,10.300)	(18.200,10.300)
ε_x (nm·rad)	3.567	3.596
(ξ_x, ξ_z)	(-0.004,1.405)	(0.006,-0.035)

Table 2: Comparison of the horizontal and vertical tunes (ν_x, ν_z), the horizontal emittance (ε_x) and the horizontal and vertical chromaticities (ξ_x, ξ_z) computed by the ELEGANT version 25.1.0 and TRACY3 codes. The discrepancy of the vertical chromaticity is due to a different modeling of the dipole edge focusing implemented in the original version of ELEGANT and TRACY3 codes. This is developed in the following part.

2.4. Modified ELEGANT's Dipole Edge Focusing Model

As a result of the discrepancy in the vertical chromaticity shown in Table 2, the ELEGANT version 25.1.0 code was modified and recompiled in the SOLEIL cluster in June 2014. Eq.

26 and Eq. 27 show the definition of the new ELEGANT version 26.0.2 upgraded at Synchrotron SOLEIL:

$$x' = \frac{p_x}{(1+\delta)} = x'_0 + \frac{1}{\rho(1+\delta)} \tan\left(\theta/2\right) z_0, \tag{26}$$

$$z' = \frac{p_z}{(1+\delta)} = z'_0 - \frac{1}{\rho(1+\delta)^2} \tan\left(\theta/2 - \psi\right) z_0. \tag{27}$$

The next section is dedicated to demonstrate the agreement between TRACY3 and the local ELEGANT version 26.0.2 studying the tune shifts with transverse amplitudes and energy.

2.5. Tune Shifts with Transverse Amplitudes and Energy

For benchmarking nonlinear dynamics, a method is to compare the tune shifts with amplitudes and energy. More generally, comparison of frequency maps will exhibit the full transverse dynamics, representing the footprint of a particle in the tune space for any stable transverse amplitude and energy offset.

It is convenient to write the transverse tune shifts in terms of angle and action coordinates to easily solve the equations of motion (Goldstein, 1980). The angles (φ_x, φ_z) for the linear motion are the betatron phase advance and actions (J_x, J_z) are the invariant of the motion.

So that the horizontal and vertical tune shifts with amplitudes $(\nu_x(J_x, J_z), \nu_z(J_x, J_z))$ and energy $((\nu_x(\delta), \nu_z(\delta))$ are expressed as:

$$\nu_x(J_x, J_z) = \nu_{x0} + a_{xx}J_x + a_{xz}J_z + O(2) + \cdots \tag{28}$$

$$\nu_z(J_x, J_z) = \nu_{z0} + a_{zx}J_x + a_{zz}J_z + O(2) + \cdots \tag{29}$$

$$\nu_x(\delta) = \nu_{x0} + \xi_x\delta + O(2) + \cdots \tag{30}$$

$$\nu_z(\delta) = \nu_{z0} + \xi_z\delta + O(2) + \cdots \tag{31}$$

where, ν_{x0} and ν_{z0} are the horizontal and vertical tunes given by the linear optics, the real coefficients a_{xx}, a_{xz} express the variation of the horizontal and vertical tunes with respect to the action J_x, $a_{zx} = a_{xz}$, a_{zz} with respect to the action J_z, and δ is the relative energy offset. These coefficients depend on nonlinear terms such as sextupole strengths and other multipolar field components. In addition, ξ_x and ξ_z define the variation of the tune with the relative energy offset at first order in both planes, that is the horizontal and vertical chromaticities respectively.

ELEGANT features several parameters for the dipole definitions (Borland, 2012). The parameter EDGE_ORDER allows the control of the order of the transfer matrix taken into account during computations: for value equal to 1 the dipole is approximated as a thick lens using a first-order transfer matrix; for value equal to 2 the second order Brown transfer matrix (Brown, 1982) is introduced. To compute the transverse tune shifts, the

parameter SQRT_ORDER controls the expansion of the square root with δ of the non-canonical coordinate x' (Eq. 26) defined as follows:

$$x'(p_x, p_z) = \frac{p_x}{\sqrt{(1+\delta)^2 - p_x^2 - p_z^2}}, \tag{32}$$

where p_x and p_z are the horizontal and vertical canonical momentum of the fringe field, respectively. The default value 0 takes into account the full square root and the value 1 is related to the first order of its Taylor expansion with δ, that is:

$$x'(p_x, p_z) = \frac{p_x}{\sqrt{(1+\delta)^2 - p_x^2 - p_z^2}} \approx p_x \left(1 - \delta + \frac{\delta^2}{2} + \cdots\right). \tag{33}$$

The dipole configurations tested to compare the tune shifts with amplitudes and energy between the two versions of ELEGANT and TRACY3 codes are:

- ELEGANT version 25.1.0 with EDGE_ORDER=1 and SQRT_ORDER=0, considering the edge effects of a dipole thick lens (configuration implemented per default).
- ELEGANT version 25.1.0 with EDGE_ORDER=1 and SQRT_ORDER=1, taking into account the edge effects of a dipole thick lens and the expansion of the square root with δ of the non-canonical coordinate x'.
- ELEGANT version 25.1.0 with EDGE_ORDER=2 and SQRT_ORDER=0, considering the dipole edge effect approximated as a second order Brown transfer matrix.
- ELEGANT version 25.1.0 with EDGE_ORDER=2 and SQRT_ORDER=1, considering the dipole edge effect as a second order Brown transfer matrix and the expansion of the square root with δ of the non-canonical coordinate x'.
- ELEGANT version 26.0.2 with EDGE_ORDER=1 and SQRT_ORDER=0, considering the edge effects of a dipole thick lens (configuration implemented per default).
- ELEGANT version 26.0.2 with EDGE_ORDER=1 and SQRT_ORDER=1, taking into account the edge effects of a dipole thick lens and the expansion of the square root with δ of the non-canonical coordinate x'.

The results of the tune shifts with the horizontal and vertical amplitudes and energy are shown in Figure 5, Figure 6 and Figure 7, respectively.

Figure 5 shows the horizontal and vertical tune shifts with the horizontal amplitude for all dipole configurations previously described. Looking carefully, there is a good agreement of the horizontal and vertical tune shifts with horizontal amplitude between both versions of ELEGANT and TRACY3 codes. There is a small influence of the choice of EDGE_ORDER and SQRT_ORDER parameters.

Figure 6 shows the horizontal and vertical tune shifts with the vertical amplitude for the same dipole configurations case previously plotted in Figure 5. The agreement is good and expected as well because both codes model similarly the sextupoles and have similar transverse dependence.

Concerning the horizontal tune shifts with the energy offset of Figure 7a, the horizontal case agrees with the results of TRACY3 between -4 % and 6 %. This range is considered acceptable to use ELEGANT inside MOGA-ELEGANT because it stays within the interest area for the energy acceptance range of the SOLEIL storage ring. Beyond this range, the results disagree due to the different coordinates used in both codes as explained previously.

In the vertical plane (Figure 7b), the tune shifts with energy offset with the corrected version of ELEGANT 26.0.2 are very close to the results obtained with TRACY3: the acceptable range of agreement goes from -5 % to 3 % approximately. Looking carefully, among all models, the closest one is the model characterized by a first-order Brown formula and the full square root of the coordinate x', that is, the case with EDGE_ORDER=1 and SQRT_ORDER=0 computed by ELEGANT 26.0.2.

These results are confirmed in Table 3, where the horizontal and vertical tunes (ν_x,ν_z) the horizontal emittance (ε_x) and the horizontal and vertical chromaticities (ξ_x,ξ_z) computed by the ELEGANT versions and TRACY3 codes are compared taken into account different configurations of EDGE_ORDER and SQRT_ORDER parameters. It can be seen that 1) the correction of the dipole edge focusing in the ELEGANT version 26.0.2 corrects the discrepancy in the vertical chromaticity and 2) the second order Brown formula enables to recover the right vertical chromaticity in the ELEGANT version 25.1.0. However, the model with the second order Brown formula cannot be used for long-term tracking because it is not symplectic. Indeed, it would introduce some fake damping and time dependence (turns) of the tunes.

Hence, in conclusion, applying the same energy dependence as in TRACY3 code allows us to get a good agreement to keep long-term tracking correct.

Parameter	**ELEGANT 25.1.0**	**ELEGANT 25.1.0**	**ELEGANT 26.0.2**	**TRACY3**
	EDGE_ORDER=1 SQRT_ORDER=0	EDGE_ORDER=2 SQRT_ORDER=0	EDGE_ORDER=1 SQRT_ORDER=0	
(ν_x, ν_z)	(18.200, 10.300)	(18.200, 10.300)	(18.200, 10.300)	(18.200, 10.300)
ε_x (nm·rad)	3.567	3.567	3.567	3.596
(ξ_x, ξ_z)	(-0.004, 1.405)	(0.006, -0.03)	(0.004, -0.071)	(0.006, -0.035)

Table 3: Comparison of the horizontal and vertical tunes (ν_x, ν_z), the horizontal emittance (ε_x) and the horizontal and vertical chromaticities (ξ_x, ξ_z) computed by the two ELEGANT versions and TRACY3 including different configurations of EDGE_ORDER and SQRT_ORDER parameters.

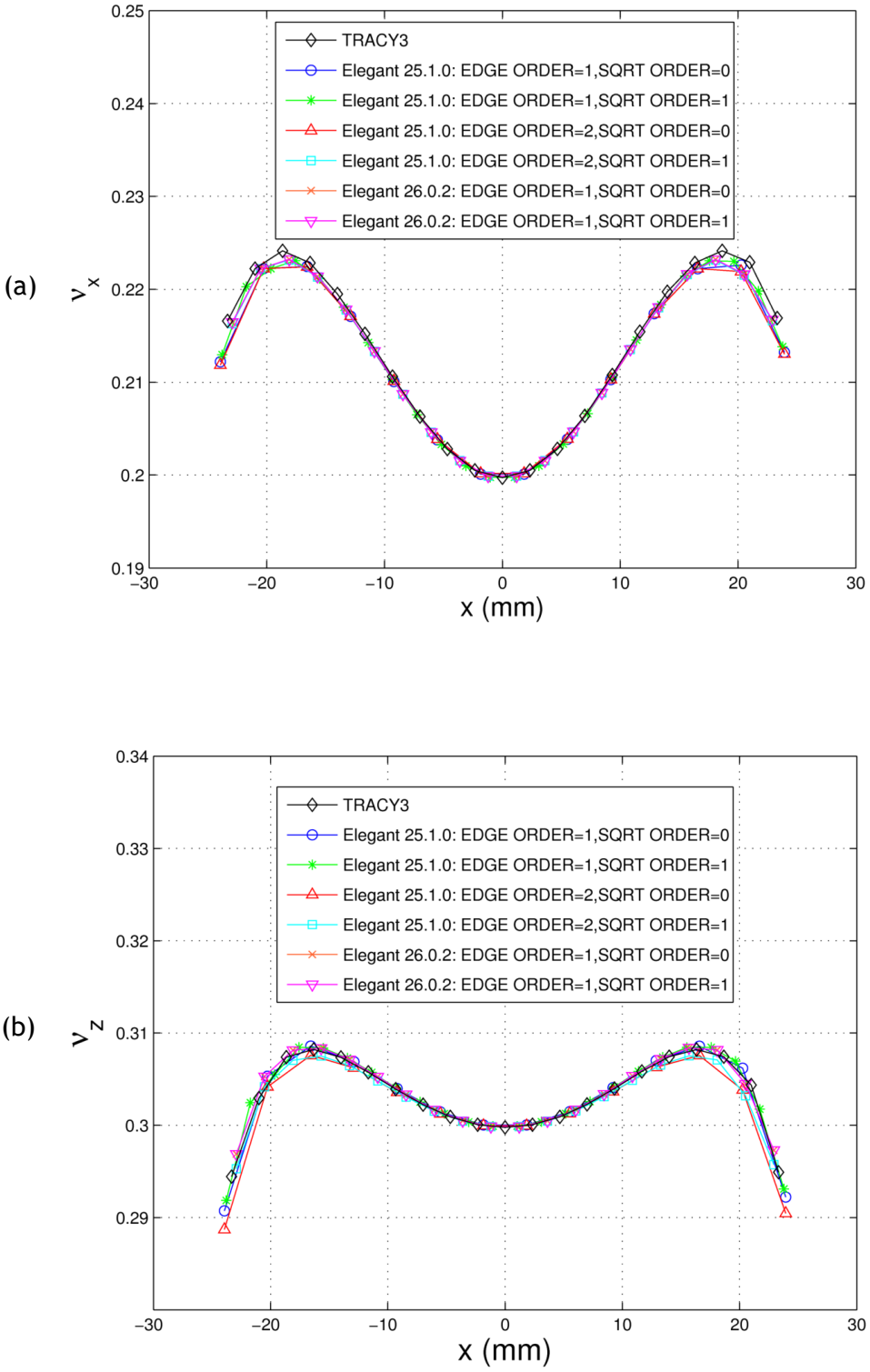

Figure 5: Comparison of the horizontal (a) and the vertical (b) tune shifts with the horizontal amplitude between TRACY3 (black ◊) and different configurations of the dipole edge focusing (EDGE_ORDER) and of the square root with δ of the non-canonical coordinate x' (SQRT_ORDER) of ELEGANT version 25.1.0 and ELEGANT version 26.0.2: ELEGANT 25.1.0 with EDGE_ORDER 1 and SQRT_ORDER 0 (blue o); ELEGANT 25.1.0 with EDGE_ORDER 1 and SQRT_ORDER 1 (green *), ELEGANT 25.1.0 with EDGE_ORDER 2 and SQRT_ORDER 0 (red Δ); ELEGANT 25.1.0 with EDGE_ORDER 2 and SQRT_ORDER 1 (cyan □); ELEGANT 26.0.2 with EDGE_ORDER 1 and SQRT_ORDER 0 (orange x); ELEGANT 26.0.2 with EDGE_ORDER 1 and SQRT_ORDER 1 (magenta ∇). 4D-tracking parameters: 1,000 turns, a range of [-0.030, 0.030] m in the horizontal plane and 30 points.

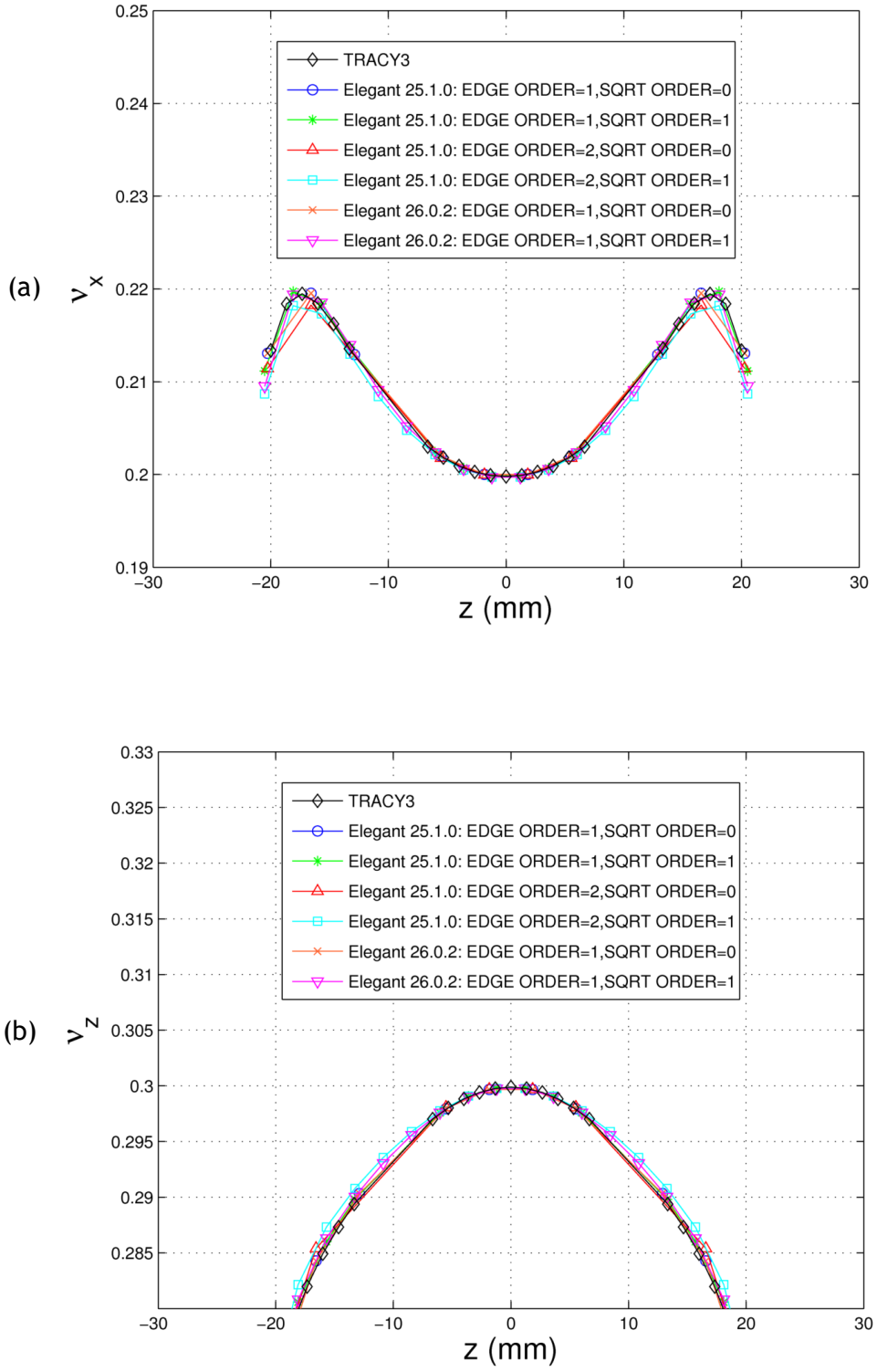

Figure 6: Comparison of the horizontal (a) and the vertical (b) tune shifts with the vertical amplitude between TRACY3 (black ◊) and different configurations of the dipole edge focusing (EDGE_ORDER) and of the square root with δ of the non-canonical coordinate x' (SQRT_ORDER) of ELEGANT version 25.1.0 and ELEGANT version 26.0.2: ELEGANT 25.1.0 with EDGE_ORDER 1 and SQRT_ORDER 0 (blue o); ELEGANT 25.1.0 with EDGE_ORDER 1 and SQRT_ORDER 1 (green *), ELEGANT 25.1.0 with EDGE_ORDER 2 and SQRT_ORDER 0 (red Δ); ELEGANT 25.1.0 with EDGE_ORDER 2 and SQRT_ORDER 1 (cyan □); ELEGANT 26.0.2 with EDGE_ORDER 1 and SQRT_ORDER 0 (orange x); ELEGANT 26.0.2 with EDGE_ORDER 1 and SQRT_ORDER 1 (magenta ∇). 4D-tracking parameters: 1,000 turns, a range of [-0.030, 0.030] m in the vertical plane and 30 points.

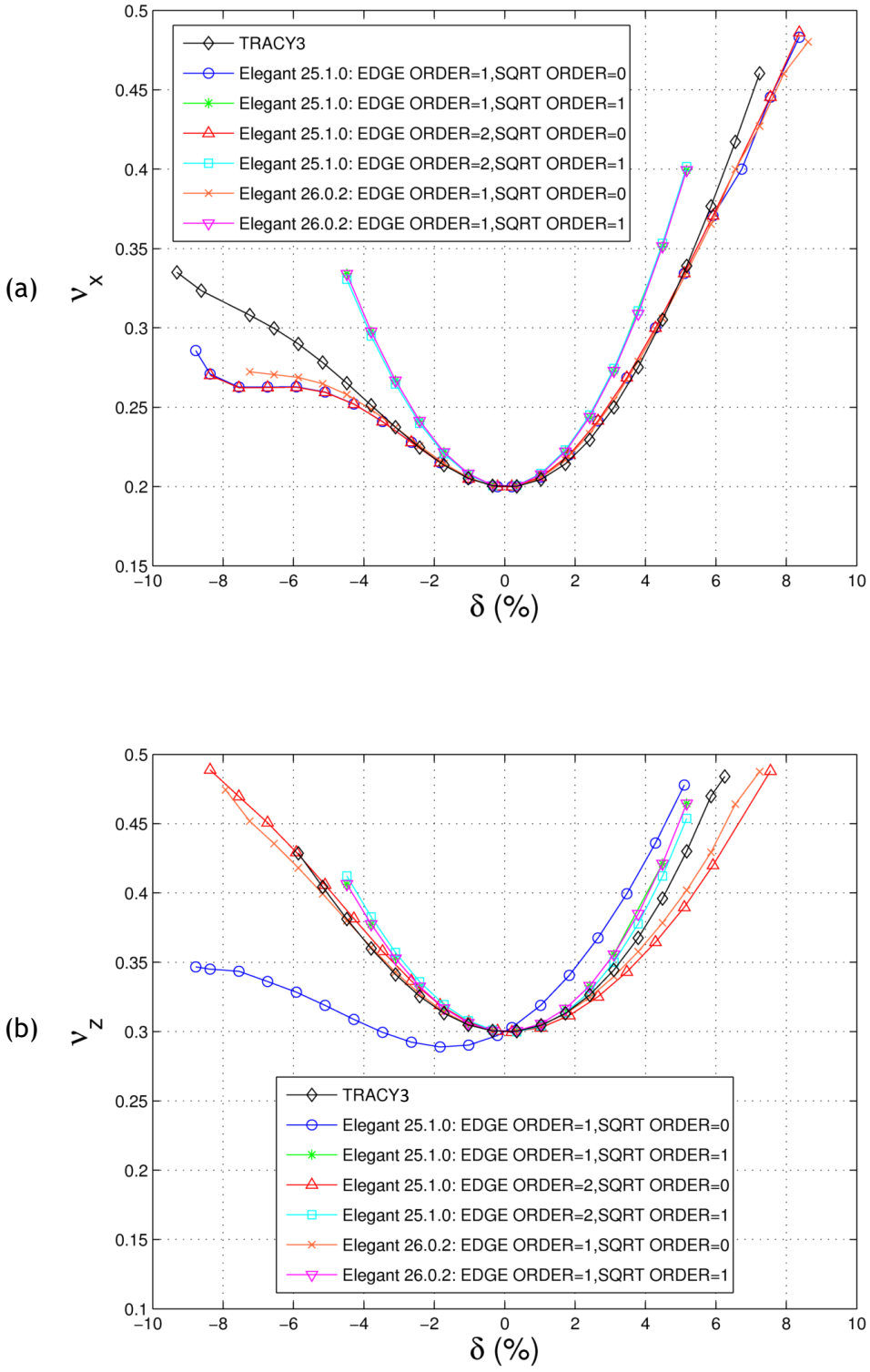

Figure 7: Comparison of the horizontal (a) and the vertical (b) tune shifts with the energy offset between TRACY3 (black ◊) and different configurations of the dipole edge focusing (EDGE_ORDER) and of the square root with δ of the non-canonical coordinate x' (SQRT_ORDER) of ELEGANT version 25.1.0 and ELEGANT version 26.0.2: ELEGANT 25.1.0 with EDGE_ORDER 1 and SQRT_ORDER 0 (blue o); ELEGANT 25.1.0 with EDGE_ORDER 1 and SQRT_ORDER 1 (green *), ELEGANT 25.1.0 with EDGE_ORDER 2 and SQRT_ORDER 0 (red Δ); ELEGANT 25.1.0 with EDGE_ORDER 2 and SQRT_ORDER 1 (cyan □); ELEGANT 26.0.2 with EDGE_ORDER 1 and SQRT_ORDER 0 (orange x); ELEGANT 26.0.2 with EDGE_ORDER 1 and SQRT_ORDER 1 (magenta ∇). 4D-tracking parameters: 1,000 turns, a range of [-10, 10] % m in the horizontal plane and 30 points.

3. BENCHMARKING USING A LATEST LATTICE OF THE SOLEIL STORAGE RING: SOLEIL2013

3.1. SOLEIL2013 LATTICE: MAIN PARAMETERS

The SOLEIL2013 present lattice will be from now on used in the study for tracking calculations and comparison. The lattice was modified in 2013 as a significant upgrade of the long straight section 13 (Loulergue, 2010). In order to accommodate two in-vacuum 5.5 mm full gap insertion devices, a quadrupole triplet was added in the middle of the straight section in order to obtain a double low-vertical betatron function at the two canted in-vacuum insertion device locations and breaks down the 4-fold symmetry. Figure 8 shows the optics of SOLEIL2009 lattice for the straight section 13 and Figure 9 shows the optics of the upgraded SOLEIL2013 lattice for the same straight section. In SOLEIL 2013, the numbers of quadrupoles, sextupoles, dipolar correctors and BPMs were also increased. There are now 11 families for both quadrupoles and sextupoles.

Table 4 summarizes the main parameters of the optics and Figure 10 displays the optical functions along the full ring. Furthermore, the physical acceptances and multipolar field components are not taken into account for simplicity.

Parameters	Values
Energy E (GeV)	2.739
Lorentz Factor γ	5360.2
Natural Emittance ε_x (nm·rad)	3.90
Magnetic Rigidity $(B_0\rho)$ (T·m)	9.14
Circumference C (m)	354.097
Symmetry/Super Period	1/1
Horizontal / Vertical Betatron Tunes (ν_x/ν_z)	18.155,10.228
Horizontal / Vertical Natural Chromaticities $(\xi_x^{nat}/\xi_z^{nat})$	-53/-19
Horizontal / Vertical Corrected Chromaticities (ξ_x/ξ_z)	1.2/2.0
Momentum Compaction Factor (1/2 order) (α/α_2)	$4.2\ 10^{-4}/4.6\ 10^{-3}$
Energy Spread σ_E	$1.029\ 10^{-3}$
Dipole Number/Angle (°)/Field (T)	32/11.25/1.71
Quadrupole Number/Family Number/Max. Field (T/m)	163/11/23
Sextupole Number/Family Number/Max. Field (T/m^2)	120/11/320
Damping Partition Number H/V/L	0.995/1.000/2.005
Energy Loss per Turn U_0 (keV)	928.9
RF-Frequency f_{RF} (MHz)	352.2
Harmonic Number h	416
Number of Straight Sections (LSS/MSS/SSS)	4/12/8
Horizontal Betatron Function β_x (LSS/MSS/SSS) (m)	11.54/4.2/14.15
Vertical Betatron Function β_z (LSS/MSS/SSS) (m)	7.91/2.28/2.74
Horizontal Dispersion Function η_x (LSS/MSS/SSS) (m)	0.22/0.17/0.22

Table 4: Physical parameters of the SOLEIL2013 storage ring lattice obtained from TRACY3 code.

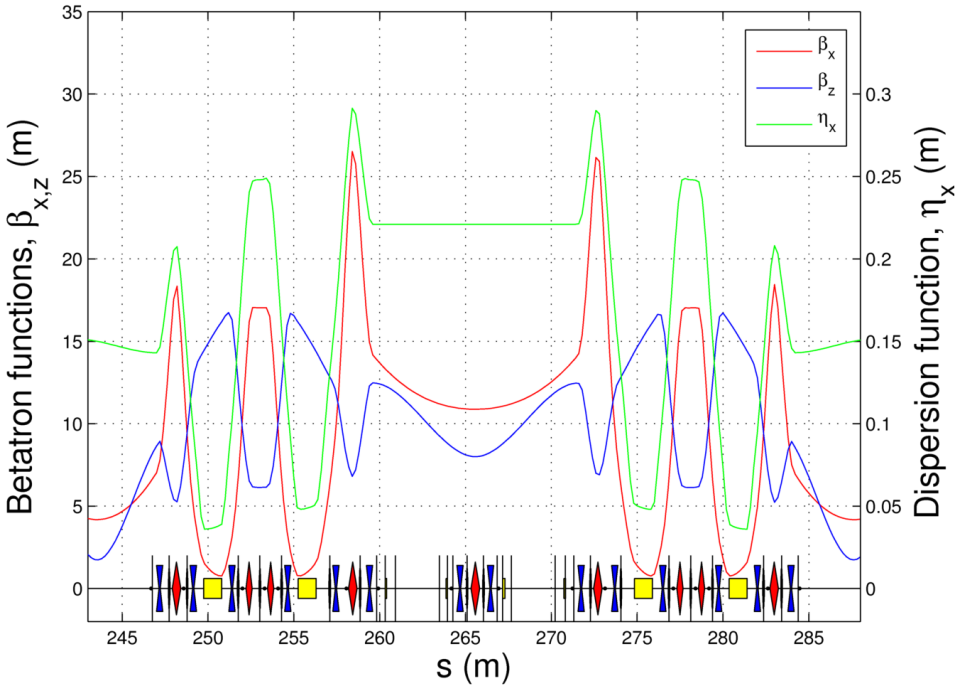

Figure 8: Horizontal and vertical betatron functions (β_x, β_z) and the horizontal dispersion function (η_x) of the SOLEIL2009 storage ring lattice in the long straight section 13 computed by TRACY3. The triplet of quadrupoles located at the middle of the straight section is switched off.

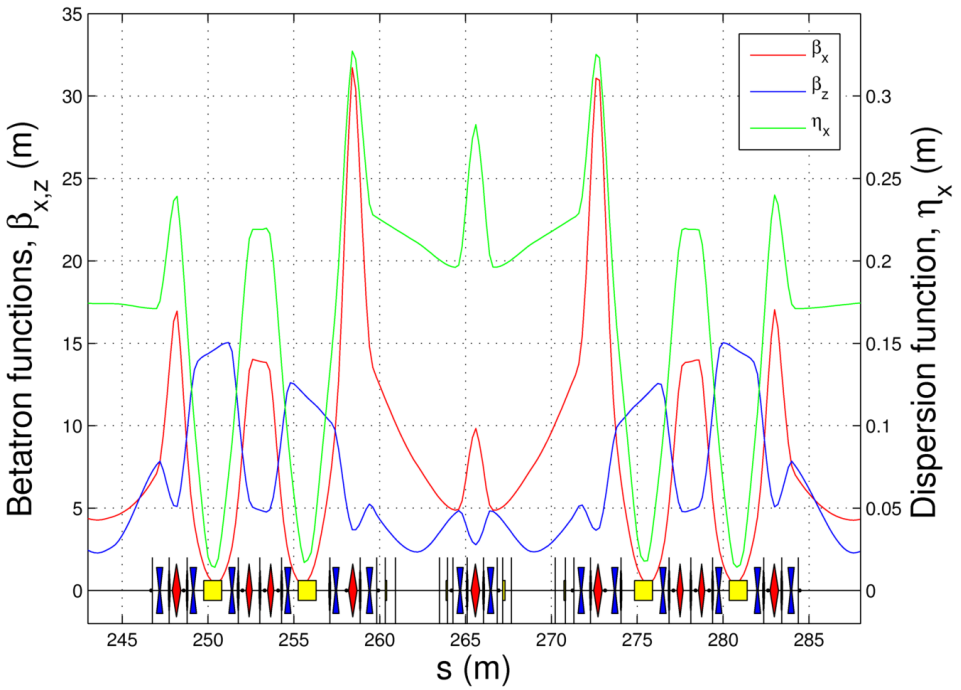

Figure 9: Horizontal and vertical betatron functions (β_x, β_z) and the horizontal dispersion function (η_x) of the upgraded SOLEIL2013 storage ring lattice in the long straight section 13 computed by TRACY3. β_z is reduced in the middle of both half of the long straight section to accommodate the two in-vacuum 5.5 mm full gap insertion devices.

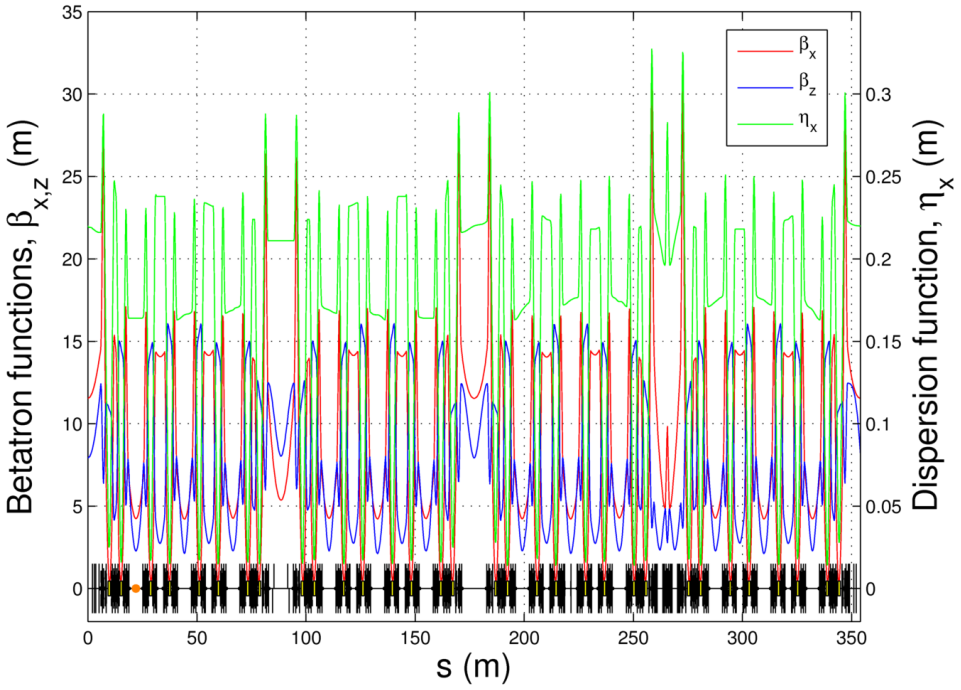

Figure 10: Optical functions of the SOLEIL2013 nominal lattice along the ring computed by TRACY3. The upgraded long straight section 13 is shown in detail in Figure 9 (the middle is located at 265.8 m).

From now on, the only version of ELEGANT used is version 26.0.2 introducing the local dipole edge field correction of Eq. 26 and Eq. 27. Table 5 shows the comparison between ELEGANT and TRACY3 for the horizontal and vertical tunes (ν_x, ν_z), the horizontal emittance (ε_x) and the horizontal and vertical chromaticities (ξ_x, ξ_z) of the SOLEIL2013 lattice. All parameters agree as expected. The small differences are due to the different models used by both codes as discussed earlier.

Parameters	ELEGANT 26.0.2	TRACY3
(ν_x, ν_z)	(18.157,10.229)	(18.155,10.228)
ε_x $(\mathrm{nm} \cdot \mathrm{rad})$	3.873	3.902
(ξ_x, ξ_z)	(1.852,1.935)	(1.757,1.959)

Table 5: Comparison of the horizontal and vertical tunes (ν_x,ν_z) the horizontal emittance (ε_x) and the horizontal and vertical chromaticities (ξ_x,ξ_z) computed by the ELEGANT and TRACY3 for the SOLEIL2013 lattice.

3.2. Dynamic Aperture

The dynamic apertures computed by ELEGANT and TRACY3 codes are compared in terms of amplitude step size and number of turns.

3.2.1. ELEGANT: OPTIMIZATION OF STEP SIZE PARAMETER

Figure 11a compares the dynamic aperture of the SOLEIL2013 lattice calculated by TRACY3 and the one calculated by ELEGANT for different values of the step size in the horizontal plane and 4D-tracking. The parameters taken into account by ELEGANT and TRACY3 codes to compute the DA are listed in Table 6. It should be noted that ELEGANT excludes the particles trapped in a resonance island on the border of the dynamic aperture applying a clipping process. This explains why particles with vertical amplitude larger than 12 mm are discarded. The conclusion of this study is that ELEGANT results agree well with TRACY3 ones for an amplitude step size of 31.

ELEGANT			**TRACY3**	
Parameters	**Values**		**Parameters**	**Values**
Number of Turns	1,000		Number of Turns	1,000
Number of Lines	21		Horizontal Range (m)	(-0.035, 0.035)
Horizontal Range (m)	(-0.035, 0.035)		Vertical Range (m)	(0.000, 0.020)
Vertical Range (m)	(0.000, 0.020)		Number of Points in H. Plane	201
Step Back (*n_split*)	1		Number of Points in V. Plane	101
Number of Subdivisions (*split_fraction*)	10			

Table 6: Main parameters used by ELEGANT (left) and TRACY3 (right) codes to compute the dynamic aperture.

3.2.2. ELEGANT: OPTIMIZATION OF NUMBER OF TURNS

Figure 11b compares the dynamic aperture computed by TRACY3 with 1,000 turns and ELEGANT for different number of turns of the SOLEIL2013 storage ring lattice. The step size is 31 and 4D-tracking computation is taken into account. As a result, the computation of the dynamic aperture does not change for numbers of turns beyond 600 turns for 4D-tracking.

3.2.3. CONCLUSION

As conclusion, the case with amplitude step size equal to 31 and 600 turns agrees well enough with the dynamic aperture computed by TRACY3 code.

(a)

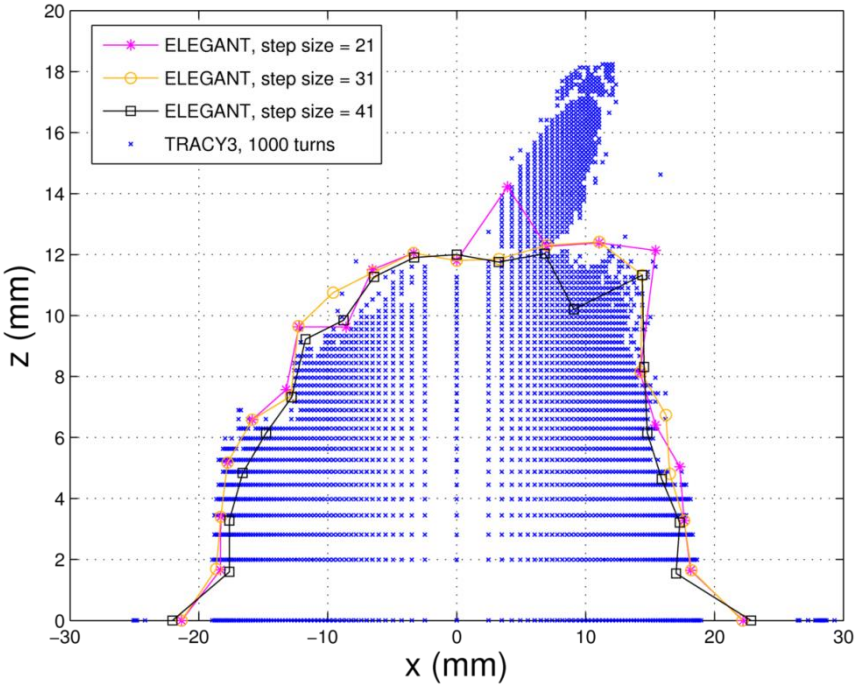

(b)

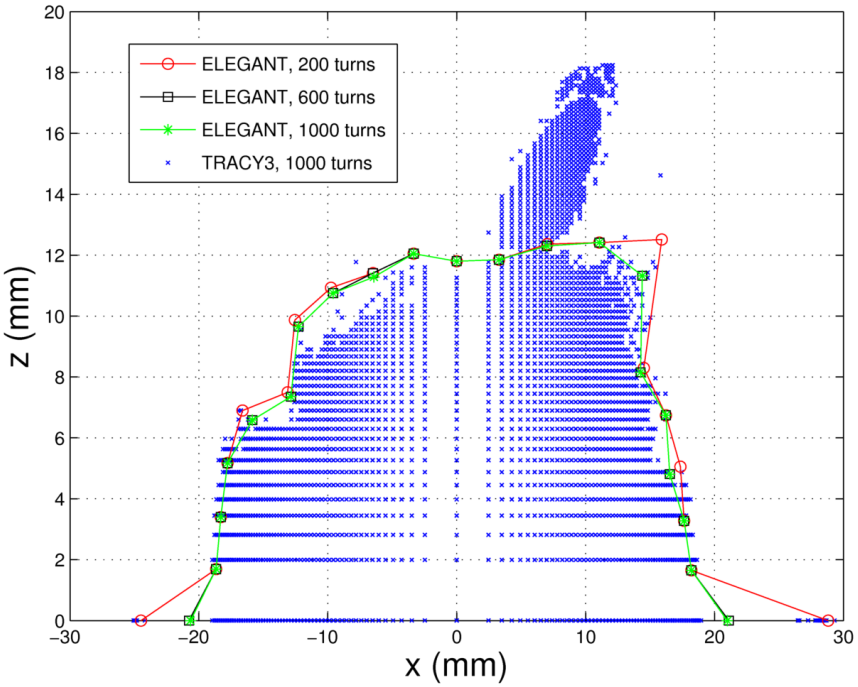

Figure 11: Comparison of the dynamic aperture of the SOLEIL2013 lattice calculated by TRACY3 with 1,000 turns (blue □)) and ELEGANT with 4D-tracking using parameters of Table 6 for different ELEGANT step sizes (a) and number of turns (b). a) The step sizes taken into account by ELEGANT are 21 (magenta *), 31 (orange o), 41 (black □) and 51 (green ∇) and the number of turn is 1,000. b) The number of turns taken into account is 200 turns (red o), 600 turns (black □) and 1,000 turns (green *) and the step size is 31.

3.3. MOMENTUM APERTURE

This type of calculation is much more time consuming that the computation of the first figure of merit, the dynamic aperture. Therefore it is even more critical to determine the ELEGANT parameters to obtain the momentum aperture as quickly as possible. For these reasons, the momentum aperture will be only computed at the position of the most nonlinear elements that is to say the sextupole magnets for this study case.

The computation of the momentum aperture performed by ELEGANT depends mainly on two parameters (Borland, 2012):

1. The number of subdivisions. The process that refines the identification of the particles lost divides the previous energy step in a certain number of subdivisions: when the energy of the lost particle is found, the second method goes back by a number of energy offsets defined by the user and splits the last division in a user-defined number of subdivisions.
2. The number of turns chosen to perform the computation.

3.3.1. OPTIMIZATION OF ENERGY STEP SIZE AND SUBDIVISIONS

Figure 12a compares the local momentum aperture of the SOLEIL2013 lattice calculated by ELEGANT and TRACY3 codes using 6D-tracking with 2.665 MV for different energy step sizes to search the energy of the lost particles: 0.1 % and 0.25 %. The parameters used in both codes to compute the momentum aperture are listed in Table 7.

The positive local momentum acceptance of the case ELEGANT with an energy step size of 0.1 % is much closer to the TRACY3 results than the one with an energy step size of 0.25 %. This was expected because the range of 0.1 % is smaller than the other one and is exactly the same as TRACY3. Hence, it is desirable to use an energy offset of 0.1 % to obtain similar local momentum apertures as TRACY3.

ELEGANT			TRACY3	
Parameters	**Values**		**Parameters**	**Values**
Number of Turns	1,000		Number of Turns	1,000
Initial Conditions (x_0, z_0) (m)	(10^{-6}, 10^{-4})		Initial Conditions (x_0, z_0) (m)	(10^{-6}, 10^{-4})
Energy Range (%)	(-10, 10)		Energy Range (%)	(-10, 10)
Step Back	1		Step Size (%)	0.1
Subdivision Factor	10			

Table 7: Main parameters used in ELEGANT and TRACY3 codes to compute the local momentum aperture of SOLEIL2013 lattice shown in Figure 12.

(a)

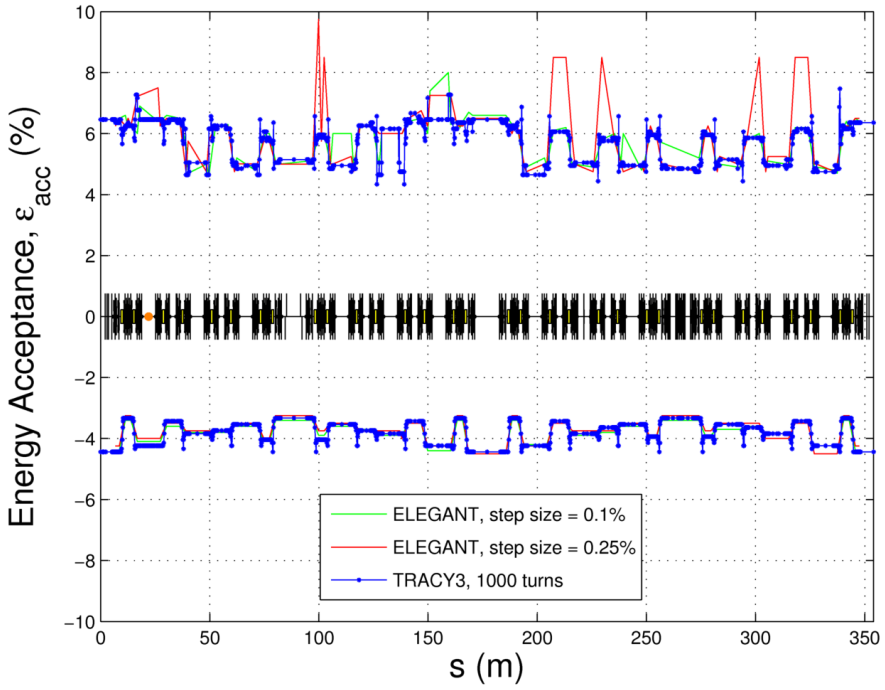

(b)

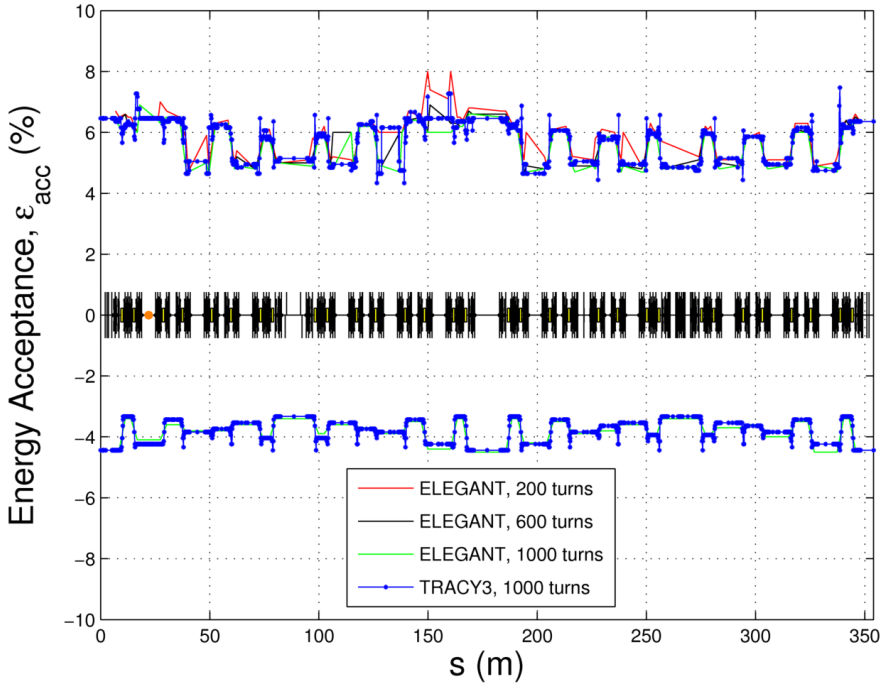

Figure 12: Comparison of the local momentum aperture of the SOLEIL2013 lattice calculated by TRACY3 and ELEGANT codes using 6D-tracking and a RF-voltage of 2.665 MV for different ELEGANT energy step sizes (a) and number of turns (b). In both figures the TRACY3 results (blue line) are computed with 1,000 turns and an energy step size of 0.1%. a) The ELEGANT steps size is 0.1 % (green line) and 0.25 % (red line) and the number of turns is 1,000. b) The number of turns used by ELEGANT is 200 turns (red line), 400 turns (black line) and 1,000 turns (green line) and the energy step size is 0.1 %. 6D-tracking parameters of Table 7.

3.3.1. SELECTION OF NUMBER OF TURNS

Figure 12b shows the comparison of the local momentum aperture of the SOLEIL2013 lattice obtained by TRACY3 and ELEGANT codes for different values of turns. 6D-tracking is taken into account in all cases with 2.665 MV of RF-voltage. The parameters used for the tracking are given in Table 7. The results show that the local momentum acceptances are much closer to the TRACY3 results increasing the number of turns. Then, 1,000 turns are considered a good case to apply to MOGA-ELEGANT taken into account the synchrotron oscillation of 4.29 kHz (or 197.14 turns) in 6D-tracking.

3.3.2. CONCLUSION

The optimum parameters for ELEGANT to compute the dynamic and momentum aperture are at least 600 turns and an amplitude step size of 31 for the dynamic aperture, and 1,000 turns and an energy step size of 0.1 % for the momentum aperture.

3.4. SOLEIL2013 LATTICE WITH PHYSICAL LIMITATIONS

After studying the dynamic and momentum apertures of an ideal model of the current lattice of SOLEIL 2013, the physical limitations of the vacuum chamber are added to approach a more realistic model. These limitations are shown in Figure 13 and listed in Table 8 and are defined only on the first quarter of the ring. The horizontal aperture is defined by the injection septum located in one long straight section (LSS), by the vacuum chamber aperture location of the medium (MSS) and of one short straight section (SSS). The vertical aperture is defined by the LSS and MSS vacuum chamber apertures. The maximum half dimensions of the SOLEIL vacuum chamber are 0.0350 m in the horizontal plane and 0.0125 m in the vertical one.

Vacuum Chamber Locations	s (m)	Horizontal Dimensions (mm)	Vertical Dimensions (mm)
Septum	1.50	(-20.0, 28.0)	(-7.0, 7.0)
LSS	5.20	(-28.0, 28.0)	(-7.0, 7.0)
MSS	24.78	(-21.0, 21.0)	(-5.0, 5.0)
SSS	34.05	(-30.0, 25.0)	(-12.5, 12.5)

Table 8: Transverse dimensions of the main elements defining the vacuum chamber of SOLEIL over half a super period. The s-column corresponds to the s-location of the beginning of the element from the injection point.

The comparison of the dynamic and momentum apertures computed with ELEGANT and TRACY3 codes for the SOLEIL2013 lattice including the physical limitations are shown in Figure 14 and Figure 15, respectively. The parameters used for tracking are given in Table 6 adding an amplitude step size of 31 for ELEGANT dynamic aperture case and in Table 7 with an energy step size of 0.1 % for momentum aperture case. The value of the RF-voltage in the momentum aperture case is also 2.665 MV.

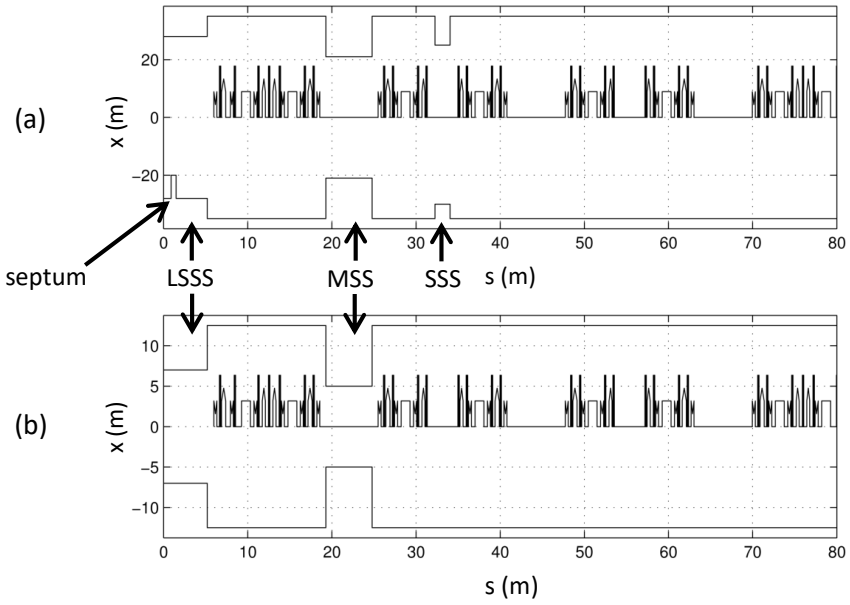

Figure 13: Horizontal (a) and vertical (b) vacuum chamber dimensions along one quarter of the SOLEIL2013 circumference. The septum of the injection section, the long (LSS), medium (MSS) and short (SSS) straight sections are indicated.

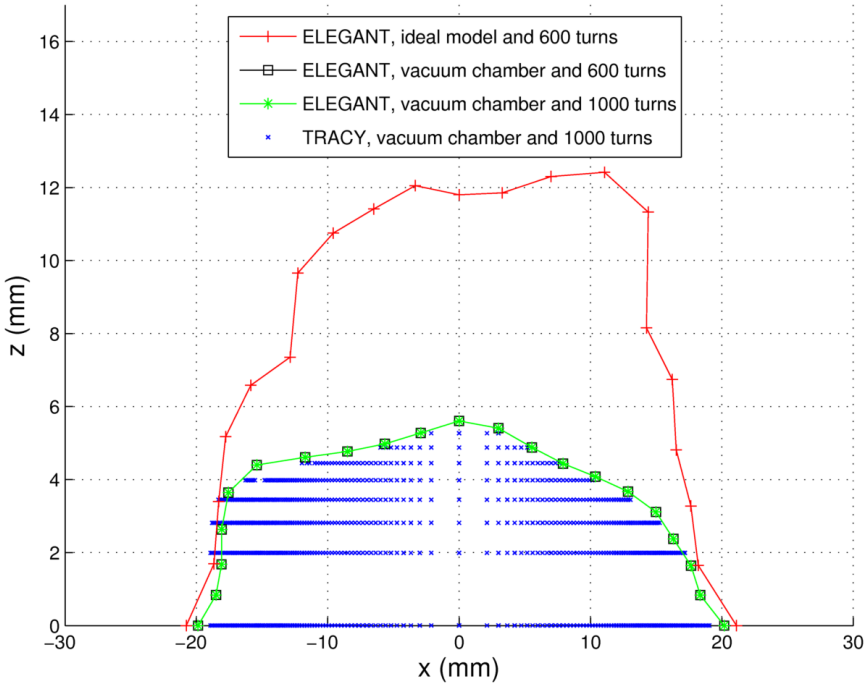

Figure 14: Comparison of the dynamic aperture of the lattice SOLEIL2013 obtained by TRACY3 with physical limitations and by ELEGANT using parameters of Table 6, with and without the physical dimensions and for different number of turns: without taking into account the physical limitations and 600 turns (red +), adding the physical limitations and 600 turns (black □), and 1,000 turns (green *) and computed by TRACY3 adding the physical limitations and 1,000 turns (blue x).

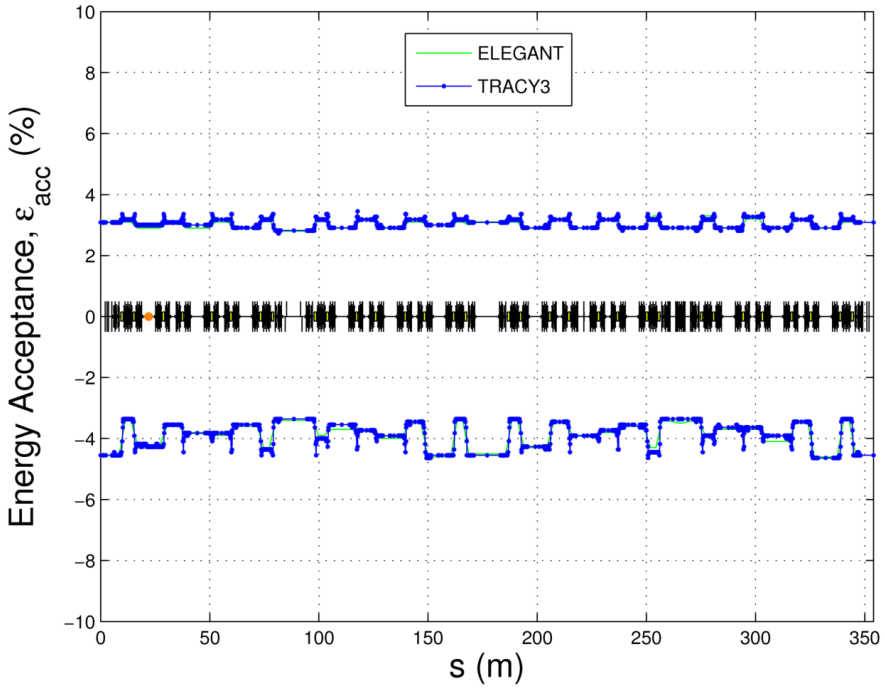

Figure 15: Comparison of the local energy acceptance of the SOLEL2013 lattice adding the vacuum chamber dimensions computed by ELEGANT (green line) and TRACY3 (blue line) codes with 6D-tracking, 2.665 MV of RF-voltage and 1,000 turns. Parameters of Table 7 with an energy step size of 0.1 % for ELEGANT.

Figure 14 shows that the dynamic aperture is reduced with respect to the ideal case as expected and that 600 turns is enough for long-term tracking. Both momentum apertures are lower than the ones computed without physical limitations of Figure 12b as expected. Figure 15 shows a good agreement of the momentum apertures computed by ELEGANT respect to the one computed by TRACY3 with 1,000 turns and 0.1 % of step size. The momentum aperture is particularity sensitive to the number of turns in 6D-tracking due to the synchrotron oscillation: when increasing the number of turns, the determination of the energy of the lost particle is more precise and the detection of the resonance lines is more accurate. Table 9 summarizes the parameters found in this chapter to efficiently compute the dynamic and momentum apertures with ELEGANT code and to obtain the same results as TRACY3 code for long-term tracking, valid with and without physical limitations.

	Dynamic Aperture	**Momentum Aperture**
Parameters	**Values**	**Values**
Number of Turns	600	1,000
Step Size	31	0.1 %

Table 9: Optimum parameters to compute the dynamic and momentum apertures within ELEGANT code and match the results obtained with TRACY3 code for long-term tracking.

3.5. Frequency Map Analysis

The Frequency Map Analysis (FMA) (Laskar, 1990 and 1995; Nadolski, 2001 and 2003) is a refined, fast converging numerical Fourier analysis technique used the last 15 years to study the stability of the dynamic system with conservative energy. It is particularly

adapted to analyze the transverse beam dynamics since it constructs a 2-dimensional map called Frequency Map where a color code is used to identify the diffusion rate (Nadolski, 2001). Then, it eases up the identification of resonances limiting the dynamics and shows nicely the stable, nonlinear and chaotic area both on the frequency map and within the dynamic aperture. The *diffusion rate d* is defined as:

$$d = log_{10}\left(\sqrt{\left(\nu_x^{(2)} - \nu_x^{(1)}\right)^2 + \left(\nu_z^{(2)} - \nu_z^{(1)}\right)^2}\right), \quad (34)$$

where ν_x and ν_z are the horizontal and vertical tunes and the indices (1) and (2) refer to the tunes values computed over 1 to N turns for index (1) and over N+1 to 2N turns for index (2). It is coded with a color scale from blue color for small tune variation (stable dynamics) to red color for nonlinear dynamics induced by the excitation of resonances and large amplitude oscillations. The resonance lines are also well identified: they always appear slight yellowish to reddish-colored because the particle oscillates transversally or longitudinally along the resonance line even if their oscillation amplitude is confined and their motion stable. Figure 16 and Figure 17 show the dynamic aperture and the variation of the horizontal amplitude with energy with their FMA of the SOLEIL2013 storage ring lattice using TRACY3 code, respectively. The vacuum chamber dimensions and the multipolar components are also included in the model. Six-dimensional tracking is computed with 1,000 turns and a RF-voltage of 2.665 MV. The parameters used to compute the dynamic aperture and the variation of the horizontal amplitude with the energy offset are listed in Table 10. Figure 16 and Figure 17 will be compared with the dynamic aperture and the variation of the horizontal amplitude with energy of the optimized solutions of MOGA-ELEGANT of Chapter IV.

The main resonance lines present in Figure 16 and Figure 17 are easily identified with a post-processing subroutine created in the local version of Accelerator Toolbox installed in SOLEIL cluster: $2\nu_x+3\nu_z$=67 (1), $\nu_x - 5\nu_z$=-33 (2), $6\nu_x$=109 (3), $5\nu_x+\nu_z$=101 (4), $9\nu_z$=92 (5).

Dynamic Aperture 4-D Tracking			**Variation H. Amplitude with Energy 6-D Tracking**	
Parameters	**Values**		**Parameters**	**Values**
Number of Turns	1,000		Number of Turns	1,000
Number of Points H. Plane	1001		Number of Points H. Plane	201
Number of Points V. Plane	501		Number of Points V. Plane	601
H. Amplitude Range (m)	(-0.04, 0.04)		H. Amplitude Range (m)	(-0.04, 0.04)
V. Amplitude Range (m)	(0.00, 0.01)		V. Amplitude Range (m)	(0.00, 0.01)
			V. Amplitude z(m)	10^{-4}
			Energy Range (%)	(-10,10)

Table 10: Main parameters used in TRACY3 to compute the dynamic aperture and the variation of the horizontal amplitude with the energy offset of the SOLEIL2013 lattice plotted in Figure 16 and Figure 17.

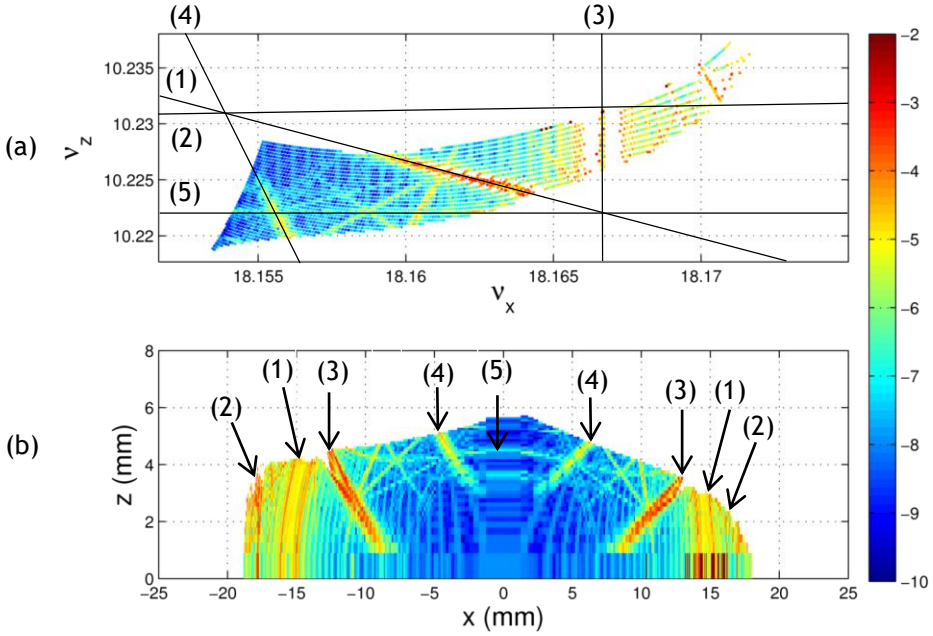

Figure 16: Dynamic aperture (b) and its frequency map (a) for the SOLEIL2013 storage ring lattice calculated by TRACY3 code adding the vacuum chamber dimensions and the multipolar field components. The main resonance lines are identified: $2\nu_x + 3\nu_z$=67 (1), $\nu_x - 5\nu_z$=-33 (2), $6\nu_x$=109 (3), $5\nu_x + \nu_z$=101 (4), $9\nu_z$ =92 (5). 4D-tracking parameters of Table 10. The color bar indicates the diffusion rate with blue color for lower values.

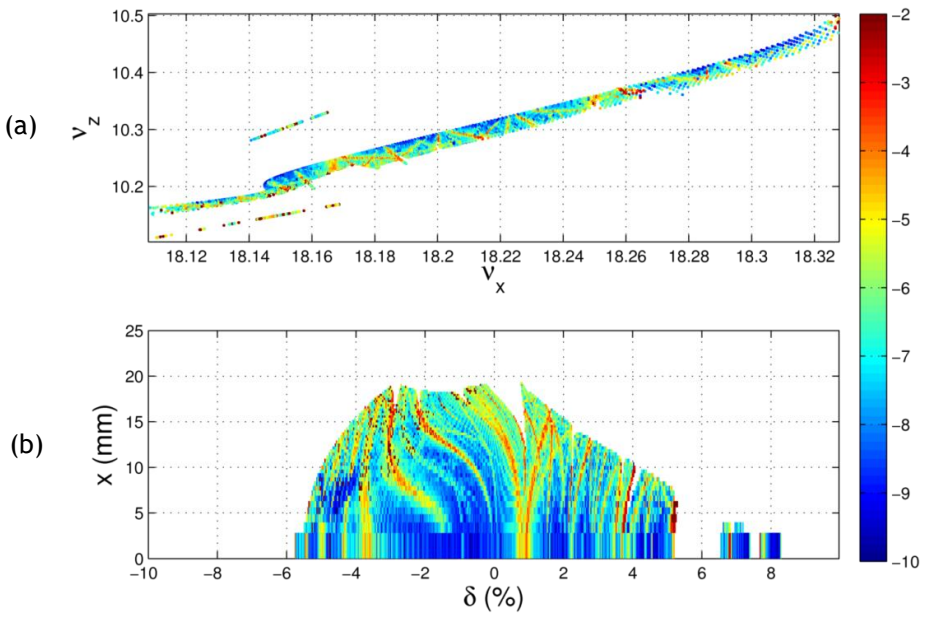

Figure 17: Variation of the horizontal amplitude (b) with relative energy offset and its frequency map (a) for the SOLEIL2013 storage ring lattice calculated by TRACY3 code adding the vacuum chamber dimensions and the multipolar field components. 6D-tracking parameters of Table 10. The color bar indicates the diffusion rate with blue color for lower values.

3.1. COMPARISON OF TOUSCHEK FORMALISM AND SENSITIVITY OF TOUSCHEK LIFETIME

It is interesting to study the sensibility of the Touschek lifetime with the horizontal emittance, the emittance coupling and the energy acceptance in the range of interest of SOLEIL. For that, a common case of the SOLEIL2013 storage ring lattice adding the physical limitations is taken into account for all cases presented below. The 6D-tracking is done for 1,000 turns and 2.665 MV of RF-voltage. The momentum aperture considered is obtained in Figure 15. The values of energy spread, bunch current and bunch length took into account in all cases are reported in Table 11.

Parameters	Values
Energy Spread σ_E	$1.0136\ 10^{-3}$
Bunch Length σ_l (mm)	6
Bunch Current I_b (mA)	1

Table 11: Values of energy spread, bunch length and bunch current used to evaluate the sensitivity of the Touschek lifetime with the horizontal emittance, the coupling and the energy acceptance plotted in Figure 18.

3.1.1. COMPARISON OF BRUCK AND PIWINSKI FORMULAS

The Touschek lifetime values computed from ELEGANT and TRACY3 with the Bruck and Piwinski formulas are shown in Table 12. The comparison of the lifetime values obtained from both codes exhibits an unexpected large disagreement of 19 % even for the same local momentum acceptance and independent of the physical aperture limitation. After investigation it turned out that the formula used in TRACY3 is not valid anymore for the case of SOLEIL and overestimate the Touschek lifetime. This is a major finding of this study. A quick parameter study and comparison of the two formulas will be performed in the following subsections.

τ_{Tous} (h)	ELEGANT Piwinski	TRACY3 Bruck	TRACY3 Piwinski
Ideal Model	61.8	69.0	58.4
Ideal Model adding Physical Limitations	27.2	32.4	26.6

Table 12: Comparison of the Touschek lifetime values of the SOLEIL2013 lattice calculated by ELEGANT and TRACY3 codes using the Bruck and the Piwinski formulas. Two models are taken into account: the SOLEIL current lattice of 2013 with and without vacuum chamber limitations, respectively. 6D-tracking parameters: 1,000 turns and 2.665 MV of RF-voltage. Touschek lifetimes: local momentum acceptances obtained in Figure 12b for the ideal model and Figure 15 adding the physical limitations and with the parameters shown in Table 11.

3.1.2. TOUSCHEK LIFETIME AND HORIZONTAL EMITTANCE AND COUPLING VALUE

Figure 18a gives the numerical dependency of the Touschek lifetime as a function of the horizontal emittance for a coupling of 1 %. The disagreement between the two formulas in-

(a)

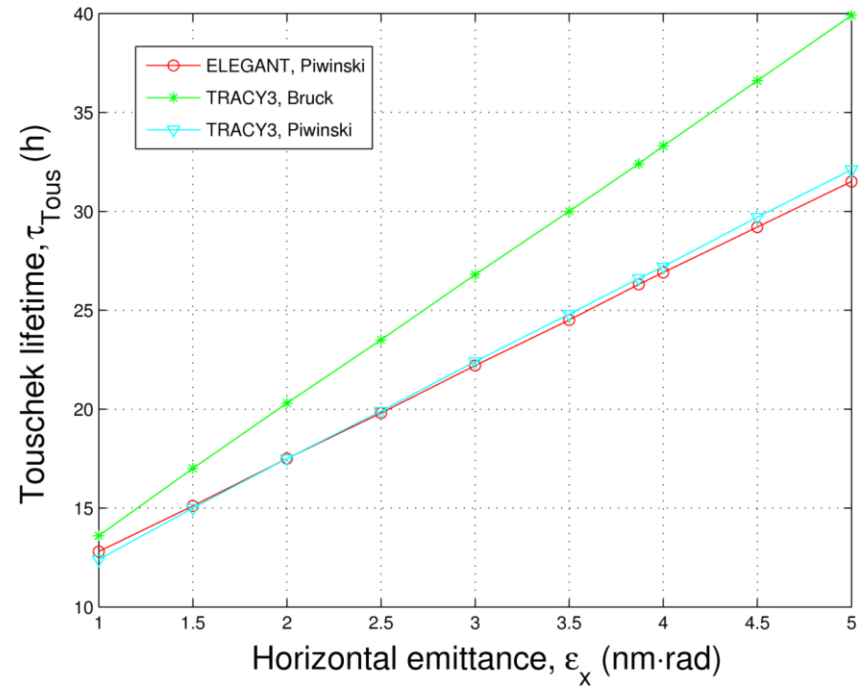

(b)

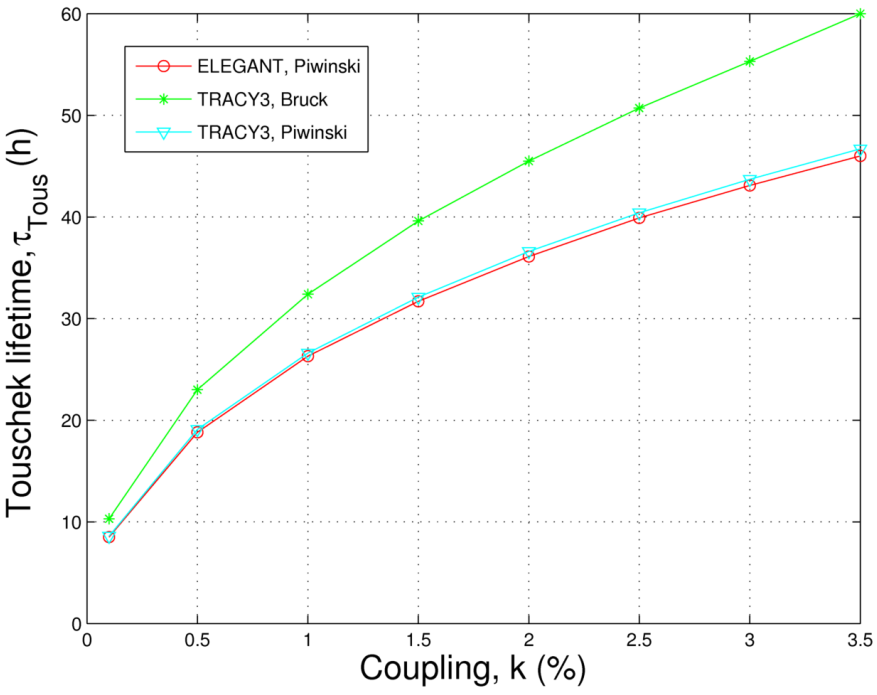

Figure 18: Touschek lifetime versus coupling (a) and horizontal emittance (b) calculated by the Piwinski formula of ELEGANT (red o), the Bruck formula (green *) and the Piwinski formula implemented in TRACY3 (cyan ∇). Parameters of Table 11 and local momentum acceptance of Figure 15b are used.

crease with the emittance value. Figure 18b shows the dependency of the Touschek lifetime with the coupling calculated with similar assumptions and the nominal horizontal emittance of 3.87 nm·rad. The results are similar to the previous case: the discrepancy between the Bruck and Piwinski formulas increase with the coupling value as well. The results obtained with ELEGANT are close to the Piwinski formula implemented in TRACY3 as it was expected. The discrepancy in the lifetime values between ELEGANT and TRACY3 with Piwinski formula corresponds to the approximation done in ELEGANT to compute the momentum aperture only in the sextupole locations.

3.1.3. Touschek Lifetime and Energy Acceptance

Figure 19 shows the dependency of the Touschek lifetime versus the energy acceptance computed by ELEGANT, and by TRACY3 with the Bruck and Piwinski formulas. For this study, the momentum acceptance is supposed s-independent and symmetric with respect to zero. The disagreement between Bruck and Piwinski formulas enlarges with large energy acceptance. By taking the 3 % average positive energy acceptance and the -3.9 % negative energy acceptance of Figure 15b, one recovers the 26.6 h and 32.4 h obtained previously.

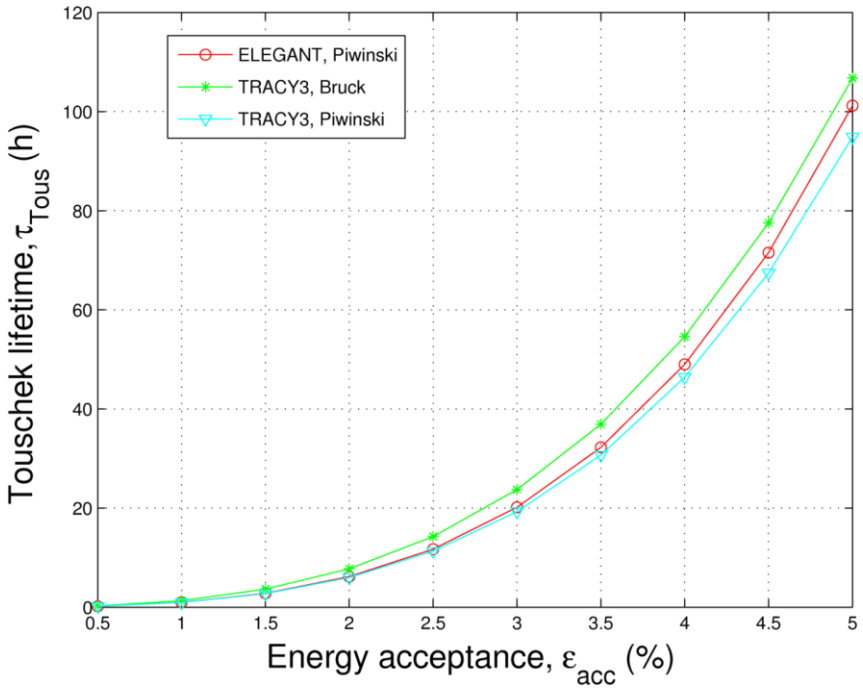

Figure 19: Touschek lifetime versus energy acceptance computed by ELEGANT (red o), the Bruck (green *) and the Piwinski formulas (cyan ∇) implemented in TRACY3 code. Parameters of Table 11 and local momentum acceptance of Figure 15 are used.

4. Conclusion

The linear and nonlinear beam dynamics have been compared between ELEGANT and TRACY3 codes. Concerning the linear beam dynamics, a shift of 1.4 units in the linear vertical chromaticity initially observed between the ELEGANT version 25.1.0 firstly

installed at SOLEIL and TRACY3 has been corrected. This discrepancy was originated from the inexact modeling of the dipole edge focusing in ELEGANT. A local version of ELEGANT 26.0.2 is now installed at SOLEIL with the same model of dipole edge focusing as TRACY3 and hence providing agreement on vertical chromaticity calculation.

After this correction, the dynamic and momentum apertures of the SOLEIL current lattice of SOLEIL 2013 computed by the new upgraded ELEGANT version 26.0.2 and TRACY3 show a good agreement with and without the physical limitations. The tracking parameters used in ELEGANT computation of the dynamic and momentum apertures have been optimized to reproduce as close as possible the computation done by TRACY3 and are listed in Table 9.

Another important result of this chapter is the identification of a discrepancy in the calculation of the Touschek lifetime between the Piwinski formula implemented in ELEGANT and the Bruck formula implemented in TRACY3, for parameters of SOLEIL. It has been shown that the Bruck approximation implemented in TRACY3 works well for low values of energy acceptance but disagrees for medium and high values of energy acceptances. For the local energy acceptance of SOLEIL (around 3 %) this difference is a relevant 19 %. Hence, the Piwinski formula has been implemented in TRACY3 to correct this significant discrepancy following the spirit done in ESRF by the accelerator group (Nash, 2015).

Finally, we now trust the new version of the ELEGANT code and it can be used by MOGA to perform as accurate linear and nonlinear lattice optimization as TRACY3 does.

BIBLIOGRAPHY

(Belgroune, 2003) M. Belgroune, P. Brunelle, A. Nadji, and L. S. Nadolski. Refined Tracking Procedure for the SOLEIL Energy Acceptance Calculation. Proceedings of 2003 Particle Accelerator Conference, pp. 896–898, Portland, Oregon, USA, 2003.

(Belgroune, 2005) M. Belgroune. Investigations Théorique et Expérimentale sur la Dynamique Non Linéaire des Particules Chargées dans les Anneaux de Stockage de Troisième Génération. PhD thesis, Paris Sud-Paris XI University, 2005, 2005PA112153.

(Bengtsson, 1994) J. Bengtsson and M. Meddahi. Modeling of Beam Dynamics and Comparison with Measurements for the Advanced Light Source. London, UK, 1994.

(Bengtsson, 1997) J. Bengtsson, E. Forest, and H. Nishimura. Tracy3 User's Manual.

(Boege, 1999) M. Boege. Update on TRACY-2 Documentation. PSI internal report, SLS-TME-TA-1999-0002, Switzerland, June 1999.

(Borland, 2000) M. Borland. Elegant: A Flexible SDDS-Compliant Code for Accelerator Simulation. Proceedings of the 2000 International Computational Accelerator Physics Conference, Darmstadt, Germany, 2000.

(Borland, 2010) M. Borland, L. Emery, H. Shang, and R. Soliday. User's Guide for SDDS-Toolkit version 2.8. Advanced Photon Source, 2010.

(Borland, 2012) M. Borland. User's Manual for ELEGANT. Program Version 25.1.0. Advanced Photon Source, 2012.

(Borland, 2013) M. Borland. Features and Applications of the Program Elegant. Proceedings of the 2013 International Particle Accelerator Conference, pp. 3139-3143. Shanghai, China, 2013.

(Borland, 2016) M. Borland. User's Manual for ELEGANT. Program Version 30.0.0. Advanced Photon Source, 2016.

(Brown, 1982) K. Brown. A First and Second Order Matrix Theory for the Design of Beam Transport Systems and Charged Particle Spectrometers. Internal report, SLAC-75. 1982.

(Bruck, 1966) H. Bruck. Accélérateurs Circulaires de Particules: Introduction à la Théorie. Presse Universitaires de France, Éd. 14, Paris, France, 1996.

(Brunelle, 2010) P. Brunelle, A. Loulergue, A. Nadji, L. S. Nadolski, and M.-A. Tordeux. Nonlinear Beam Dynamics Studies at SOLEIL using Experimental Frequency Map Analysis. Proceedings of 2010 International Particle Accelerator Conference, pp. 4653–4655, Kyoto, Japan 2010.

(Brunelle, 2016) P. Brunelle. Private communication.

(Einfeld, 2009) D. Einfeld. Comparison of Lattice Codes. In lecture during the Nonlinear Beam Dynamics Workshop, Rutherford Laboratory and Diamond Light Source, UK, November 2009.

(Forest, 1994) E. Forest, M.F. Reusch, D.L. Bruhwiler, and A. Amiry. The Correct Local Description for Tracking in Rings. Particle Accelerators, vol. 45, pp. 65-94, 1994.

(Forest, 1998) E. Forest. Beam Dynamics: A New Attitude and Framework. Harwood Academic Publisher, 1998.

(Forest, 2006) E. Forest. Geometric Integration for Particle Accelerators. Journal of Physics A: Mathematical and General, 39(19):5321, 2006.

(Goldstein, 1980) H. Goldstein. Classical Mechanics. 2nd Ed., Addison Wesley, Reading, MA, 1980.

(Herr, 2013) W. Herr. Mathematical and Numerical Methods for Non-linear Beam Dynamics. CERN Yellow Report CERN-2014-009, pp. 157-198. Trondheim, Norway, 2013.

(Kernighan, 1988) B. W. Kernighan and D. M. Ritchie. The C Programing Language. Prentice-Hall, Englewood Cliffs, N. J., 2nd Ed., 1988.

(Laskar, 1990) J. Laskar. The Chaotic Motion of the Solar System. A Numerical Estimate of the Size of the Chaotic Zones. Icarus, vol. 88, pp. 266-291, 1990.

(Laskar, 1995) J. Laskar. Introduction to Frequency Map Analysis. Proceedings of 3DHAM95 NATO Advanced Institute, S'Agaro, June 1995, C. Simo Ed., pp 134-150.

(Loulergue, 2010) A. Loulergue, C. Benabderrahmane, F. Bouve, P. Brunelle, M.-E. Couprie, J.-C- Denard, J.-M. Filhol, C. Herbeaux, P. Lebasque, V. Leroux, A. Lestrade, O. Marcouillé, J.-L. Marlats, J. Moreno, A. Nadji, L. S. Nadolski, F. Polack, A. Somogyi, M.-A. Tordeaux. Double Low Beta Straight Section for Dual Canted Undulators at SOLEIL. Proceeding of 2010 International Particle Accelerator Conference, pp. 2496-2498, Kyoto, Japan, 2010.

(Nadolski, 2001) L. S. Nadolski. Application de L'Analyse en Fréquence à L'Étude de la Dynamique des Sources de Lumière. PhD thesis, Paris Sud-Paris XI University, July 2001, 2001PA112120.

(Nadolski, 2002a) L. S. Nadolski. Comparison BETA/TRACY3. Private Communication.

(Nadolski, 2002b) The TRACY code was written by J. Bengtsson, É. Forest, and H. Nishimura, then translated by M. Böge at SLS, extented by L. Nadolski at SOLEIL (2002), revised by J. Bengtsson at BNL (2005). A compact user interface was added at SOLEIL by J. Zhang (2011).

(Nadolski, 2009a) L. S. Nadolski. Note Technique sur les Codes de Tracking MADX/PTC et TRACY III-Champ de Fuite de Quadrupoles. SOLEIL internal report SOU-PM-NT-I-3698, 2009.

(Nadolski, 2009b) L. S. Nadolski. Progress for the Linear and Nonlinear Modeling of SOLEIL Storage Ring. In lecture during the second Nonlinear Beam Dynamics Workshop, Rutherford Laboratory and Diamond Light Source, UK, 2009.

(Nadolski, 2003) L. S. Nadolski and J. Laskar. Review of Single Particle Dynamics for Third Generation Light Sources through Frequency Map Analysis. Phys. Rev. ST. Accel. and Beams, 6(11), 114801, 2003.

(Nishimura, 1988) H. Nishimura. TRACY, A Tool for Accelerator Design and Analysis. Proceedings of 1988 European Particle Accelerator Conference, pp. 803-805, Rome, Italy, 1988.

(Nash, 2015) B. Nash, N. Carmignani, L. Farvacque, and S. M. Liuzzo. New Functionality for Beam Dynamics in Accelerator Toolbox (AT). Proceedings of 2015 International Particle Accelerator Conference, pp. 113-116, Richmond, USA, 2015.

(Obrain, 1989) S. K. Obrien. Turbo Pascal 5.5: The Complete Reference. Borland Osborne/McGraw-Hill, ISN 0078815010, 1989.

(Ousterhout, 1994) John K. Ousterhout, Tcl and the Tk Toolkit, Addison-Wesley, Reading, MA, USA, ISBN 0-201-63337-X, 1994.

(Piwinski, 1998) A. Piwinski. The Touschek Effect in Strong Focusing Storage Rings. Technical report 98-179, DESY, 1998.

(Tordeux, 2009) M.-A. Tordeux, P. Brunelle, A. Loulergue, A. Nadji, and L. S. Nadolski. Linear and Nonlinear Model Optimization for SOLEIL Storage Ring. Proceedings of 2009 Particle Accelerator Conference, pages 3931-3933, Vancouver, Canada, 2009.

(Wheeler, 2011) B. Wheeler. Tcl/Tk Programing Cookbook. Published by Packt Publishing Ltd. 1st Ed., Birmingham, 2011.

(Wolski, 2014) A. Wolski. Beam Dynamics in High Energy Particle Accelerators. Imperial College Press, 1st Ed., 2014.

(Xiao, 2007) A. Xiao and M. Borland. Touschek Effect Calculation and its Application to a Transport Line, ANL, Argonne, IL 60439, USA, 2007.

(Zhang, 2013) J. Zhang and L. Nadolski. User's Manual for SOLEIL. SOLEIL internal report, 2013.

CHAPTER III
BEAM-BASED EXPERIMENTS AT SOLEIL: BEAM LIFETIME MEASUREMENTS

CONTENTS

The beam lifetime may become a critical parameter for a light source. Most of the third generation light sources are dominated by the Touschek lifetime (C. Bernardini, 1963) when operating at large current per bunch and with low coupling value. Gas contribution becomes important especially when low gap in-vacuum undulators are installed in the ring. It is essential to understand the beam loss mechanism during lifetime electron loss-induce in order to reduce the activation of the component of the accelerator, avoid losing beam near beam line front ends and inside the insertion devices. Moreover a large lifetime enables the reduction of the injection frequency and saving the injectors (power consumption, age of the components, etc.).

Many laboratories have already performed beam-based experiments about beam lifetime. Lifetime contributions differ depending on the characteristics of each accelerator. Examples of analysis of the beam lifetime dependency with the vertical scrapers to determine the elastic component of the gas lifetime are reported in Ref. (Decking, 1998; Khan, 199; Streun, 2001; Huttel, 2003; Spencer, 2007; Steier, 2009; Huang, 2011; Hansson, 2013; Carmignani, 2014). Measurements the dependency of the Touschek lifetime with the coupling value or RF-voltage are numerous: for instance for coupling, at ALS (Streun, 2001), UVSOR (Mochihashi, 2007), SLS (Steier, 2009), SPEAR3 (Huang, 2011) and ESRF (Carmigniani, 2014) and for the RF-voltage at ALS (Decking, 1998), BESSY-II (Khan, 1999), SLS (Streun, 2001), ANKA (Huttel, 2003), ESRF (Carmignani). Studies of the beam lifetime dependency with the current can be found for ALS (Decking, 1998), ANKA (Huttel, 2003), SLS (Streun, 2001), SPEAR3 (Huang, 2011) and NSLS-II (Podobedov, 2015) for different filling patterns.

The set of experiments presented in this thesis follows the work done previously; a set of experiments has been performed in three machine dedicated shifts in order to improve the understanding of the electron beam lifetime measured in the SOLEIL storage ring. This is the first time that this type of work is performed to this extent at SOLEIL. The main contributions to the electron beam lifetime are reviewed starting from the modeling and assumptions and specificities of SOLEIL. The Touschek and the gas lifetime are presented in great detail. Finally, these models are confronted against the experimental data. Different experiments were performed to measure the variation of the total beam lifetime with coupling value, physical aperture, and bunch current in order to get a complete vision of each contribution to the total lifetime in the SOLEIL2013 storage ring. The storage ring lattice considered in this report corresponds to the settings used in operation since December 2013 (see Chapter II Section 3.1). Two types of filling patterns have been studied whose main parameters are given in Table 1.

Number of Bunches	I (mA)	I_b (mA)	P (mbar)	k (%)	V_{RF} (MV)
8	50	6.25	$2.5\ 10^{-10}$	1	2.665
312	430	1.4	$4.8\ 10^{-10}$	1	2.665

Table 1: Main parameters of the two filling patterns studied during the experiments.

1. ELECTRON BEAM LIFETIME CALCULATION

The total lifetime (τ) of the electron beam stored in the SOLEIL storage ring is a composition of two major contributions: the gas scattering lifetime (τ_{gas}) and the Touschek lifetime (τ_{Tous}) (Le Duff, 1985):

$$\frac{1}{\tau} = \frac{1}{\tau_{gas}} + \frac{1}{\tau_{Tous}}. \quad (1)$$

The objective of this chapter is to describe the physics behind the various lifetimes, estimate their respective contributions for the SOLEIL2013 lattice and then use this knowledge to analyze lifetime measurements, and compare them with simulation ones.

1.1. GAS SCATTERING LIFETIME

The gas scattering lifetime is a consequence of the scattering processes between the beam of electrons and the residual gas inside the vacuum chamber. This scattering process depends on four phenomena described below (Le Duff, 1985).

1.1.1. ELASTIC NUCLEUS SCATTERING (COULOMB OR RUTHERFORD SCATTERING)

The electrons are deflected with conservation of energy leading to an angular kick of the betatron motion. The cross section is given by the Rutherford cross section that depends strongly on the physical acceptance of the chamber and is expressed as follows (Le Duff, 1985):

$$\frac{1}{\tau_{ENS}} = \frac{2\pi r_0^2}{\gamma^2} Z^2 \rho c \left[\langle \beta_x \rangle \left(\frac{\beta_x}{a^2} \right) + \langle \beta_z \rangle \left(\frac{\beta_z}{b^2} \right) \right], \quad (2)$$

where r_0 is the classical electron radius, c is the speed of light, γ the Lorentz factor, Z is the atomic number of the atoms of a diatomic gas, $\rho[\mathrm{m}^{-3}] = 6.6\ 10^{22}\ P\ [\mathrm{mbar}]$ is the atomic nucleus density where P is the mean pressure, $\langle \beta_x \rangle$ and $\langle \beta_z \rangle$ are the average values of the horizontal and vertical betatron functions along the ring, $\left(\frac{a^2}{\beta_x}\right) = \min_s \left(\frac{a(s)^2}{\beta_x(s)}\right)$ and $\left(\frac{b^2}{\beta_z}\right) = \min_s \left(\frac{b(s)^2}{\beta_z(s)}\right)$ are the horizontal and vertical physical acceptances where $a(s)$ and $b(s)$ are the horizontal and vertical vacuum chamber half sizes respectively along the ring. Equation 2 is valid only if the dynamic aperture is larger than the physical aperture, which is true in this study.

The parameters used to compute the elastic Coulomb scattering lifetime are the following:

- The nominal scraper values are (-28, 33) mm in the horizontal plane and (-3.6, 3.6) mm in the vertical plane.

- The average values of horizontal and vertical betatron functions along the ring obtained by ELEGANT: $\langle\beta_x\rangle$ = 8.23 m and $\langle\beta_z\rangle$ = 7.94 m.
- The horizontal physical acceptance is defined by one of the following elements: the injection in-vacuum septum, the positive (external) and negative (internal) horizontal scrapers, the extremities of long (LSS), medium (MSS) and short straight sections (SSS) vacuum chambers where the betatron functions are maximized[1]. Table 2 gives the different cases taking into account that some apertures are sometimes asymmetric. For a given element, it was verified that the local physical acceptance is the minimum between the positive and negative contributions for asymmetric aperture.
    - It can be concluded that the physical horizontal aperture is defined by the septum blade.
    - This is in accordance with the simulations through on-momentum tracking where nonlinearities are taken into account (such as betatron function variation with amplitude).
    - The quantity of particles lost in the negative scraper location is higher than the particles lost at the positive one (Figure 1). As the two horizontal scrapers are not located at the same place in the ring, the optical functions are not the same for both scrapers and then the physical aperture limitation is not the same (as seen in the analytical calculations of Table 2).
    - The horizontal physical acceptance is plotted in Figure 2 and Figure 3 at the beginning and at the end of the ring, respectively, where typical horizontal limitations are located.
- The vertical physical acceptance is defined as the minimum value of the quantity $\left(\frac{b^2}{\beta_z}\right)$ along the storage ring circumference. The main limitations are given at SOLEIL by the LSS, the vertical scrapers, the MSS and the SSS vacuum chambers. Table 2 shows that the vertical scraper defines the vertical physical acceptance. Figure 4 exhibits the vertical physical acceptance for the first quarter of the ring.

Substituting the above parameters into Eq. 2, the Elastic Nucleus Scattering lifetime can be written as a function of the pressure P and the atomic number Z as:

$$\tau_{ENS}[h] = \frac{1.24\ 10^{-6}}{P[mbar]\ Z^2}, \tag{3}$$

[1] In a straight section, the betatron function evolution is quadratic: if $\beta_0$is the betatron function at the center (symmetry point), the betatron function $\beta(s)$ at a distance s from the center is: $\beta(s) = \beta_0 + s^2/\beta_0$.

Vacuum Chamber Location	s (m)	Horizontal Apertures (mm)	Vertical Apertures (mm)	β_x (m)	β_z (m)	$\left(\frac{a^2}{\beta_x}\right)$ (10^{-5} m·rad)	$\left(\frac{b^2}{\beta_z}\right)$ (10^{-6} m·rad)
Septum	1.50	(-20.0, 28.0)	(-7.0, 7.0)	11.735	8.203	**3.41**, 6.68	5.97
LSS	5.20	(-28.0, 28.0)	(-7.0, 7.0)	13.886	11.319	5.65, 5.65	4.33
VS	4.29	(-35.0, 35.0)	(-3.6, 3.6)	13.140	10.237	9.32, 9.32	**1.27**
HNS	12.47	(-28.0, 35.0)	(-12.5, 12.5)	14.914	4.411	5.26, 8.21	35.42
MSS	24.78	(-21.0, 21.0)	(-5.0, 5.0)	6.064	5.667	7.27, 7.27	4.41
SSS	34.05	(-30.0, 25.0)	(-12.5, 12.5)	14.132	3.099	6.37, 4.42	50.42
HPS	341.28	(-35.0, 33.0)	(-12.5, 12.5)	14.446	4.745	8.48, 7.54	32.93

Table 2: Vacuum nominal chamber dimensions of SOLEIL adding the vertical (VS), the horizontal positive (HPS) and negative (HNS) scraper apertures. The maximum horizontal and vertical betatron functions for each location are also included. The last two columns show the local physical acceptance.

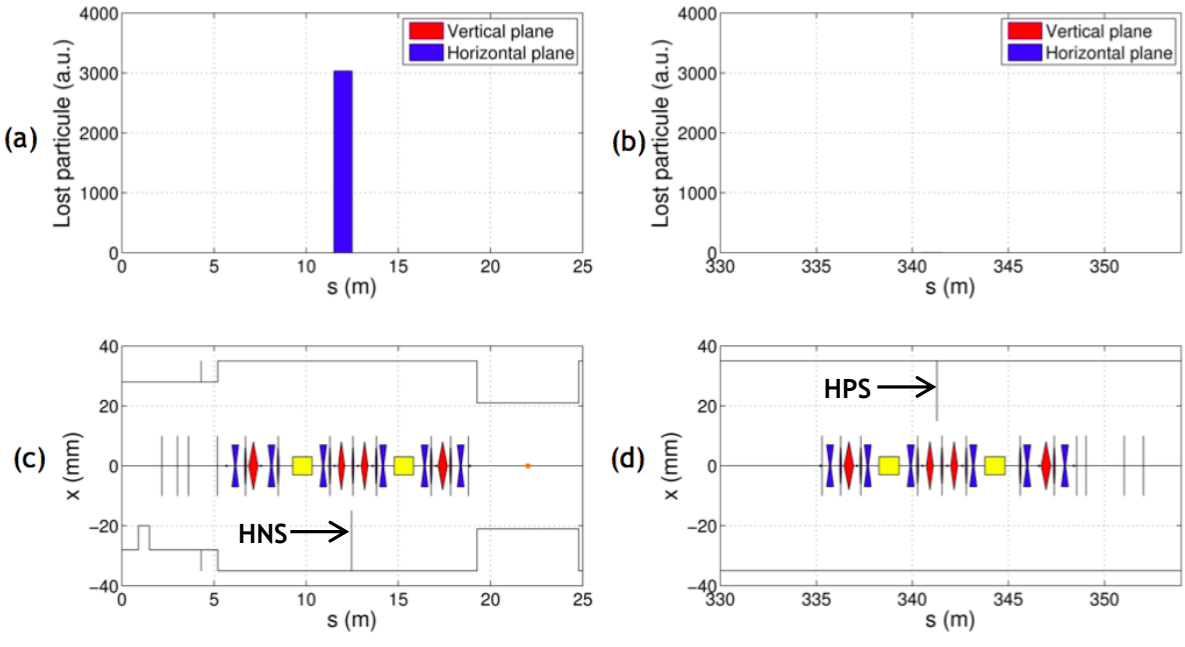

Figure 1: Particle loss locations (a) and (b) closing the internal (c) and external (d) horizontal scrapers at (-15, 15) mm position. For the same aperture of the two scrapers, the losses on the internal horizontal scraper are higher than the external one.

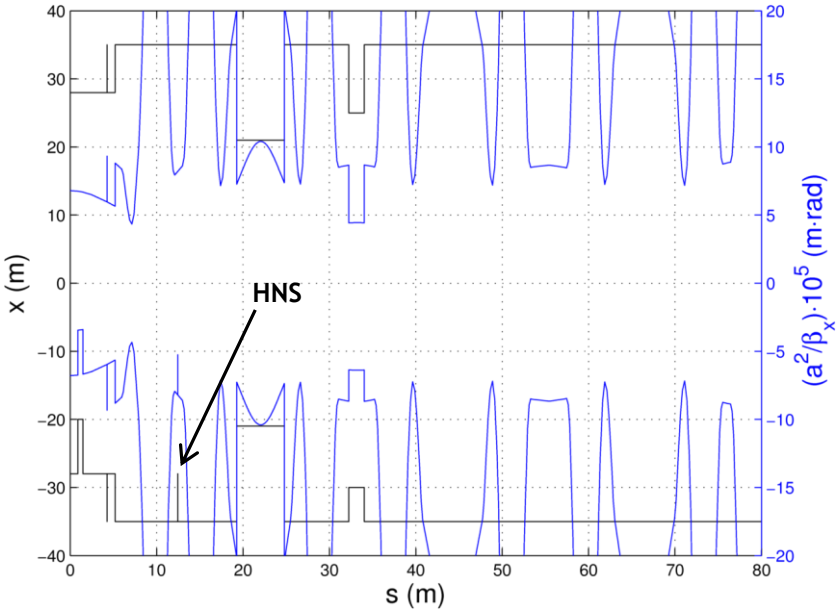

Figure 2: Horizontal physical acceptance of the first ¼ of the SOLEIL circumference with the scrapers at nominal positions. The minimum value is located at the septum location. The horizontal negative scraper (HNS) is marked at its nominal position (-28 mm).

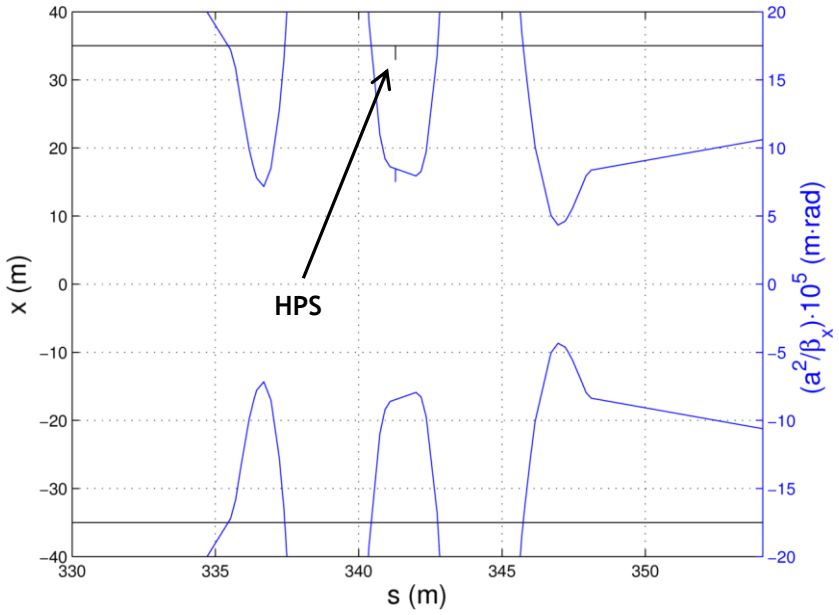

Figure 3: Horizontal physical acceptance of the last ¼ of the SOLEIL circumference with the scrapers at nominal positions. The horizontal positive scraper (HPS) at nominal position (+33 mm) is indicated.

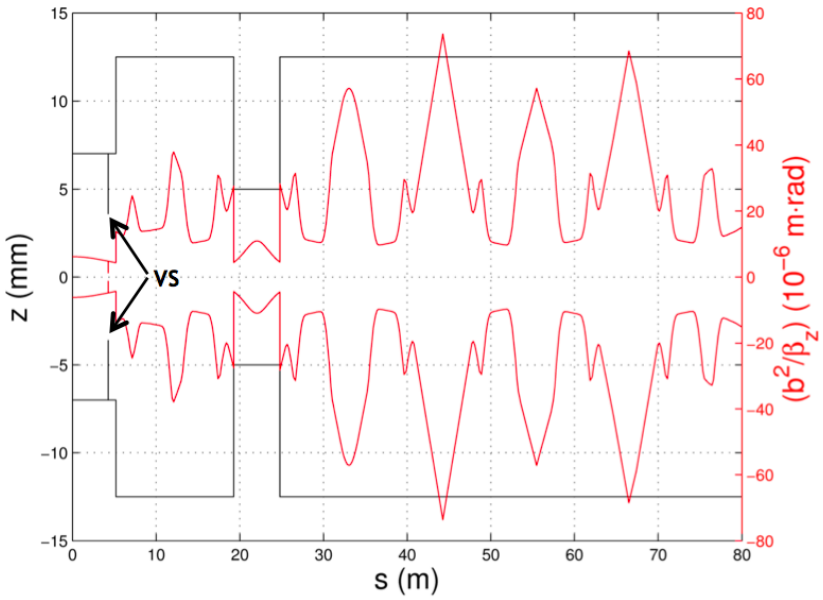

Figure 4: Vertical physical acceptance of the first ¼ of the SOLEIL circumference with the scrapers at nominal positions. The vertical scrapers (VS) at nominal position (+/- 3.6 mm) are indicated.

1.1.2. Elastic Shell Electron Scattering

The stored electrons are colliding with electrons of the gas atoms and molecules. Then electrons transfer elastically their energy to the atom of the residual gas. The event probability depends on the averaged energy acceptance (ε_{acc}) (Le Duff, 1985):

$$\frac{1}{\tau_{ESS}} = \frac{2\pi r_0^2}{\gamma} Z\rho c \, \frac{1}{\varepsilon_{acc}}, \tag{4}$$

where the parameters r_0, c, γ, Z, ρ have already been defined previously.

The energy acceptance (ε_{acc}) can be defined as the maximum energy deviation that one particle can have just before to become lost. This quantity depends on the location along the ring due to its dependency with the dispersion and betatron functions. The energy acceptance is either limited by the RF-energy acceptance defined by the longitudinal bucket size, or by the transverse dynamics including the physical aperture (Nadji, 1998). As a first approximation, when the RF-system is the main limitation, the energy acceptance can be expressed as:

$$\varepsilon_{acc}^{RF} = \pm \sqrt{\frac{2eU_0 \, |\sin \phi_s|}{\pi |\alpha| h E_0} \left(\sqrt{q^2 - 1} - \cos^{-1}\left(\frac{1}{q}\right) \right)}. \tag{5}$$

In this case, U_0 is the energy loss per turn, α is the first order momentum compaction factor, h is the harmonic number, E_0 is the energy and q = $^{eV_{RF}}/_{U_0}$ the overvoltage factor. When the energy acceptance is limited by the transverse dynamics, it depends on the location in the ring, and positive and negative values are not necessarily equal. Then, a

representative value can be calculated as the average of the positive and negative values along the ring. For the SOLEIL nominal lattice of 2013, the average value is around 3 %. This value will be the reference value in this chapter to calculate analytically the different contributions to the gas lifetime. The 3 % value will be discussed in the experimental part.

Writing Eq. 4 as a function of the pressure P and the atomic number Z, it transforms in Eq. 6 as:

$$\tau_{ESS}(h) = \frac{4.51\ 10^{-5}}{P[mbar]\ Z}. \tag{6}$$

1.1.3. INELASTIC NUCLEUS SCATTERING (BREMSSTRAHLUNG)

The stored electrons are colliding with nuclei and the process leads to an energy loss of the electrons. If the energy loss is larger than the energy acceptance ($\varepsilon_{\mathrm{acc}}$), the particle motion is not any more stable and the particle get lost. The Inelastic Nucleus Scattering lifetime (τ_{INS}) is expressed as follows (Le Duff, 1985):

$$\frac{1}{\tau_{INS}} = \frac{16 r_0^2}{411} Z^2 \rho c\ ln\left(\frac{183}{Z^{\frac{1}{3}}}\right)\left(ln\left(\frac{1}{\varepsilon_{acc}}\right) - \frac{5}{8}\right), \tag{7}$$

where the parameters r_0, c, γ, Z, ρ are defined previously and $\varepsilon_{\mathrm{acc}}$ is the energy acceptance of the storage ring.

Considering an averaged energy acceptance of 3 %, a measured mean pressure P and the atomic number Z, Eq. 7 transforms in:

$$\tau_{INS}[h] = \frac{1.57\ 10^{-5}}{P[mbar]\ Z^2\ ln\left(\frac{183}{Z^{\frac{1}{3}}}\right)}. \tag{8}$$

1.1.4. INELASTIC SHELL-ELECTRON SCATTERING

This contribution is due to the scattering of the stored electrons with the electrons of the atoms or gas molecules and the process leads to an energy loss of the electrons. It also depends on the averaged energy acceptance ($\varepsilon_{\mathrm{acc}}$) as follows (Le Duff, 1985):

$$\frac{1}{\tau_{ISS}} = \frac{16 r_0^2}{411} Z \rho c\ \left\{ln\left(\frac{2.5\gamma}{\varepsilon_{acc}}\right) - 1.4\right\}\left\{ln\left(\frac{1}{\varepsilon_{acc}}\right) - \frac{5}{8}\right\}. \tag{9}$$

Considering an energy acceptance of 3 %:

$$\tau_{ISS}[h] = \frac{1.35\ 10^{-6}}{P[mbar]\ Z}. \tag{10}$$

1.1.5. ANALYSIS OF THE RESIDUAL GAS

The elastic and inelastic contributions of the gas lifetime depend strongly on the composition of the residual gas inside the storage ring vacuum chamber. Often the atomic number found in the literature is Z = 7. This is convenient because ion pumps, gauges are calibrated in pressure equivalent to di-nitrogen. After a few years of vacuum conditioning, the composition of the gas at SOLEIL has been deeply modified with the disappearance of almost all heavy elements: the composition is mostly made of di-hydrogen gas. Almost 50 % of the circumference is coated with Non-Evaporable-Getter NEG (ternary alloy TiZrVa) acting like a distributed pump. The effect at SOLEIL will be that the concentration of high-Z molecules will even be lower than in other existing accelerators. So the computation of an effective atomic number becomes of primordial importance. The 27 GeV storage ring HERA-e at DESY has reported an effective of 3.6 (Seidel, 2008).

For the Elastic Scattering case, the factor PZ^2 used in Eq. 3 must be calculated taking into account the partial pressure P_i of the molecule i and the atomic number of each atom j in the molecule i as (Wiedemann, 2007):

$$PZ^2 \rightarrow \sum_{i,j} P_i Z_j^2 = P \sum_{i,j} k_i Z_j^2. \tag{11}$$

The composition of the residual gas of the storage ring was measured and analyzed at SOLEIL during the shutdown of August 2015 (Béchu, 2015). The data was measured using spectrometers Residual Gas Analysis (RGA) (Herbeaux, 2008) disseminated along the ring. The composition of the residual gas in the arc of the storage ring (outside the straight sections) is shown in Table 3, where κ_i is defined as the ratio between the partial pressure P_i of the molecule i, and P is the total pressure.

Residual Gas Molecule	$\boldsymbol{\kappa_i}$	$\sum_j \mathbf{Z_j}$	$\sum_{i,j} \boldsymbol{\kappa_i Z_j}$	$\sum_j \mathbf{Z_j^2}$	$\sum_{i,j} \boldsymbol{\kappa_i Z_j^2}$
H_2	0.885	2	1.770	2	1.770
CH_4	0.080	10	0.800	40	3.200
CO	0.026	14	0.364	100	2.600
H_2O	0.005	10	0.050	66	0.330
CO_2	0.001	22	0.022	164	0.164
Ar	0.002	18	0.036	324	0.648
sum	1	76	3.042	8.712	8.712
N_2	1	14	14	98	98

Table 3: Residual gas composition measured at SOLEIL. κ_i is the gas concentration and Z_j the atomic number of each atom j in the molecule i. Courtesy of C. Herbeaux and N. Béchu.

It can be seen from Table 3, that the sum of the factor PZ^2 for all residual gas molecules is 11 times smaller than the factor associated with the residual gas composed by N_2 or CO as it is usually assumed in the bibliography (Huttel, 2003; Spencer, 2007). In other words, the effective atomic number $Z_{ENS,eff}$ for the Elastic Nucleus Scattering has been overestimated 3.3 times considering the gas residual fully composed by N_2 or CO: the new effective atomic number value is $Z_{ENS,eff}$ = 2.1. Similarly the Inelastic and Elastic Shell-Electron Scattering scale as Z: the effective atomic number becomes $Z_{ESS,eff} = Z_{ISS,eff}$ = 1.5.

At the same time, the Inelastic Nucleus Scattering (Bremsstrahlung) with the presence of different types of molecules in the residual gas, must be calculated as (Wiedemann, 2007; Seidel, 2008):

$$\frac{1}{\tau_{INS}\,(h)} = -\frac{4}{3}\,\frac{c}{1.013}\sum_{i}\frac{P_i(bar)}{L_{r,i}}\,ln\,\varepsilon_{acc}, \tag{12}$$

where c is the speed of light, ε_{acc} the energy acceptance of the storage ring and $L_{r,i}$ the radiation length of gas molecules of type i. The radiation length is the distance over which electron loses its energy by a factor 1/e. Then, comparing the effective radiation length of the SOLEIL gas composition and the corresponding one considering the gas fully composed by N_2 or CO (Table 4), a factor 10 larger is found for SOLEIL. The effective atomic number calculated from Eq. 7 is $Z_{INS,eff}$ = 2.2. It is close to the effective atomic number deduced in the Elastic Nucleus Scattering case.

From now on, the new effective atomic number will be noted concisely as Z_{eff}.

Residual Gas Molecules	$\boldsymbol{\kappa_i}$	$\mathbf{L_{r,i}\ (m)}$	$\frac{\boldsymbol{\kappa_i}}{\mathbf{L_{r,i}\ (m)}}$
H_2	0.885	7527	$1.78\ 10^{-4}$
CH_4	0.080	696	$1.15\ 10^{-4}$
CO	0.026	321	$8.10\ 10^{-5}$
H_2O	0.005	477	$1.05\ 10^{-4}$
CO_2	0.001	197	$5.08\ 10^{-6}$
Ar	0.002	118	$1.70\ 10^{-5}$
sum	1	1995	$5.01\ 10^{-4}$
N_2	1	326	$3.07\ 10^{-3}$

Table 4: Effective radiation and inelastic interaction length calculation taken into account the residual gas composition measured at SOLEIL. κ_i is the gas concentration for each molecule i. The radiation length $L_{r,i}$ for molecule i is the distance over which electron loses its energy by a factor 1/e. Radiation lengths are well tabulated in literature (Seidel, 2008; PDB, 2015).

1.1.6. GAS LIFETIME CALCULATION

The total gas lifetime can be expressed as a combination of Eq. 2, Eq. 4, Eq. 7 and Eq. 9:

$$\tau_{gas}\,[h] = \left(\frac{1}{\tau_{ENS}} + \frac{1}{\tau_{ESS}} + \frac{1}{\tau_{ISS}} + \frac{1}{\tau_{INS}}\right)^{-1}. \quad (13)$$

Table 5 shows the calculation of the different contributions to the gas lifetime τ_{ENS}, τ_{ESS}, τ_{INS} and τ_{ISS} as well as the total gas lifetime τ_{gas}. The parameters used are an energy acceptance of 3 %, the pressures measured during the experiments and the two values of the effective atomic number: Z = 7 taking into account the gas composed by N_2 or CO, the effective atomic number Z_{eff}. The scraper apertures are the nominal ones. The calculation is done for the two filling patterns studied during the experiments (Table 1). Comparing all cases, the Elastic Shell-Electron Scattering lifetime is very large and its contribution can be neglected with respect to the other gas contributions.

Z	Number of Bunches	P (mbar)	τ_{ENS} (h)	τ_{ESS} (h)	τ_{INS} (h)	τ_{ISS} (h)	τ_{gas}* (h)
7	8	$2.5\ 10^{-10}$	101.1	25800.0	281.5	774.1	67.9
	312	$4.8\ 10^{-10}$	52.7	13438.0	146.6	403.2	35.3
Z_{Eff}	8	$2.5\ 10^{-10}$	1145.1	118820	2559.5	3564.7	647.5
	312	$4.8\ 10^{-10}$	596.4	61883.0	1333.1	1856.6	337.2

Table 5: Calculation of the Elastic lifetimes (τ_{ENS}, τ_{ESS}), Inelastic lifetimes (τ_{INS}, τ_{ISS}), and total gas lifetime (τ_{gas}) contributions for the two filling patterns studied during measurements. The pressures are the ones measured during the experiments and the atomic numbers of 7 and Z_{eff}. The scraper apertures correspond to the nominal ones. * Calculated neglecting the τ_{ESS} contribution.

Equation 13 can be written in a more convenient way for the analysis of the experimental data:

$$\frac{1}{\tau_{gas}} = Q\left(\frac{\beta_x}{a^2}\right) + K\left(\frac{\beta_z}{b^2}\right) + \lambda, \quad (14)$$

where:

- β_x and β_z are the horizontal and vertical betatron functions where the horizontal and vertical physical acceptances are located respectively (Table 2).
- *a* and *b* are the horizontal and vertical half sizes of the smallest physical aperture.
- Q and K are coefficients that depend on the parameters defined in Eq. 2. The theoretical values for the measured pressure are defined by the following expressions:

$$Q^{THE} = \frac{2\pi r_0^2}{\gamma^2} {Z_{ENS,eff}}^2 \rho c \langle \beta_x \rangle\,, \quad (15)$$

$$K^{THE} = \frac{2\pi r_0^2}{\gamma^2} {Z_{ENS,eff}}^2 \rho c \langle \beta_z \rangle. \quad (16)$$

- The inelastic contribution of the gas scattering is represented by the factor $\lambda = \frac{1}{\tau_{INS}} + \frac{1}{\tau_{ISS}}$. Note that the dependence of this parameter with energy acceptance is not negligible. The value is changed by 40 % for an average momentum acceptance between 1 % and 3 %.

The calculated values of Q, K and λ are given in Table 6.

Z	Q (m rad h^{-1})	K (m rad h^{-1})	λ (h^{-1})
7	2.4 10^{-8}	2.3 10^{-8}	9.3 10^{-3}
Z_{eff}	2.1 10^{-9}	2.0 10^{-9}	1.3 10^{-3}

Table 6: Parameters for gas lifetime assuming an average pressure of 4.8 10^{-10} mbar and a 3 % of energy acceptance.

1.2. TOTAL BEAM LIFETIME

The total beam lifetime is calculated using Eq. 1. The bunch current (I_b), the mean pressure (P), the RF-voltage (V_{RF}) and the coupling (k) used to calculate the simulated Touschek and gas lifetimes are shown in Table 1.

The gas lifetime (τ_{gas}) is calculated using Eq. 13 and neglecting the contribution of the Elastic Shell-Electron Scattering phenomena. The different contributions are calculated considering the analytical formulas Eq. 2, Eq. 7 and Eq. 9. The gas beam lifetime is related to the mean pressure as follows:

$$\tau_{gas}[h] = \frac{A}{P\ [mbar]}, \tag{17}$$

where A is a constant and P is the mean pressure of the residual gas measured during the experiment.

The Touschek lifetime has been studied in detail in Chapter II. The formula that will be used in this chapter is the exact formula called Piwinski formula (Eq. 5 of Chapter II) based on TRACY3 outputs. The energy acceptance calculated with TRACY3 takes into account the nominal physical aperture described in Table 2. In order to calculate the Touschek lifetime, it is also important to take into account the effect called *bunch lengthening* with current. The bunch lengthening ($\Delta\sigma_l(I_b)$) is a consequence of the interaction between the electron beam and the vacuum chamber (Wiedemann, 2007). It is defined, for each bunch current, as the increase factor of the bunch length with respect to the bunch length at zero current:

$$\Delta\sigma_l(I_b) = \sigma_l(I_b)/\sigma_l(0). \tag{18}$$

where $\sigma_l(I_b)$ is the bunch length measured experimentally and $\sigma_l(0)$ is the bunch length at zero current calculated using the experimental voltage value as follows:

$$\sigma_l = \sqrt{\frac{2\pi\alpha hc^2}{(2\pi \cdot f_{RF})^2 \cdot cos\phi_s} \frac{E}{eV_{RF}}}\sigma_E. \quad (19)$$

To characterize the bunch lengthening at SOLEIL, the experimental variation of the bunch length has been measured versus the bunch current in May 2013 for a RF-voltage of 2.8 MV. The experimental data are shown in Figure 5 and fitted (R^2=0.9995) as follows:

$$\sigma_l\ RMS[ps] = 0.0020\ I_b^3[(mA)^3] - 0.0904\ I_b^2[(mA)^2] + 2.5021\ I_b[mA] + 15.8270 \quad (20)$$

For each bunch current, the bunch length is deduced from Eq. 20 (corresponding to V_{RF} = 2.8 MV) and then scaled with the experimental RF-voltage according to Eq. 19. The bunch length values corresponding to the experiment conditions are summarized in Table 7.

It is worth noting that a fit using a simple power law of the bench length with respect to the bunch current shows a deviation of the standard 1/3 power law. This deviation needs further investigation to understand the impedance contribution. This is beyond the scope of this work.

$$\sigma_l\ RMS[ps] = 14.98 + 3.53\ I^{0.72}[\ (mA)^{0.72}]. \quad (21)$$

The calculated total, gas and Touschek lifetimes are given in Table 8 for the two filling patterns and for the two values of the effective atomic number.

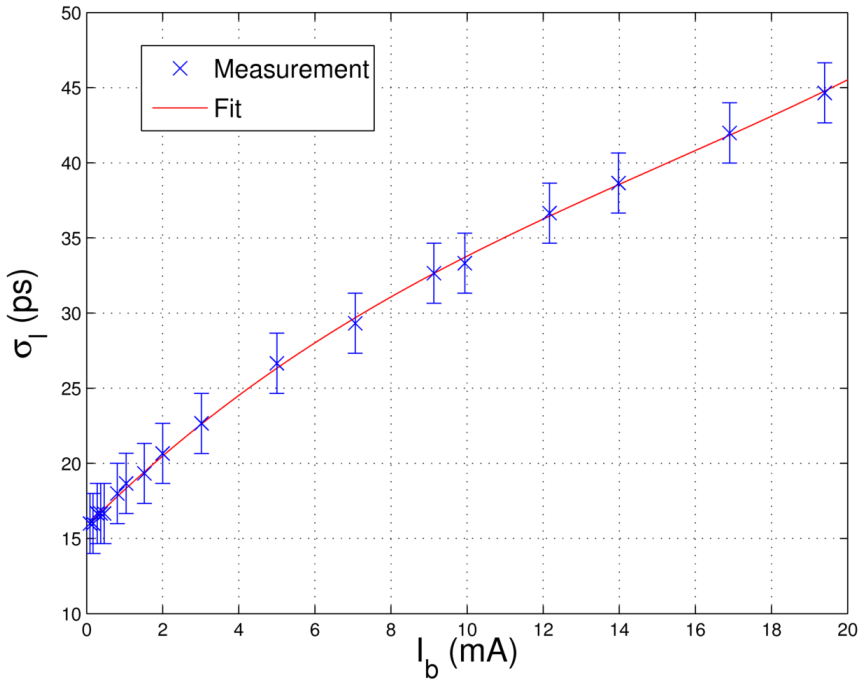

Figure 5: RMS bunch lengthening measured at SOLEIL in May 2013 for a 2.8 MV RF voltage using a picosecond streak camera (courtesy of M. Labat).

Number of Bunches	k (%)	V_{RF} (MV)	I_b (mA)	$\sigma_l(I_b)$ (ps)	$\sigma_l(0)$ (ps)	$\Delta\sigma_l(I_b)$
		2.800	0	15.8	15.8	1.0
8	1	2.665	6.25	29.1	16.2	1.8
312	1	2.665	1.40	19.5	16.2	1.2

Table 7: RMS bunch length values deduced from the bunch lengthening measurement performed in May 2013 with a RF-voltage of 2.8 MV.

Number of Bunches	Z	τ_{gas}^{SIM} (h)	τ_{Tous}^{SIM} (h)	τ^{SIM} (h)
8	Z_{eff}	647.5	6.9	6.8
312		337.2	20.2	19.1
8	7	67.9	6.9	6.3
312		35.3	20.2	12.8

Table 8: Simulated total (τ^{SIM}), Touschek (τ_{Tous}^{SIM}) and gas lifetimes (τ_{gas}^{SIM}) calculated for each filling pattern studied during the experiment. The gas lifetimes are calculated for two values of the effective atomic number Z, for an energy acceptance of 3 % and for parameters of Table 1.

2. ELECTRON BEAM LIFETIME MEASUREMENTS

A list of beam-based experiments was carried out to obtain a global view of the contribution of the Touschek and gas lifetimes in the total beam lifetime of the SOLEIL2013 nominal lattice. In this case, the beam lifetime was measured in function of the coupling, the physical aperture (horizontal and vertical scraper positions), and the bunch current. These experimental results will be compared with the simulation ones and the goal is to extract from both some evaluation of the experimental gas and Touschek lifetimes. Firstly, each experiment is explained and analyzed individually and secondly the conclusions and the comparison of all the results will be discussed. The considerations given as follows are available for all the experiments:

- The conditions for all the experiments (except the last one where bunch current was varied) are the follows: a ¾ operation mode with 430 mA of intensity, a coupling of 1 %, the RF-voltage of 2.665 MV, a bunch length of 19.5 ps (see Table 7) and a pressure of 4.8 10^{-10} mbar.
- The horizontal and vertical scrapers are positioned at their nominal positions: (-28, 33) mm for the horizontal (external, internal) scrapers and (-3.6, 3.6) mm for the vertical one. The dimensions of the vacuum chamber and the multipolar field components are also taken into account.

- The gas lifetime is calculated using Eq. 2, Eq. 7 and Eq. 9 for two values of the effective atomic number (Z=7 and Z_{eff}). The horizontal physical acceptance remains limited by the septum aperture but the vertical is now limited by the vertical scraper aperture. As seen in Table 5, the Elastic Shell-Electron Scattering lifetime is very large and its contribution will be neglected.
- The energy acceptance is calculated with TRACY3 using a 6D-tracking over 1,000 turns. The Touschek lifetime is then calculated using Piwinski formula (Eq. 5 of Chapter II). Figure 6 shows the energy acceptance obtained from TRACY3 for the particular configuration of the scrapers at their nominal positions described before.
- Among all cases studied during the experiment, this particular case of 1 % coupling will be the reference case to compare with other experiments.
- The total beam lifetime was measured using a DCCT (Direct-Current Current Transformer). The decay of the current signal is measured during a fixed interval of time. Measurement errors coming from the DCCT will be given.

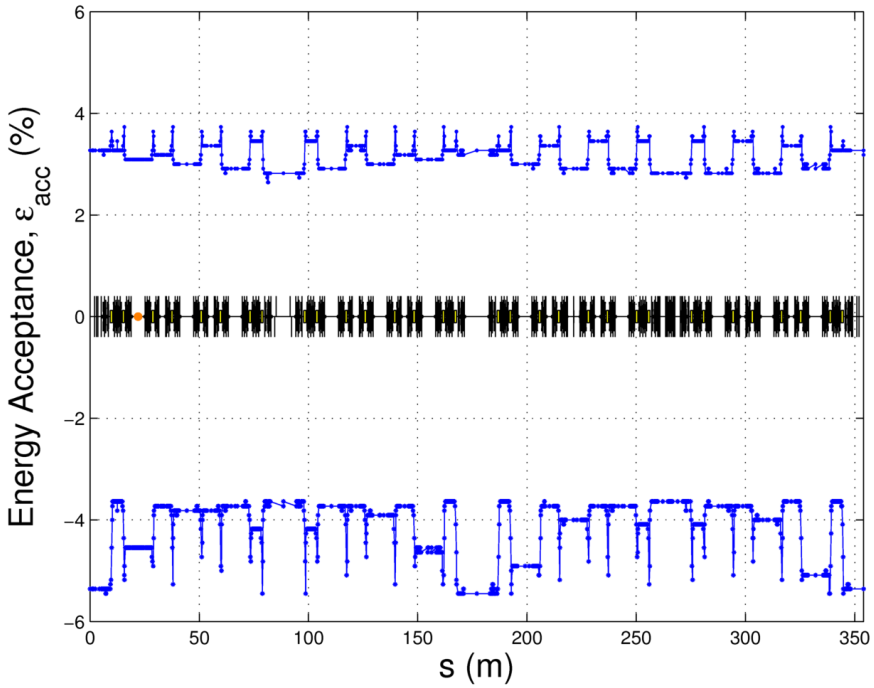

Figure 6: Variation of the energy acceptance along the ring obtained from TRACY3 for the nominal lattice of SOLEIL for a RF-voltage of 2.665 MV and the scrapers at nominal positions.

2.1. Variation of Beam Lifetime With Coupling

The filling pattern used for measurements is the 312 bunch mode which parameters are given in Table 1. The RF-voltage and the physical aperture remain constant. The coupling was varied by controlling the vertical dispersion using 32 skew quadrupoles without increasing the betatron coupling. The nonlinear dynamics should not depend on the coupling value and the energy acceptance should remain the same for all cases. Moreover the gas lifetime will be the same for all cases so the Touschek lifetime is the only

contribution to vary with coupling. Considering that the Touschek lifetime depends on the square root of coupling (Eq. 6 of Chapter II), Eq. 1 transforms as follows:

$$\frac{1}{\tau^{MEAS}} = \frac{1}{\tau_{gas}^{DED}} + \frac{1}{\sqrt{k} \cdot cte}. \tag{22}$$

Table 9 presents the measurements of beam lifetime (τ^{MEAS}) as a function of the coupling (k) measured during the experiment. The experimental conditions are exactly the same as the conditions explained before.

Measurement Number	k (%)	τ^{MEAS} (h)	Measurement Number	k (%)	τ^{MEAS} (h)
1	0.20	5.07 ± 0.03	11	1.80	16.70 ± 0.10
2	0.31	6.66 ± 0.03	12	1.99	17.30 ± 0.10
3	0.49	8.73 ± 0.03	13	3.09	20.80 ± 0.10
4	0.70	10.66 ± 0.08	14	4.02	22.70 ± 0.10
5	0.78	11.40 ± 0.10	15	6.24	25.40 ± 0.10
6	0.91	12.13 ± 0.07	16	7.05	25.60 ± 0.10
7	1.00	12.70 ± 0.10	17	8.31	25.10 ± 0.10
8	1.19	13.70 ± 0.10	18	10.17	23.40 ± 0.10
9	1.41	15.00 ± 0.10	19	14.06	16.90 ± 0.10
10	1.59	15.70 ± 0.10			

Table 9: Total beam lifetime measured as a function of the coupling. The filling pattern is the 312-bunch mode which parameters are given in Table 1.

The analysis of the invert of the lifetime in function of the inverse of the square root of coupling presented on Figure 7 shows three different regimes:

1. At high coupling values, the regime is nonlinear. The skew quadrupole introduce strong multipolar field components degrading the Touschek lifetime.
2. A second region between slightly below 1 % and intermediate values of the coupling showing a linear regime.
3. A third regime linear as well at lower coupling values.

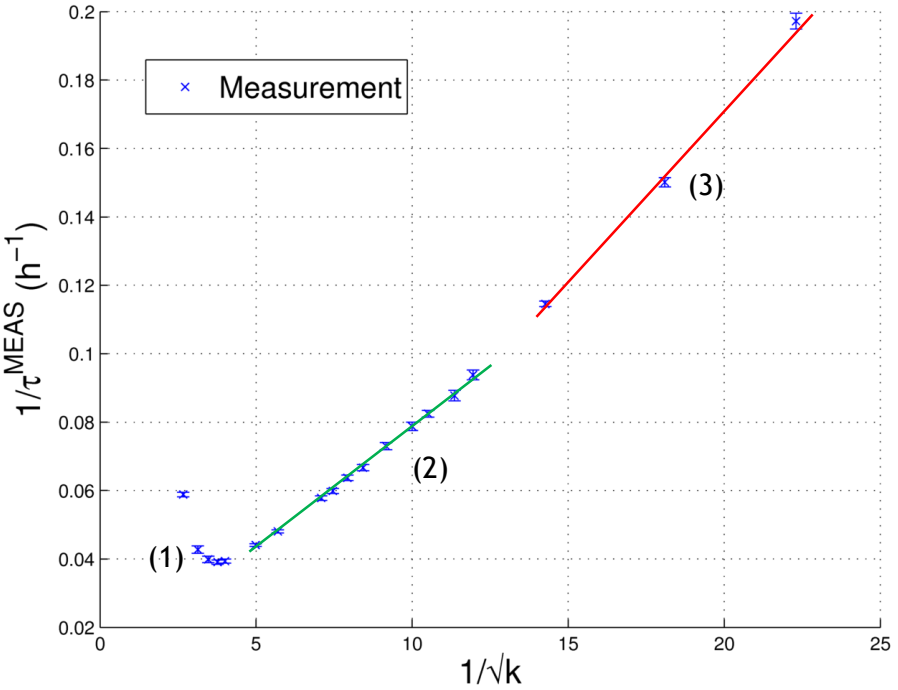

Figure 7: Inverse of the measured total beam lifetime in function of the inverse of the square root of the coupling value. Three different regimes are shown: one non-linear (1) and two linear (2) and (3).

It was then decided to carry out another set of experiment (Table 10) at the end of a user operation (500 mA, 416 bunches, RF voltage = 2.46 MV, mean pressure 5 10^{-10} mbar) for a restricted range of coupling value: 0.16 % to 1 %. Eq. 22 was fitted (Figure 8) and gives:

$\tau_{gas}^{DED} = (60 \pm 15)\ h,$

$\tau_{Tous}^{DED} = (15.7 \pm 0.6)\ h,$ for 1 % coupling.

When applying a scaling on parameters to come back to the reference case with 312 bunches (see Table 1), these values become:

$\tau_{gas}^{DED} = (62.5 \pm 13)\ h,$

$\tau_{Tous}^{DED} = (13.0 \pm 0.5)\ h$ for 1 % coupling.

Measurement Number	k (%)	τ^{MEAS} (h)	Measurement Number	k (%)	τ^{MEAS} (h)
1	1.00	12.4 ± 0.2	6	0.37	8.2 ± 0.2
2	0.86	11.7 ± 0.2	7	0.28	7.4 ± 0.2
3	0.71	11.0 ± 0.2	8	0.22	6.6 ± 0.1
4	0.58	10.0 ± 0.2	9	0.18	6.0 ± 0.1
5	0.47	9.2 ± 0.2	10	0.16	5.7 ± 0.1

Table 10: Total beam lifetime measured as a function of the coupling. The filling pattern is a 416-bunch mode with a 500 mA total beam current.

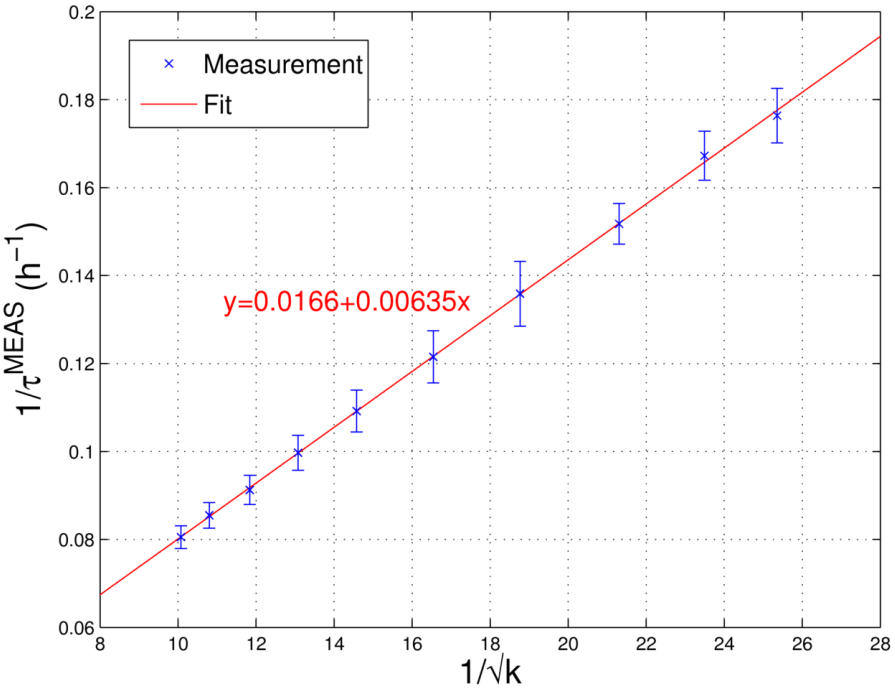

Figure 8: Inverse of the measured total beam lifetime in function of the inverse of the square root of the coupling for coupling values between 0.16 % and 1.00 %. The slope is the inverse of the Touschek lifetime and the crossing of the y-axis gives the inverse of the gas lifetime during the experiment (500 mA, 4/4 filling pattern).

2.2. Variation of Beam Lifetime with Bunch Current

2.2.1. Beam Lifetime Measurements

Measurements were also done to analyze the relation between the total beam lifetime and the bunch current. In this case, the measurements were done with 8 bunch filling pattern while varying the bunch current. The scrapers were at their nominal positions: (-28, 33) mm for the horizontal scrapers and (-3.6, 3.6) mm for the vertical one. The RF-voltage was V_{RF} = 2.665 MV and the coupling was k = 1 %.

Table 11 shows the beam lifetimes measured in the experiment versus the bunch current. As already mentioned in section 1.2, when the bunch current is increased, the bunch length is increased too. The bunch lengthening factor $\Delta\sigma(I_b) = \sigma(I_b)/\sigma(0)$ measured with a RF-voltage of 2.8 MV has been scaled with the experimental RF-voltage of 2.665 MV according to Eq. 19. The bunch lengthening factor values corresponding to the experiment are given in the Table 11.

Figure 9 shows the comparison between measurements and calculations for both values of the two values of the atomic number Z = 7 and Z_{eff} while the bunch current increases from 1 to 10 mA in the 8-bunch filling pattern. Measurements and simulation results are in better agreement for Z = 7, showing that the real gas composition is not exactly the one described in Table 3.

I_b (mA)	τ^{MEAS} (h)	$\Delta\sigma = \sigma(I_b)/\sigma(0)$
10.11	3.40 ± 0.01	1.99
8.83	3.65 ± 0.01	1.90
7.63	4.00 ± 0.02	1.81
6.25	4.57 ± 0.07	1.70
5.22	5.3 ± 0.2	1.61
3.81	6.7 ± 0.4	1.47
2.0	10.3 ± 0.4	1.26
1.03	14.3 ± 0.2	1.14

Table 11: Total beam lifetime measured as a function of the bunch current and corresponding bunch lengthening with bunch current. The filling pattern is an 8-bunch mode.

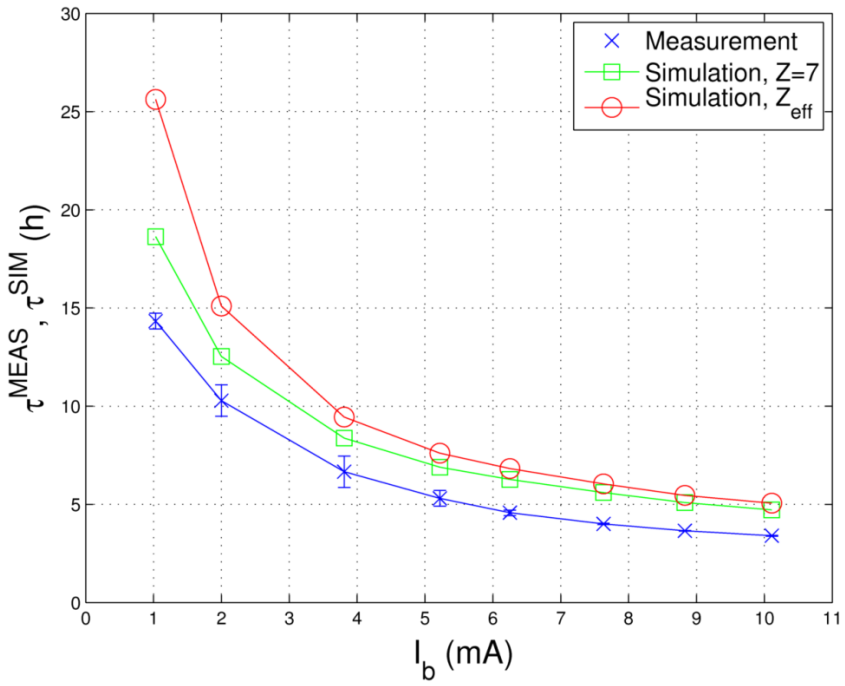

Figure 9: Variation of the measured and simulated total beam lifetime versus bunch current for the 8-bunch filling pattern. Simulated beam lifetimes are calculated for two different values of atomic number: Z_{eff} and Z = 7.

2.2.2. *Deduced Gas and Touschek Beam Lifetimes*

The Touschek lifetime can be expressed as a function of the bunch current (I_b) as $\tau_{Tous} = \frac{\alpha\,\Delta\sigma}{I_b}$. Then the variation of the total beam lifetime τ with the bunch current I_b can be expressed as follows:

$$\frac{1}{\tau} = \frac{1}{\tau_{gas}} + \frac{1}{\tau_{Tous}} = \frac{1}{\tau_{gas}} + \frac{I_b}{\alpha\, \Delta\sigma} \tag{23}$$

where α is constant and independent of the bunch current.

Figure 10 shows the variation of the inverse of the measured beam lifetime versus bunch current. The model of Eq. 23 is being used to fit the experimental data and deduce the experimental gas and Touschek lifetime values. The mean pressure can be considered as constant because the total beam current varies from 8 to 80 mA, and in this range, the pressure is low and does not vary a lot. Then the constant term in the fitting will represent the inverse of the gas lifetime and the Touschek lifetime will be deduced by subtracting the deduced gas lifetime to the measured one. The measurement fitting is done with a second order polynomial (R^2 = 0.9991, Figure 10) and the deduced Touschek and gas lifetimes for a bunch current of 6.25 mA are:

$$\tau_{gas}^{DED} = (31 \pm 8)\ h,$$
$$\tau_{Tous}^{DED} = (5.4\ \pm 0.8)\ h$$

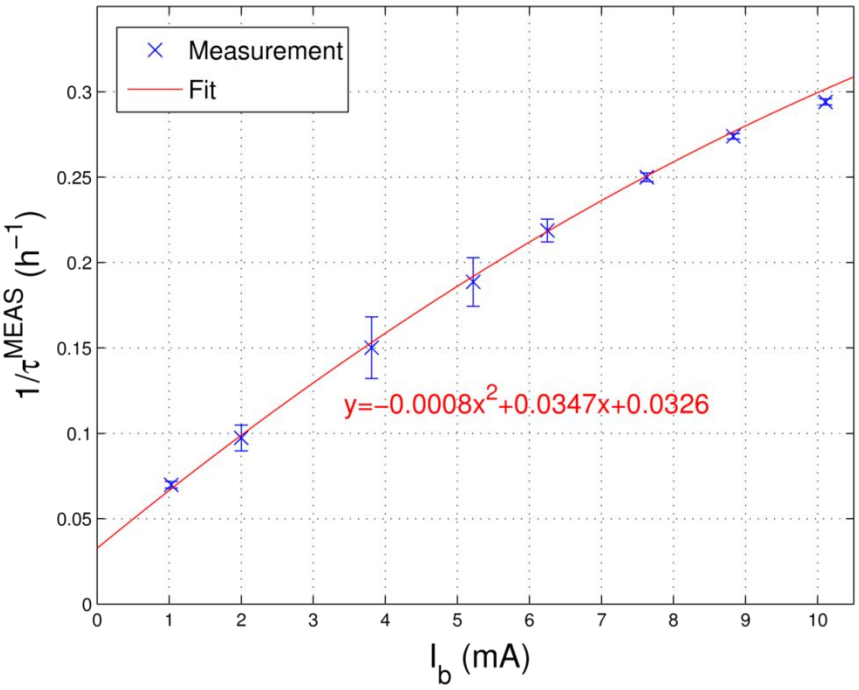

Figure 10: Variation of the inverse of the measured total beam lifetime versus bunch current for the 8-bunch filling pattern with a quadratic fitting.

2.2.3. Bunch Lengthening Determination from Beam Lifetime Measurements

It has been shown in section 1.2 that the variation of the bunch length with current measured with a streak camera, can be fitted by a 3rd order polynomial (see Eq. 20). Using the row data of Table 11 it is also possible to deduce the bunch lengthening equation as well by fitting with the Eq. 23. To proceed we introduce the polynomial equation $\Delta\sigma(I_b) =$

$\sigma(I_b)/d = (aI_b^3 + bI_b^2 + cI_b + d)/d$ into Eq. 23, where a, b, c and d are constant coefficients, to get the following expression:

$$\frac{1}{\tau} = \frac{1}{\beta} + \frac{I_b\, d}{\alpha(aI_b^3 + bI_b^2 + cI_b + d\,)}. \tag{24}$$

Table 12 shows the coefficients a, b and c obtained from the fitting of the measurements using Eq. 24 and a comparison with the ones obtained from streak camera measurements. The term *d* is fixed to the measured bunch length value of 16.2 ps. The agreement with the streak camera measurements is satisfactory.

Remark: it has been discovered in 2015 that the RF-voltage seen by the electron beam was larger by an offset of 0.3 MV than the re-read value given by the equipment. Of course this information is of great importance to deduce the bunch length from streak camera measurement as a scaling in square root of V_{RF} is used. Then calculation were performed considering that the RF-voltage seen by electrons during streak camera experiment is 2.8 + 0.3 = 3.1 MV and that the one used during measurement is 2.665 + 0.3 = 2.965 MV. This offset does not modify significantly the calculation results and does not explain the difference between calculated values and measurements.

	a (10^{-3} s A^{-3})	b (10^{-6} s A^{-2})	c (10^{-9} s A^{-1})
Deduced Values	0.002	-0.11	2.0
Streak Camera Measurements	0.002	-0.09	2.3

Table 12: Fitted coefficients a, b and c for bunch lengthening model. A comparison is made with the coefficients obtained by fitting the streak camera measurements (see Eq. 20).

2.3. Variation of Beam Lifetime with Physical Aperture

2.3.1. Vertical Scraper Experiment

During this experiment, the internal and external horizontal scrapers remain at their nominal positions. The vertical scraper aperture was varied from ± 2 mm to ± 7 mm. Table 13 shows the beam lifetimes measured in the experiment versus the vertical scraper positions. Figure 11 compares the measured beam lifetimes with the calculated ones. Figure 12 shows that the theoretical energy acceptances calculated by TRACY3 remain unchanged when the vertical scraper aperture is reduced because of the constant horizontal physical aperture. The Touschek lifetime is then independent of the vertical scraper aperture and the dependence of the total lifetime versus vertical scraper aperture is only due to the gas contribution. The measurements (inverse of the beam lifetime versus β_z/b^2) can be fitted using Eq. 1 and Eq. 14 and the only parameter that can be deduced without any approximation is K. The linear variation is obtained for the measurements 3 to

6 which correspond to the cases where the vertical scraper aperture is limiting the physical aperture of the ring (Figure 13). The deduced value of K is K^{DED} = 1.3 10^{-8} m·rad·h^{-1}.

Measurement Number	b (mm)	τ^{MEAS} (h)
1	(-7, 7)	13.7 ± 0.2
2	(-6, 6)	13.6 ± 0.2
3	(-5, 5)	13.6 ± 0.2
4	(-4, 4)	13.1 ± 0.2
5	(-3, 3)	12.2 ± 0.1
6	(-2, 2)	9.8 ± 0.1

Table 13: Variation of the measured beam lifetime versus the aperture of the vertical scraper (b).

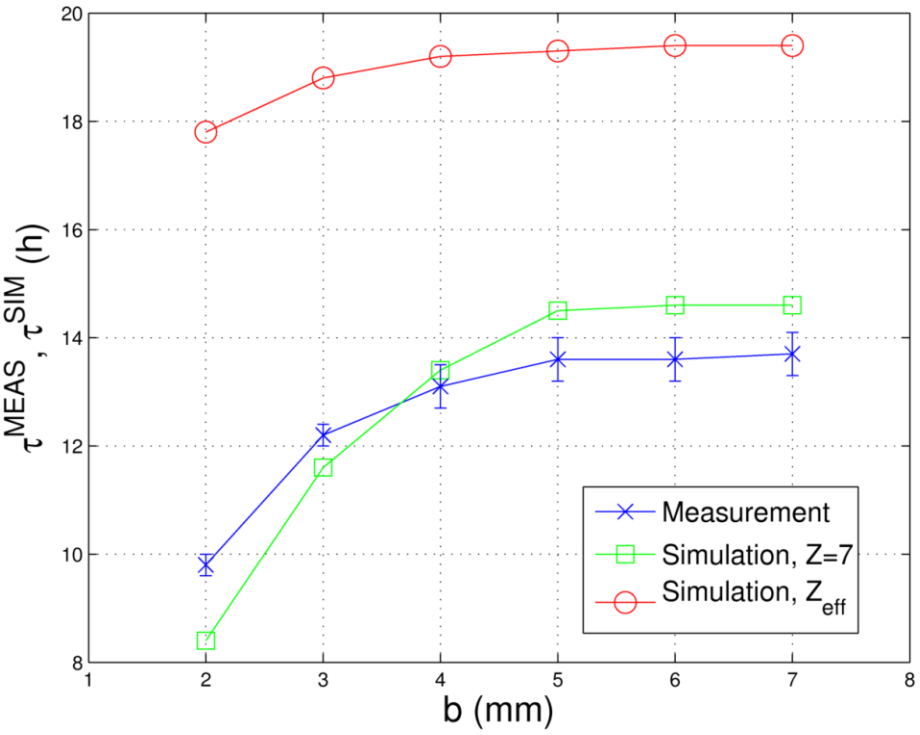

Figure 11: Variation of the measured and simulated total beam lifetime versus vertical scraper aperture (b). The simulated beam lifetimes are calculated for two different values of atomic number: Z = Z_{eff} and Z = 7.

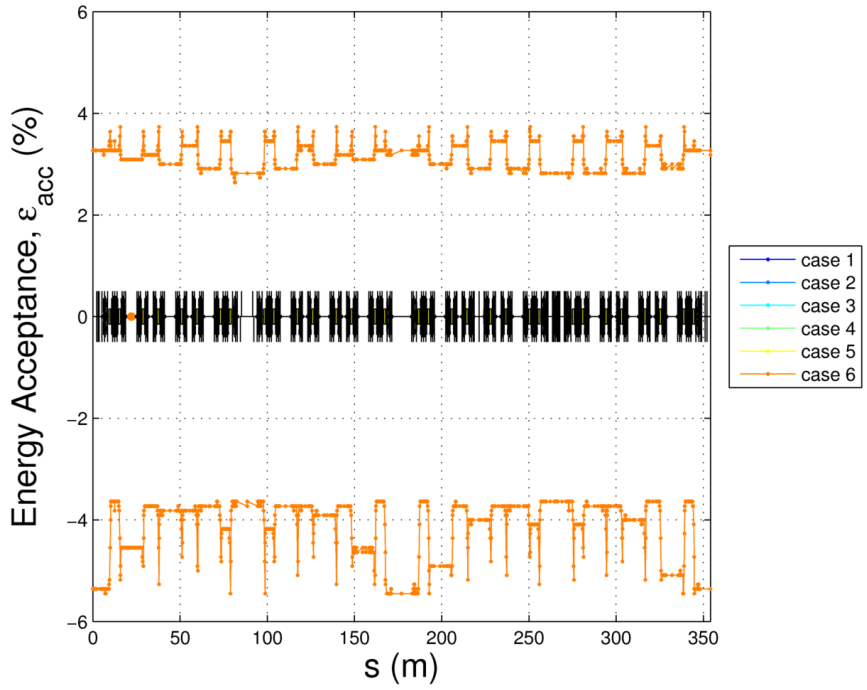

Figure 12: Variation of the energy acceptance along the ring calculated by TRACY3 for all the vertical scraper configurations of Table 13.

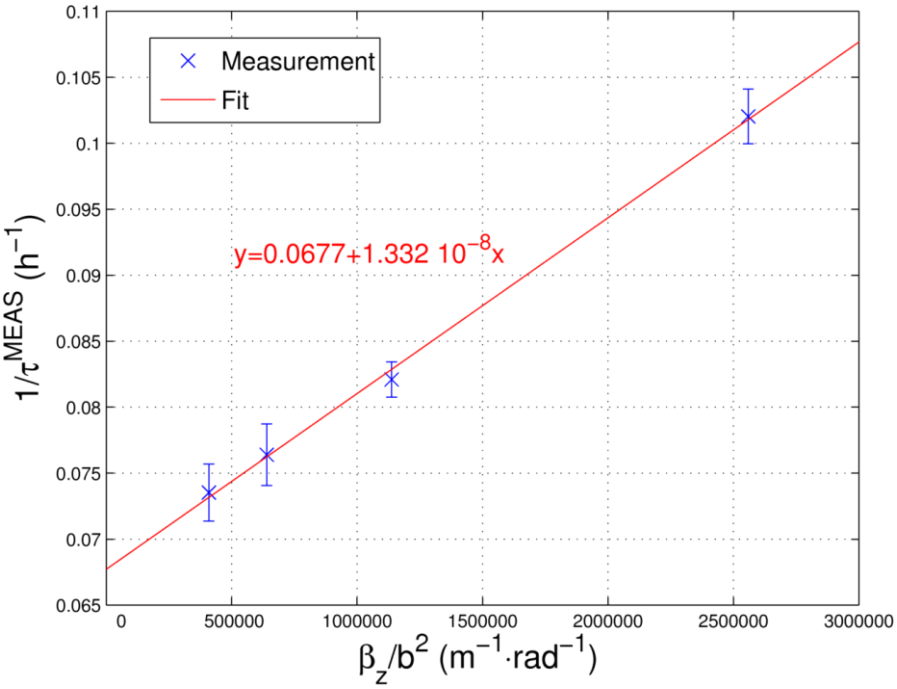

Figure 13: Inverse of the measured total beam lifetime versus the inverse of the vertical physical acceptances of the measurements n°3 to 6 of Table 13.

2.3.2. EXTERNAL HORIZONTAL SCRAPER EXPERIMENT

During this experiment, the internal horizontal scraper and the vertical scraper remain at their nominal positions. The external scraper was moved from 33 mm to 8 mm. Table 14 shows the beam lifetimes measured in the experiment versus the horizontal external scraper positions. Figure 14 compares the measured beam lifetimes with the calculated ones for the two values of the atomic number 7 and Z_{eff}. The energy acceptance value used to calculate the gas lifetime is the 3 % constant value.

In both measurements and calculations, the beam lifetime remains constant for high values of the external horizontal scraper apertures (measurements 1 to 6) because the horizontal physical aperture remains limited by the septum (gas contribution) and the energy acceptance is not reduced (Touschek lifetime) as can be seen on Figure 15 that presents the theoretical energy acceptances calculated by TRACY3 for all the experimental cases.

In this experiment, the reduction of the horizontal physical aperture has an influence on all the contributions of the gas lifetime by the mean of both the physical and energy acceptances (see Eq. 2, 4, 7 and 9), and of course on the Touschek lifetime by the mean of the energy acceptance. Then the assumed constant value of the energy acceptance for gas lifetime calculation is no correct anymore. As a consequence, the very good agreement between measurements and calculations for the Z = 7 value of the atomic number remains true for the shape of the curve but not for the level of the curve.

Moreover, the analytical formula that describes the dependence of the total beam lifetime versus the external horizontal scraper aperture a becomes then very complex and it is therefore impossible to deduced parameters without assuming many theoretical values.

Measurement Number	**a (mm)**	τ^{MEAS} **(h)**	**Measurement Number**	**a (mm)**	τ^{MEAS} **(h)**
1	(-28, 33)	12.90 ± 0.10	7	(-28, 16)	12.50 ± 0.10
2	(-28, 28)	13.00 ± 0.10	8	(-28, 14)	10.25 ± 0.08
3	(-28, 24)	12.80 ± 0.10	9	(-28, 12)	6.79 ± 0.02
4	(-28, 22)	12.70 ± 0.10	10	(-28, 10)	4.11 ± 0.03
5	(-28, 20)	12.90 ± 0.10	11	(-28, 8)	2.15 ± 0.02
6	(-28, 18)	12.80 ± 0.10			

Table 14: Variation of the beam lifetime measured versus the aperture (a) of the external horizontal scraper.

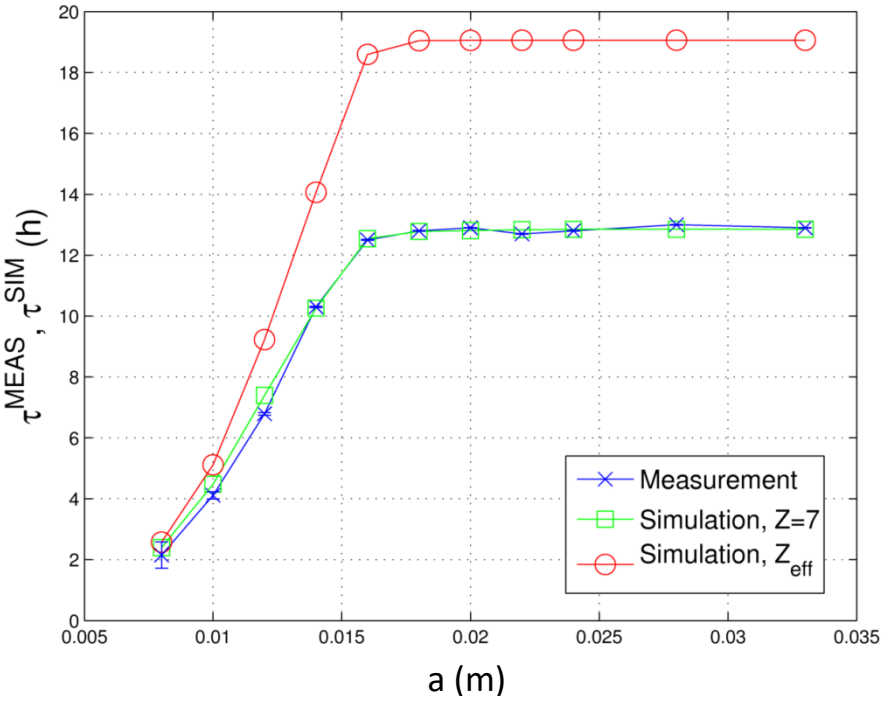

Figure 14: Variation of the measured and simulated beam lifetime the versus the horizontal external scraper aperture (a). The simulated gas beam lifetimes are calculated for two different values of the atomic number: Z_{eff} and Z=7 for a constant energy acceptance of 3 %.

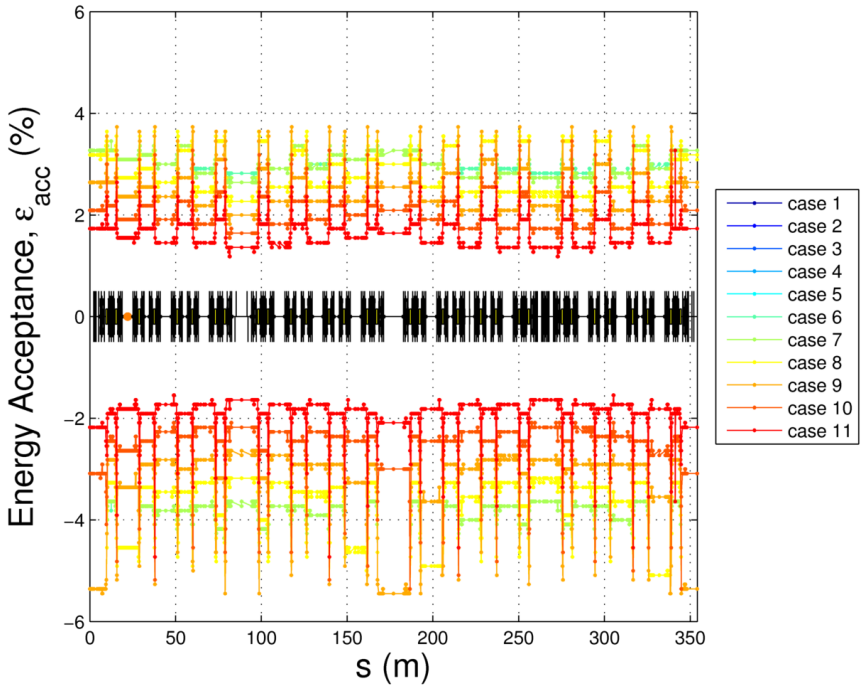

Figure 15: Variation of the energy acceptance along the ring calculated by TRACY3 for all the external horizontal scraper configurations of Table 14.

3. SUMMARY AND CONCLUSIONS

Two types of experiments have been performed to deduce both Touschek and gas experimental lifetimes: two experiments where beam properties are modified (vertical size by mean of the coupling, bunch current) and two experiments where the physical aperture of the ring is modified by mean of scraper aperture reduction. For the particular case of the nominal lattice of SOLEIL, this seems to be a powerful tool to test the validity of the models used up to now. Table 15 presents a summary of the experimental deduced results and a comparison with the expected values from the models for the two types of experiments.

Experiment	τ_{gas}^{SIM} **(h)**		τ_{Tous}^{SIM} **(h)**	τ_{gas}^{DED} **(h)**	τ_{Tous}^{DED} **(h)**
	Z=7	**Z_{eff}**			
Variation of the Coupling 312 bunches (I_b = 1.4 mA)	35.3	337.2	20.2	**62.5**	**13.0**
Variation of the Bunch Current 8 bunches (I_b = 6.25 mA)	67.9	647.5	6.9	**30.7**	**5.4**
Variation of the Vertical Scraper position 312 bunches (I_b = 1.4 mA)	**K^{SIM}** **(m rad h^{-1})**		**K^{DED}** **(m rad h^{-1})**		
	$2.3\ 10^{-8}$	$6.6\ 10^{-9}$	**$1.3\ 10^{-8}$**		

Table 15: Touschek and gas lifetime comparison between the simulation and experimental results for the different experiments. The simulated gas lifetime is calculated for two values Z = 7 and Z_{eff}. The Touschek lifetime is calculated with the Piwinski formula, a 1 % coupling, a RF-voltage of 2.665 MV and the nominal physical aperture.

The conclusions for the Touschek beam lifetime are:

- The deduced values from experiments are smaller than the expected ones by a factor of 30-40 % nevertheless the shapes of the experimental curves are very close to the expected ones.
- Then it can conclude that the energy acceptance is calculated properly with the ELEGANT and TRACY3 codes as a function of the longitudinal position in the ring.
- The integration of this energy acceptance in the Piwinski formula is confirmed to be a good method to estimate the Touschek lifetime in the case of SOLEIL. The use of the simplified Bruck formula is not precise enough.
- The variation of the bunch length with bunch current is an important effect that has to be taken into account in the calculation.

The conclusions for the gas beam lifetime are:

- The contribution of the vertical aperture limitation in the Elastic Nucleus Scattering is the only parameter that can be deduced from physical aperture experiments.

- The deduced gas lifetime values from the experiments are significantly closer to the expected ones calculated with the atomic number Z = 7 but there is still a factor of 2 between deduced and expected values.
- First we have checked that an error of even 10 % of the betatron functions at the location of each physical limitation along the ring cannot be the explanation of the disagreement between simulated and experimental gas lifetimes.
- The explanation should be that the real vacuum environment seen by the beam is not the one described in the calculations in terms of effective atomic number and mean pressure in the ring. Indeed the measurement of these two parameters is delicate in a synchrotron light source and in the case of SOLEIL, the presence of many in-vacuum undulators modifies strongly locally the pressure and the gas composition at these locations. Their distribution along the ring represents about 10 % of the total ring circumference. Figure 16 shows that the measurements performed at these locations show that the pressure can be 5-10 times larger than the mean pressures in the ring.
    - For instance, in the injection straight section, the pressure is almost 10 times larger than the average pressure taken in the computation. The gas composition in close to the effective atomic numbers $Z_{ENS,eff} = Z_{INS,eff} = 2.1$ and $Z_{ESS,eff} = Z_{ISS,eff} = 1.5$ as described previously. This section is not NEG coated and hosts many ceramic chambers for the injection kicker and the septum.
    - At the location of in-vacuum undulators, the average is not locally larger with a factor up to 6, the gas composition is also very different with higher Z components as measured recently: Table 16 gives the very recent results obtained by the residual gas analyzes of the insertion for a hybrid 450 mA filling pattern. The effective atomic number increased to $Z_{ENS,eff} = Z_{INS,eff} = 5.5$ and $Z_{ESS,eff} = Z_{ISS,eff} = 4.2$. In reality even higher Z-species could be present locally, these numbers are only a crude approximation. This is in a better agreement with the results of our measurements showing that the average effective Z should be close to 7.

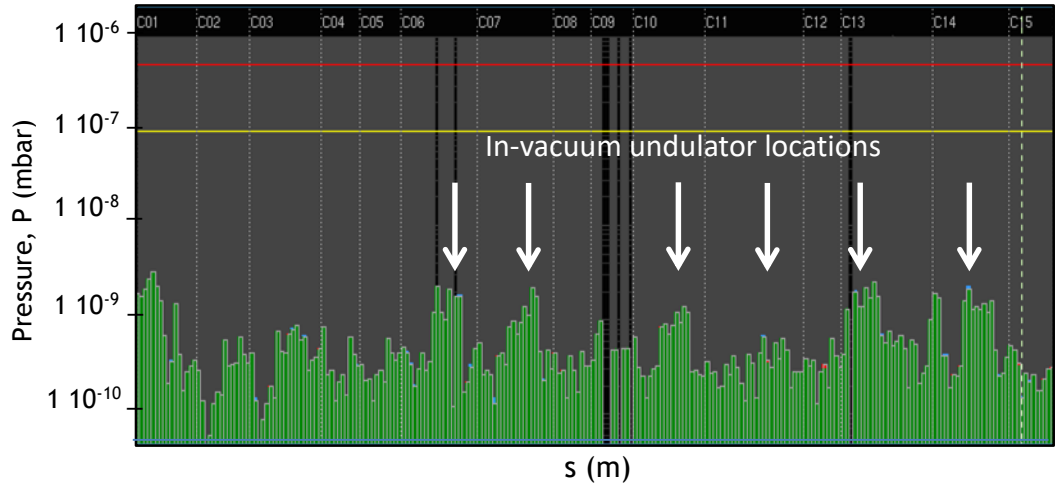

Figure 16: Variation of the local pressure (mbar) in logarithm scale along the ring (cells C01 to C16). The locations of the in-vacuum undulators are highlighted.

Residual Gas Molecule	κ_i	$\sum_j Z_j$	$\sum_{i,j} \kappa_i Z_j$	$\sum_j Z_j^2$	$\sum_{i,j} \kappa_i Z_j^2$
H_2	0.585	2	2	1.170	1.170
CO	0.242	14	100	3.388	24.200
N_2	0.040	14	98	0.560	3.920
CF_4	0.036	42	360	1.512	12.960
F_2	0.070	18	162	1.260	11.340
HCl	0.015	18	290	0.270	4.350
CO_2	0.012	22	164	0.264	1.968
sum	1	130	1176	**8.424**	**59.908**
N_2	1	14	98	14	98

Table 16: Residual gas composition measured at SOLEIL representing the environment of an in-vacuum insertion device. κ_i is the gas concentration and Z_j the atomic number of each atom j in the molecule i. Courtesy of C. Herbeaux and N. Béchu.

BIBLIOGRAPHY

(Béchu, 2015) Measurement performed by N. Béchu and C. Herbeaux (Ultra-Vacuum Group).

(Bernardini, 1963) C. Bernardini, G. F. Corazza, G. Di Guigno, G. Guido, J. Hassinski, P. Marin, R. Querzoli, and B. Touschek. Lifetime and Beam Size in a Storage Ring. Physical Review Letters, vol. 10, nº9, 1963.

(Carmignani, 2014) N. Carmignani. Touschek Lifetime Studies and Optimization of the ESRF: Present and Upgraded Lattice. PhD Thesis, Pisa University, Italy, 2014.

(Decking, 1998) W. Decking, J. Byrd, C. Kim, and D. S. Robin. Lifetime Studies at the Advanced Light Source. Proceedings of the 1998 European Particle Accelerator Conference, pp. 1262-1265, Stockholm, 1998.

(Hansson, 2013) A. Hanssom, A. Andersson, J. Breulin, G. Skripa, and E. Wallén. Studies of the Electron Beam Lifetime at MAX III. Proceedings of the 2013 International Particle Accelerator Conference, pp. 208-210, Shangai, China, 2013.

(Herbeaux, 2008) C. Herbeaux, N. Béchu, A. Conte, P. Manini, A. Bonucci, and S. Raimondi. NEG Coated Chambers at SOLEIL: Technological Issues and Experimental Results. Proceedings of the 2008 European Particle Accelerator Conference, pp. 3711-3713, Genoa, Italy, 2008.

(Huang, 2011) X. Huang and J. Corbett. Measurement of Beam Lifetime and Applications for SPEAR3. Nuclear Instruments and Methods in Physics Research Section A: Accelerators, Spectrometers, Detectors and Associated Equipment, 629(1):31–36, 2011.

(Huttel, 2003) E. Huttel, I. Birkel, A.-S. Müller, F. Perez, and M. Pont. Studies of Beam Lifetime at ANKA. Proceedings of the 2003 Particle Accelerator Conference, pp. 893-895, Portland, USA, 2003.

(Khan, 1999) S. Khan. Study of the BESSY-II Lifetime. Proceedings of the 1999 Particle Accelerator Conference, pp. 2831-2833, New York, USA, 1999.

(Le Duff, 1985) J. Le Duff. Current and Current Density Limitations in Existing Electron Storage Rings. Nuclear Instruments and Methods in Physics Research, A239, pp. 83-101, 1985.

(Mochihashi, 2007) A. Mochihashi, M. Katoh, M. Hosaka, Y. Takashima, and Y. Hori. Touschek Lifetime Measurement with a Spurious Bunch in Single-bunch Operation in the UVSOR-II Electron Storage Ring. Nuclear Instruments and Methods in Physics

Research Section A: Accelerators, Spectrometers, Detectors and Associated Equipment, 572(3):1033–1041, 2007.

(Nadji, 1998) A. Nadji, G. Flynn, J.-L. Laclare, M.-P. Level, P. Nghiem, and J. Payet. Energy Acceptance and Touschek Lifetime Calculations for the SOLEIL Project. Proceeding of the 1997 Particle Accelerator Conference, pp. 1517-1549, Vancouver, Canada, 1997.

(PDG, 2015) Particle Data Book, http://pdg.lbl.gov.

(Podobedov, 2015) B. Podobedov, W. Cheng, Y. Hidaka, H.-C. Hseuh, and G. Wang. NSLS-II Beam Lifetime Measurements and Modeling. Proceedings of the 2015 International Particle Accelerator Conference, pp. 415-417, Richmond, VA, USA 2015.

(Seidel, 2008) M. Seidel and K. Zapfe, Chapter 8, "Particle Accelerators" in *Vacuum electronics: components and devices*. Springer Science & Business Media, J. A., Eichmeier and M. Thumm (Eds.), 2008.

(Spencer, 2007) M. J. Spencer, M. J. Boland, R. T. Dowd, G. LeBlanc, and Y. E. Tan. Lifetime Contribution Measurements at the Australian Synchrotron. Proceedings of the 2007 Particle Accelerator Conference, pp. 914-916, New Mexico, USA, 2007.

(Steier, 2009) C. Steier and L. Yang. Touschek Lifetime Measurements at Small Horizontal Emittance in the ALS. Proceedings of the 2009 Particle Accelerator Conference, pp. 3269–3271, Vancouver, BC, Canada , 2009.

(Streun, 2001) A. Streun. Beam Lifetime of the SLS Storage Ring. SLSTME-TA-2001-0191 (2001).

(Wiedemann, 2007) H. Wiedemann. Particle Accelerator Physics. Springer-Verlag Berlin and Heidelberg GmgH & Co. K, 3rd edition (2007).

CHAPTER IV
OPTIMIZATION OF THE TRANSVERSE BEAM DYNAMICS OF THE SOLEIL NOMINAL LATTICE

CONTENTS

The aim of this chapter is to present optimized lattices of SOLEIL obtained by using the genetic-based optimization code MOGA-ELEGANT. The main objective is to validate experimentally this type of algorithm to optimize the lattice of today or for future upgrades at SOLEIL. During this work, only the SOLEIL current storage ring lattice was considered. This lattice has been optimized over the years to maximize the beam performance especially in presence of the 26 insertion devices controlled freely by the users. The lattice is considered to be robust and to give a fair trade-off between the electron beam lifetime and injection efficiency in the storage ring. As a first step, solutions from the Pareto-optimal front were selected. Then they were further studied using the long-term tracking code TRACY3 where a more complete model of the magnetic defaults (multipolar field components) and quadrupole fringe field were included along with a full description of the physical aperture restricting the transverse oscillations of the beam. To end, a set of best candidate solutions were tested experimentally in terms of optics settings and beam performance (injection efficiency and Touschek beam lifetime).

1. MOGA OPTIMIZATION RESULTS

1.1. STARTING POINT OF THE OPTIMIZATION

For MOGA-ELEGANT computation, ELEGANT uses a model describing a perfect lattice of SOLEIL, that is to say, a model that does not include the multipolar field components of the main magnets and corrector magnets but including the physical aperture (see Chapter II.3.4). In this study, insertion devices are not considered although they may strongly impact the beam dynamics and lower the physical aperture considering in-vacuum devices. The lattice considered is very similar to the lattice set until today in the control room for user's operation (namely SOLEIL2013 presented in Chapter II): only the first sextupole family strength (S1) is slightly different (3.1 % weaker) for machine radiation protection purpose. This will be the starting point (SP) for all the MOGA-ELEGANT simulations.

The lattice performance is evaluated using proxies: the Touschek lifetime and injection efficiency related to the off- and on-momentum beam dynamics respectively (see Chapter I.3.1). The off-momentum parameter is the energy acceptance calculated all around the ring. It is the smallest acceptance between transverse and RF acceptances. It will be used to calculate the Touschek lifetime. The on-momentum parameter is the area of the dynamic aperture calculated at the injection point location.

For saving the high-demanding computation time of MOGA-ELEGANT, the model of the SOLEIL vacuum chamber dimensions is taken into account only in the first quarter of the ring circumference.

1.2. OPTIMIZATION PARAMETERS

The variables taken into account by the MOGA-ELEGANT optimization are the two quadrupole families Q7 and Q9 used to modify the horizontal and vertical tunes. The error bars of horizontal and vertical tunes are set to 0.01 using the soft operator of ELEGANT (similar to Eq. 40 in Chapter I). The nonlinear optimization uses the 11 sextupole families as nonlinear knobs. Among them, the sextupole families S9 and S10 will be further used to fit the chromaticity values to 1.2 and 2.0 in the horizontal and vertical planes respectively. The parameter space is then of dimension 13.

The tracking process is six-dimensional (6D) including the synchrotron oscillation using a RF-cavity with a voltage of 2.665 MV and the number of turns used is 1,000. Synchrotron radiation and radiation damping are also taken into account during the off-momentum tracking.

The parameters taken into account in ELEGANT to compute the dynamic and momentum apertures are listed in Table 1. These values are the same as the values found in Chapter II except the vertical amplitude range for the DA computation: it is reduced down to 10 mm due to the introduction of the physical aperture limitations. The Touschek lifetime is calculated using 1 mA of bunch current, 1 % coupling, 6 mm bunch length and the horizontal emittance and energy acceptance of each particular solution.

As explained in Chapter I, the tune scan region was constraint so that the fractional part of the tunes could vary between 0.1 and 0.4. Therefore solutions close to the integer or half-integer resonances are rejected since the final optics will suffer from instabilities: close orbits diverge for tunes close to integer resonance and quadrupole error effects are amplified when one of the tunes is in the vicinity of a half-integer resonance. The errorLevels controlling the genetic algorithm are found to be optimum for (e_s,e_v) = (0.5 m^{-3}, 0.001) respectively for sextupole and quadrupole strength variations (see Eq. 42 and Eq. 44 in Chapter I).

Dynamic Aperture			**Momentum Aperture**	
Parameters	**Values**		**Parameters**	**Values**
Number of Turns	1,000		Number of Turns	1,000
Number of Lines	21		Initial Conditions (x_0, z_0) (m)	(10^{-6}, 10^{-4})
H. Amplitude Range (m)	(-0.035, 0.035)		Energy Range (%)	(-10, 10)
V. Amplitude Range (m)	(0.000, 0.010)			
Step Size	31		Step Size (%)	0.1
Step Back Number (*n_split*)	1		Step Back Number	1
Number of Subdivisions (*split_fraction*)	10		Subdivision Factor	10

Table 1: Main parameters used by MOGA-ELEGANT to compute the dynamic and momentum apertures during the optimization of SOLEIL2013 lattice.

1.3. Simulation Results

1.3.1. MOGA Result for the Nominal Lattice of SOLEIL

Figure 1 shows the optimization results obtained by MOGA-ELEGANT for the Touschek lifetime and the area of the dynamic aperture of the optimized solutions starting from the SOLEIL2013 lattice. A population of circa 48,000 (46,000 stable) individuals was obtained after one month of computation using 200 of the CPUs available in the computation cluster; 240 generations were evaluated to build the Pareto-optimal front that shows a convergence.

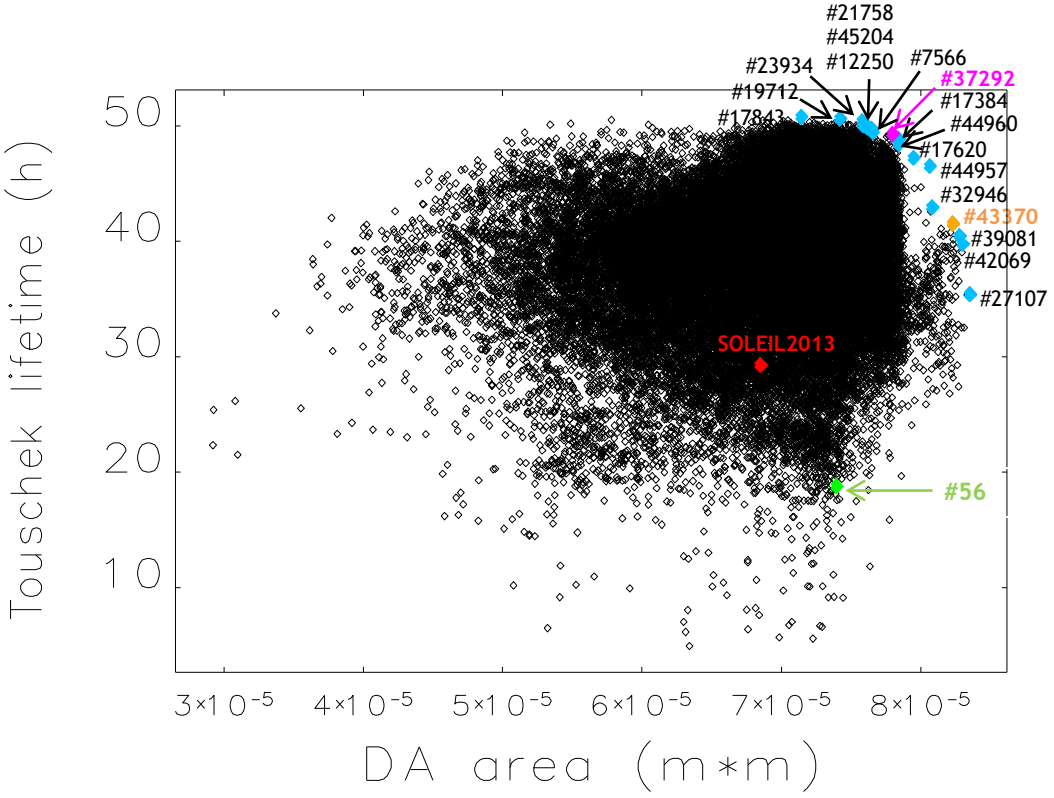

Figure 1: Optimized solutions of the SOLEIL2013 storage ring lattice obtained by MOGA-ELEGANT after 1 month of computation using 200 CPUs in terms of area of dynamic aperture and Touschek lifetime. The red point is the SOLEIL2013 lattice called starting point and the cyan points with ID numbers are points of the Pareto-optimal front. The solutions chosen for experiments are highlighted in green (#56), magenta (#37292) and orange (#43370). The black points are the solutions dominated by the Pareto-optimal front. 6D-tracking parameters: 2.665 MV of RF-voltage and 1,000 of turns including the synchrotron radiation and the radiation damping for the off-momentum acceptance calculation.

The starting SOLEIL2013 lattice is represented in red on Figure 1 with an already large Touschek lifetime of 29 hours and it enables an injection with a 95 % to 100 % efficiency meaning that the dynamic aperture is already maximized. The Pareto-optimal front is depicted using blue dots and ID numbers for identification and is made of 17 solutions with different values of Touschek lifetime ranging from 35.4 h to 50.8 h (Table 2). The Pareto-optimal solutions dominate the rest of stable represented in black. They are the solutions with the largest dynamic apertures for a

given Touschek lifetime or with the largest Touschek lifetimes for a given dynamic aperture. The results give a maximum improvement of the Touschek lifetime by 73% and of the area of the dynamic aperture by 24% with respect to the starting point.

Besides the Pareto-optimal solutions, Figure 1 also exhibits three solutions #56 (green dot), #37292 (magenta dot) and #43370 (orange dot) that will be discussed in more details in the next sections.

Lattice	DA Area (m^{-2})	Touschek Lifetime (h)	ν_x	ν_x
Nominal	6.85 10^{-5}	29.3	18.157	10.229
Solutions belonging to the Pareto-optimal front				
#7566	7.65 10^{-5}	49.5	18.095	10.236
#12250	7.65 10^{-5}	49.8	18.095	10.236
#17384	7.84 10^{-5}	48.9	18.101	10.268
#17620	7.95 10^{-5}	47.2	18.121	10.257
#17843	7.14 10^{-5}	50.8	18.105	10.245
#19712	7.42 10^{-5}	50.6	18.095	10.236
#21758	7.61 10^{-5}	49.9	18.095	10.236
#23934	7.58 10^{-5}	50.4	18.105	10.245
#27107	8.35 10^{-5}	35.4	18.173	10.258
#32946	8.08 10^{-5}	43.0	18.112	10.258
#37292	7.80 10^{-5}	49.3	18.101	10.268
#39081	8.28 10^{-5}	40.4	18.163	10.258
#42069	8.30 10^{-5}	39.8	18.163	10.258
#43370	8.23 10^{-5}	41.5	18.163	10.258
#44957	8.06 10^{-5}	46.5	18.118	10.258
#44960	8.06 10^{-5}	46.5	18.112	10.258
#45204	7.58 10^{-5}	50.1	18.105	10.245
Specific solution not belonging to the Pareto-optimal front				
#56	7.40 10^{-5}	18.8	18.156	10.229

Table 2: Dynamic aperture area and Touschek lifetime for each point of the Pareto-optimal front and a specific solution obtained by MOGA-ELEGANT after 30 days of computation (200 CPUs). Touschek lifetime is calculated for 1 mA bunch current, 1 % coupling and 6 mm bunch length.

Figure 2 shows the tune scan region explored by MOGA-ELEGANT optimizing the SOLEIL2013 storage ring lattice using a color code proportional to the area of the dynamic aperture (Figure 2a) or the Touschek lifetime (Figure 2b). The tune fractional part region of the optimization process is limited between 0.1 and 0.4 to avoid the effects of the integer and half integer resonance lines on the performance of the real machine.

It is worth noting that MOGA-ELEGANT finds different groups of solutions. One group has low horizontal tune close to 18.1. As other users of MOGA-ELEGANT have

reported it during a workshop of Eucard2 Low Emittance Ring in 2015 (LER, 2015), there might be a bias in the algorithm. Practically, this type of solution is often of poorer performance in terms of sensitivity of the closed orbit to errors and of the horizontal phase advance during the off-axis injection process (accumulation, top-up injection).

Another group of solutions has larger horizontal tunes (solutions #42096, #43370, #39081 and #27107). None of these solutions were ever explored up to now. Moreover many solutions of lower rank exhibit interesting performance.

Figure 3 and Figure 4 show histograms of the distribution of the sextupole settings. Among the sextupoles, the strength variation can reach 10 % to 15 %. For all distribution the black vertical line represents the SOLEIL2013 settings of the magnets. Similar histograms are given for the horizontal and vertical tunes (Figure 5). It is interesting to notice that for some sextupole families the distribution is centered far away from the starting value.

As a second stage of this study and time demanding work, the solutions of the Pareto-optimal front were carefully evaluated using Frequency Map Analysis so to analyze the diffusion process that characterizes the beam dynamics. TRACY3 code was used for this purposed with a refined model including multipolar field components and quadrupole fringe field. In terms of tune diffusion, a special care was given to the injection area in the dynamic aperture around -8 mm in the horizontal plane. The solutions were then sorted. Two of them labeled #37292 (low horizontal tune) and #43370 (higher horizontal tune) were selected because of their high-expected performance for being tested with beam-based measurements. Another solution, #56, was chosen for its much lower Touschek lifetime than the nominal case in order to check the validity of both the genetic algorithm and of the magnetic model used to describe the lattice. Numerical results are presented in the next section in terms of beam dynamics, tune shifts with amplitudes and energy, and the dynamic and momentum apertures with their respective FMAs.

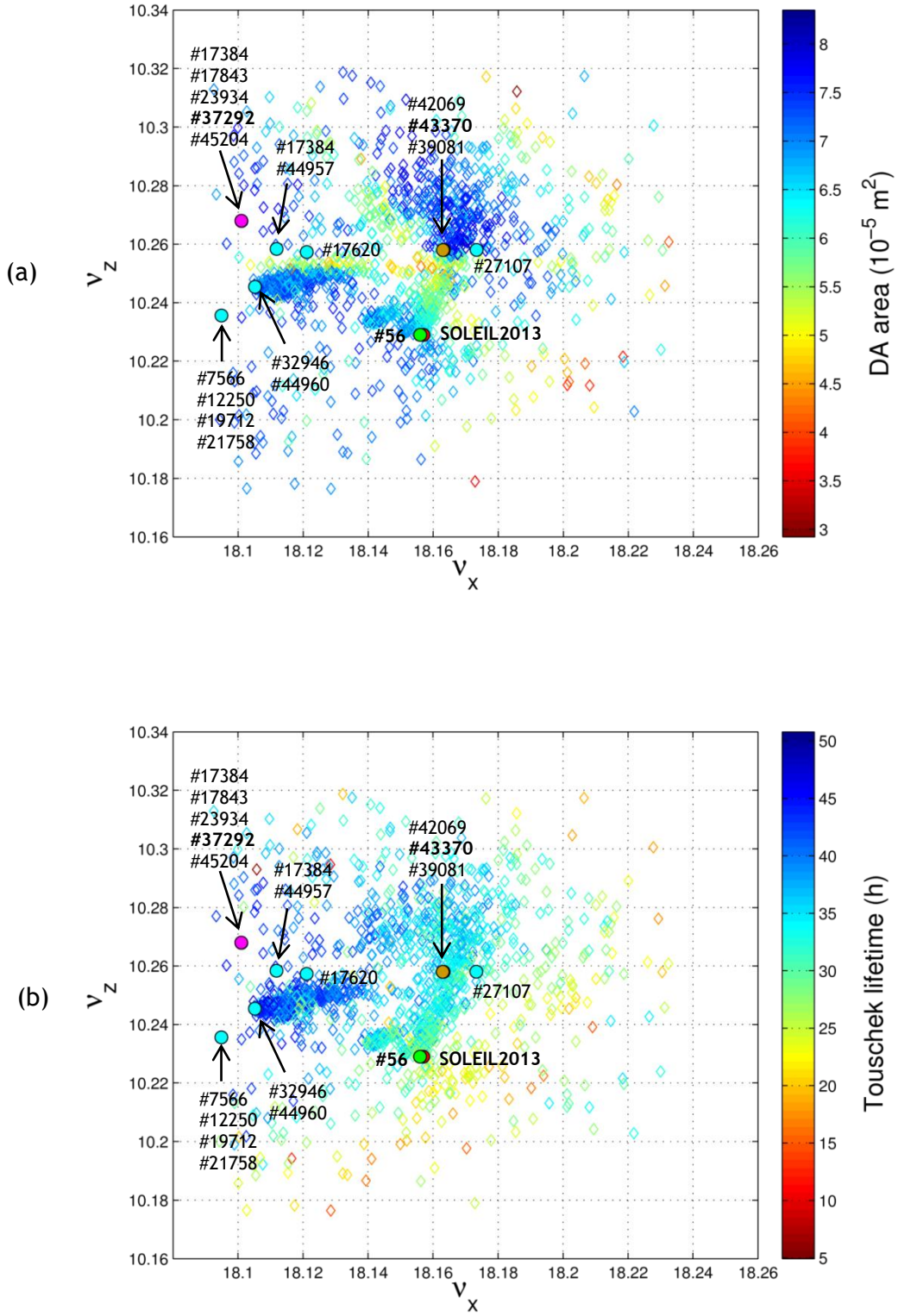

Figure 2: Tune region explored by MOGA-ELEGANT algorithm color-coded with the area of the dynamic aperture (a) and the Touschek lifetime values (b) for the SOLEIL2013 lattice. The SOLEIL2013 lattice (SP), the Pareto-optimal solutions and the solutions selected for experiments are indicated.

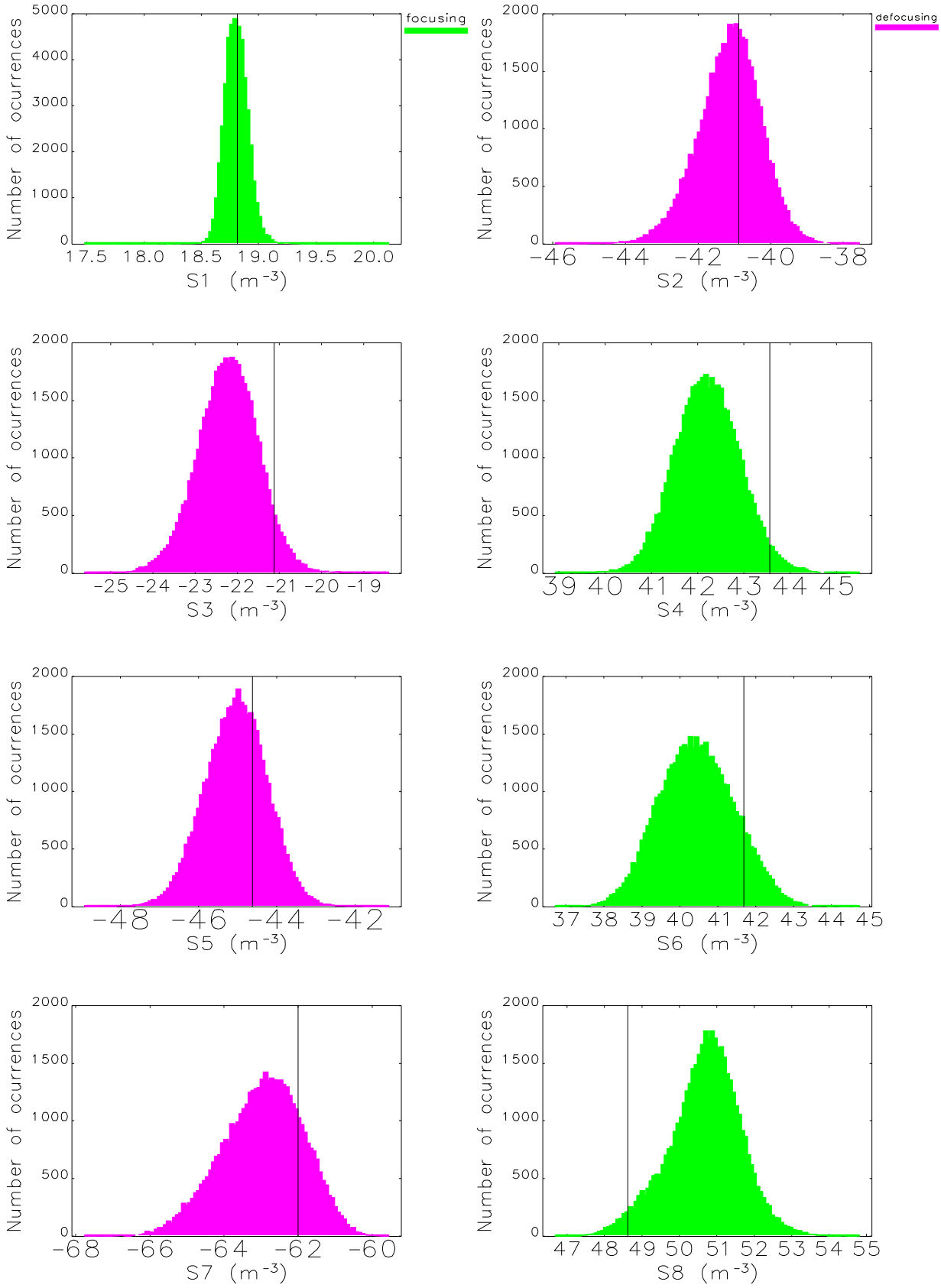

Figure 3: Histograms of the sextupole strengths (S1 to S8) for all the stable solutions found by MOGA-ELEGANT. The starting point for the magnet strengths is shown as a vertical black line. Focusing sextupoles are represented in green and defocusing ones in magenta.

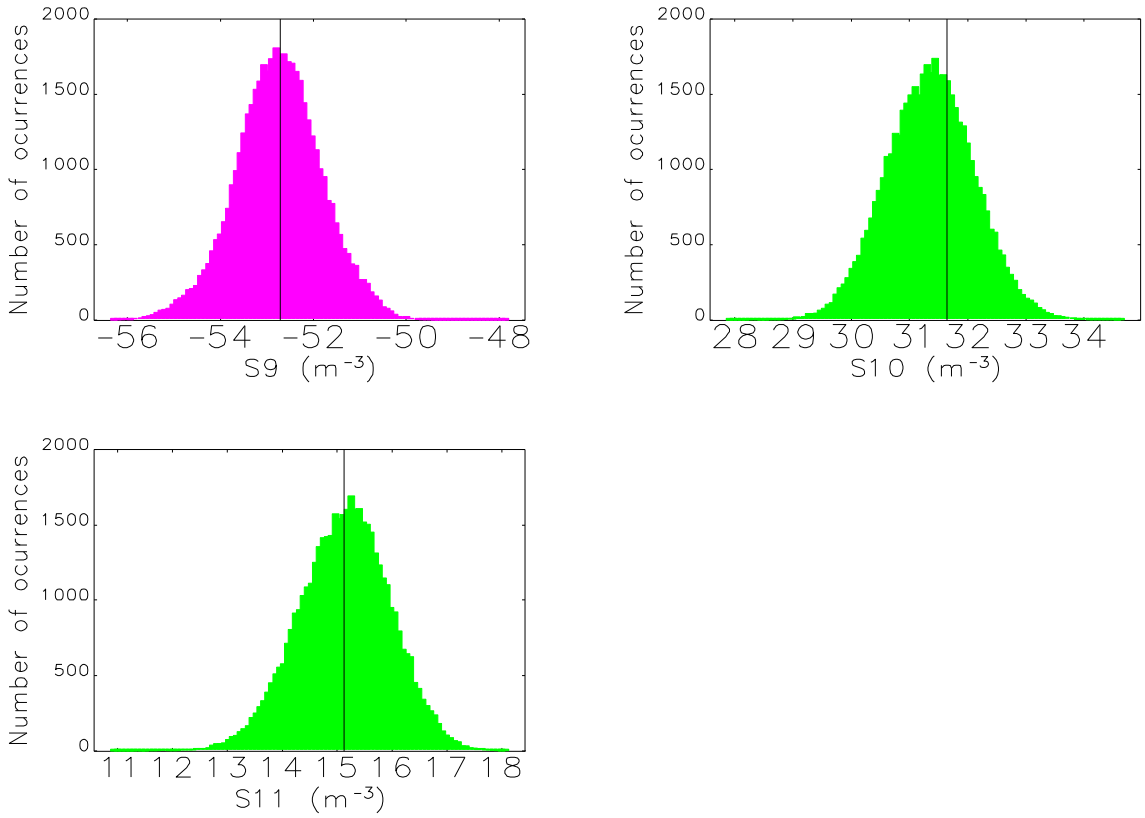

Figure 4: Histograms of the sextupole strengths (S9 to S11) for all the stable solutions found by MOGA-ELEGANT. The starting point for the magnet strengths is shown as a vertical black line. Focusing sextupoles are represented in green and defocusing ones in magenta color.

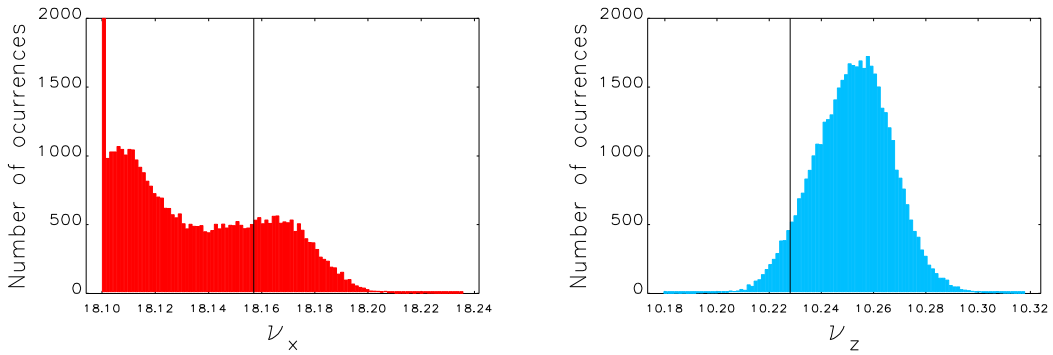

Figure 5: Histograms of the horizontal and vertical tunes (ν_x, ν_z) for all the stable solutions found by MOGA-ELEGANT. The starting point tunes are shown as a vertical black line. For the horizontal plane, the number of solutions with a tune of 18.10 is 8,000.

1.3.2. SELECTION OF CANDIDATE LATTICES

1.3.2.1. On- and off-Momentum Apertures

Figure 6 shows the dynamic aperture and the frequency map of the solution #37292 (low H-tune solution). The DA is dominated by strong resonance lines of orders 5 and 7 close to the injection point of -8 mm, but for vertical amplitudes that are larger than the injection ones. Then the injection efficiency should not be affected except by the effect of the proximity of the horizontal integer resonance.

Figure 7 shows the variation of the horizontal amplitudes with the relative energy offset together with its frequency map for the same lattice. The negative energy acceptance is larger than the nominal lattice shown in Figure 17b of Chapter II.

Figure 8 shows the dynamic aperture and their frequency map of the solution #43370 (high H-tune solution). In this case, the DA (Figure 8b) is better than the solution #37292 in terms of diffusion rates and then may give better injection efficiency.

Figure 9 shows the variation of the horizontal amplitudes with the relative energy offset together with its frequency map of the solution #43370: there is an improvement of the negative side up to 7 % with respect to the nominal of Figure 17b of Chapter II. Then, the momentum aperture and the Touschek lifetime are larger than the nominal case.

Figure 10 shows the dynamic aperture and their frequency map of the solution #56. The diffusion rate is low at the injection location of -8 mm (Figure 10b). This point should have similar injection performance than the nominal lattice. The frequency map presents a fold for larger horizontal tunes.

Figure 11 shows the variation of the horizontal amplitudes with the relative energy offset together with its frequency map: the negative momentum acceptance (Figure 11b) is smaller by almost 2% than the nominal case (Figure 17b of Chapter II) reducing the contribution of the momentum aperture and the Touschek lifetime. This lattice will be used, as a counter-example, to test whether the storage ring lifetime is as low as predicted by the model while preserving a large fraction horizontal tune and the injection efficiency.

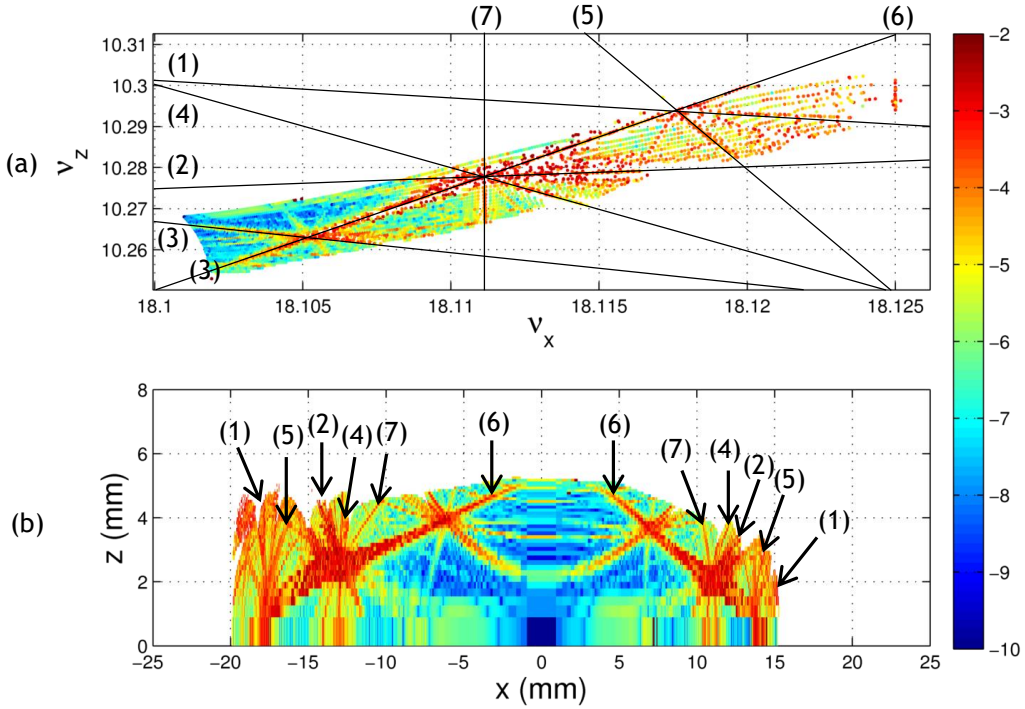

Figure 6: Dynamic apertures (a) and its frequency maps (b) for the MOGA-ELEGANT solution #37292 (low H-tune) calculated by TRACY3 adding the dimensions of the vacuum chamber and the multipolar field components. The main resonance lines are identified: $\nu_x+3\nu_z=49$ (1), $\nu_x+4\nu_z=23$ (2), $2\nu_x+3\nu_z=67$ (3), $4\nu_x+2\nu_z=93$ (4), $6\nu_x+\nu_z=119$ (5), $5\nu_x-2\nu_z=70$ (6), $9\nu_z=173$ (7). The 6D-tracking uses the parameters of Table 10, Chapter II. The color indicates the diffusion rate with blue color for lower values.

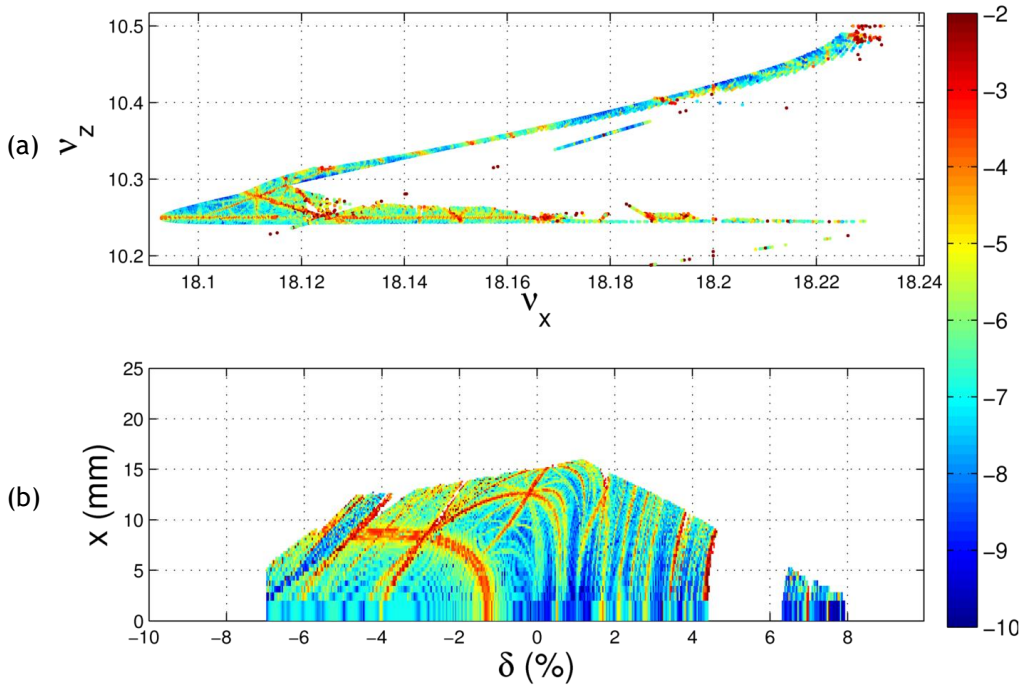

Figure 7: Variation of the horizontal amplitudes with the energy offset (b) with its frequency map (a) for the MOGA-ELEGANT solution #37292 (low H-tune) calculated by TRACY3 adding the dimensions of the vacuum chamber and the multipolar field components. The 6D-tracking uses the parameters of Table 10, Chapter II. The color indicates the diffusion rate with blue color for lower values.

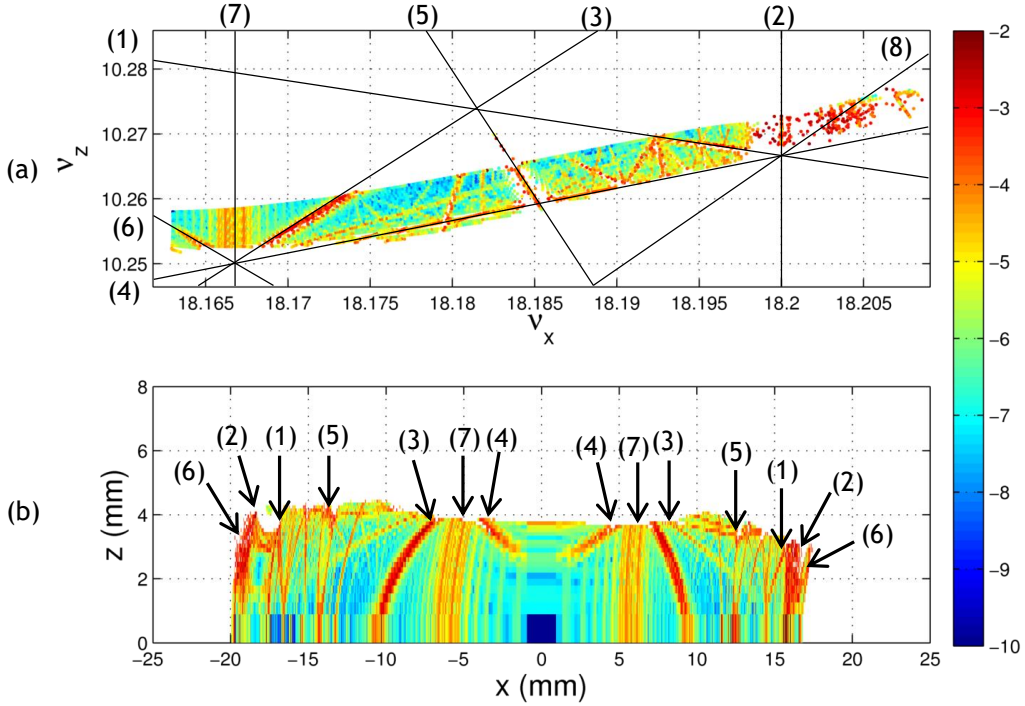

Figure 8: Dynamic apertures (a) and their frequency maps (b) for the MOGA-ELEGANT solution #43370 (high H-tune) calculated by TRACY3 adding the dimensions of the vacuum chamber and the multipolar field components. The main resonance lines are identified: $\nu_x+3\nu_z=49$ (1), $5\nu_z=91$ (2), $3\nu_x+2\nu_z=34$ (3), $3\nu_x+2\nu_z=75$ (4), $4\nu_x+\nu_z=83$ (5), $4\nu_x+3\nu_z=42$ (6), $7\nu_z=72$ (7), and $6\nu_x+3\nu_z=140$ (8). 6D-tracking parameters of Table 10, Chapter II. The color indicates the diffusion rate with blue color for lower values.

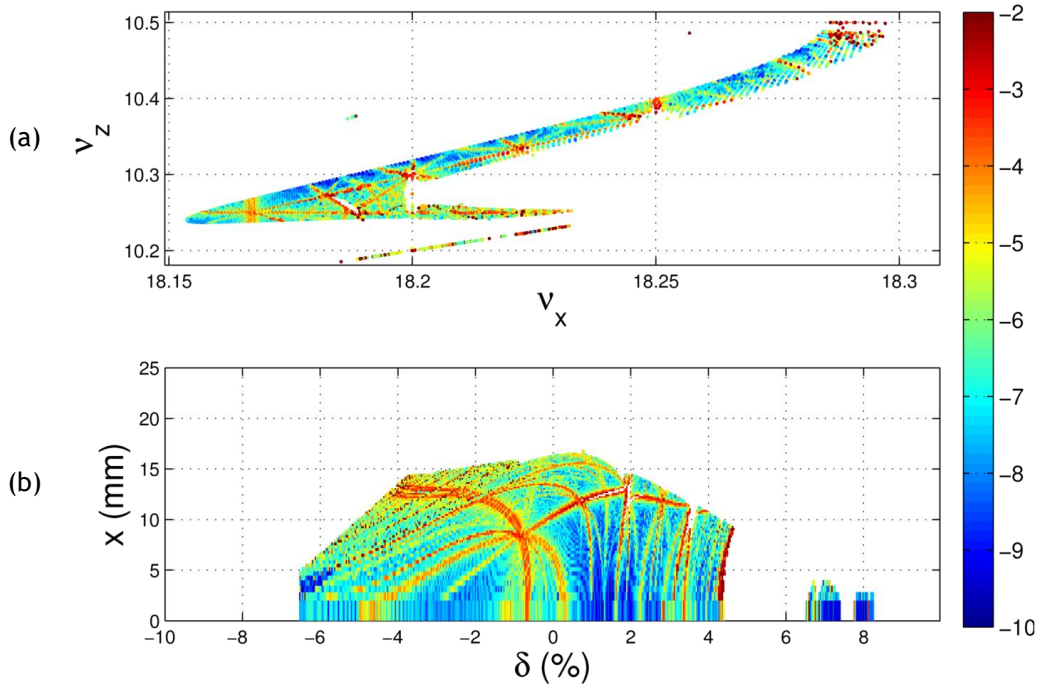

Figure 9: Variation of the horizontal amplitudes with the energy offset (b) with its frequency map (a) for the MOGA-ELEGANT solution #43370 (high H-tune) calculated by TRACY3 adding the dimensions of the vacuum chamber and the multipolar field components. 6D-tracking parameters of Table 10, Chapter II. The color indicates the diffusion rate with blue color for lower values.

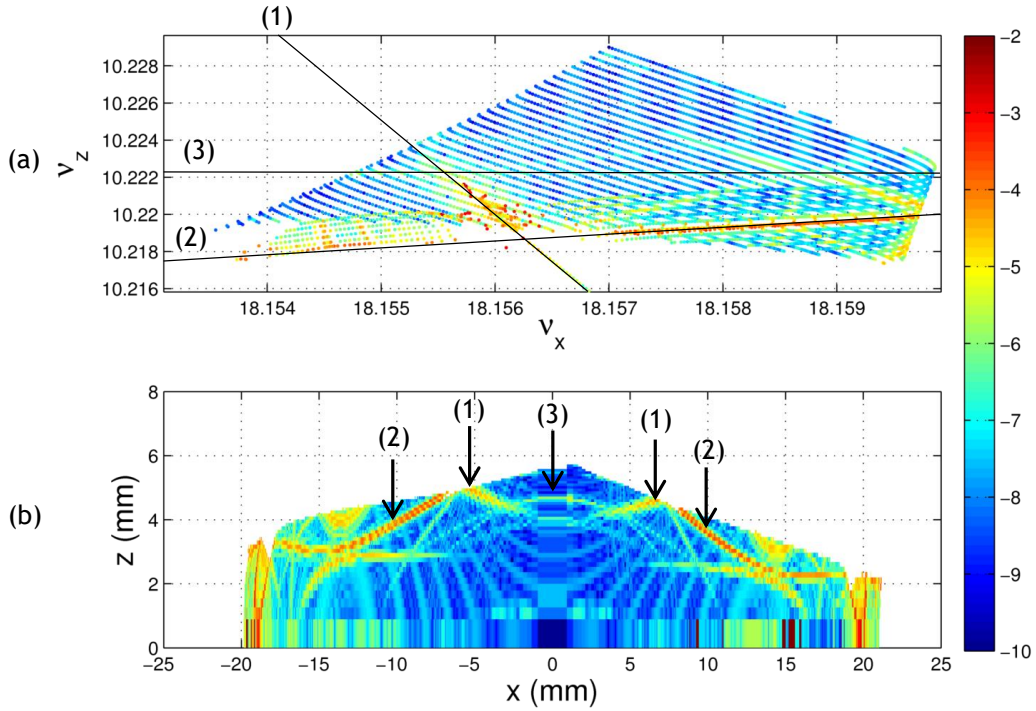

Figure 10: Dynamic apertures (b) and their frequency maps (a) for the MOGA-ELEGANT solution #56 calculated by TRACY3 adding the dimensions of the vacuum chamber and the multipolar field components. The resonance lines are identified: $5\nu_x+\nu_z=101$ (1), $4\nu_x-3\nu_z=42$ (2) and $2\nu_x-6\nu_z=-25$ (3). 6D-tracking parameters of Table 10, Chapter II. The color indicates the diffusion rate with blue color for lower values.

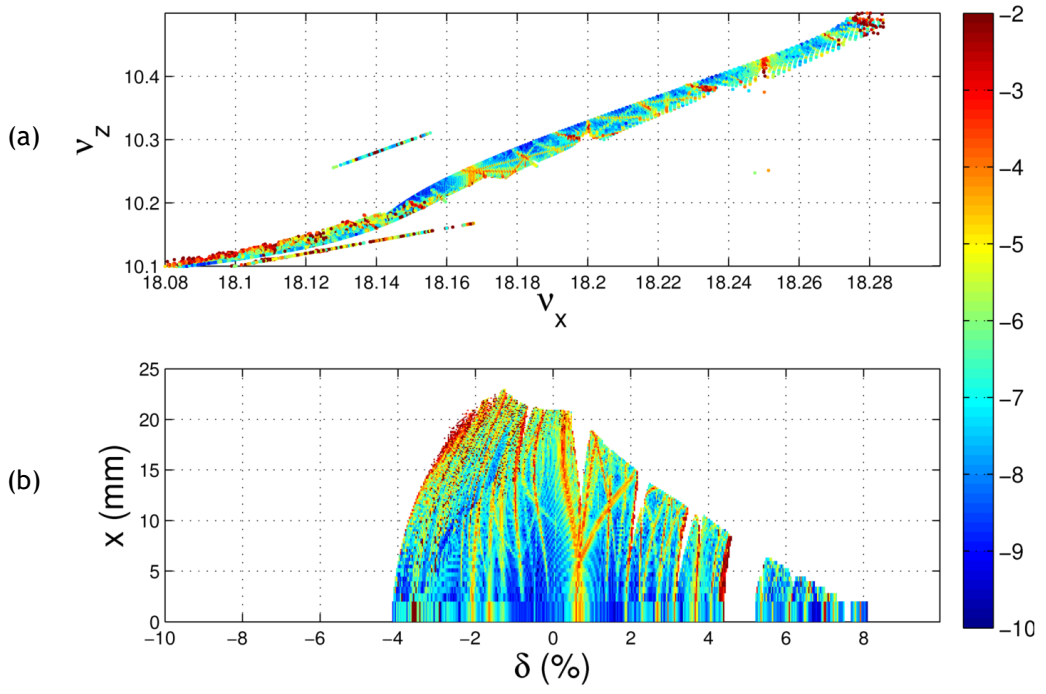

Figure 11: Variation of the horizontal amplitudes with the energy offset (b) with their frequency maps (a) for the MOGA-ELEGANT solution #56 calculated by TRACY3 adding the dimensions of the vacuum chamber and the multipolar field components. 6D-tracking parameters of Table 10, Chapter II. The color indicates the diffusion rate with blue color for lower values.

1.3.2.2. Tune Shifts with Transverse Amplitudes and Energy Offsets

The tune shifts with the transverse horizontal and vertical amplitudes and energy offset of the SOLEIL2013 storage ring lattice and the three optimized solutions selected from the optimization process of MOGA-ELEGANT are shown in Figure 12, Figure 13 and Figure 14, respectively. This is another standard way of presenting the performance of a given lattice. The parameters used by TRACY3 code to compute the tune shift versus horizontal and vertical amplitudes and energy offset are listed in Table 3.

Tune Shifts with Amplitude			**Tune Shifts with Energy**	
Parameters	**Values**		**Parameters**	**Values**
Number of Turns	1,000		Number of Turns	1,000
Horizontal Range (m)	(-0.04, 0.04)		Energy Range (%)	(-10, 10)
Vertical Range (m)	(-0.01, 0.01)		Number of Points	100
Number of Points in H. Plane	100			
Number of Points in V. Plane	100			

Table 3: Main parameters used by TRACY3 code to compute the tune shift versus transverse horizontal and vertical amplitudes and energy.

Figure 12 shows the tune shifts with the transverse horizontal amplitude for the SOLEIL2013 storage ring lattice and the three studied solutions selected from MOGA-ELEGANT. The horizontal tune shifts of the optimized solutions changes significantly with respect to the nominal lattice. The change in sextupole strengths and tunes does not modify the tune shift with horizontal amplitude.

Figure 13 shows the tune shifts with the vertical amplitude for the SOLEIL2013 lattice and the three selected solutions from MOGA-ELEGANT. The tune shift with vertical amplitude is almost constant since the dynamics is almost linear with maximum 4 mm amplitude of oscillation.

Figure 14 shows the horizontal and vertical tune shift with energy offset of the SOLEIL2013 storage ring lattice and the three solutions selected from MOGA-ELEGANT. Here, the tune shifts with energy are significantly modified in both horizontal and vertical planes for the negative energy derivation values. The key ingredient is the higher orders of the nonlinear chromaticities that curve back the tunes away from the integer resonance line. The starting optic is limited around -5% where the horizontal tune crosses the integer resonance. Besides the transverse off-momentum beam dynamics is limited by the half-integer resonance.

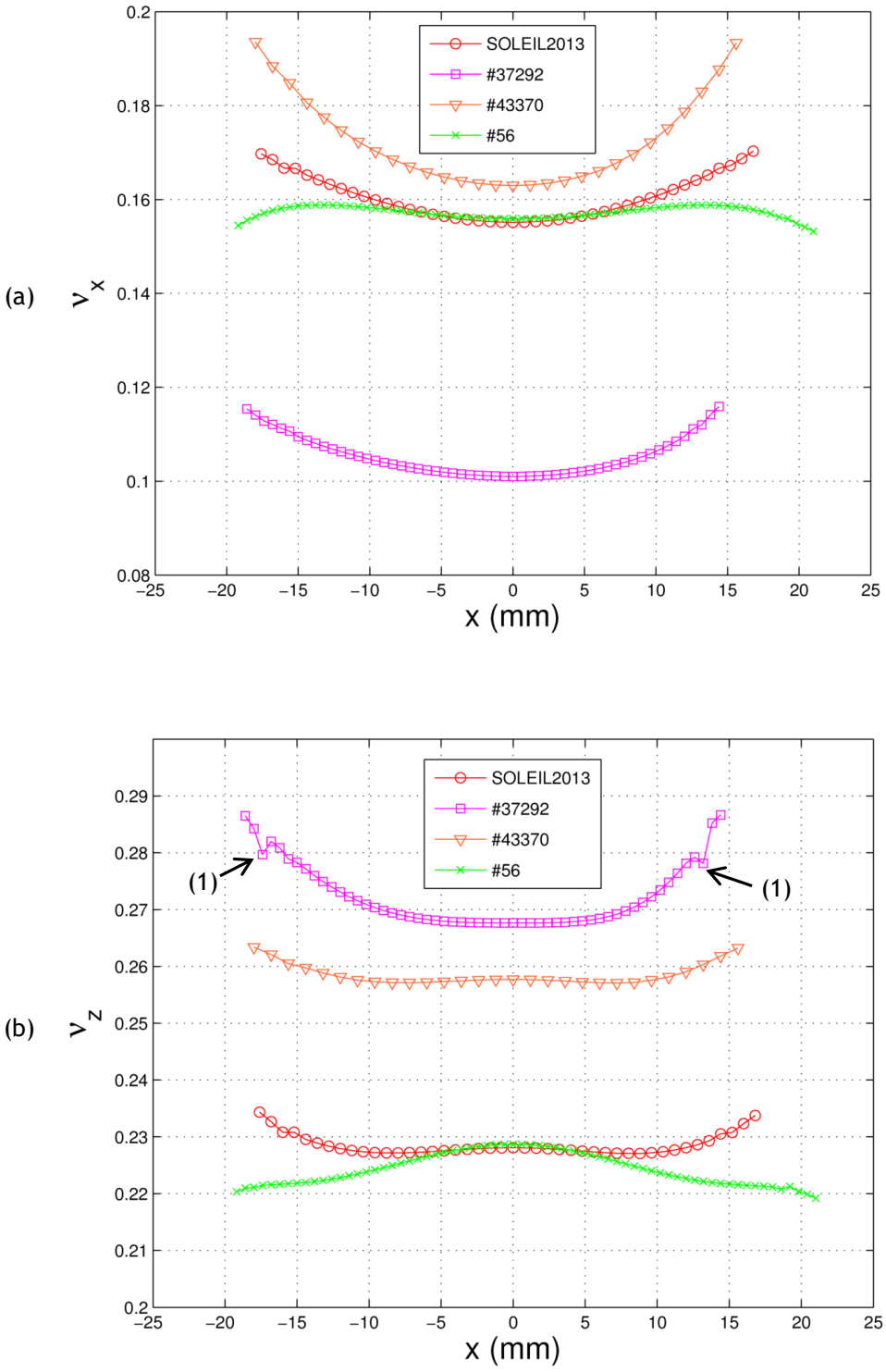

Figure 12: Comparison of the horizontal (a) and the vertical (b) tune shifts with the horizontal amplitude between the SOLEIL2013 storage ring lattice (red o) and the optimized solutions #56 (green x), #37292 (magenta □) and #43370 (orange Δ) obtained by MOGA-ELEGANT and calculated by TRACY3 including the vacuum chamber and the multipolar field components. The resonance lines $5\nu_x$-$2\nu_z$=70 (1) is identified. The parameters used by TRACY3 code to compute the tune shifts with the horizontal amplitude are shown in Table 3.

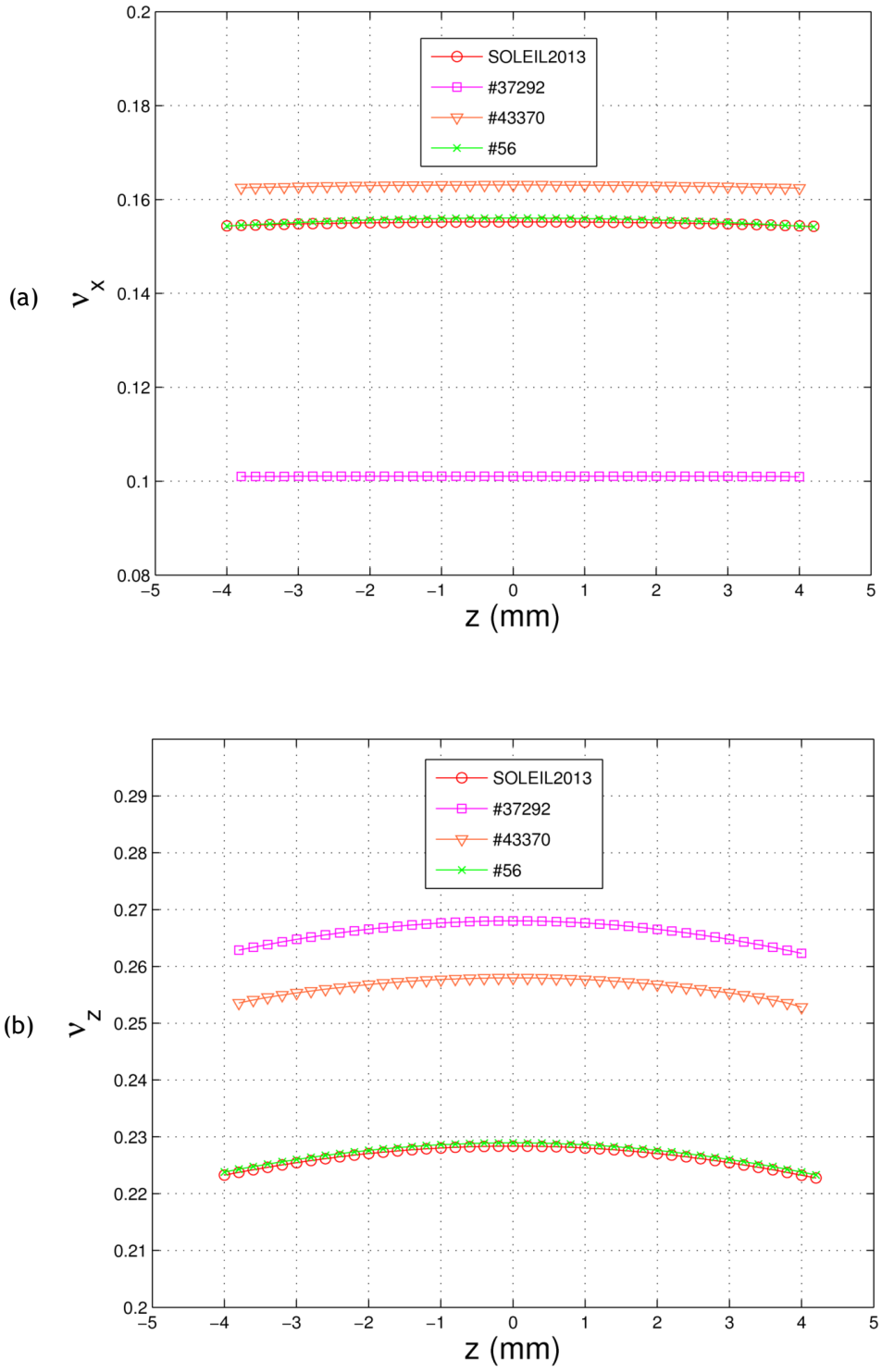

Figure 13: Comparison of the horizontal (a) and the vertical (b) tune shifts with the vertical amplitude between the SOLEIL2013 storage ring lattice (red o) and the optimized solutions #56 (green x), #37292 (magenta □) and #43370 (orange ∇) obtained by MOGA-ELEGANT and calculated by TRACY3 including the vacuum chamber and the multipolar field components. The parameters used by TRACY3 code to compute the tune shifts with the horizontal amplitude are shown in Table 3.

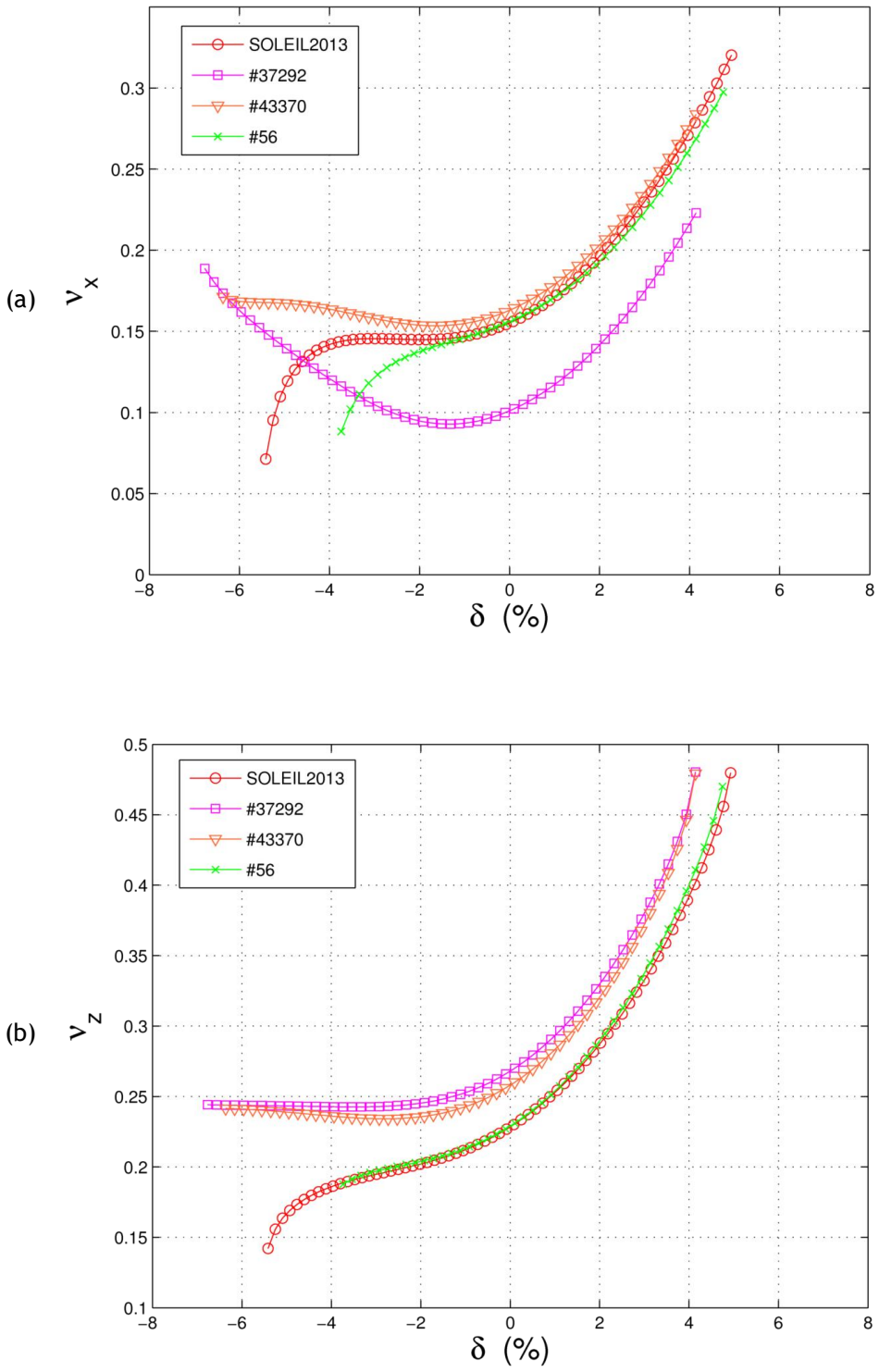

Figure 14: Comparison of the horizontal (a) and the vertical (b) tune shifts with energy between the SOLEIL2013 storage ring lattice (red o) and the optimized solutions #56 (green x), #37292 (magenta □) and #43370 (orange ∇) obtained by MOGA-ELEGANT and calculated by TRACY3 including the vacuum chamber and the multipolar field components. The parameters used by TRACY3 code to compute the tune shifts with the horizontal amplitude are shown in Table 3.

1.3.2.3. 6D-Momentum Acceptance along the Storage Ring and Touschek Lifetime

The comparison of the momentum acceptances calculated by ELEGANT and TRACY3 codes for the SOLEIL2013 lattice and the three optimized solutions considered in this study are shown in Figure 15 (6D tracking with 1,000 turns and 2.665 MV of RF-voltage are taken into account). The parameters used by TRACY3 code to compute the momentum aperture are given in Table 1.

The optimized solutions #37292 and #43370 show larger momentum acceptances compared to the nominal case. The improvement seen before on the horizontal and vertical tune shift with energy of Figure 14 is confirmed.

Table 4 gives the Touschek lifetime calculated for the optimized solutions #37292 and #43370 together with the degraded solution #56 computed by ELEGANT and TRACY3 codes with and without the multipolar field components. As a result, the improvement of the Touschek lifetime calculation obtained from ELEGANT is confirmed by TRACY3 with a more realistic model. The slight difference between ELEGANT and TRACY3 values is well understood and originates from the approximation applied in ELEGANT to compute by tracking the momentum acceptance at the sextupole locations and only for one quarter of the ring circumference.

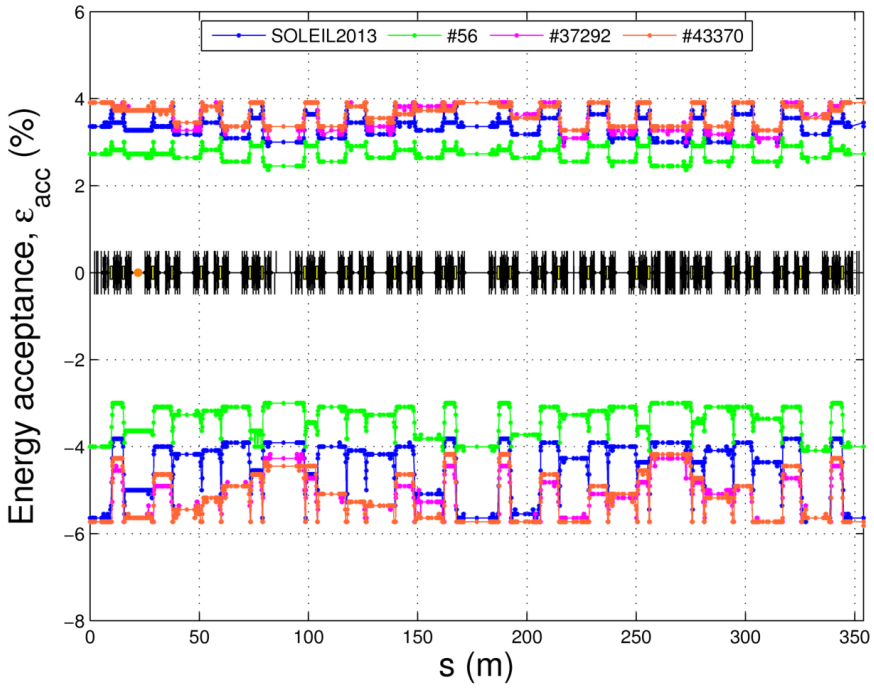

Figure 15: Comparison of the momentum apertures calculated by TRACY3 code for the SOLEIL2013 lattice (blue line) and the two optimized solutions #37292 (magenta line) and #43370 (orange line) and the low-lifetime lattice #56 (green line) found by MOGA-ELEGANT. 6D tracking with 1,000 turns and 2.665 MV of RF-voltage are taken into account adding the dimensions of the vacuum chamber and the multipolar field components. MA computation parameters are given in Table 1.

Lattice	ε_x (nm rad)	Touschek Lifetime (h)		
		ELEGANT	TRACY3 Multipolar Field Components	
			Without	With
Nominal	3.87	29.3	32.3	35.3
#37292	3.97	49.3	50.3	50.8
#43370	3.87	41.5	45.2	47.3
#56	3.87	18.8	17.7	18.1

Table 4: Touschek lifetime of the SOLEIL2013 storage ring lattice and the optimized solutions obtained by MOGA-ELEGANT #37292, #43370, and #56 computed from ELEGANT and TRACY3 energy acceptances, with and without multipolar field components. The Touschek lifetime is computed with 1 % of coupling, 6 mm of bunch length, 1 mA of bunch current.

1.3.3. Summary of Selected Lattices

Three lattices have been selected for beam-based experiment:

- Two lattices for their promising performance with respect to the nominal lattice in terms of Touschek lifetime (50 h): one with low (#37292) and one with large (#43370) fractional part of the horizontal tune.
- One lattice (#56) with a predicted degradation of the Touschek beam lifetime but large dynamic aperture and large fractional part of the horizontal tune.

2. Experiments: Testing MOGA Solutions in the Real Storage Ring

An 8-hour shift was dedicated to check out whether the predicted performance (improvement or degradation) of the aforesaid lattices was met with the electron beams.

The SOLEIL storage ring lattice was prepared for the experiment:

- Magnets were cycled on their nominal setting.
- All electromagnetic insertion devices (IDs) were switched off.
- All mechanical insertion devices were open to their maximum gaps (rest gaps for in-vacuum IDs for avoiding locally random outgassing that could jeopardize lifetime measurements).
- All scrapers were opened to their maximum values.
- Then after tune, chromaticity corrected to the model values, an orbit response matrix was measured and analyzed to verify that the optics is close to the model one (LOCO analysis, (Safranek, 2002)). The residual beta beating was found to be below one percent peak value, which corresponds to the standard symmetrisation of the storage ring.

The machine was then set to 1 % coupling to mimic the machine setup used in the calculation of the Touschek lifetime. The betatron tunes were set to the model values: 18.1548 ± 0.0005 and 10.2294 ± 0.0005 using the two quadrupole families Q7 and Q9.

During the same day, lifetime and injection efficiency were measured for both the nominal lattice and the MOGA-ELEGANT lattices. These results are reported in the next sections.

2.1. QUADRUPOLE AND SEXTUPOLE STRENGTH CONVERSION

In order to test the new lattices, the first step consists of converting magnet strengths into currents feeding the power supplies of the quadrupole and sextupole magnets. To be more precise, the quadrupole and sextupole strengths have to be converted from physics units of (m^{-2}) and (m^{-3}) respectively to hardware units of current (A). A Matlab routine is used for that purpose encoding the magnetic calibration performed during magnetic measurements before the commissioning of SOLEIL (Brunelle, 2006). The results of this conversion are given in Table 5 using the Accelerator Toolbox (Terebilo, 2001). The quadrupole and sextupole strengths are expressed up to the fourth decimal due to the power supply precision:

- 1 mA corresponds to the Least Significant Bit (LSB) of the 20 bit quadrupole power supplies.
- 5 mA corresponds to the Least Significant Bit (LSB) of the 20 bit sextupole power supplies.

	Reference Lattice		MOGA ID					
	SOLEIL 2013		#37292		#43370		#56	
Magnet Families	Strengths (m^{-2})	Currents (A)	Strengths (m^{-2})	Currents (A)	Strengths (m^{-2})	Currents (A)	Strengths (m^{-2})	Currents (A)
Q7	2.034	206.477	2.031	206.093	2.035	206.559	2.034	206.442
Q9	-1.357	-161.680	-1.360	-162.043	-1.362	-162.285	-1.357	-161.680
Magnet Families	Strengths (m^{-3})	Currents (A)	Strengths (m^{-3})	Currents (A)	Strengths (m^{-3})	Currents (A)	Strengths (m^{-3})	Currents (A)
S1	17.5626	81.685	18.7613	87.378	18.7583	87.364	18.9482	88.266
S2	-40.8670	-192.740	-40.8470	-192.606	-41.9827	-198.038	-41.1569	-194.088
S3	-20.5422	-98.600	-21.4389	-100.099	-23.2049	-108.492	-20.4060	-95.192
S4	43.5625	205.603	41.5311	195.878	42.0925	198.564	44.2078	208.6967
S5	-44.625	-210.697	-44.0502	-207.941	-44.9865	-212.432	-44.9611	-212.309
S6	41.6875	196.624	40.0953	189.008	41.7478	196.913	40.8363	192.552
S7	-62.0000	-294.959	-63.2662	-301.225	-65.1094	-310.386	-62.9133	-299.476
S8	48.6250	229.916	50.8281	240.531	51.7695	245.072	48.0718	227.254
S9	-52.8803	-250.436	-52.2136	-247.217	-48.7588	-230.560	-52.0707	-246.526
S10	31.1999	146.544	30.6508	143.928	30.0148	141.000	32.2452	151.526
S11	15.1250	70.112	15.2917	70.904	14.0244	64.889	14.0709	65.109

Table 5: Quadrupole and sextupole strengths and corresponding currents for the nominal lattice and the three MOGA-ELEGANT lattices (ELEGANT units).

The maximum relative change in quadrupole strengths is 0.3 % and in sextupole strengths is 9.8 % for all the lattices (see Table 6). Figure 16 shows the relative changes for the sextupole families between the SOLEIL2013 nominal lattice and the three solutions selected for experiments.

Lattice	Relative Change of the Magnet Strengths												
	Q7 (%)	**Q9** (%)	**S1** (%)	**S2** (%)	**S3** (%)	**S4** (%)	**S5** (%)	**S6** (%)	**S7** (%)	**S8** (%)	**S9** (%)	**S10** (%)	**S11** (%)
#37292	0.30	0.03	6.8	2.7	9.8	3.4	0.8	0.1	5.0	6.5	7.5	5.2	7.3
#43370	0.03	0.03	7.9	0.7	3.4	1.5	0.8	2.0	1.5	1.1	1.2	1.9	7.0
#56	0.00	0.00	6.8	0.1	1.5	4.7	1.3	3.8	2.0	4.5	0.9	3.1	1.1

Table 6: Relative changes of the 11 sextupole strengths and of the 2 quadrupole strengths of the three selected MOGA solutions with respect to the nominal lattice SOLEIL2013.

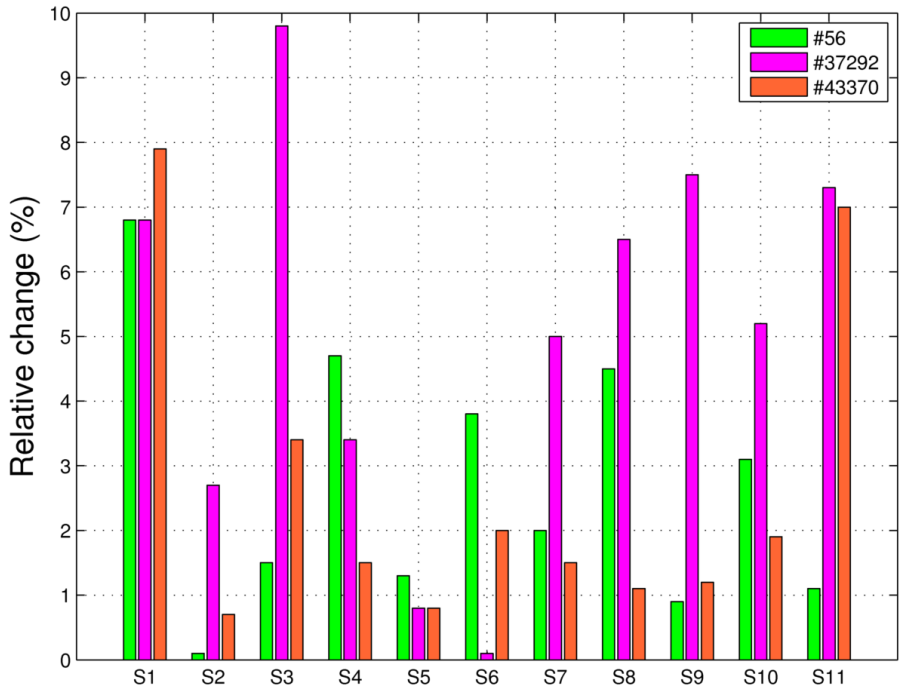

Figure 16: Relative changes of the sextupole family strengths of the solutions #56, #37292 and #43370 with respect to the SOLEIL2013 lattice.

2.2. Experimental Results for MOGA Solutions

Table 7 summarizes the experimental conditions of RF-voltage (V_{RF}), total beam current (I), filling pattern, coupling (k) and pressure (P). The beam current and the filling pattern were selected to perform the experiments are 150 mA and ¼ in order to maximize the contribution of the Touschek lifetime. By this choice, the total beam current is lower leading to a less contribution of the gas.

Machine Configuration			Measured Beam Parameters	
Parameters	**Values**		**Parameters**	**Values**
V_{RF} (MV)	2.7*		ξ_x	1.2 ± 0.1
I (mA)	150		ξ_z	2.0 ± 0.1
Bunch Current (mA)	1.4		ε_x (nm rad)	4.18 ± 0.01
Filling Pattern	1/4		ε_z (pm rad)	41 ± 0.1
H-scraper Position (mm)	(-35, 35)		k (%)	1.00
V-scraper Position (mm)	(-12.5, 12.5)		P (mbar)	3.0 ± 0.1 10^{-10}

Table 7: RF-voltage (V_{RF}), total beam current (I), filling pattern, coupling (k), average pressure around the ring (P), betatron tunes and chromaticities set for the beam-based measurements of the SOLEIL2013 lattice and the selected solutions #37292, #43370 and #56. (*) Effective RF-voltage seen by the beam.

All selected MOGA-ELEGANT lattices were tested successfully: the nominal total beam lifetime was increased from 16.8 h to 23.5 h for lattice #43370 and even to 25.3 h for lattice #37292 (60 % increased) as predicted by MOGA-ELEGANT. Detailed results are reported in Table 8 that shows the comparison between the measured and simulated total beam lifetimes (τ^{MEAS}, τ^{SIM}), the deduced and simulated Touschek lifetimes ($\tau^{DED}_{Tous}, \tau^{SIM}_{Tous}$), and injection efficiencies measured during the experiment for the three new lattices and the reference SOLEIL2013 lattice. The theoretical beam lifetimes are computed using Eq. 1 of Chapter III: the gas contribution is computed by Eq. 11 of Chapter III with the measured mean pressure of 3.0 10^{-10} mbar, that is 102.4 h, and the Touschek lifetimes are computed from TRACY3 taking into account the multipolar field components and the quadrupole fringe fields to be as close as possible to the real machine.

Lattice	ε_x **(nm·rad)**	ν_x	ν_x	τ^{SIM}_{Tous} **(h)**	τ^{DED}_{Tous} **(h)**	τ^{SIM} **(h)**	τ^{MEAS} **(h)**	**Injection Efficiency (%)**
Nominal	3.87	18.155	10.229	23.8	20.1 ± 0.7	19.8	16.8 ± 0.5	90
#37292	3.97	18.101	10.268	34.2	33.6 ± 0.9	26.1	25.3 ± 0.5	67
#43370	3.87	18.163	10.258	29.9	30.5 ± 0.8	24.8	23.5 ± 0.5	95
#56	3.87	18.157	10.229	12.2	10.7 ± 0.6	11.1	9.7 ± 0.5	95

Table 8: Comparison of simulated (TRACY3) and measured total and Touschek lifetimes for all the lattices tested experimentally. The injection efficiency is also shown. Emittance values correspond to the model values. Computation hypothesis: 102.4 h for the gas lifetime, 1 % coupling, 6 mm bunch length and 1.4 mA bunch current.

As a first remark, the horizontal emittance measured in the control room is slightly larger than the modeled one. For lattice #43370, the measured emittance was 4.4

nm·rad due to the proximity of the horizontal tune to the integer. The Touschek lifetime was renormalized for a fair comparison with the other points.

The lattice #43370, the MOGA-ELEGANT solution with higher H-tune, preserves the injection efficiency while increasing the total beam lifetime by about 40 %. This corresponds to a net increase of the Touschek contribution 30.5 h, close to the prediction of 29.9 h.

The lattice #37292, the MOGA-ELEGANT solution with low horizontal tune, gives the best lifetime with an increase of 50 % of the total lifetime corresponding to the doubling of the Touschek lifetime with a total measured value of 33.6 hours (expected 34.2 h). The lower injection efficiency can be explained by the lower horizontal tune. Indeed for a tune close to 18.1, the injected beam after one turn gets an unfavorable phase advance bringing part of the beam directly on the septum sheet of the injection septum; on average the rise-fall time of the 4 injection kickers is 6 turns. This fact was not included in the simulation and whence not predicted by ELEGANT or TRACY3.

The lattice #56 presents a significant decrease of the lifetime while keeping the injection efficiency. The lifetime decreased by 42 %. The measured Touschek lifetime 10.7 h is slightly different to the predicted value 12.2 h.

The lattice #43370 was tested with a setting of the skew quadrupoles leading to a minimum coupling value of 0.14 %. The total beam lifetime time was measured to be 8h instead of 5.5 h for the nominal lattice. This gives an increase of 31 % of the total lifetime and an increase of 49 % of the Touschek lifetime (from 5.8 h to 8.7 h), which is coherent with the measurement at 1 % of coupling.

2.3. SUMMARY AND CONCLUSIONS

There is a good agreement between simulated and measured beam lifetimes. Then, the improvement of the Touschek lifetime predicted by MOGA-ELEGANT has been validated. These results are the first application of MOGA-ELEGANT at SOLEIL. The success of the experiment with the beam in the control room enables us to validate both the optimization method based on genetic algorithm and the magnetic model of the storage ring lattice.

The improvement was large concerning beam lifetime since the nominal lattice was expected to be already well optimized in terms of beam lifetime and injection efficiency. For many years, the choice of any working point at SOLEIL has shown that a compromise was necessary between beam lifetime and injection efficiency. MOGA-ELEGANT has revealed several new groups of solutions with improvement for both figures of merit. The next step will be to check the robustness of the lattice with respect to the insertion device configuration and to study the localization of the losses due to beam lifetime or after a beam dump. Both these topics are of special importance for using the new lattice for daily operation.

In a close future, the storage ring will be operated with lower coupling value. In order to run with a 0.2 % coupling, it becomes primordial to increase the Touschek lifetime since it will be fully dominant. Considering that the shielding walls of the accelerator are built to sustain a minimum total beam lifetime of 4 h, the new sextupole setting should be very helpful. Otherwise the radiation safety would become a strong showstopper in this project.

For long-term projects, an upgrade study program has been started at SOLEIL in order to lower the horizontal emittance by a factor a least 20. The storage ring lattice will be fully redesigned replacing the standard double bend lattice by a multibend lattice. The strong focusing new lattice will be extremely challenging in terms of dynamic aperture and lifetime optimization. MOGA-ELEGANT and genetic based algorithms could be a key ingredient for helping optimize nonlinear dynamics and making the project viable (Nagaoka 2012, 2013, 2014; Nadolski, 2014).

BIBLIOGRAPHY

(Brunelle, 2006) P. Brunelle, C. Benabderrahmane, P. Berteaud, F. Briquez, L. Dubois, M. Girault, A. Madur, F. Marteau, A. Nadji, F. Paulin, J. Vétéran, and A. Daël. Magnetic Measurements Results of the Dipoles, Quadrupoles and Sextupoles of the SOLEIL Storage Ring. Proceedings of the 2006 European Particle Accelerator Conference, pp. 3278-3280, Edinburgh, Scotland, 2006.

(LER, 2015) https://indico.cern.ch/event/395487/timetable/#20150915.detailed

(Nadolski, 2014) L. S. Nadolski P. Brunelle, X. N. Gavaldà, A. Loulergue, A. Nadji, R. Nagaoka, and M.-A. Tordeux. Study of Upgrade Scenarios for the SOLEIL Storage Ring. Proceedings of the 2014 International Particle Accelerators Conference, pp. 203-205, Dresden, Germany, 2014.

(Nagaoka, 2012) R. Nagaoka, P. Brunelle, L. S. Nadolski, and A. Nadji. Study of a Lower Emittance Lattice at SOLEIL. Proceedings of the 2012 International Conference Particle Accelerators, pp. 1155-1157, New Orleans, USA, 2012.

(Nagaoka, 2013) R. Nagaoka, P. Brunelle, L.S. Nadolski, A. Nadji, X.N. Gavaldà, M. Klein, A. Loulergue, and M.-A. Tordeux. Study of Low Emittance Optics using Multi-Bend-Achromat Lattice at SOLEIL. Proceedings of the 2013 International Conference Particle Accelerators, pp. 76-78, Shanghai, China, 2013.

(Nagaoka, 2015) R. Nagaoka, P. Brunelle, F. Cullinan, X.N. Gavaldà, A. Loulergue, A. Nadji, L.S. Nadolski, and M.-A. Tordeux. Study of Optimal MBA Lattice Structures for the SOLEIL Upgrade. Proceedings of the 2015 International Conference Particle Accelerators, pp. 106-108, Richmond, USA, 2015.

(Safranek, 2002) J. Safranek, G. Portmann, A. Terebilo, and C. Steier, MATLAB-based LOCO. Proceedings of the 2002 European Particle Accelerator Conference, pp. 1184-1186, Paris, France, 2002.

(Terebilo, 2001) A. Terebilo, Accelerator Toolbox for MATLAB. SLAC Technical Report SLACPUB-8732, USA, 2001.

CONCLUSIONS AND PERSPECTIVES

The optimization of the nonlinear beam dynamics of the current lattice of SOLEIL with Multi-Objective Genetic Algorithm (MOGA) has been performed with success. The model of the SOLEIL lattice has been used including two quadrupole families and the eleven sextupole families as optimization variables and adding all physical limitations. The simulated results obtained after 1 month of computation in the SOLEIL cluster using 200 CPUs show a significant improvement of the dynamic aperture and especially of the Touschek lifetimes (70%), the objectives of the optimization process.

The experimental results obtained by beam-based experiments agree with the simulated ones. Two optimized solutions of the Pareto-optimal front have been tested in the control room of SOLEIL showing an important improvement of 40–50 % in the total beam lifetime while preserving close to 100% of the injection efficiency of the storage ring. MOGA was able to predict the performance of the optimized lattice in terms of Touschek lifetime and injection efficiency. These results rely on the fine modeling of the magnetic lattice including all the measured multipolar components prior to the commissioning of the machine. A degraded solution has also been tested. Its lower Touschek lifetime with respect to the nominal lattice is well confirmed.

This is the first time that MOGA or any GA has been applied for the SOLEIL storage ring optimization. As advantages, MOGA enables the discovery of solutions that were never explored before. The relative changes of 10–15 % in terms of sextupole settings are larger than the changes obtained with the other methods applied during the on-line optimization of the working point at SOLEIL. MOGA also opens a new window to explore and optimize the present and future lattices of SOLEIL: it is flexible and can be used to optimize other figures of merit for forthcoming studies, as for example, the horizontal emittance for the future low-emittance upgrade of SOLEIL lattice to a level of hundred picometers.

As a disadvantage, MOGA is slow, CPU demanding, and needs a high-performance computing system. The tracking computation of especially the momentum aperture is very time consuming even with the approximations applied in this thesis. To ensure solutions with dynamic apertures free from major resonances, the diffusion rate from frequency map analysis could be used as a figure of merit. The calculation of the tune shift with amplitude and energy can also be used to speed up the selection of the Pareto-optimal front and even the code ELEGANT can be replaced by a faster tracking code. The use of other algorithms as the Robust Conjugate Direction Search (RCDS) much robust and efficient than MOGA could be another way to speed up the optimization process. The last results of RCDS reported in this

thesis are promising and it could be applied to optimize the nominal lattice of SOLEIL online directly in the control room in an optimum way.

In parallel, the comparison between ELEGANT and the version of TRACY3 installed and developed at SOLEIL has become important for this thesis. Firstly, TRACY3 is a beam-based validated code; it has been used to introduce the multipolar field components into the optimized model in an easier way. Secondly, the disagreement of the vertical chromaticity between the version 25.0.1 of ELEGANT and TRACY3 has allowed the definition of the dipole edge focusing of ELEGANT to be corrected. In addition, the Bruck formula originally implemented to compute the Touschek lifetime in TRACY3 has been replaced by the Piwinski formula resulting in more exact values of the Touschek lifetime. Finally, the post-process routines of TRACY3 to analyze for example the Frequency Maps and the tune shift with amplitudes and energy offset has become crucial to compare the solutions of the Pareto-optimal set among them and select the best solutions to be tested using beam-based experiments.

The second main result of this thesis is the experimental study of the beam lifetime and the respective Touschek and gas lifetime contributions. The beam lifetime has been measured varying the coupling value, the vertical scraper aperture, and the bunch current for the nominal lattice of SOLEIL. For the filling patterns used in SOLEIL, the results show a strong contribution of the Touschek lifetime in the total beam lifetime and a good agreement between the simulated and measured Touschek lifetimes. This confirms the reliability of the lattice model and the accuracy of the energy acceptance calculation with ELEGANT and TRACY3.

The study of the gas beam lifetime has shown that there is a disagreement between simulated and measured gas lifetimes due to difficulty to determine experimentally the effective atomic number of the residual gas and the pressure felt by the beam in the storage ring. Concerning the effective atomic number, Residual Gas Analyzer (RGA) measurements have shown a difference of the gas composition between the sector of the storage ring and the sections hosting in-vacuum undulators. This difference comes from the use of NEG coated chambers in almost 50 % of the circumference that makes the gas composition change over time and make molecules with small atomic numbers dominate the gas. However, the zones of the storage ring free of NEG coated surfaces, like the straight sections hosting in-vacuum undulators, present a gas composition with higher Z-molecules close to the atomic number equal to 7, the atomic number supposing a gas composted by N_2 or CO commonly referenced in the bibliography. The comparison between simulated and measured beam lifetime shows that this effective atomic number of 7 is better representing the reality and that the gas scattering should be mainly generated in the small part of the circumference where there is not NEG coating.

Actually a specific type of thermocouple was discovered to release heavy elements in the vacuum pipe. In the near future a new type of RGA most fast will be installed to refine the measurement of components of the gas. In addition, at these locations much higher pressures

dominate, increasing indeed the contribution of the gas lifetime. Other places host ceramic chambers for current measurement systems, kicker magnets, injection septa, and RF-cavity bellows that are known to rise in temperature and then increasing locally the gas pressure. The measure of the pressure is delicate as well due to the limited number of ions pumps distributed along the ring.

This PhD has enabled the increase of knowledge of the accelerator physics group. Many minor and major upgrades of the storage ring lattice are foreseen at SOLEIL. The lifetime and injection efficient will remain some of utmost figures of merit. The success depends heavily on a good knowledge of the magnetic measurement of the magnets, the magnetic errors, a good modeling of the physical aperture. The large time devoting during the magnetic measurements and their analysis pays off. This is one of the guarantees to assure that model-based optimized lattice will show similar performance in the real world. It is also clear that the detailed modeling and online measurement of the pressure along the ring is of paramount importance; for future light sources where the physical aperture is 10 to 20 mm of diameters, this is even more relevant. The studies have shown that a dedicate care should be given to reducing any local increase in the pressure, especially at the location of ceramic chambers and in-vacuum undulator whose future full gap will be 4 to 5 mm.

I would like to finish by discussing points about the methodology of optimizing the forthcoming strong focusing lattices of the diffraction limited light sources. Genetic based-algorithms are really an added value and should be fully part of the toolbox of the accelerator physicists. This is true both for off- and on-line algorithms. The later ones have never been tested at SOLEIL and should be tested and they will certainly show equivalent success to that of ESRF, SPEAR3, for example. GAs are time-consuming, complex, and often require High-Performance Computers. This work was just an introduction; many developments need to be done for the optimization of both linear and nonlinear beam dynamics. The workload will likely necessitate a dedicated engineer to maintain and develop GAs. Even if the algorithm could be sped-up, the computer resources are critical for the future simulation. As it was done during the work, several dedicated queues of the cluster should be exclusively reserved for this type of computation using parallel optimization.

université PARIS-SACLAY | ÉCOLE DOCTORALE PHENIICS

Titre : Application d'Algorithmes Génétiques Multi-Objectifs et Études Expérimentales de la Durée de Vie du Faisceau de l'Anneau de Stockage du Synchrotron SOLEIL

Mots clés : Sources de Lumière, Dynamique de Faisceau, Algorithmes Génétiques, Durée de Vie, Études Expérimentales

Cette thèse est consacrée à l'optimisation des sources de lumière synchrotron. La dynamique de faisceau non linéaire de l'anneau de stockage du synchrotron SOLEIL est optimisée à l'aide d'algorithmes génétiques multi-objectifs (MOGA-ELEGANT). Le code ELEGANT est d'abord comparé avec le code étalon de SOLEIL, TRACY3. Le code MOGA est ensuite utilisé pour obtenir les meilleures configurations possibles en termes d'ouvertures dynamiques et d'acceptances en énergie, qui sont fortement en rapport avec l'efficacité d'injection et la durée de vie Touschek respectivement. Après un mois de calcul sur le cluster de calcul de haute performance de SOLEIL en utilisant 200 CPU, un ensemble de solutions est trouvé. Elles sont testées expérimentalement dans la salle de contrôle de SOLEIL. L'amélioration de la durée de vie Touschek obtenue est confirmée par les mesures : la durée de vie du faisceau de l'anneau de stockage de SOLEIL est augmentée de 40 à 50%.

La deuxième partie de ce travail de thèse présente une étude expérimentale de la durée de vie du faisceau de l'anneau de stockage de SOLEIL. En particulier les contributions de la durée de vie Touschek et de la durée de vie du gaz sont étudiées. La durée de vie du faisceau est mesurée en fonction de paramètres importants tels que le couplage, l'ouverture des collimateurs horizontaux et verticaux, et le courant par paquet. Les résultats expérimentaux sont comparés avec les durées de vie Touschek calculées par la formule Piwinski mise en œuvre dans le code TRACY3 et la durée de vie du gaz calculée analytiquement. Cette étude permet de montrer que la composition du gaz résiduel et la pression locale varient de manière importante le long de toute la machine: l'effet des onduleurs sous vide est dominant. Des nombres atomiques effectifs sont obtenus. La forme des courbes expérimentales est proche des courbes simulées et est compatible avec un nombre atomique effectif proche de 7.

Title: Multi-Objective Genetic based Algorithms and Experimental Beam Lifetime Studies for the Synchrotron SOLEIL Storage Ring

Keywords: Synchrotron Light Sources, Beam Dynamics, Genetic Algorithms, Beam Lifetime, Beam-Based Experiments

Abstract: This thesis is dedicated to the optimization of the nonlinear beam dynamics of synchrotron radiation light sources using Multi-Objective Genetic Algorithms (MOGA-ELEGANT). In the first part the ELEGANT code is benchmarked against TRACY3; then MOGA is tuned and used to find the best settings of quadrupole and sextupole magnets in order to maximize the dynamic and momentum apertures, strongly related with the Touschek lifetime and the injection efficiency respectively. Solutions obtained after one month of computation in the high level computational cluster of SOLEIL using 200 CPUs are analyzed. The improvement of the Touschek lifetime obtained with MOGA is confirmed by the beam-based experiments. The beam lifetime of the SOLEIL storage ring is increased 40-50 %.

The second part this PhD work is devoted to study experimentally the beam lifetime of the SOLEIL storage ring to improve the understanding of the beam lifetime and its contributions: the Touschek and gas lifetimes. The beam lifetime is measured in function of important parameters as coupling, horizontal and vertical scrapers, and bunch current. The experimental results are compared with the simulated ones. The Piwinski formula is implemented in the tracking code TRACY3 to replace Bruck approximation. The gas lifetimes were computed using analytical models. This study allows understanding that the composition of the residual gas and the local pressure along the entire machine vary significantly between the arcs and the in-vacuum insertion devices: new effective atomic numbers are obtained. This type of measurement remains difficult to analyze without a large error margin; in-vacuum insertions have a dominant contribution. The shape of the experimental curves is closed to the expected ones and compatible with an effective atomic number of about 7.